ABROGATION OF LIVER CANCER WITH THERMAL ABLATION AND TARGETED HEAT SHOCK INHIBITION

by

Yizhe Chen

A dissertation submitted to the faculty of
The University of Utah
in partial fulfillment of the requirements for the degree of

Doctor of Philosophy

Department of Pharmaceutics and Pharmaceutical Chemistry

The University of Utah

May 2015

The University of Utah Graduate School

STATEMENT OF DISSERTATION APPROVAL

The dissertation of **Yizhe Chen**

has been approved by the following supervisory committee members:

Hamidreza Ghandehari	, Chair	11/12/2014 Date Approved
You Han Bae	, Member	11/16/2014 Date Approved
James Herron	, Member	11/12/2014 Date Approved
Darin Furgeson	, Member	11/18/2014 Date Approved
Courtney Scaife	, Member	11/12/2014 Date Approved

and by **David Grainger**, Chair/Dean of

the Department/College/School of **Pharmaceutics and Pharmaceutical Chemistry**

and by David B. Kieda, Dean of The Graduate School.

ABSTRACT

Thermal ablation is widely used, first line local-regional therapy for unresectable hepatocellular carcinoma (HCC). Although high temperature delivered by thermal energy results in efficient coagulation necrosis in tumor cells, various factors including tumor size, shape, location, and cirrhosis can lead to un-uniform heat distribution and inefficient cell damage. As a result, the incomplete ablation causes high rates of tumor recurrence and poor survival for HCC patients. Cells that are not completely ablated can induce heat shock proteins (HSPs), which are cellular gatekeepers to protect tumor cells from thermal damage and prepare them for future neoplastic growth. Synchronous adjuvant chemotherapy targeting those cells can achieve more complete tumor abrogation and prevent future tumor recurrence. This dissertation describes a strategy to combat postablation recurrence by synchronous inhibition of heat shock protein 90 (HSP90) by thermo-responsive, elastin-like polypeptide (ELP)-based biopolymer conjugates. ELP copolymer carries high concentrations of a potent HSP90 inhibitor, geldanamycin (GA), which inhibit the induction of HSP90 and further destabilize numerous HSP90 client proteins critical for cell survival. It is hypothesized that combination of thermal ablation with concomitant inhibition of HSP90 via ELP-GA conjugates can achieve synergistic anticancer effect. Specifically, the ablation-created hyperthermia will sensitize tumor cells to be more vulnerable to the drug, which will be conjugated with high concentrations through thermally targeted, ELP-based biopolymer systems. The ELP conjugates, in turn, will reach and kill the remaining viable

cells to prevent future recurrence. ELP-GA conjugates that ferry multiple GAs and rapidly respond to hyperthermia were synthesized, characterized, and evaluated for activity in HCC models. The cytotoxicity of ELP-GA conjugates was enhanced with hyperthermia treatment, and effective HSP90 inhibition was achieved in HCC cell lines. In a tumor-bearing mouse model, electrocautery-based thermal ablation offered effective destruction of tumor core and created a hyperthermia zone for targeted delivery and accumulation of ELP-GA conjugates.

Results demonstrate that the combination of thermal ablation and targeted HSP90 inhibition can enhance the anticancer effect and cellular delivery of macromolecular chemotherapeutics to achieve safe, synergistic, and long-term anticancer effect with no tumor recurrence observed. The combination approach paves the way for developing molecular-targeted intervention to increase the efficacy of first-line local-regional therapies for HCC.

TABLE OF CONTENTS

LIST OF TABLES

LIST OF FIGURES

ABBREVIATIONS

17-AAG	17-ally-17-desmethoxygeladanamycin-tanespimycin
17-DMAG	17-desmoethoxy-17-N,N-dimethylaminoethylaminogeldanamycin-alvespimycin
AAADA	Aminoacetaldehyde diethyl acetal
AFB1	Aflatoxin B1
AFP	α–fetoprotein
ALT	Alanine aminotransferase
ASO	Antisense oligonucleotide
AST	Aspartate aminotransferase
BLCL	Barcelona-clinic liver
BUN	Blood urea nitrogen
CAF	Cancer-associated fibroblasts
CCl4	Carbon tetrachloride
CDD	Choline deficient diet
CIP	Calf intestinal alkaline phosphatase
CLIP	Cancer of the Liver Italian Program
CMC	Critical micelle concentrations
CT	Computed tomography
DCP	Des-y-carboxyprothrombin

DEB	Drug eluting beads
DEN	N-nitrosodiethylamine
DLS	Dynamic light scattering
DMEM	Dulbecco's modified Eagle's medium
DMSO	Dimethyl sulfoxide
EC	Electrocautery
EDC	1-ethyl-3-(3-dimethylaminopropyl) carbodiimide
EGF	Epidermal growth factor
ELP	Elastin-like peptide
EPR	Enhanced permeability and retention
FBS	Fetal bovine serum
FDA	Food and drug administration
FGF	Fibroblast growth factor
HBV/HCV	Hepatitis B/C viruses
HCC	Hepatocellular carcinoma
HCSC	Hepatic cancer stem cells
HGF	Hepatocyte growth factor
HIF-1	Hypoxia induced factor-1
HIFU	High intensity focused ultrasound
HSP	Heat shock protein
HT	Hyperthermia
IGF	Insulin-like growth factor
LT	Liver transplantation

MALDI-TOF-MS	Matrix-assisted laser desorption ionization-time of flight mass spectrometry
MRI	Magnetic resonance imaging
MSC	Mesenchymal stem cells
MTD	Maximum tolerated dose
MWA	Microwave ablation
NASH	Nonalcoholic steatohaptitis
Nd-YAG	Neodymium yttrium-aluminum-garnet
NF-κB	Nuclear factor kappa B
NHS	sulfo-*N*-hydroxysuccinimide
NIPAAm	N-Isopropylacrylamide
OERCA	Overlap extension rolling circle amplification
PDGF	Platelet-derived growth factor
PEG	Poly(ethylene) glycol
PET	Positron emission tomography
PMA	Premarket approval
RDL	Recursive directional ligation
RES	Reticuloendothelial system
RFA	Radiofrequency ablation
SABR	Stereotactic ablative radiotherapy
SBRT	Stereotactic body radiation therapy
SCID	Severe combined immune deficient
SDS-PAGE	Sodium dodecyl sulfate polyacrylamide gel electrophoresis

SELP	Silk elastin-like polypeptide
SLP	Silk-like polypeptide
TA	Thermal Ablation
TAA	Hepatotoxin thioacetamide
TAM	Tumor associated macrophages
TEM	Transmission electron microscopy
TER	Thermal enhancement ratio
TGF-α	Tumor growth factor alpha
TKI	Tyrosine kinase inhibitors
UPR	Unfolded protein response
VEGF	Vascular endothelial growth factor
UPR	Unfolded protein response

ACKNOWLEDGEMENTS

The work described in this dissertation is the product of the efforts of multiple individuals.

Dr. Furgeson, my research advisor and formal chair of my Ph.D. supervisory committee, provided continuous, unwavering support for me during my graduate studies. It was my great honor to be able to do this project with him, and I was deeply inspired by his unique way of thinking. He offered me space to set my own pace and allowed me to develop independent research skills. He has been actively seeking outside collaborations so I am exposed to various other disciplines and experts related to the drug delivery field. He is not only my research mentor, but also a reliable "big brother" who helped my transition to the US, supported me when I had visa issues, and taught me driving, writing, and even life-saving skills. He never hesitated to share his own experiences to motivate me when things were not working.

Dr. You Han Bae, a member of my Ph.D. supervisory committee, has consistently provided feedback on my research and prompt assistance to my request of literature and experimental design. He is particularly inspiring to me with his scientific insight. His constructive criticism has helped me develop critical thinking and challenge the status quo to probe the truth behind the phenomenon. I also had the opportunity to work with him as a teaching assistant, where I gained a broad understanding of drug delivery and appreciation of the effort professors made into each single lecture. I deeply appreciate his

motivation, encouragement, and high standards which drive me to grow consistently throughout my Ph.D. study.

Dr. Ghandehari, who volunteered to be the chair of my Ph.D. supervisory committee, has played a significant role in my graduate studies. He carries with him a vast understanding and knowledge in the drug delivery field. Every individual meeting with him I would acquire valuable information not only about the research techniques and related literature, but also a deeper understanding of experts related to my research. To me and my fellow students, he is a prime example of a scientist with wide connections and entrepreneurship.

Dr. James Herron, also a member of my Ph.D. supervisory committee, has also played a significant role during my course of studies. As my graduate study advisor, he provided various guidance on my transition from a complete foreign school to US graduate school. During my SAC year, he also helped me to be a better department coordinator. I enjoyed his individual committee meetings, which not only guided my research design, but also enriched my understanding of the project and utilization of the department resources. Dr. Herron has a tremendous reservoir of knowledge which allows him to point out things that I miss. I am very impressed with his interest in China, which added much joyful flavor into our individual meetings.

Dr. Courtney Scaife is also one of my committee members. She stepped in right after my previous surgeon member left and offered as much help as she could to push the project forward. She is the one who did the most hands-on experiments and trained me on various surgical skills. She also provided keen insight from a surgeon's perspective and also offered valuable guidance on my presentation skills.

Dr. Pysher, division chief of clinical and pediatric pathology, has contributed tremendously in my research. In addition to providing detailed instructions on immunohistochemistry studies, he spent a lot of effort reviewing the data and offered in-depth discussion not only on the project, but also on a general scale.

Dr. Grainger, our department chair, also provided tremendous support for my course of study. He served as a co-mentor in my last Ph.D. course and offered a nourishing environment to cultivate my presentation skills. He also played a vital role during my SAC year where he responded in a timely fashion with a truly caring heart for students. He sets an excellent sample for students as a world- class researcher and mentor.

I would also like to acknowledge the Furgeson Lab group, especially Pilju Youn, for being a reliable, supportive, and caring lab member throughout my study. We truly worked as a team and tried our best to help with each other's project. Being an international student, she understands most of my struggles and offers life tips. Her emotional support helped me through hard and tough times. The friendship we have developed during our studies will definitely continue and benefit both our future careers.

Dr. Lim's lab provided valuable guidance and training for my molecular biology experiments. Dr. Shawn's lab also offered valuable suggestions for my histology experiments. Their continuous support, kindness, and generosity helped my research go more smoothly and created a working environment in a big family.

CHAPTER 1

INTRODUCTION

1.1 Introduction

1.1.1 Hepatocellular carcinoma

Hepatocellular carcinoma (HCC), a cancer of the liver, is a deadly disease with no ultimate cure at the present time; In fact, its mortality rate is the third among all cancer types[(1)]. Surgical resection and transplantation currently represent the best options for HCC patients; however, the majority of the patients cannot undergo surgery due to impaired liver function, location of the tumor, or lack of donor resources. HCC is more prevalent in the Asia Pacific region, where 58% of the liver cancers, often in those infected with Hepatitis B Virus (HBV), are diagnosed in China[(2)]. In Western countries, the Hepatitis C Virus (HCV) is the major virus driving HCC carcinogenesis[(3)]. Over the years, there have been enormous improvements in our understanding regarding the etiology, progression, and ultimately, the treatment of the disease. Local-regional therapies, including ablation, embolization, and radioembolization, have shown an improved success rate and are used more widely in clinics. One of the problems of treating HCC is the lack of proper guidance, as each treatment is limited by several factors, including the tumor characteristics, stage of progression, liver function, and patient ethnicity. The newly available HongKong liver staging system is rising in popularity as the most accurate guidance for medical oncologists[(4)], but the

comprehensive algorithm needs to be improved. Similarly, posttreatment remains a challenge, with a high recurrence rate existing among patients receiving all forms of treatment. In most cases, HCC patients will undergo a series of treatments unless they are still in the very early stages of the disease. HCC also presents multiple barriers for effective drug delivery. Few drugs will enter directly into the tumor but instead into "healthy" hepatocytes, potentially making the already compromised liver even "sicker" and less likely to be operable or able to receive future treatments. As a result, there is less enthusiasm towards using systemic chemotherapy as first-line treatment, but often as an essential adjuvant therapy for liver cancers unless no other options are available. Also, since many of the patients cannot undergo surgery or liver transplant, the local-regional therapies have become more widely used as potential cures for certain liver tumors. The local-regional therapies also provide a bridge to later-stage liver cancers, so that patients can be treated with more advanced/curable techniques.

1.1.2 Current status of thermally targeted drug delivery carriers

The concept of chemotherapy was pioneered by Paul Ehrlich and later developed into the concept of a 'magic bullet' to kill specific targets inside cells. Over the years, the ideal concept has been challenged by the fact that this 'bullet' needs to be highly specific to tumor tissues and survive long enough in the blood circulation to reach its intended target. Clearly, this is not the case with any cancer types. In an effort to increase overall drug delivery and avoid systemic toxicity, macromolecular drug carriers have been used to ferry high concentrations of antineoplastic agents, with some success in the clinic. However, the high molecular weight of those carriers has not been sufficient to solve all the carrier issues, since there exist multiple barriers to efficient delivery of drugs to tumor

(Table 1.1). As a result, more advanced systems have been developed to further increase the specificity, biocompatibility, and translatability of cancer drug treatments. Among those systems, stimuli-responsive drug carriers are gaining more interest among researchers due to their ability to achieve controlled drug release, localized therapeutic effects, as well as reduced systemic toxicity. Elastin-like polypeptides (ELPs) are the leaders in the nonchemical biomaterials and boast unique phase transition behaviors[(5)]. ELP-based biopolymers provide modularity in sequence design, precise control of molecular weight, low polydispersity, and efficient purification with high yields suitable for industrial scale-up. In addition, ELP-based biopolymers provide the common advantages of water soluble, biodegradable polymers, whereas hydrophobic drugs must either be physically capsulated or chemically conjugated to achieve high loading. Similar to other macromolecular drug carriers, ELPs have been shown to evade renal filtration via the glomeruli, resulting in longer circulation time so that more drug can be delivered to the site of disease[(6)]. Most importantly, the aggregation of ELP-based biopolymers during hyperthermia can provide additional active targeting as well as an enhanced permeability and retention (EPR) effect. Despite these advantages, however, developing clinical applications for these thermally responsive therapeutics remains a challenge due to toxicity issues and overall low tumor drug delivery. Thus, a new carrier is needed that can enhance the cytotoxic effects of thermal ablation with low systemic toxicity and the postablation killing of remaining tumor cells at the ablated margins.

1.1.3 Thermal ablation and heat shock pathway

Thermal ablation is the most widely used local-regional therapy for HCC[(7)]. It has been widely adopted as the major treatment option for unresectable HCCs and is even an

Table 1.1 Barriers for drug delivery to tumors (modified from ref ([2])).

Chemical barriers	Biological barriers	Physical barriers	Clinical barriers
Low solubility	Renal filtration	Vascular endothelium	Low efficacy
Low stability	Hepatic degradation	Perivascular space	Side effects and toxicity
Low molecular weight	Tumor cell heterogeniety	Tumor stroma	Need for hospitalization
Large volume of distribution	High tumor cell density	Cellular membrane	Frequent administration
Charge interactions	High interstitial fluid pressure	Nuclear membrane	Low cost-effectiveness
	Drug efflux pumps		Little guidance on dosing regimen

equivalent choice for operable patients. However, the major problem of this treatment is the high tumor recurrence rate suffered in all ablation modalities. This is, by and large, due to the fact that not all cells are exposed to high temperature for a sufficient amount of time, and as a result, cells can rescue themselves from protein degradation and DNA damage in order to prevent apoptosis or necrosis[8]. To ensure survival under thermal stress, cancer cells induce heat shock proteins (HSPs) to refold and stabilize aggregated or misfolded proteins to bring them back to their normal condition[9]. Thus, the overexpression of heat shock proteins attenuates the thermal injury by ablation and triggers a network of cellular pathways critical for cell survival[10]. Two major observations support this assumption. First, a sublethal heating rim (periphery of the coagulation zone) does exist in all ablation modalities. The stressed but still living cells at the ablated tumor margins can trigger upregulation of HSPs by 2-4-fold. Second, HSPs are found to chaperone over 200 cancer-related proteins, including Akt, mTOR, mutant P53, etc.[11]. Therefore, abrogation of those stressed tumor cells through targeted, sustained release of heat shock inhibitors is essential, and can be realized through a thermally responsive drug carrier that ferries high concentrations of drugs to the hyperthermic tumor sites **(Figure 1.1)**. The double abrogations of tumor cells by heat shock protein inhibition and thermal ablation can therefore have augmented anticancer efficacy and prevent future tumor recurrence.

1.2 Specific aims

To achieve the aforementioned anticancer effect and effective inhibition of heat shock proteins, a thermo-responsive polymer conjugate needs to be designed, engineered, and

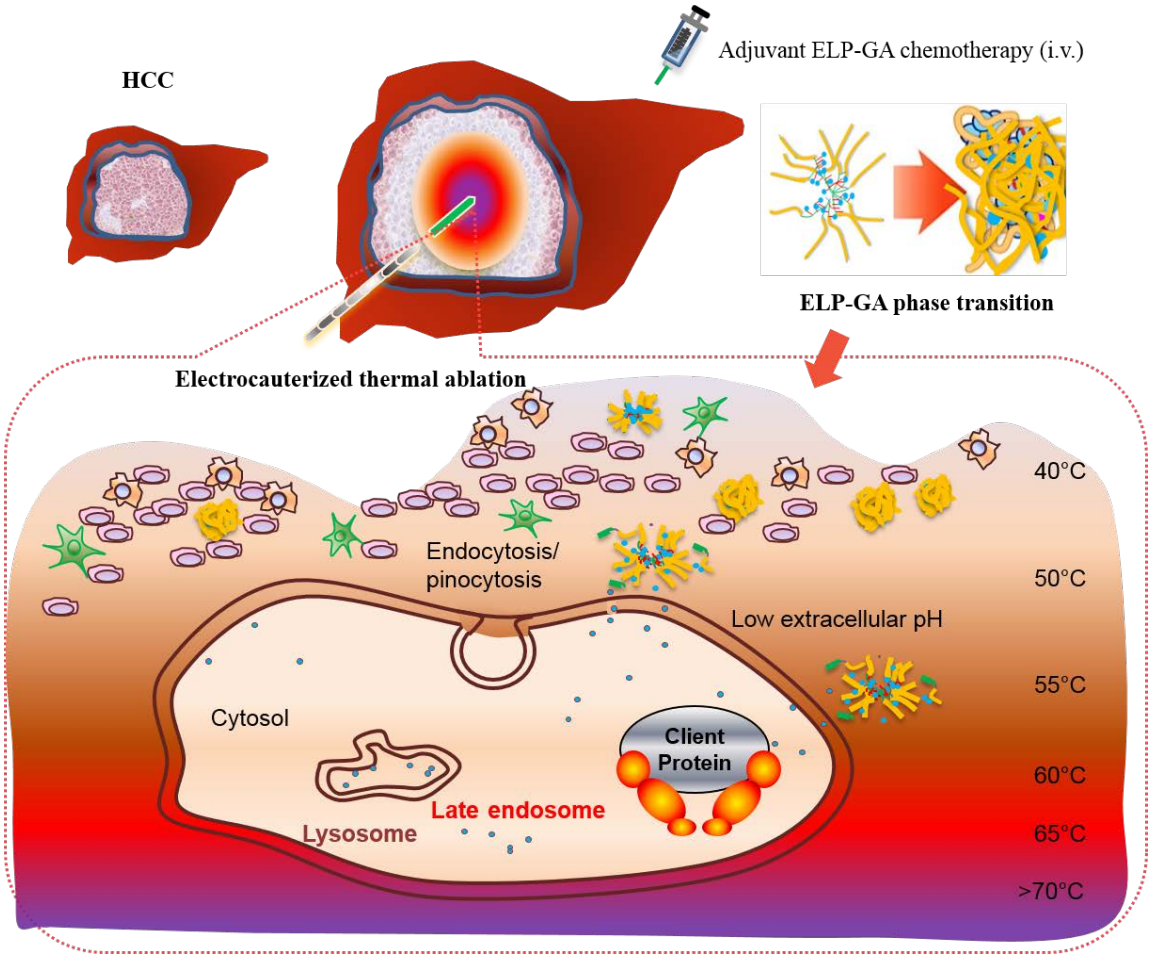

Figure 1.1. Rationale of double targeting of tumors by focal thermal ablation at the tumor core and heat shock inhibition at the ablated tumor margins.

evaluated with a clinically relevant thermal ablation device in HCC tumors. This hypothesis was tested by the following specific aims:

1. Constructing and characterizing multifunctional biopolymer-geldanamycin (GA) conjugates for thermo-targeted drug delivery.
2. Evaluating cytotoxicity and HSP90 expression in HCC cancer cells treated by biopolymer-GA and hyperthermia.
3. Preventing macroscopic tumor recurrence with systemic administration of multi-targeted biopolymer-GA and thermal ablation (electrocautery).

1.3 Scope and organization

Chapter 2 provides the necessary background on polymer therapeutics and conjugates, with an emphasis on thermally responsive biopolymers. Discussion of the challenges to their clinical utilization in anticancer therapies is also provided. A detailed background on thermal ablation, hyperthermia, and their influences on the tumor microenvironment is presented, along with the role of HSPs in the combination therapy. Specifically, the role of HSP90 and its implications in the treatment of HCC will be extensively reviewed. The local thermal ablation modality used in this study was delivered though electrocautery. Therefore, a brief discussion of this technique is also included with other thermal modalities commonly used in the clinic. In Chapter 3, a detailed description of first-generation, diblock ELP-based biopolymers and GA conjugates is presented. Diblock copolymers and conjugates with acute thermal responsiveness to hyperthermia and high drug conjugation ratios have been successfully achieved. A preliminary study in rabbits showed that ELP-based polymers are biocompatible and exert palliative effects on end-stage cancer in animals. The relatively low thermal transition temperature poses a

potential risk for lung embolisms; therefore, a new polymer with a higher transition temperature was constructed and is described in Chapter 4. Detailed characterizations were provided in Appendix A. A novel cloning strategy was introduced to make a new ELP library to decrease hydrophobicity of the whole polymer. The *in vitro* cytotoxicity and ability to inhibit heat shock proteins were then evaluated. The synergy between hyperthermia and the thermo-responsiveness of ELP-GA conjugates was studied, both *in vitro* and in a tumor-bearing mice model. The *in vivo* tumor accumulation and biodistribution of ELP-based biopolymers were investigated in Chapter 5. Additional rabbit study was provided in Appendix B. Finally, Chapter 6 summarizes the major findings, clinical implications, study limitations, and suggested future directions.

1.4 References

1. Singh S, Singh PP, Roberts LR, Sanchez W. Chemopreventive strategies in hepatocellular carcinoma. Nat Rev Gastroenterol Hepatol 2014;11:45-54.

2. Lammers T. Improving the efficacy of combined modality anticancer therapy using HPMA copolymer-based nanomedicine formulations. Adv Drug Deliv Rev 2010;62:203-30.

3. Seeff LB, Hoofnagle JH. Epidemiology of hepatocellular carcinoma in areas of low hepatitis B and hepatitis C endemicity. Oncogene 2006;25:3771-7.

4. Yau T, Tang VY, Yao TJ, Fan ST, Lo CM, Poon RT. Development of Hong Kong liver cancer staging system with treatment stratification for patients with hepatocellular carcinoma. Gastroenterology 2014;146:1691-700.

5. Meyer DE, Chilkoti A. Genetically encoded synthesis of protein-based polymers with precisely specified molecular weight and sequence by recursive directional ligation: examples from the elastin-like polypeptide system. Biomacromolecules 2002;3:357-67.

6. Liu W, Dreher MR, Chow DC, Zalutsky MR, Chilkoti A. Tracking the in vivo fate of recombinant polypeptides by isotopic labeling. J Control Release 2006;114:184-92.

7. Maluccio M, Covey A. Recent progress in understanding, diagnosing, and treating hepatocellular carcinoma. CA Cancer J Clin 2012;62:394-9.

8. Lepock JR. How do cells respond to their thermal environment? Int J Hyperthermia 2005;21:681-7.

9. Ciocca DR, Calderwood SK. Heat shock proteins in cancer: diagnostic, prognostic, predictive, and treatment implications. Cell Stress Chaperone 2005;10:86-103.

10. Hanahan D, Weinberg RA. Hallmarks of cancer: the next generation. Cell 2011;144:646-74.

11. da Silva VC, Ramos CH. The network interaction of the human cytosolic 90 kDa heat shock protein Hsp90: A target for cancer therapeutics. J Proteomics 2012;75:2790-802.

CHAPTER 2

LITERATURE BACKGROUND

2.1 Introduction

The first-ever cancer case in the world is still unknown, yet starting a long time ago, ancient Greek and Roman physicians have utilized heat to treat breast masses. Since the heart and circulation mystery was resolved, cancer treatment has started to advance as doctors used surgery to remove “movable” tumor tissues[(1)] . Over the years, various treatment options have developed for cancer, including surgery, chemotherapy, immunotherapy, targeted therapy, and various other adjuvant therapies. However, the number of cancer patients far outgrows the number of available treatments each year and the challenging health burden is shared among all types of countries for all walks of life. The reason for a person to grow a tumor remains a mystery, which may be related to exposure to carcinogens, family history or acquired genetic mutation, unhealthy life style, and chronic mental issues. Contrary to many other diseases, the understanding of the carcinogenesis remains limited; therefore, the multidisciplinary cancer teams are never sure if they can cure or even control the progress of the disease. As a result, cancer treatment becomes a chronic battle where patients suffer from long-term exposure to chemotherapy, systemic toxicity, and associated pain, not to mention other economic and mental burdens. About 15 million new cases occur each year and the number is projected to be 21.4 million in 2030[(2)]. The cost and market associated with the US alone will be as

high as 35 billion dollars by 2018[3].

As people are eagerly obtaining knowledge about cancer, there has been increasing awareness to avoid chronic treatment which is very likely to prevent us from getting the curative treatment. It is a frustration for patients, medical professionals, and health care agents to suffer repeated, long-term treatments with little benefit. Therefore, there is a critical need to develop controlled drug delivery to maximize therapeutic effect and minimize toxicity. Over the years, we have learned the “brutal” fact that cancer cells can renew, acquire drug resistance, and evade immune surveillance. Chances for a single therapy as the ultimate cure are infinitely small. Hence, it is quite convincing to use combination therapy to synergistically increase the therapeutic benefit. In a routine clinical setting, combination therapy with established treatments either concomitantly or sequentially is widely adopted. However, it is quite challenging to design the type and use of combination. When it comes to chemotherapy, combination chemotherapy usually involves two or more drugs with different mechanisms administered in a certain sequence to the patients. This approach has achieved remarkable breakthroughs in pediatric leukemia treatment with less side effects and drug resistance[4]. However, even when no drug-drug interactions are present, the success of the combination approach still depends on the delivery of the active agents to the tumor site. In this chapter, we introduce a combination therapy for hepatocellular carcinoma (HCC), a lethal cancer type with high recurrence rates among major treatments. As a result, HCC patients usually have to go back to the doctors again with more aggressive treatments. Thermal ablation is widely used in HCC patients yet incomplete ablation frequently results in tumor recurrence, followed with chronic treatments. As an effort to increase the efficacy of ablation as well

as to prevent recurrence, we introduce targeted drug delivery systems to offer high concentrations of drugs specifically in the ablated tumor tissues to achieve more complete tumor abrogation.

In this chapter, a detailed discussion of the disease—HCC— will be provided with the emphasis on tumor recurrence, which provides the rational of designing a targeted drug delivery system using biocompatible, thermo-responsive, elastin-like peptide (ELP)-based biopolymers. The use of polymeric drug conjugates will also be reviewed, along with the discussion of limitations and challenges of those systems. Since the combination therapy involves thermal ablation and hyperthermia, review about the current clinical techniques, tissue responses, and heat-drug interaction will be presented, with the central emphasis on heat shock response. In particular, the function of heat shock protein 90 (HSP90) and its role in cancer will be discussed.

2.2. Hepatocellular carcinoma (HCC)

2.2.1 HCC statistics, diagnosis, prognosis

Hepatocellular Carcinoma (HCC) is currently the third leading cause of cancer-related deaths[(5)]. It accounts for about 80% of all cases of liver cancer. Globally, three-quarters of a million new cases are reported every year. The death rate, which nearly equals the incidence rate, continues to rise[(6)]. Major risk factors include infection by hepatitis B/C viruses (HBV/HCV), mutagen exposure such as aflatoxin B (AFB), and metabolic abnormality, including obesity, diabetes, fatty liver disease, and/or nonalcoholic steatohepatitis (NASH)[(7)] . Among those factors, chronic HBV patients have 100 times higher risk of HCC than noncarriers[(8)], although the exact molecular mechanism is not fully understood. Liver toxic compounds—such as alfatoxin B1 (AFB1), heavy alcohol,

and oral contraceptives—are found to be contributing factors[9]. Due to the lack of diagnosis of HCV during the 1940s through the 1960s, HCC cases driven by HCV infection rapidly increased, even in developed countries[10]. The economic burden of HCC becomes enormous, costing up to an estimated 455 million dollars annually in the US alone[11].

Currently, HCC is diagnosed by analyzing serum α-fetoprotein (AFP) levels and utilizing liver imaging with ultrasounds or CT/PET/MRI. AFP level, however, remains highly variable among different patients as well as at different stages of HCC. AFP concentration has also been shown to be similar between patients bearing HCC or those just having cirrhosis or hepatitis[12]. Changes in AFP level over the course of treatment[13] have allowed doctors to detect early HCC recurrence. Recently, Huang *et al.* screened the tissues of 50 HCC patients, and found that two metabolites, betaine and propionylcarnitine, serve as a combination tool to differentiate HCC from nonmalignant liver disease[12] . Still, very limited biomarkers are available for diagnosis and prognosis of HCC. In fact, imaging currently provides the only way to diagnose HCC through typing/staging, and standardization has not yet been established in imaging, resulting in significant mistyping and misstaging[14]. The assessment of tumor aggressiveness is also limited. Edmondson-Steiner's grading system, which is not applied internationally, is the only recognized system for tumor morphological grading due to the low sensitivity of imaging methods[15]. To address these limitations, new biomarkers and molecular prognostic parameters are being developed and evaluated in various clinical trials, including the application of des-y-carboxyprothrombin (DCP) in combination with AFP subfraction L3 (AFP-L3) as biomarkers to evaluate the efficacy of transarterial

chemoembolization (TACE)(#NCT01360255). Nautel *et al.* developed a robust microarray system that tracks 5 gene signatures to predict the clinical outcome of patients who have undergone curative resection[16]. Another strategy is to identify gatekeeper pathways at each specific tumor stage in order to guide chemoprevention. More effort is required to develop an accurate, reproducible, and clinically-relevant prognostic algorithm that better manages this challenging cancer type.

One major obstacle for prognosis of HCC is the high recurrence suffered by almost all treatment options. In fact, patient survival gets worse as a result of recurrent HCCs[17], which are often metachronous and multicentric in nature[18]. As a result, there is a critical need to prevent tumor recurrence through comprehensive understanding of the biology and targeted intervention at early stages of the treatment.

2.2.2 Pathophysiology of HCC and recurrent HCC

The exact mechanism for hepatic carcinogenesis is still poorly understood. It has been suggested that gradual accumulation of genetic mutation and malignant cell transformation finally results in the formation of single or multiple lesions[19], which are often associated with liver cirrhosis. 80% of HCC patients are carriers of hepatitis viruses[20], which induce growth factors that promote abnormal hepatocyte proliferation. HCV infection, in particular, activates tumor growth factor alpha (TGF-α) and NF-κB, which contribute to the formation of cirrhosis[21]. At the genetic level, HCV disrupts the signaling pathways for tumor suppression via p53 inactivation[22]. HBV, on the other hand, activates the promoters for various oncogenes, causing DNA rearrangement, chromosomal damage, and elevated oxidative damage harmful to genomic stability[23]. In addition to p53, multiple genes are related to carcinogenesis, such as PTEN[24] and

TERT[25]. Increased telomerase activity is found in more than 80% of HCC tumors with shortened telomere length[25, 26], which is commonly observed in many cancer types. More importantly, a positive correlation has been found between telomerase retroviridase and recurrence of HCC post transplantation[27].

HCC has a strong tendency to spread via the portal venous system. Recurrence can result from *de novo* carcinogenesis or intrahepatic dissemination of the primary tumor[28]. In addition to aggressive vascular invasion, high expression of osteopontin[29-31] and transforming growth factor-β (TGF-β) are clinically associated with the postoperative recurrence of HCC[31].

2.2.3 Hepatic tumor microenvironment

Due to the complex nature of HCC, a comprehensive understanding of the tumor microenvironment is essential to design effective intervention strategies that block tumor recurrence. In this chapter, the physical environment, cellular-molecular components, and hepatic tumor margins will be discussed.

2.2.3.1 Physical environment

2.2.3.1.1 Tumor vasculature. Dominant proangiogenic factors, like the vascular endothelial growth factor (VEGF), are actively involved in the vascularization of HCCs. Other growth factors—such as platelet-derived growth factor (PDGF), fibroblast growth factor (FGF), and epidermal growth factor (EGF)—also play supporting roles in tumor angiogenesis. Similar to many other tumor types, HCC features a leaky vasculature due to deficiency in pericytes and perivascular cells. The leakiness of the vasculatures provide chances of vascular invasion, as seen in 88% of the patients who experience

recurrence after transplantation[32].

2.2.3.1.2 Hypoxia. Another common physical features of tumor microenvironment is the deficiency of oxygen level, which leads to genomic instability, irreversible DNA damage, and induction of prooncogenes[33]. The invasion and expansion of the tumor increases the glycolytic rate, causing the microenvironment to be even more hypoxic. As a response to this environment, hypoxia-induced factor-1 (HIF-1) is often induced, which further enhances glycolysis[34] to support tumor growth, represses genes to prevent DNA repair[35], induces expression of growth factors, and promotes angiogenesis for vascular invasion[36].

2.2.3.2 Cellular and molecular components

It has been well recognized that multiple cell types are involved in hepatic tumor lesions, which makes HCC an excellent model to understand tumor microenvironment. The major players are cancer-associated fibroblasts (CAFs), endothelial cells, hepatic stellate cells, tumor-associated macrophages (TAMs), and cancer stem cells. CAFs are widely involved in HCC progression and invasion since they produce a variety of growth factors[37]. TAMs, a group of highly polarized cells, which act as either cleaners (M1) or food callers (M2), secret numerous cytokines to support tumor progression[38]. Similar to other tumor types, endothelial cells play an important role in feeding the tumor by creating tumor vasculature. These cells express a variety of receptors involved in angiogenesis, such as VEGR, EGFR, and PDGFR. In addition, it has also been found that CD1-5^{+} HCC endothelial cells contribute to resistance to chemotherapy[39]. It has been noticed that bulk tumor cells diversely interact with tumor stroma, which recruit tumor cells to meet at the margins and prepare them for neoplastic growth[40].

Hepatic cancer stem cells (HCSCs) have the same characteristics as cancer stem cells: self-renewal, differentiation, tumorigenecity, and radio-chemo resistance[41-43]. Similar to CSCs in many other solid tumors, HCSCs are heterogeneous with vast difference in cell markers expression due to diverse cellular origins. Multiple cell markers such as EpCAM[44], CD44[45], CD133[46], and CD24[47] have been found to be overexpressed on the cell surface. However, medical professionals should be cautious about using each of them as the only marker to distinguish stem cells.

Multiple signaling pathways are involved in malignant hepatocytes' formation from normal stem cells, including Wnt[48, 49], Notch[50], sonic hedgehog[51], STAT3[52, 53], AKT[54], and TGF-β[55]. The modulation and cooperation among each pathway ensure normal liver growth. However, due to limited understanding about how stem cells develop into differentiated hepatocytes, the exact mechanism of their malignant transition to liver cancer cells remains to be elucidated. Over the years, it has been suggested that TGF-β played dual functions of tumor suppression and promotion of stem cell transition to malignant tumor cells[55]. Although further studies are warranted, impaired TGF-β signaling pathway may serve as a marker to distinguish normal stem cells from cancer stem cells[56].

HCSCs have been shown to be involved in HCC invasion, metastasis, and recurrence. Therefore, profiling cell markers' expression—combined with other diagnostic markers, such as AFP levels—can improve diagnosis and prognosis of this lethal disease. Further understanding of the biology of hepatic stem cells is also warranted in order to develop targeted therapies without harming normal stem cells and hepatocytes.

2.2.3.3 Signaling pathways

Various signaling pathways are deregulated in human HCC. The major families include growth factors [e.g., insulin-like growth factor (IGF), EGF, FGF, hepatocyte growth factor (HGF), VEGF, and platelet-derived growth factor (PDGF)] and signaling pathways that are involved in liver development, such as AKT/mTOR, WNT/β-Catenin, Notch and Hedgehog, and TGF-β (details in stem cell session).

Four main strategies have been used to block the signaling pathways critical for tumor progression and metastasis: (i) Block the expression and production via RNA interference or small molecular inhibitors, which is the major strategy used in this dissertation; (ii) Suppress the activity by neutralizing antibodies; (iii) Competitively bind soluble receptors to disrupt the natural interaction of protein with its receptor; and (iv) Inhibit receptor signaling using small molecules, such as tyrosine kinase inhibitors (TKI)[57].

2.2.4 Treatment options

Since HCC is such a complex disease, it has been a daunting task for clinicians to determine an optimal treatment for individual patients. Without a standard staging system in hand, proper evaluation of the potential response to a specific treatment is problematic. Liver function (Child-Pugh grading system), tumor pathology, prognostic variables (size, tumor numbers, locations, vascular invasion, etc.) all need to be taken into consideration. However, no current staging systems—including the Barcelona-Clinic Liver (BLCL) cancer staging system and the Cancer of the Liver Italian Program (CLIP) classification—has been able to fulfill all the requirements. A guideline for treatment decision needs to be optimized continuously to incorporate all possible variables. One of the important features shared by all treatment options is that tumor recurrence, especially

for 5-year recurrence, has been high which is the major reason for patient death. A summary of recurrence rate among major treatments is listed in **Table 2.1** and a brief introduction of major therapies is discussed below.

2.2.4.1 Liver transplantation and resection

Liver transplantation (LT) possibly achieves the ultimate cure for patients with severely impaired liver function. The carefully selected (based on Milan criteria) patients who undergo LT are able to get 5-year survival > 70% and < 10% recurrence[58]. However, LT is not feasible for patients who show multiple modules of tumors and/or show tumors of more than 3 cm in any dimension. In particular, patients with a single tumor that is > 5 cm are not recommended for LT. Some of the major problems with LT include the sacristy of donor and potential immune rejection. Since the waiting time is often unpredictable, drop-out rates are high and patients usually experience vascular invasion before LT, which can drive recurrence up to 20%[59]. Curative resection is not feasible for > 80% of HCC patients, who usually also suffer from severe cirrhosis and fibrosis. Moreover, even after "thorough" resection, the 1-year recurrence rate has increased to about 25%, thus calling for a more vigorous postsurgery surveillance and intervention. Although surgical resection requires low hepatic venous pressure gradient and patients have high level reserve of liver function, the recurrence rate rises to 50% in 5 years, and the 10-year actual survival rate is as low as 7.2%[60]. Currently, no adjuvant therapies have clinically been proven to reduce post-resection recurrence[61].

Table 2.1 Recurrence rate of HCC after treatment.

Treatment	5-Year Recurrence Rate (%)	Ref
Surgical resection	14-51	(62-64)
Liver transplantation	5-39	(65)
Radiofrequency ablation	26-84	(66)
Microwave ablation	31-65	(67, 68)
Cryoablation	31-55	(69)
High intensity focused ultrasound	15-58	(70, 71)
Transcatheter arterial chemoembolization	5-79	(72, 73)

2.2.4.2 Catheter-based therapies

The hepatic artery is the major nutrient supplier for HCC. Therefore, this unique route has been exploited to deliver a large dose of drug to the tumor bed. Over the past three decades, various embolization technologies have been developed to administer therapeutic agents through a catheter placed in the patient's artery. The most developed technologies to date include transarterial chemoembolization (TACE), chemoembolization with drug eluting beads (DEB), bland embolization, and Yttium-90-based radioembolization. However, there have been no randomized trials suggesting the superiority of embolization to other surgical treatments. Moreover, the off-target effect can devastate the lungs and gastrointestinal tract. Without portal vein involvement, radioembolization achieves a paltry 25-50% response rate[(74)].

2.2.4.3 Ablation

Ablation is one of the most used local-regional treatment strategies in clinic practice. Depending on the type of energy used for ablation, tumor cells can be destroyed by chemicals (percutaneous ethanol injection), extreme temperatures (thermal ablation or cryoablation), irreversible electroporation (IE), and high intensity focused ultrasound (HIFU). Among all the ablation methods, thermal ablation has been performed most widely on nonresectable HCC patients. Generally, doctors perform radiofrequency ablation (RFA) on tumors less than 3 cm and microwave ablation (MWA) for larger tumors (>5 cm). HCC is an ideal target for ablation due to the "oven effect", which can be exploited to enhance ablation efficiency since the liver tumor is surrounded by a fibrosis region where the heat is insulated. Ablation also helps to diffuse drug into the relatively soft tumor tissues while keeping them away from the cirrhotic liver. RFA is the

most widely used ablation method for early stage or small tumors less than 3 cm[75, 76]. RFA offers flexibility on tumor locations other than subcapsular or those close to gall bladder and major vessels. Recent finding suggests that RFA exhibits equivalent efficacy surgery on resectable patients. However, the heat sink effect, which is caused by the blood vessel adjacent to the ablation tip, attenuates the heat killing effect and remains a major risk factor of recurrence for all thermal ablation modalities. In addition, the difficulty in ablating all tumor cells, particularly in the tumor (ablated) margins, is not overcome. Those untreated and stressed tumor cells trigger induction of heat shock proteins (HSPs), which help tumor cells to survive and further proliferate.

2.2.4.4 Chemotherapy

Chemotherapy is often used among more advanced stage of HCC patients. Due to their already-damaged liver conditions, the efficacies of chemotherapies are limited since patients may not be able to finish the entire treatments. Common systemic therapies are summarized in **Table 2.2.** To date, the only FDA-approved targeted chemotherapy, Sorafenib, a multikinase inhibitor, has been widely used in the clinic. Yet, phase II and phase III trials suggest only a 3-month advantage over the control group due to early termination of the study[77]. Treatment by Sorafenib has also been linked to slow wound healing, hypertension, diarrhea, and proteinuria[78]. A loss of efficacy with time has been also observed in 20-38% patients[79]. Various other kinase inhibitors, with similar molecular mechanisms that target growth factor signaling pathways, are in clinical trials[10, 80]. These include Erlotinib for EGFR and brivanib for VEGFR/FGFR. Numerous clinical trials have combined Sorafenib with other treatment such as radioembolization , TACE, and ablation[81]. Although the enthusiasm became lukewarm after the initial

Table 2.2. Approved nanomedicines used in HCC patients[82].

Chemotherapy	Mechanisms of action
Doxorubicin and mitoxantrone	Topoisomerase II inhibition and free
5-Fluorouracil	Thymidylate synthase inhibitor
Gemcitabine, irinotecan, and thalidomide	DNA synthesis inhibitor
Cisplatin-based	Alkylating agents
Sorafenib	Multikinase inhibitor
Sunitinib and Bevacizumab	VEGF inhibitor
Erlotinib, Cetuximab	EGFR inhibitor
Tamoxifen, megestrol, octreotide,	Hormones(estrogen receptor) antagonist

clinical trial, combination with other treatment has shown a better efficacy profile since the patients stay on the chemo long enough to get the desired benefit. These clinical observations also suggest great potential of using combination treatment for HCC.

2.2.4.5 Other therapies

Two rising radiation therapies including stereotactic body radiation therapy (SBRT) or stereotactic ablative radiotherapy (SABR) can precisely deliver high-dose radiation in tumor fractions resulting in low toxicities[83, 84]. More information and data are needed, however, to achieve selection criteria. Immunotherapy based on oncolytic viral agents and vaccines has been tried in HCC since their great success in treating liquid cancers[85]. However, the heterogeneity in HCC caused by various etiologic factors still pose great obstacles for efficacy[86]. Another new approach is “miRNA replacement therapy” in which the downregulated miRNAs expressing tumor suppressors are delivered. Two miRNAs, miR-26a and miR-34a, have shown preliminary efficacy in HCC xenograft models[87, 88].

2.2.4.6 Combination therapies

In order to address the limitation of single treatment/ modality, several combinations have been tried in the clinics to achieve augmented anticancer effect. Particularly, RFA was performed with coadministration of TACE and the tumor progression rate showed to be reduced from 39% to 6%[89]. One recent study combining RFA, TACE, and sorafenib has shown overall survival benefit from 12.8 to 39.6 months[90]. However, high dose of sorafenib resulted in thrombosis in one third of the patients and clear guidance on a dosing regimen is missing. To rationally improve the benefit of combination therapy,

both the initial treatment and postsurveillance needs to be put at equal weight for HCC. The understanding of the molecular events related to recurrence will significantly help to design targeted adjuvant therapies to achieve a better clinical outcome.

2.2.5 Hepatic tumor margins

The recurrence rate has been high for HCC since the difficulty in defining a safe margin for both surgical resection[91, 92] and thermal ablation[93, 94]. Practically, in order to avoid liver injuries, surgeons have to leave a certain thickness of margins; however, it was suggested that the thinness of the margins does not correlate with the overall patient outcomes. Similarly, no ablation device has been efficient enough to ablate each individual cell in the liver tumor microenvironment. A significant number of tumor cells, either not even reached, or inadequately treated, play a pivotal role to trigger series of cellular and molecular events for survival, progression, and final relapse. It has been recognized that adjuvant intervention needs to be followed up after either of those treatments[90, 95], especially after those treatments that will lower the viral load and inflammatory activities[96]. On the other hand, more complete surgical excision has been tried using a novel probe device— Margin Probe, (Dun medical, Israel), which has been approved for Premarket Approval (PMA) by the FDA in January 2013. The machine differentiates viable tumor cells at the margins based on their unique electrical magnetic properties. It has been shown that with the aid of device, the repetition of open breast surgery was reduced to 50% in clinical trials, and achieved 97% sensitivity for large breast tumors. However, it was not as effective for breast tumors smaller than 0.7mm and is so far limited to breast tumors.

2.2.6 Heat shock proteins (HSPs) in signaling pathways in HCC

HSPs are recognized as key mediators in the hallmarks of cancer[97, 98]. Typically, HSPs are 2-3-fold up-regulated in common cancers[99], specifically up to 7-fold with HCC[100], providing increased molecular chaperoning duties[101]. Moreover, HSPs are induced under thermal stress caused by hyperthermic ablations which lead to thermo-tolerance[102-104]. As previously stated, multiple signaling pathways, including growth factors (VEGF, PEFG, EGF, HGF), phophatidylinositol-3 kinase (PI3K)/AKT[105, 106] WNT/β catenin pathway[107], and RAF/MEK/ERK pathways, are perturbed in HCC [108-112]; many of the signaling proteins are direct clients of HSP90.

HSP90 also interact with cells important in the hepatic tumor microenvironment. Hepatic stellate cells, which are the major armies for liver fibrosis and carcinogenesis[113, 114], can be induced to apoptosis by HSP90 inhibitors[115]. HSP inhibition has also been shown to suppress the unfolded protein response (UPR) as a result of severe hypoxia. Therefore, HSP90 inhibition alone has the multitarget potential to disrupt multiple signaling pathways in HCC. Given timely, the adjuvant HSP chemotherapy can further increase the ablation-induced tissue coagulation and, most importantly, eradicate the thermal stressed, residual viable cells at HCC tumor margins.

2.2.7 HCC model for therapeutic evaluation

2.2.7.1 Murine models

Various agents have been used in mice models due to their similarity to the injury–fibrosis–malignancy cycle in humans. Those agents damage the normal liver proliferation, such as N-nitrosodiethylamine (DEN)[116], AFB[117], and carbon tetrachloride(CCl4)[118]. The major disadvantages of those models are waiting time since most of the tumors, even

with high success rate, take 1-2 years to form[119]. The reproducibility is also a key issue due to requirement of skillful surgical techniques. AFB and CCl4 have also been injected to rats but the success rate (~30%) was not comparable to mice models. Choline-deficient diet (CDD) has also been used to induce HCC in mice and rats which triggered the fibrosis or cirrhosis crucial for hepatocellular carcinogenesis[120]. Other agents such as hepatoxin thioacetamide (TAA) can induce tumor formation via elevated oxidative stress, but again, it can take as long as 10-15 weeks[121].

2.2.7.2 Transgenic mice model

Transgenic models have been used to understand the carcinogenesis, metastasis, and multidrug resistance of HCC. Since most of the oncogenes have been mutated to various degrees in HCC patients, special cell lines have been developed in mice such as PLC/PRF/5 (p53-mutant, KRas-mutant, and B-Raf-wild type)[122] cell lines. Another cell line having inactivated Rb and p53 genes with dual activation of c-myc-TGF-α and c-myc-E2F1 pathways formed liver cancer in as fast as 8 months, versus 20 months for normal mice[123, 124]. These models suggest the key roles of deregulated tumor suppression genes for HCC development. Other types of special HCC models include nude mice bearing xenograft of metastatic human HCC LCI-D20 and metastatic human HCC cell line MHCC9 [125, 126]. These models provided understanding of the molecular biology of tumor metastasis[127]. With a similar goal to test the role of certain genes in HCC, Shouval *et al.* developed cancer cells overexpressing multidrug resistance gene (MDR 1) grown as intrahepatic xenografts in immunocompromised (SCID) mice. This type of tumor serves as a good model to study acquired drug resistance which commonly developed shortly after chemotherapy[128].

2.2.7.3 Xenograft mouse models

Xenograft models are most widely used in laboratory routines due to fast tumor growth. Human HCC cells are injected into immuno-deficient mice (Athymic nude mice or SCID mice[129]). There are two major categories for xenograft models: i. Ectopic model where the tumor cells are injected subcutaneously in the mice flank; ii. Orthotopic model where the tumor cells are injected directly into the liver. This model has high fidelity to the actual environment in liver, where a portal system and drug-detoxifying enzymes exist. The organ environment has profound effects on the response of tumor cells to chemotherapy. Studies have shown that response to chemotherapeutic agents varies depending on whether the tumor was ectopic or orthotopic[125]. The pay-off of the xenograft model is their poor correlation to human tumor progression, but they can be used to evaluate drug efficacy specifically to the models tested. The interaction of the mice tumor with its surrounding tissue is unlikely to be the same as the tumor-stroma interaction in human. However, economically, the flank tumor model remains the most widely used in the laboratory setting. The efficacy of various agents can be tested in those efficient models. Routine cell lines such as human HepG2/ Hep 3B have been frequently transplanted into nude mice, including athymic nude mice, B6C3F1 mice[130], CB-17/SCID mice[131], and BALB/c mice[132].

2.2.7.4 VX2 rabbit model

One of the most used animal models for HCC study is the VX2 rabbit model. In 1933, Shope and Hurst first found a particular virus which can induce papillomas in the skin of domestic rabbits[133]. Three years later, Kidd *et al.* reported cutaneous carcinoma through inoculation of this virus for up to 10 months[134]. Since it was the first-ever success in the

history of virus-induced tumor inoculation, it was designated as the ground-breaking “V1” tumor. However, the second trial failed. Later, Kidd was able to maintain a new cell line up to 14 generations and it was successfully transplanted to multiple animals[135]. These transplantable new cells were then called “V2” cells. Since then, the inoculation method has widely adopted by numerous researchers, and the carcinoma is now universally designated as the “VX2 tumor”, which is mostly proliferated in rabbits.

Unlike other mammalian cancer cell lines, culturing VX2 cells in a tissue flask has proven to be a daunting task. Very few successful cases have been reported so far. Glasako *et al.* first commented on the survival of VX2 cells *in vitro* back in 1976[136], followed by Dickson[137] and Easty *et al.*[138]. However, there is no report after 20 years of these publications proving that VX2 can grow and maintain its aggressiveness *in vitro*. Recently, Handel *et al*. reported a new passaging method to ensure subsequent implantation of cultured VX2 cells in rabbit bones[139]. They found that the initial cell density and transplant sites are deciding factors for tumor survival and growth. This might be an encouraging sign for VX2 culture studies; however, the reproducibility remains to be seen.

Due to the trickiness of the VX2 culturing technique, as well as the poor correlation usually seen between *in vitro* and *in vivo* studies, researchers almost universally maintain the cell proliferation through *in vivo* transplantation. Because of their aggressiveness and rapid growth, VX2 tumor cells have been implanted into various organs and tissues, such as liver[140], lung[141], thigh muscle[142], kidney[143], mucosa in the tongue[144], gastrointestinal[145-147] , brain[148, 149], and intraocular[150] among various other types[151-153]. Usually, 1-3 million cells are required to be implanted at the site of interest. Liver and

thigh muscle are among the most frequently injected sites, but the implantation methods are not the same. Single cell suspensions, either fresh made or frozen cell stocks, are used for growing intramuscular tumors. Fresh cell fragments, however, seem to ensure a successful and fast tumor propagation in the liver[154].

One of the most important advantages of VX2 tumors is their fast growth kinetics. A direct comparison of liver tumor models in mice, rats, and rabbits shows the VX2 rabbit model to be most efficient in terms of success rate, tumor growth rate, and animal survival time. Most importantly, the incidence of primary liver tumors has been shown to be directly linked to virus infection caused by HBV/HCV[8]. It is clinically proven that the presence of the virus contributes largely to the onset, progression, and metastasis of liver tumors. Therefore, the virus-derived nature of the VX2 tumor provides the unique advantage of mimicking the biological features of human liver tumors. Indeed, VX2 liver tumors have been mostly widely used as a model to understand and treat primary liver tumors and associated metastases. Another unique advantage of the VX2 tumor is its ability to grow to a large size in a short period of time. We have observed that the VX2 tumor can reach 4 cm in diameter in rabbits without signs of significant distress. Given the fact that human liver tumors often grow as big as 5, or even 7 cm[155], the VX2 tumor can serve as a clinically relevant model to test modalities such as thermal ablation and TACE, etc., which are hard to perform on small animals like mice and rats. However, there have been no reports of genetically modified rabbits that are designed to mimic or understand oncogene-mutated, drug-resistant tumors commonly observed in human patients' specimens.

2.2.7.5 Other HCC models

About 10% of liver tumor models are rat-based. Non-cell-induced carcinogenesis has also been tried in rats[156], which exhibits lower variability and high metastasis potential. Recently, a new tumor derived from Reuber H 35 hepatoma has induced solid tumors in ACI male rats, a rare but rapid tumor model with a doubling time of about 49 h[157]. Most other rat models suffer from slow growth rate and small tumor size similar to those in mice. However, they do have larger vessels which provide technical easiness for therapies like TACE[158].

Woodchuck has been suggested to be a relevant model since tumor generation is related to hepatitis virus (WHV)[159]. Although this virus has the impressive ability to cause liver cancer in all animals[160], working with the host of the virus in general is hard and very little literature is available using woodchuck for a liver tumor model.

Researchers have used zebrafish as a model to understand the molecular basis of carcinogenesis in human livers. The regulation of oncogenes involved in both human and transformed zebrafish liver tumor cells have been identified by efficient RNA analysis. The zebrafish model has the advantage for high throughput screening to identify new targets to develop new drugs for HCC[161, 162].

In this dissertation, we used both the HepG2 ectopic murine model as well as the VX2 rabbit model to evaluate the performance of ELP biopolymer GA conjugates. Most of the study was performed on athymic nude mice due to economic reasons. The pilot study of conjugates on the VX2 tumor is provided in Appendix B.

2.3 Macromolecular drug delivery and polymer-drug conjugates

Macromolecular drug carrier is typically composed of a macromolecule linked to a therapeutic agent. In 1975, Ringsdorf first proposed a rational model to achieve pharmacological effect from the macromolecular drug carriers based on active polymers[(163)]. This Ringsdorf model is widely used in polymeric drug delivery systems today. Briefly, the model consists of three basic components: 1) a solubilizer that can offer hydrophilicity to carry high concentrations of drugs, which usually exhibit poor water solubility; 2) a drug, either covalently attached to the polymer backbone through various linkers, or physically encapsulated into a secondary structure of the polymers; 3) a targeting moiety which provides a pharmacological recognition of the polymer conjugates to reach the desired target of disease. Over the years, pharmaceutical scientists develop, optimize, and expand the model so various advanced models (such as theranostics) have been proposed and reviewed elsewhere[(164)]. A significant effort has been put into anticancer polymer drug conjugates where most chemotherapies are very hydrophobic and the clinical use has been plagued by dose-dependent toxicity and poor bioavailability. Those problems can be partially solved by using polymer conjugates since the water soluble polymers have large capacity to carry a high dose of drugs on one polymer backbone. Second, the drugs attached to the polymer can be engineered to nanoscale with a controlled drug release profile. As a result, the duration and concentration can be custom designed to achieve the desired pharmacological effect. Last but not least, polymer conjugates also offer the opportunity to alter the pharmacokinetics and biodistribution of the drug as poor drug accumulation inside tumor remains a daunting challenge. Less than 1% of the chemotherapy can reach tumor tissues by

systemic injection and the carrier can bring the quantity up to 5-10-fold. However, systemic toxicity remains an issue due to high nonspecific accumulation in vital organs such as liver, kidney, spleen, and lung.

So far, there are very limited polymer conjugates that are on the market, as shown in **Table 2.3**. Most of them are poly(ethylene) glycol (PEG)-based systems. PEG has been regarded as a biocompatible polymer and offers a variety of functionalized derivatives that are commercially available[165]. Precise control of molecular weight, narrow size distribution, and large capacity of scale up has been achieved in the industry[166]. However, like many other polymer therapeutics, degradability and potential risk of long-term accumulation inside the body remains unclear. As a result, there are no specific and clear guidelines from both scientific and regulatory areas on the "ideal" parameters of the polymer conjugates.

2.3.1 Strategies to improve versatility of polymer-drug conjugates

2.3.1.1 Targeting system

Over the past decades, enormous efforts have been made to improve the targetability of polymer conjugates to avoid systemic toxicity and fast clearance. From the drug delivery perspective, there are two major types of targeting: passive targeting and active targeting. The latter gained widespread passion among researchers as it has potential to be the ultimate magic bullet by attaching a specific ligand to the polymer. Bae *et al.*[167] pointed out that although active targeting is ideal due to recognition of the target cells, the heterogeneity of the cancer cells both in a patient and among patient cohorts, the multiple barriers to overcome before reaching the tumor bed, as well as the engineering complexity of the advanced drug delivery systems render the strategy far from being

Table 2.3. Approved macromolecular medicine for cancer treatment [168, 169].

Trade Name	Active Ingredient	Indication	Company	Approval
Abraxane	Albumin protein-bound paclitaxel	Metastatic breast cancer	Celgene	2005
Alimta	Pemetrexed	Nonsquamous NSCLC, malignant pleural mesothelioma	Lilly	2004
DaunoXome	Liposomal daunorubicin citrate	HIV-associated Kaposi's sarcoma	Galen	1996
Depocyt(e)	Liposomal cytosine arabinoside	Lymphomatous meningitis	Pacira	1999
Doxil	Pegylated-stabilized liposomal doxorubicin	AIDS-related Kaposi's sarcoma, refractory ovarian cancer,	Janssen	1995
Eligard	Leuprolide acetate and PLGH polymer	Advanced prostate cancer	Sanofi	2002
Oncaspar	PEG-asparaginase	Acute lymphocytic leukemia	Sigma Tau	1994
Rexin G	Targeting protein tagged phospholipid/micro	Sarcoma, osteosarcoma, pancreatic cancer	Epeius Biotechnology Corp.	Phase III
Ontak	Interleukin-2 diphtheria toxin fusion protein	Cutaneous T-cell lymphoma	Eisai	1999
Thermodox	Heat activated liposomal encapusaltion of doxorubicin	Breast cancer and primary liver cancer	Celsion	2013

mature. Passive targeting, on the other hand, is mainly mediated by EPR effect, which is based on the longevity of the pharmaceutical carrier in the blood and its accumulation in pathological sites with leaky vasculature in tumor[170]. Although there is limited evidence in human cancers, EPR effect has been shown in multiple animal models and higher accumulations inside tumor were achieved by numerous research groups. In addition, various stimuli have been used to further increase the effect of passive targeting by applying heat, light, magnetic field, ultrasound, etc. Those stimuli-responsive systems are found to have the greatest versatility in drug delivery. In this chapter, the temperature-responsive system based on ELP is reviewed in a separate section.

In summary, the unique challenge of the development of polymer conjugates lies in the perfect matching of polymer conjugates that can target a specific medical condition. It is too ideal to find “one size fits all” polymer conjugates that are both effective and safe for all kinds of cancers, and treatment with various other methods is desired. As a result, the clinical translatibility of polymer conjugates can be successful not only from the engineer side, but with a critical understanding of the biological characteristics of the disease which is discussed earlier. From the polymer perspective, most synthetic polymers suffer challenging synthesis, wide poly-dispersity, nondegradability, and resultant toxicity. Although it has been proposed widely that polymers can alter or improve drug accumulation, no pharmacokinetic model has been established for macromolecular drug delivery systems. All these issues remain to be solved.

2.3.1.2 Stimuli triggered drug release

The acid labile linker is stable at physiological pH but hydrolyzes under acidic conditions. Therefore, various linkers **(Figure 2.1)** have been exploited to achieve site-

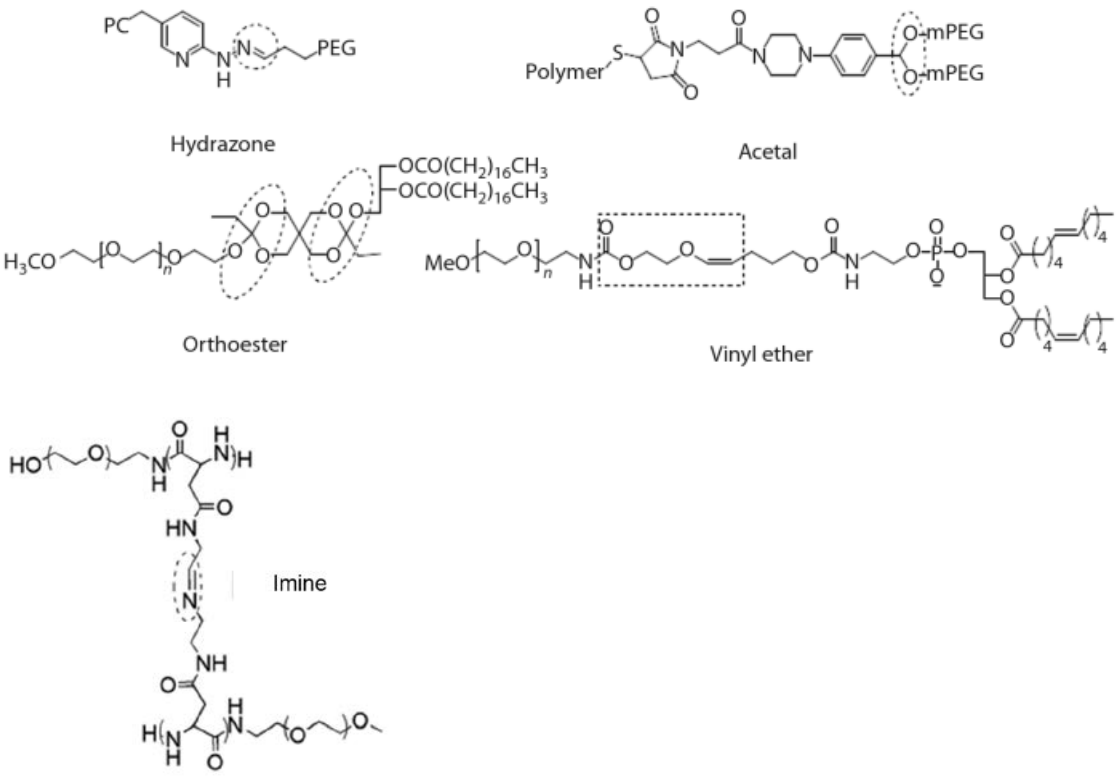

Figure 2.1. Acid labile systems used in macromolecules drug delivery systems.

Modified from reference hydrazone[171, 172], acetal[173], orthoester[174], vinyl ether[175, 176], and imine[177].

specific drug release under two major conditions. First is the slightly acidic tumor microenvironment (pH 6.0-6.5)[178, 179] where both acid labile linkers as well as charge reversal on the whole polymer have been utilized. The other is intracellular low pH cell compartments such as lysosome and late endosomes where pH is below 5.0[180].

2.3.1.3 Polymeric nanoparticles

Drug encapsulating nanoparticles are one of the most widely used polymeric delivery systems due to their desirable physicochemical properties, including sub-100 nm size, large capacity to solubilize hydrophobic drugs, and various engineering choices to include targeting ligands, imaging, and long half-life in blood (stealth micelle). One of the nanoparticles from the Kataoka group is the Poly(Asp)-PEG copolymer that has entered clinical trials yet more dose escalating and toxicity profiles need to be revealed[181, 182]. The downside of the polymeric nanoparticles often comes from the synthetic difficulty, high poly-dispersity, and nondegradable nature of the polymer. The long-term accumulation has been shown to induce toxicity in vital organs like liver, kidney, and spleen. Therefore, biodegradable and biocompatible polymers which offer the benefit of macromolecular vehicles should be put into more emphasis and development of those polymers can provide promising materials that can be translated into clinical use.

In this dissertation, a recombinant-based, elastin-like polypeptide (ELP) is used as the macromolecule to deliver chemotherapeutics to HCC. Special emphasis is placed to address limitations of polymer conjugates discussed above. ELP belongs to a class of genetically engineered biopolymers. A brief introduction will be presented followed by detailed background information of ELPs. The versatility of the polymer design, high

quality of product control, controlled drug release through sensitive linkers, thermal-responsiveness, and excellent biocompatibility along with enhanced drug accumulation are discussed. The potential of ELP-based polymers for various medical applications is also briefly discussed.

2.4 Genetically engineered protein biopolymers

Protein or polypeptide biopolymers are natural or unnatural amino acid repeats produced from prokaryotes or eukaryotes. Since the biopolymer is designed at the genetic level, the sequence and length can be precisely controlled. By changing a specific amino acid in the repetitive motif, many proteins with distinct hydrophobicity, charges, and secondary structures can be obtained. In addition to its appealing physicochemical properties, these biopolymers are biodegradable where the amino acids can be broken down though proteolysis[183, 184]. Among all biopolymers, ELP, silk-like polypeptides (SLP), and silk-elastin-like polypeptides (SELP) are the most developed for drug delivery or tissue engineering purposes. Applications for SLP[185] and SELP[186] can be found elsewhere while ELP will be thoroughly discussed in the following section.

ELPs belong to a unique library of natural proteins found in human skin, blood vessel, and lungs[187]. They are originally derived from tropoelastin, and are comprised of pentapeptide (VPGXG) repeats where X can be any amino acid except proline[188]. ELPs have gained wide popularity in drug delivery, regenerative medicine, diagnostic imaging, biosurface engineering, and various other health care applications. ELPs provide great modularity in design and synthesis, with little compromise of biocompatibility lacked by chemically synthetic counterparts. The physicochemical and mechanical properties are highly amenable to specific treatment needs. More importantly, ELPs offer easy scale-up,

efficient purification, and high yield which make them excellent candidates for medical products.

2.4.1 Cloning strategies

The construction of the first generation of ELPs was realized through monomer concatemerization. This method is fast but suffers from mixed population of oligomerization products with wide distribution of gene lengths[189]. A more precise control is achieved by using the recursive directional ligation (RDL) approach developed by Meyer *et al.*[190]. RDL realizes seamless ligation with two monomer genes using type II restriction enzymes and leads to a precise dimer without unwanted insertion of other amino acids. Depending on the cloning vectors, dozens of enzyme pairs can be used. This method, however, can be very laborious when constructing ELPs with very large molecular weight, and multiple species of different gene length are still observed frequently. A modified method was recently developed by McDanial *et al.*[191] who ligated two half-vectors, each containing monomer with compatible sticky ends to eliminate the products other than the desired dimers. This method also increases screening efficiency since the realization of transformation in bacteria can only be achieved by successful ligation, which lowers the possibility of mismatch or mutations. To further expand the chemical modularity of ELPs, noncanonical ELPs comprising unnatural amino acids, which can provide site-specific conjugation, become genetically possible using another recently developed technique by Amiram *et al.*[192]. The so-called overlap extension rolling circle amplification (OERCA) method, a high-throughput gene amplification method, has achieved excellent yield and fidelity products from circular DNA templates. Their drawback, however, lies inherently in the PCR part of the method

where longer genes (> 2kb) have low success rate.

ELPs do have some limitations due to the recombinant nature of the polymers. For example, since the proteins are expressed in *E Coli* (bacteria), there are no posttranslational modifications such as glycosylation or phosphorylation. As a result, the proteins do not have a secondary structure to provide or maintain biological function. If the ELPs are too hydrophobic, they form aggregates in inclusion bodies as part of the natural defense from the bacteria[193]. In ideal cases, the molecular weight can be precisely controlled. However, a certain degree of misread, single nucleotide mutation, or methionine cleavage has been frequently observed in our laboratories and those of others. Postpurification modification, which involves multiple conjugation schemes, still yields a mixed species of conjugates with different degrees of labeling/encapsulation. This wide distribution can be partly addressed using noncanonical amino acids, where azidohomoalanine (AHA) can be introduced to achieve site-specific labeling through click chemistry. However, the technique has been developed with limited success so far.

2.4.2 Thermodynamics of ELP folding

The unique property of ELP lies in its ability of inverse temperature transition. This coacervation process is driven by the entropy gain of water molecules around ELPs and entropy loss driven by hydrophobic folding of ELPs. This effect has been extensively characterized by Urry and coworkers[194] using circular dichroism (CD), electron microscopy, infrared spectroscopy, fast field filtration, etc. The thermal properties of ELPs have been well correlated with its chain length (molecular weight), concentration, guest residue compositions, and ambient ionic strength. Precise control of the ELP transition has been improved over the years with molecular dynamics (MD)

simulations[195-197], yet a more comprehensive model covering larger ELPs and its derivatives is still needed.

2.4.3 Methods of genetic engineering, expression, and purification

Due to the unique inverse transition behaviors of ELPs, a wide variety of ELP-based copolymers or ELP-fusion proteins can be produced with high yield without tedious chromatography-based purification[198]. More importantly, ELP provides a unique platform where a highly positively charged, antibacterial sequence can be coexpressed in bacteria[199, 200], and be separated from ELP using cleavable linkage like intein[201]. ELP-based fusion proteins have also been expressed in plant systems including tobacco.

The purification method is termed inverse transition cycling (ITC). Typically, 3-4 rounds of ITC can yield a highly purified product (>98%). In a typical cycle, a high concentration (1-5 M) of salts are added to the protein solution to induce the hydrophobic collapse of ELP-based proteins. At the same time, a high temperature is applied and the protein solution is centrifuged at 40 °C to yield an ELP pellet, along with other aggregated protein impurities. Then the insoluble proteins, which remain aggregates at cold temperatures (4°C), will be removed by a cold spin where the ELPs resolubilize to stay in the supernatant. **Figure 2.2** represents a typical round of ITC procedure in a laboratory setting.

2.4.4 ELP-based diblock, triblock copolymers

The traditional amphiphilic diblock or triblock copolymers have a prototype of AB or ABA (BAB), where the A and B block exhibits vast difference in the hydrophilicity (**Figure 2.3**). The adjustment of the hydrophilicity/hydrophobicity balance can be tuned

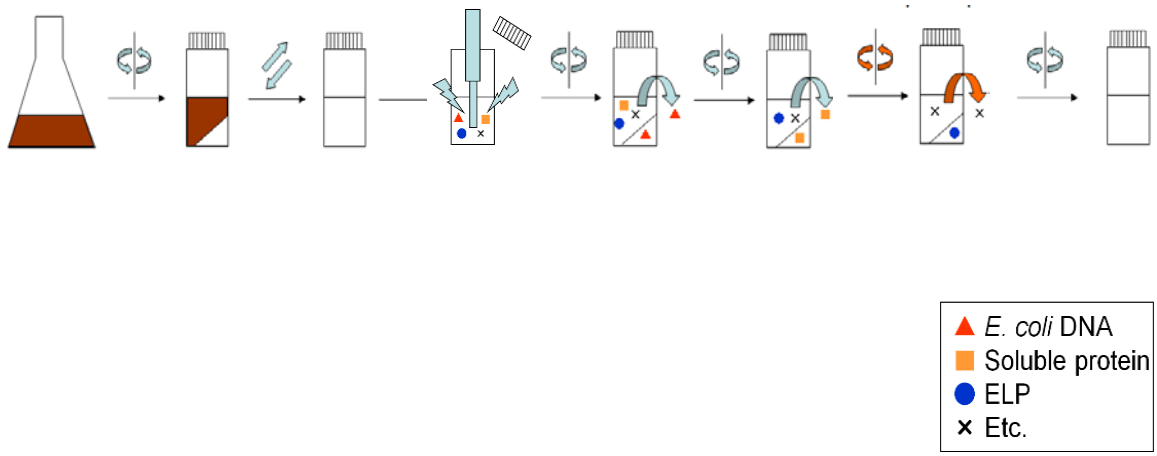

Figure 2.2. ELP purification steps from cell culture harvest.

After 24 h of shaking at 37 ºC, cells are harvested and sonicated. DNA is first removed by PEI precipitation. Soluble proteins are removed first by hot spin where ELP is aggregated with other insoluble impurities. ELP is then resolubalized into supernatant in cold PBS in the cold spin and insoluble aggregates will be discarded.

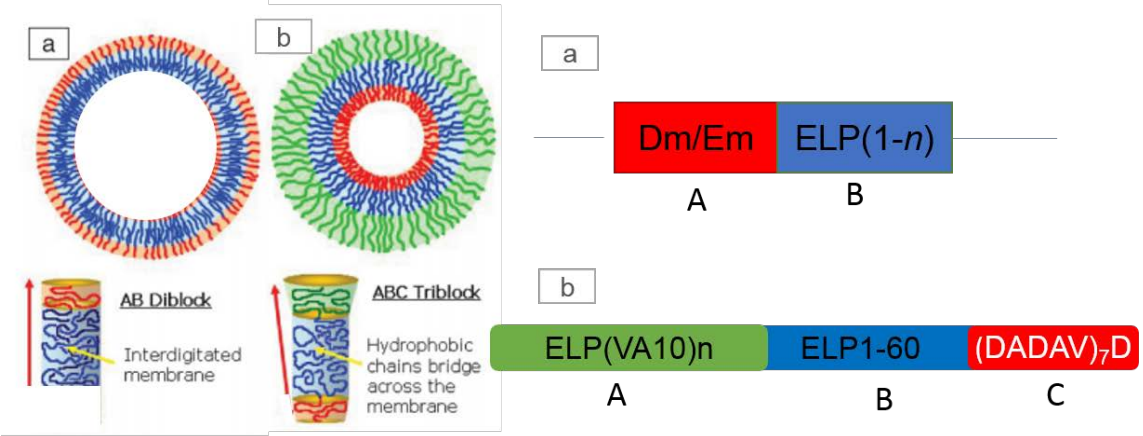

Figure 2.3. Representative ELP copolymers and possible morphologies.

a) AB diblock copolymers alone, b) ABC triblock copolymer conjugates (where C block is loaded with hydrophobic drugs): the green chains are preferentially at the outer face due to their relatively larger volume and less hydrophobicity (decrease of hydrophobicity in the arrow direction).

based on the relative ELP length, which can offer a tremendous advantage over conventional amphiphiles. Therefore, ELP-based copolymers can form micelles in very low concentrations with highly stable and size tunable aggregates for controlled drug delivery. What's more, the thermo-responsiveness of ELP copolymers by entropy-driven hydration makes the polymer change from nanoparticles/nanovesicles easily into micellar clusters.

The amphiphilic ELP diblocks form a unique class of drug delivery vehicles and are the major focus of this dissertation. Cargos include targeting ligands, small hydrophobic drugs, therapeutic peptides, or even large biologicals including antibodies fragments fused to ELP. The formation of the micelles by the loading cargo is dependent on the hydrophobicity of each block and the agent to be encapsulated[202]. Although ELP copolymers enjoy very narrow size distribution, polymer conjugates, on the other hand, still suffer relatively large polydispersity since the conjugate chemistry cannot be precisely controlled. Limited synthetic schemes are available for some chemical labile amino acids which can largelyjeopardize the yield of ELPs. Noncanonical amino acids have rendered site-specific conjugation[203] through azidohomoalanine followed by click chemistry. However, no application in ELPs has been published so far.

The diblock copolymer can be easily expanded to multiple blocks (e.g., triblock) to offer more desired physicochemical properties. In addition to adding more control over the hydrophobicity-hydrophilicity balance, the added block can also introduce reactive amino acids for chemical conjugation. Since the third block is usually designed with distinct hydrophilicity, it triggers even faster self-assembly than the diblock copolymers. Last but not least, the triblock can potentially reduce the interaction with the reticulo-

endothelial system (RES) with less hydrophobic corona but can form macroscopic gels above the transition temperature (Tt)[204, 205].

Two types of interactions are vital after ELPs' administration into cell culture media or living animals. One interacts with the water-based system (media, blood), the other happens at the lipid bilayer critical for cellular uptake. The understandings of both are still in their infancy due to the difficulty to simulate large molecular weight of ELPs (>7000Da). The mechanical study of ELPs revealed that hydrogen bond breakage mainly drives the overall entropy gain, resulting in a stretch of the ELPs[206].To understand and predict the interaction between ELP and biological membranes, all-atom and CG simulations were performed to elucidate the structures of ELPs which turned out to be quite distinct from its state in water. The ELPs in lipid bilayers have more random-coil structure than those in water-based solvents, suggesting a more dynamic hydrophobic interaction which can be exploited to achieve enhanced cellular uptake.

2.4.5 Biocompatibility

In addition to ELPs' unique physicochemical properties, they also provide extraordinary biocompatibility[207, 208] displayed in multiple tissue scaffolds[209], where tissue stability and local inflammation were monitored in both short-term (21-28 days)[210, 211] and long-term (6 months)[212]. ELPs can be engineered easily to be free of immunogenicity as few reports have shown antibody generation after i.v. injection into rabbits.

The beauty of ELP lies also in the capacity to reach a wider therapeutic index window. Since a wide range of concentrations of phase transition from micelles to aggregates has been observed, ELP still retains the ability to self-assemble in diluted form to protect the

drug from rapid systemic clearance and reach the tumor bed.

Through surface engineering, aggregation upon interaction with serum proteins can be significantly reduced. For ELPs, an approach is to introduce a third block to increase the hydrophobic stability and biocompatibility. Several blood compatibility studies have shown that ELP4 (similar to ELPVA library) is regarded to be less thromogenic with less microparticle formation and platelet activation than ELP1 or ELP2 library, especially with long length[213]. Therefore, adding an ELP4 block to the ELP1/2 diblock copolymer can reduce the overall tissue response and make them a better candidate for clinical usage.

2.4.6 Pharmacokinetics of ELP

As a macromolecular drug delivery vehicle, ELP-based biopolymers can increase the half-life of therapeutic cargos and avoid rapid systemic clearance[214]. Radiolabeling has been regarded as the most sensitive method to track *in vivo* fate of many drug carriers. Since the production of ELP requires nutrients, media containing ^{14}C -labeled glucose isotope has been tried to express ELP and provides a cheaper and more reliable way to quantify ELP *in vivo*. It has been shown that ELP1-150 has a half-life of about 8.2 hours in mice[215], although the actual pharmacokinetics of the therapeutic cargo remains unknown. Radio-labeled ELPs have been shown to be more stable than a chemically labelled counterpart[216]; however, it suffers from very poor yield of ELP, rendering it not applicable to other types of more complicated ELP polymers.

2.4.7 Application of ELP in medicine

Several designs of ELP using its thermo-responsiveness have been tested in several groups. This unique advantage makes ELP an attractive vehicle in the field of drug

delivery, tissue engineering, gene delivery, and protein purification, as summarized in **Table 2.4**. Among all the applications, ELP is most appealing to be used as a thermo-targeted drug delivery vehicle. Although there are numerous studies on thermo-sensitive polymers, only a few have achieved controlled response within clinically relevant temperatures (39-44 ^{0}C) in either cell culture or animal studies. One of the most developed synthetic polymers is N-isopropylacrylamide (NIPAAm)-based polymers pioneered by Okano *et al*. The pNIPAAm offers a tunable critical solution temperature based on the copolymer composition, molecular weight, and hydrophobicity. However, toxicity remains a major issue for its clinical development.

Various chemotherapeutic agents have been encapsulated including docetaxel[217] and adriamycin[218, 219) (220]. The micelles kept the drugs at normal temperatures but released the payload much faster at hyperthermic ranges (39-45 °C)[221]. Those micelles usually have the hydrophobic drug in the core while the other type of thermo-responsive micelle undergoes structure collapse to expose the hydrophobic corona to achieve enhanced cellular uptake[222]. In this dissertation, we have developed two kinds of ELP copolymers that fully take advantage of the benefits of ELP-based biopolymers. The copolymers offer modular structure design, efficient expression and purification, high purity, and controlled thermal transition behavior at hyperthermic temperatures. The ELP triblock in Chapter 4 has shown enhanced cellular uptake through dynamic interaction with the cell membrane with an ELPVA library. The extra block not only provides a certain level of hydrophobicity, but also offers better water-solubility than the ELP diblock in Chapter 3. Therefore, ELP triblock was used to combine hyperthermia for enhanced tumor eradication. The mechanism, cellular response, and how ELP-based conjugates can

Table 2.4. Applications of ELP-based biopolymer in medicine.

Structure	Application	Reference
ELP-fusion protein	Purification tag	(201, 223, 224)
ELP-Peptide	Chaperon small peptide	(225-227)
ELP copolymer	Drug delivery	(228-232)
	Cancer therapy with hyperthermia	(233-235)
Crosse linked ELP scaffolds	Tissue engineering	(221, 236-241)
	Removal of heavy metals	(242-245)
ELP-cationic peptide/polymer	Gene delivery	(246-249)

achieve enhanced cytotoxicity under hyperthermia are discussed below.

2.5. Hyperthermia and heat shock response

Hyperthermia refers to a heat application resulted in elevated tissue temperature (from 39-45 ºC)[250]. As early as the 19th century, reports in Asia showed that high fever resulted in tumor shrinkage. Nowadays, it is often used as an (Neo) adjuvant therapy to other standard cancer treatment[251]. Hyperthermia can be applied in either the whole body through perfusion or in local, regional tissue sites with focused energy.

2.5.1 Methods to induce clinical hyperthermia

In this dissertation, hyperthermia is generated through the application of thermal ablation. Thermal ablation is the mostly used local therapy for HCC. The thermal energy can be delivered into tumor tissue in a minimally invasive fashion[252]. Various modalities have been developed to produce extreme temperatures, including RFA, MWA, HIFU, laser, and cryoablation. Cryoablation destroys cells through thawed ice balls[253], not through elevated temperature. Therefore, it will not be discussed in detail here. In this dissertation, we used electrocautery as the means of thermal ablation, which is similar to radiofrequency.

2.5.1.1 Radiofrequency

RF ablation (RFA) uses electromagnetic energy sources with frequencies ranging from 375–500 kHz[254]. The electrical resistance of tissue results in significant ion agitation, which creates friction heat around the electrode. The distinct discrepancy between the large area of ground pad and small contact zone of the electrode needle causes the heat to be focused around the needle area. A close loop is needed to deliver the energy into a

patient: RF generator, electrode needle, and an electrode (ground pads). At the early stage of development, RFA is mostly monopolar where only one needle is needed, but a limited coagulation zone can be achieved[255]. This engineer barrier has been overcome by using multiple electrodes to deliver larger volume of ablation.

Electrocautery (EC) adopts similar energy to heat targeted tissues with a slightly wider range of frequency (100 kHz-3.3 MHz)[256]. It is one of the most versatile and widely used instruments among surgeons. The electrical current generated by the generator heats the instrument (usually via an electrical pencil) first and tissue is subsequently treated by the pencil. Similar to RFA, EC requires a complete circuit for the current flow, including a generator, an applicator, and grounding pad. First developed by Bovie[257], it has been used in hepactomy[258], vessel sealing[259], as well as to ablate highly vascularized tumor[260]. Although complications are not inevitable in EC, complications associated with electrosurgical injuries and skin burns are rare in the clinical setting, which makes it an economic and effective tool in the clinics.

2.5.1.2 Microwave

MWA uses dielectric hysteresis to produce a high temperature to destroy tissue. The thermal energy results from the fast oscillation of water (polar) molecules in an applied electromagnetic field at 900–2,450 MHz[261]. Tissues with a high percentage of water, such as liver, lung, and tumor, are most conducive to this type of heating[262, 263]. The radiation of the energy from the power generator is through interstitial antenna(s)[264]. This mechanism of heating is similar to RFA with more effective propagation of heating so a large ablation volume can be achieved[265]. It has been proven that MWA is equally safe as RFA in the clinical practice, yet the choice of ablation methods largely depends

on the size of the tumor[67, 266].

2.5.1.3 Laser

Laser can generate high temperatures between 50 ºC to 100 ºC with an infrared light delivered though an optical fiber[267]. The typical wavelength (λ) is between 800 and 1100nm. The most widely used lasers are diode (λ = 800-980 nm) and Neodyium Yttrium-Aluminum-Garnet (Nd-YAG, λ =1064 nm)[268]. The generation of heat is through the absorption of photo energy by tissue-specific chromophores[269], which causes coagulation necrosis of the contact tissue. Since the energy is realized through the monochromatic light, tissue impedance will not affect the penetration of the heat. As a result, more uniform ablation zone can be achieved with limited damage to the surrounding tissue. Also, the unique mechanism of heat generation allows clinicians to monitor extent of coagulation with real-time MRI imaging[270] . However, it has been shown that a longer procedure time is needed to achieve a larger coagulation zone and there are higher incidences of bleeding in clinical practice. Therefore, only certain organs are routinely ablated using laser[271].

2.5.1.4 Ultrasound

HIFU utilizes ultrasound energy applied by extracorporeal or direct needle application (transducer) to achieve thermal tissue ablation[272, 273]. At frequencies typically between 0.8 and 1.6 MHz, ultrasound waves can be harmlessly propagated through soft tissue and result in localized hyperthermia. Specifically, sound energy is absorbed by tissue and deposited as heat at the point of focus where the temperature can quickly rise to 80°C[274]. In addition to thermal injury, ultrasound can cause mechanical cell damage due to

cavitation. When higher energies are applied, ultrasound waves interact intensively with the microbubbles of the water and the collapse of the microbubbles causes tissue vibration and damage[272]. The most appealing advantage of HIFU is that it can be applied noninvasively, and coupled with contrasting agent or MRI guidance to achieve real-time imaging. Although it depends on the characteristics of the transducers, the ablation volume is usually small[275]. The advantages of disadvantages of all ablation devices are summarized in **Table 2.5**.

In this dissertation, the hyperthermia is created at the regions where the heat is dissipated from thermal ablation (electrocautery), or at the ablated tumor margins.

2.5.2 Cell response to hyperthermia

Cell damage starts to occur when the temperature is elevated by 2-2.5 ºC[250]. Specifically, hyperthermia initiates protein misfolding, cell membrane disaggregation or increased membrane fluidity, and disruption of microtubule organization. At the molecular level, it modulates receptor expression and subsequent bio-recognition[276]. The temperature rise also alters the host immune system, produces antibodies, and specifically increases blood flow and oxygenation. At higher temperatures, typically above 50 ºC, both the misfolded and native proteins undergo denaturation, which results in a complete shutdown of protein synthesis and DNA repairs. Consequently, most cells will yield to coagulation necrosis while a subpopulation of cells that might just be sensitized still survives. It has been found that the thermal lethal effect is more profound when the cells are in mitosis[277]. **Figure 2.4** summarizes the effect of temperature on the cell fate.

Due to the heterogeneous nature of tumor microvessels, as well as the lack of smooth muscle and skeleton, tumor cells are more sensitive to heat-induced stress compared to

Table 2.5. Advantages and disadvantages of ablation devices used in the clinics.

Energy Source	Advantage	Disadvantage
Radiofrequency	Most widely used, advanced probe design	Heat sink effect
Microwave	Bigger coagulation zone, faster temperature elevation no need of grounding pad	Heat sink effect
Cryoablation	Rewarm tissues is possible, less complication rates, less blood loss	Small coagulation zone, longer procedure time
High intensity focused ultrasound	Noninvasive and offers real time imaging	Limited penetration
Laser	Deep penetration, independent of tissue impediance, real-time imaging	High incidence of bleeding, small coagulation zone

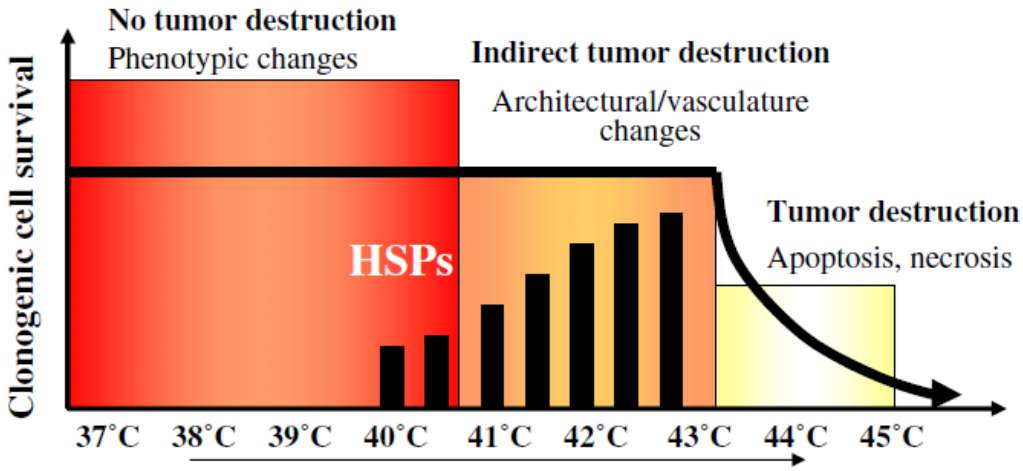

Figure 2.4. Cellular survival is dependent on temperature.

At lower temperatures (37-40 °C), few phenotypic changes are observed in the cells. HSPs start to be elevated at 40 °C. Thermal injuries increase as more HSPs are produced at higher, hyperthermic temperatures (40.5-43.5°C). Cells experience enhanced membrane permeability, morpholical changes, and collapse of vasculatures. Higher temperatures lead to cell destruction either through cell apoptosis or necrosis where cell survival starts to plunge.

the normal tissue[278]. When the ambient temperature increases over 43 ^{0}C, the tumor cells cannot dissipate heat evenly due to poor blood perfusion, which leads a blood flow stasis to cause more stress in the tumor microenvironment. The added heat stress, together with hypoxia, contributes to a lower intratumoral pH and final cell necrosis[279, 280]. Interestingly, Cho *et al.* applied heat-stressed mesenchymal stem cells (MSCs) to tumor cells (SK-OV-3) *in vitro* and showed a significant reduction of overall tumor cell viability. It has been suggested that the MSC cells, which are major components in the tumor stroma, can secrete various cytokines to destroy cytoskeleton of tumor cells[281]. Therefore, hyperthermia can kill tumor cells both directly and indirectly. However, the most important factor to determine the fate after the thermal stress has been shown to be correlated more with the degree of protein denaturation and amount of aggregation, rather than the time of heating[282, 283]. Therefore, simply relying on the temperature and time of heating will neither ensure killing of all the tumor cells nor predict the prognosis.

2.5.3 Hyperthermia and drug delivery

It has been shown in various studies that hyperthermia can increase the cytotoxic effects of certain drugs, such as cyclophosphamide, cisplatin, and bleomycin. Although exact mechanism are yet to be revealed, it has been proposed that increased sensitivity of cells to the temperature, enhanced cellular uptake, and drug accumulation contribute to the stronger cytotoxicity. As stated before, hyperthermia has been shown to increase blood permeability to small chemicals like Evans Blue[284], as well as large biomolecules such as antibodies[285-287]. Specifically, hyperthermia (and hence thermal ablation) increases vascular permeability through endothelial injury[288] [278, 289] or increases the pore size on the cell membrane to allow subsequent cellular accumulation of therapeutic

agents. As a result, the PKPD profile of therapeutic agents is altered in many aspects, as summarized by Hildebrandt *et al.*[283] in **Figure 2.5**. Critical understandings of these potential interactions are important to design a therapeutic regimen to maximize the combination effect.

In the context of cancer therapy, how hyperthermia affects drug transport depends largely on the tumor characteristics as well as the size of the delivery system. Although tumor microvasculature is known to be leaky, most tumors still have a vast number of hypo-permeable microvessels to allow very limited extravasation of larger nanoparticulate systems (>100 nm)[290]. As discussed before, hyperthermia increases the permeability of blood vessels; therefore, the effect on drug accumulation will be discussed below.

2.5.3.1 Hyperthermia increases drug accumulation

The hyperthermia has shown to increase the extravasation of large molecules to a comparable level of smaller particles[291]. The 100 nm liposome has shown similar extravasation at 42 ^{0}C compared to a 7 nm albumin particle at 34 ^{0}C. This phenomenon has been also seen in 200 and 400 nm particles, but the enhancement is limited compared to the 100 nms. Importantly, the increased extravasation is not seen in normal vessels, suggesting a tumor-specific accumulation enhancement by hyperthermia[291]. The shrinkage of endothelial cells, probably due to the disruption of the cellular skeleton[292], was proposed to result in a large cell gap to allow large particles to go through[293, 294]. However, a nonuniform distribution of the 100 nm liposomes still remains a major issue due to the heterogeneity of tumor vessels[295]. Limited extravasation of larger particles (>200 nm) suffers from a more rapid clearance from the body. As a result, low amount of

Pharmocodynamics
Acceleration of primary mode of action (alkylating reaction, protein damage, oxygen-radicals; DNA-strand breaks)
Increased intracellular drug concentration (drug uptake, membrane damage, protein damage, pH changes)
Pharmacokinetics
Drug uptake (decreased gastrointestinal or transdermal absorption)
Distribution (pH changes, fluid sequestration, increased tumor blood flow)
Metabolism and excretion (changes in hepatic and renal blood flow)

Figure 2.5. Interaction between heat and drug.

big particles can reach the tumor bed even with the application of hyperthermia.

2.5.3.2 Factors that affect the drug efficacy

2.5.3.2.1 Temperature. Under mild hyperthermic conditions (< 41 ^{0}C), cells develop thermo-tolerance by induction of heat shock proteins capable of refolding denatured proteins, and enhance stability of their client proteins vital for tumor survival. At higher temperatures (>42 ^{0}C), tumor cells tend to be more sensitized and more vulnerable to chemotherapies, as summarized in **Table 2.6**. Numerous cells from *in vitro/in vivo* studies experience 0.4-4-fold of enhancement of toxicity when they have been exposed to 30 min or more hyperthermia. The duration of hyperthermia has not been proposed to be a factor for the efficacy.

2.5.3.2.2 Heat drug sequence. It has been shown that synchronized administration of drug and hyperthermia yield the best anticancer effect in patients[296]. Adjuvant chemotherapy (post thermal ablation) shows better clinical outcome than neo-adjuvant chemotherapy (before thermal ablation). Although it highly depends on cell types, HCC cells seem to be more vulnerable to heat sensitization and have better response to chemotherapy. The optimal time of drug administration, however, should be tested in a clinical setting with the consideration of drug's specifics, such as hepatic metabolism rate and molecular pathways[297, 298].

2.5.3.2.3 Heat shock response. When cells survive after the ablation treatment due to sublethal exposure, several cellular pathways are altered to minimize cell damage and promote cell survival, including DNA damage and repair[299], cellular immune response[300] and heat shock pathway[283]. We and other groups have observed that the combined hypothermia with heat shock inhibition further augment the cytotoxic effect

Table 2.6. Thermal Enhancement Ratio (TER) of chemotherapies' cytotoxicity treated with hyperthermia.

Drug	Treatment (min)	TER 40-42 (°C)	TER 42.5-44 (°C)	Cell type	Ref
17-AAG	30	-	**1.4-2.4**	HepG2, Hep3B	
ELP-GA conjugates	30		**1.6-3**	HepG2, Hep3B	
Geldnamycin	30		**1.5-4.2**	MCF-7	(301)
Cisplatin	30	1.5-3.9	1.4-4.9	SCC-VII	(302)
Doxorubicin	30	1	1.0-2.0	C-26	(303)
Gemcitabine	60	>2	>2	Hela	(283, 304, 305)
Cyclophosphamide	30	2.3	2.7	FSa-II (*in vivo*)	(283, 304)
Bleomycin	30	1.2	1.6	FSa-II	(305)
		3.9		Osteosarcoma (*in vivo*)	(306)
Mitomycin C		1	2.8	Fsa-II	(303)

than either therapy alone. Therefore, a detailed discussion of heat shock response after hyperthermia and its impact on HCC are discussed below.

2.5.4 Heat shock proteins

2.5.4.1 Heat shock proteins (HSPs) as gate keepers

HSPs or stress proteins are highly conservative proteins present in all species. HSPs mostly reside in the cellular compartment but can also be expressed in the extracellular membrane[307]. First discovered in 1962, over 40 different HSPs have been identified so far[308]. There are mainly six families in heat shock proteins based on their molecular weight: HSP100, HSP90, HSP70, HSP60, HSP40, and small HSPs such as HSP27[309].

Under normal conditions, most HSPs are expressed at nondetectable levels[310]. However, HSPs are drastically induced under heat shock, lack of nutrients, hypoxia, or other cellular stresses up to 5% of total cellular proteins[311]. This rapid response enables them to have strong cytoprotective effect and function as molecular chaperons for many vital cellular proteins, often called client proteins. The duties of chaperon mainly lie in the restoration of protein homeostasis, including removal of misfolded or aggregated proteins and repair of disrupted regulatory complexes[307].

2.5.4.2 HSPs in HCC

The induction of heat shock proteins in liver are most dramatic upon stressed conditions, and various HSPs, including HSP27, HSP70, HSP90, and glucose regulated proteins (GRPs), are upregulated in liver cancer[312, 313]. The expression level of HSPs is shown to be correlated clinically with the clinicopathological features of HCC patients, as shown in **Table 2.7**. Therefore, HSPS can serve as both therapeutic targets and diagnostic

Table 2.7. Specific HSPs associated with clinicopathological features of HCC.

Clinicopathological features	HSPs	Reference
Large tumor size	GRP94, HSP70	(314, 315)
Advanced tumor stage	GRP75, GRP78, GRP94	(316) (317)
Early recurrence	GRP75	(317)
Poor disease-free and overall	HSP27, HSP70,GRP75,	(314, 318)
Microvascular invasion	HSP90, GRP78	(316)
High level of alpha-fetoprotein	HSP27, GRP75, GRP78	(312)

markers for a certain cohort of patients.

About 80% of HCC cases are associated with either HBV or HCV infection[319]. HSP90, GRP78, and GRP94 have been shown to be upregulated in more than 80% of HCC carrying HBV[320]. HSP27 has been identified as a partner with HCV to promote chronic liver disease[321].

2.5.4.3 Induction of HSPs upon hyperthermia

Under hyperthermia, the delicate semistable states of various proteins experience thermodynamic change, which results in misfolded, entangled, or aggregated states[322]. As a result, critical protein functions are lost and cells are in danger. At a threshold temperature, cells start the intracellular HSP-synthesis to rescue heat-damaged protein to their initial structure. This process occurs through ATP-dependent binding and hydrolysis to release the substrates, which either prevent them from aggregation or even refold them to the correct form. In addition to HSPs themselves, they can provide immunoprotective duty by interaction with other peptides[323]. Depending on the cell types, HSPs can be induced up to 2-4-fold and return to normal amount when the cell is rescued. However, at higher temperatures, HSP synthesis is inhibited and the lack of HSP induction is associated with exponential cell death. Indeed, it has been shown that the lack of HSP induction is the cause but not the result of cell death[324].

2.5.4.4 Inhibition of HSPs for cancer treatment

The unfavorable tumor microenvironment, together with hyperthermia stress, requires an increased level of heat shock proteins to aid elimination of misfolded proteins. As a result, Many HSPs have been proposed as an attractive target for cancer, including

HSP70, HSP90, and HSP27. There are three basic categories of HSP inhibition: small molecular inhibitors, protein aptamers[325], and antisense oligonucleotide (ASO)[326]. The small molecules and protein aptamers bind to the different parts of protein to inhibit its function, while the ASO binds to the mRNA to prevent protein translation. Two small molecular inhibitors under development for HSP27, quercetin and RP101, have shown antitumor effect in breast, prostate, and gastric cancer cells[327-330]. Small molecules for HSP70 and HSP40 are still in early development. One of the promising inhibitors, MKT-077, was withdrawn from clinical trials due to renal toxicity[331, 332]. Still, since HSP70 inhibition can trigger apoptosis in cancer cells[333] , new inhibitors are being evaluated with promising results. A specific antibody to HSP70 (cmHSP70.1) has made it into phase II clinical trials for non-small cell lung cancer[334]. Among all HSPs, HSP90 inhibitors are mostly developed and used in this dissertation. A detailed discussion is provided in the following section.

2.5.4.5 HSP90 and inhibitors and clinical development

HSP90 plays the central role in protein homeostasis[335]. At the transcription level, HSP90 frees the heat shock factor 1 (HSF-1), the trimerization of which leads to the induction of a variety of heat shock proteins for thermo-tolerance. Although HSP90 is not the ancestor of other HSPs, inhibition of HSP90 has profound effect on their interaction and expression and can serve as a multitarget within the heat shock pathway. Moreover, numerous oncogenic proteins have been identified as an HSP90 client protein, including HER2, EGFR, AKT, mTOR, and Erb (summarized in **Figure 2.6**). As a result, there has been increasing enthusiasm in pursuing HSP90 as an anticancer target. Indeed, HSP90 suppression has been proven effective in treating a variety of advanced cancers[336]. The

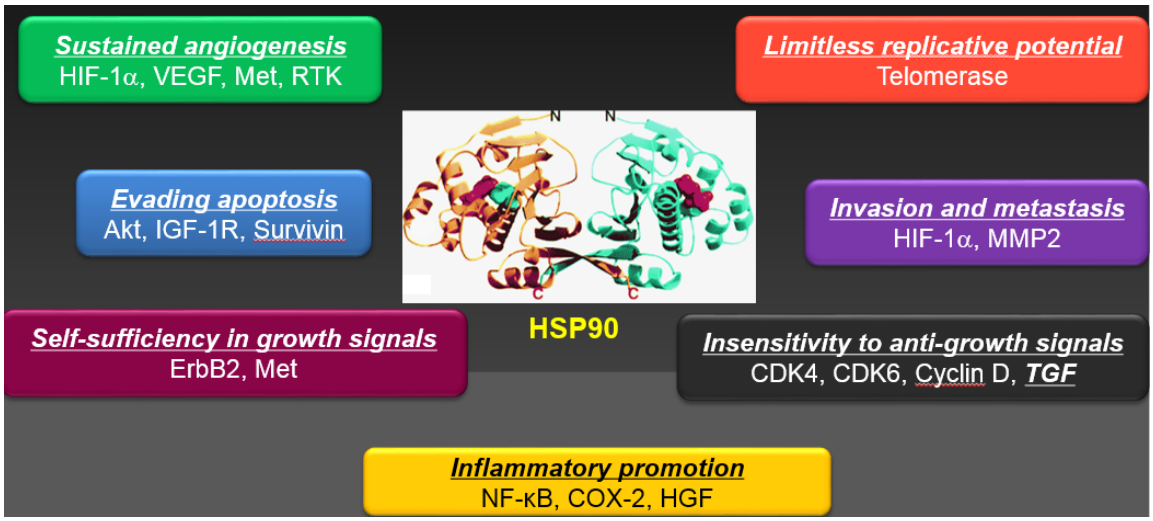

Figure 2.6. HSP90 Client proteins involved in hall marks of cancer.

HSP90 chaperones a wide varitey of proteins that are involved in hall marks of cancer. Therefore, arious siganling pathways, including angiogensis, apoptosis, inflammation, and those related to cell growth, can be suppressed via HSP90 inhition. Adapted from Hanahan *et al.*[98]

first-generation, GA (ansamycin)-based inhibitors (in **Figure 2.7**) bind to the N-terminal ATP binding pocket of HSP90[337], which lead to destabilization, ubiquitination, and proteasomal degradation of the client proteins[338, 339]. In addition to poor water solubility, GA elicited acute toxicity in preclinical studies; therefore, the unnecessary 17-methy group was replaced by amino derivatives and among these, 17-AAG (17-ally-17-desmethoxygeladanamycin-tanespimycin) advanced to Phase II clinical trials[340]. However, no objective response was obtained among multiple malignancies[341-344]. The solubility and toxicity profile was further improved in another analog 17-DMAG (17-desmoethoxy-17-N,N-dimethylaminoethylaminogeldanamycin-alvespimycin), which is used via oral or intravenous administration[345-347]. However, the clinical development of DMAG was halted due to strategic reasons despite positive response from breast cancer patients[348]. Later, a new GA derivative, IPI-504/retaspimycin, which contains reduced quinone, showed modest antitumor activity among lung cancer patients[349]; however, this drug still suffers from a series of fatal side effects including ketoacidosis and liver failure[350]. Although limited efficacy has been shown using HSP90 inhibitors as the single anticancer agent, various combinations with other drugs are being evaluated in Phase II trials (#NCT01262400, NCT01427946)[351].

Aiming to further improve the bioavailability and toxicity profiles of HSP90 inhibitors, a wide range of second-generation HSP90 inhibitors is being actively pursued both in industry and academia. Leading candidates include resorcinoal derivatives, identified by high throughput screening and purine derivatives found by structure-based design. Clearly, HSP90 suppression holds great potential in treating highly selective patients to achieve optimal therapeutic efficacy.

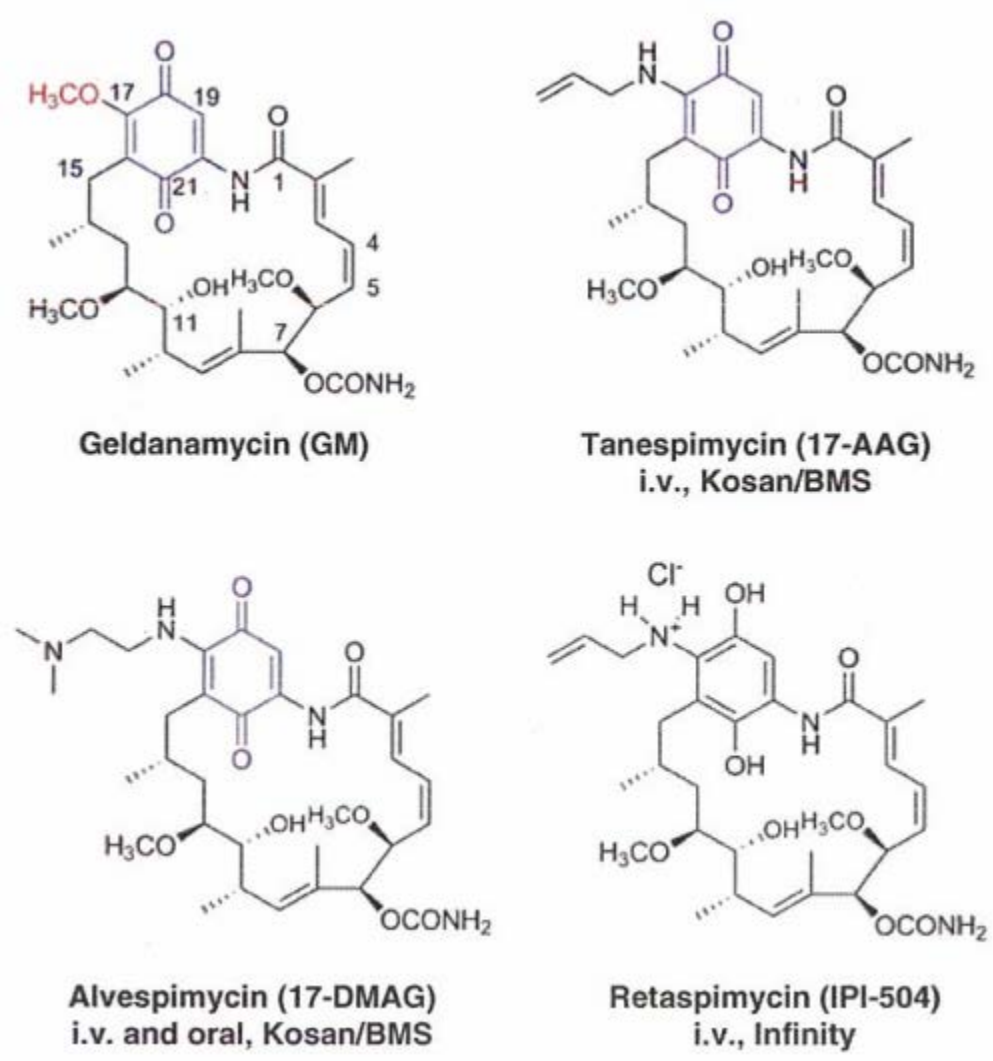

Figure 2.7. Chemical structure of ansamyin (GA)-based HSP90 inhibitors.

To ensure further clinical success of HSP90 inhibitors, it is highly necessary to identify patients whose disease progression is driven by oncogenes sensitive to HSP90 inhibition. This prescreening needs to be coupled with reliable diagnostic markers as well as close surveillance and evaluation of treatments before or after HSP90 inhibition.

In this dissertation, an aldehyde-modified geldanamycin (GA-CHO) was used to conjugate hydrazide on ELP copolymer to form a pH-sensitive, hydrazone bond. Although ketones are more widely used for hydrazone formation[352, 353], the conversion of parent hydroxyl group to the ketone resulted in significantly less HSP90 binding affinity and cytotoxicity[354]. Therefore, the aldehyde form was used in this dissertation.

2.6 Summary

HCC has high recurrence rate among all treatment options, which is the major factor of patient death. Frequently used by medical oncologist, thermal ablation is very effective in killing tumor cells at high temperatures. However, due to the theoretical limitation as well as the anatomical characteristics of tumor, ablation by itself is still inadequate to kill all tumor cells. The ablation also creates a temperature gradient where hyperthermic isotherm is formed, usually at the ablated margins where intracellular HSPs are induced to ensure survival. The upregulation of HSPs has been observed in nonablated HCC samples, with even more HSPs expressed post ablation. Among all the HSPs, HSP90 chaperones a variety of oncogenic proteins through diverse signaling pathways in carcinogenesis and is over-expressed by up to 7-fold in HCC patients. Therefore, it is of paramount importance to avoid potential risk of induced heat shock to alleviate the cell apoptosis or necrosis caused by hyperthermia and thermal ablation.

Macromolecular drug delivery systems have been used in anticancer applications to reduce the systemic toxicity, and enhance tumor accumulation and overall bioavailability of the chemotherapeutic cargo. However, traditional polymer drug delivery systems suffer from poor biocompatibility, wide size distribution, and unknown long-term toxicity to various organs. Therefore, strategies to develop an economic, modular, and safer macromolecular drug carrier to deliver sufficient chemotherapeutics are warranted. ELPs are bioorganic protein polymers that can be engineered to carry high loading of hydrophobic drugs and offer unique inverse temperature transition to serve as tunable drug depot at hyperthermic temperatures. Thus, the chemotherapeutic delivery can be increased by conjugation to the ELP backbone, and further enhanced with application of hyperthermia where the blood flow and vascular permeability of the tumor is increased.

Therefore, it is proposed that concomitant thermal ablation and enhanced delivery of HSP90 inhibition through ELP-drug conjugates at inadequately ablated, HSP90-induced tumor sites can more effectively abrogate bulk tumor cells and deplete positive margin cells to prevent future recurrence.

2.7 References

1. American Cancer Society website. The history of Cancer. 2009.

2. http://www.wcrf.org/cancer_statistics/world_cancer_statistics.php.

3. http://www.transparencymarketresearch.com/cancer-tumor-profiling.html.

4. Farber S, Diamond LK. Temporary remissions in acute leukemia in children produced by folic acid antagonist, 4-aminopteroyl-glutamic acid. New Engl J Med 1948;238:787-93.

5. Siegel R, Naishadham D, Jemal A. Cancer statistics, 2012. CA Cancer J Clin 2012;62:10-29.

6. Jemal A, Bray F, Center MM, Ferlay J, Ward E, Forman D. Global cancer

statistics. CA Cancer J Clin 2011;61:69-90.

7. Schlesinger S, Aleksandrova K, Pischon T, Fedirko V, Jenab M, Trepo E, et al. Abdominal obesity, weight gain during adulthood and risk of liver and biliary tract cancer in a European cohort. Int J Cancer 2013;132:645-57.

8. Beasley RP. Hepatitis B virus. The major etiology of hepatocellular carcinoma. Cancer 1988;61:1942-56.

9. Aravalli RN, Steer CJ, Cressman EN. Molecular mechanisms of hepatocellular carcinoma. Hepatology 2008;48:2047-63.

10. Aravalli RN, Cressman EN, Steer CJ. Cellular and molecular mechanisms of hepatocellular carcinoma: an update. Arch Toxicol 2013;87:227-47.

11. Lang K, Danchenko N, Gondek K, Shah S, Thompson D. The burden of illness associated with hepatocellular carcinoma in the United States. J Hepatol 2009;50:89-99.

12. Huang Q, Tan Y, Yin P, Ye G, Gao P, Lu X, et al. Metabolic Characterization of Hepatocellular Carcinoma Using Nontargeted Tissue Metabolomics. Cancer Res 2013; 3:4992-5002

13. Johnson PJ. The role of serum alpha-fetoprotein estimation in the diagnosis and management of hepatocellular carcinoma. Clinics in Liver Disease 2001;5:145-59.

14. Kudo M. Diagnostic imaging of hepatocellular carcinoma: recent progress. Oncology 2011;81 Suppl 1:73-85.

15. Edmondson HA, Steiner PE. Primary carcinoma of the liver: a study of 100 cases among 48,900 necropsies. Cancer 1954;7:462-503.

16. Nault JC, De Reynies A, Villanueva A, Calderaro J, Rebouissou S, Couchy G, et al. A hepatocellular carcinoma 5-gene score associated with survival of patients after liver resection. Gastroenterology 2013;145:176-87.

17. Chan EY, Larson AM, Fix OK, Yeh MM, Levy AE, Bakthavatsalam R, et al. Identifying risk for recurrent hepatocellular carcinoma after liver transplantation: implications for surveillance studies and new adjuvant therapies. Liver transplantation 2008;14:956-65.

18. Zhou Y, Sui C, Li B, Yin Z, Tan Y, Yang J, et al. Repeat hepatectomy for recurrent hepatocellular carcinoma: a local experience and a systematic review. World J of Surg Oncol 2010;8:55.

19. Farazi PA, DePinho RA. Hepatocellular carcinoma pathogenesis: from genes to environment. Nat Rev Cancer 2006;6:674-87.

20. Davis GL, Dempster J, Meler JD, Orr DW, Walberg MW, Brown B, et al.

Hepatocellular carcinoma: management of an increasingly common problem. Proceedings 2008;21:266-80.

21. Minguez B, Tovar V, Chiang D, Villanueva A, Llovet JM. Pathogenesis of hepatocellular carcinoma and molecular therapies Curr Opin Gastroenterol. 2009;25:186-94.

22. Hussain SP, Schwank J, Staib F, Wang XW, Harris CC. TP53 mutations and hepatocellular carcinoma: insights into the etiology and pathogenesis of liver cancer. Oncogene 2007;26:2166-76.

23. Branda M, Wands JR. Signal transduction cascades and hepatitis B and C related hepatocellular carcinoma. Hepatology 2006;43:891-902.

24. Abdel-Hamid M, El-Daly M, Molnegren V, El-Kafrawy S, Abdel-Latif S, Esmat G, et al. Genetic diversity in hepatitis C virus in Egypt and possible association with hepatocellular carcinoma. J Gen Virol 2007;88:1526-31.

25. Sung WK, Zheng H, Li S, Chen R, Liu X, Li Y, et al. Genome-wide survey of recurrent HBV integration in hepatocellular carcinoma. Nat Genetics 2012;44:765-9.

26. Farazi PA, Glickman J, Jiang S, Yu A, Rudolph KL, DePinho RA. Differential impact of telomere dysfunction on initiation and progression of hepatocellular carcinoma. Cancer Res 2003;63:5021-7.

27. Oya H, Sato Y, Yamamoto S, Nakatsuka H, Kobayashi T, Hara Y, et al. Comparison between human-telomerase reverse transcriptase mRNA and alpha-fetoprotein mRNA as a predictive value for recurrence of hepatocellular carcinoma in living donor liver transplantation. Transpl Proceed 2006;38:3636-9.

28. Rahbari NN, Mehrabi A, Mollberg NM, Muller SA, Koch M, Buchler MW, et al. Hepatocellular carcinoma: current management and perspectives for the future. Ann Surg 2011;253:453-69.

29. Bellahcene A, Castronovo V, Ogbureke KU, Fisher LW, Fedarko NS. Small integrin-binding ligand N-linked glycoproteins (SIBLINGs): multifunctional proteins in cancer. Nat Rev Cancer 2008;8:212-26.

30. Sieghart W, Wang X, Schmid K, Pinter M, König F, Bodingbauer M, et al. Osteopontin expression predicts overall survival after liver transplantation for hepatocellular carcinoma in patients beyond the Milan criteria. J Hepatol 2011;54:89-97.

31. Ben-Ari Z, Pappo O, Druzd T, Sulkes J, Klein T, Samra Z, et al. Role of cytokine gene polymorphism and hepatic transforming growth factor beta1 expression in recurrent hepatitis C after liver transplantation. Cytokine 2004;27:7-14.

32. Zimmerman MA, Ghobrial RM, Tong MJ, Hiatt JR, Cameron AM, Hong J, et al. Recurrence of hepatocellular carcinoma following liver transplantation: a review of

preoperative and postoperative prognostic indicators. Arch Surg 2008;143:182-8; discussion 8.

33. Bristow RG, Hill RP. Hypoxia and metabolism. Hypoxia, DNA repair and genetic instability. Nat Rev Cancer 2008;8:180-92.

34. DeBerardinis RJ, Lum JJ, Hatzivassiliou G, Thompson CB. The biology of cancer: metabolic reprogramming fuels cell growth and proliferation. Cell Metab 2008;7:11-20.

35. Koshiji M, To KK, Hammer S, Kumamoto K, Harris AL, Modrich P, et al. HIF-1alpha induces genetic instability by transcriptionally downregulating MutSalpha expression. Mol Cell 2005;17:793-803.

36. Miyoshi A, Kitajima Y, Ide T, Ohtaka K, Nagasawa H, Uto Y, et al. Hypoxia accelerates cancer invasion of hepatoma cells by upregulating MMP expression in an HIF-1alpha-independent manner. Int J Oncology 2006;29:1533-9.

37. Fransvea E, Mazzocca A, Antonaci S, Giannelli G. Targeting transforming growth factor (TGF)-betaRI inhibits activation of beta1 integrin and blocks vascular invasion in hepatocellular carcinoma. Hepatology 2009;49:839-50.

38. Rumie Vittar NB, Lamberti MJ, Pansa MF, Vera RE, Rodriguez ME, Cogno IS, et al. Ecological photodynamic therapy: New trend to disrupt the intricate networks within tumor ecosystem. Biochim Biophys Acta 2013;1835:86-99.

39. Xiong YQ, Sun HC, Zhang W, Zhu XD, Zhuang PY, Zhang JB, et al. Human hepatocellular carcinoma tumor-derived endothelial cells manifest increased angiogenesis capability and drug resistance compared with normal endothelial cells. Clin Cancer Res 2009;15:4838-46.

40. Quail DF, Joyce JA. Microenvironmental regulation of tumor progression and metastasis. Nat Med 2013;19:1423-37.

41. Dean M, Fojo T, Bates S. Tumour stem cells and drug resistance. Nat Rev Cancer 2005;5:275-84.

42. Rich JN. Cancer stem cells in radiation resistance. Cancer Res 2007;67:8980-4.

43. Yamashita T, Ji J, Budhu A, Forgues M, Yang W, Wang HY, et al. EpCAM-positive hepatocellular carcinoma cells are tumor-initiating cells with stem/progenitor cell features. Gastroenterology 2009;136:1012-24.

44. Kim JW, Ye Q, Forgues M, Chen Y, Budhu A, Sime J, et al. Cancer-associated molecular signature in the tissue samples of patients with cirrhosis. Hepatology 2004;39:518-27.

45. Zhu Z, Hao X, Yan M, Yao M, Ge C, Gu J, et al. Cancer stem/progenitor cells are highly enriched in CD133+CD44+ population in hepatocellular carcinoma. Int J Cancer

2010;126:2067-78.

46. Suetsugu A, Nagaki M, Aoki H, Motohashi T, Kunisada T, Moriwaki H. Characterization of CD133+ hepatocellular carcinoma cells as cancer stem/progenitor cells. Biochem Biophysical Res Commun 2006;351:820-4.

47. Lee TK, Castilho A, Cheung VC, Tang KH, Ma S, Ng IO. CD24(+) liver tumor-initiating cells drive self-renewal and tumor initiation through STAT3-mediated NANOG regulation. Cell Stem Cell 2011;9:50-63.

48. Tsai RY. A molecular view of stem cell and cancer cell self-renewal. Int J Biochem Cell Biol 2004;36:684-94.

49. Reya T, Clevers H. Wnt signalling in stem cells and cancer. Nature 2005;434:843-50.

50. Reya T, Morrison SJ, Clarke MF, Weissman IL. Stem cells, cancer, and cancer stem cells. Nature 2001;414:105-11.

51. Taipale J, Beachy PA. The Hedgehog and Wnt signalling pathways in cancer. Nature 2001;411:349-54.

52. Tang Y, Kitisin K, Jogunoori W, Li C, Deng CX, Mueller SC, et al. Progenitor/stem cells give rise to liver cancer due to aberrant TGF-beta and IL-6 signaling. PNAS 2008;105:2445-50.

53. Schmelzer E, Zhang L, Bruce A, Wauthier E, Ludlow J, Yao HL, et al. Human hepatic stem cells from fetal and postnatal donors. J Exp Med 2007;204:1973-87.

54. Ma S, Lee TK, Zheng BJ, Chan KW, Guan XY. CD133+ HCC cancer stem cells confer chemoresistance by preferential expression of the Akt/PKB survival pathway. Oncogene 2008;27:1749-58.

55. Mishra L, Derynck R, Mishra B. Transforming growth factor-beta signaling in stem cells and cancer. Science 2005;310:68-71.

56. Mishra L, Banker T, Murray J, Byers S, Thenappan A, He AR, et al. Liver stem cells and hepatocellular carcinoma. Hepatology 2009;49:318-29.

57. Fang H, Declerck YA. Targeting the Tumor Microenvironment: From Understanding Pathways to Effective Clinical Trials. Cancer Res 2013;73:4965-77.

58. Khorsandi SE, Heaton N. Contemporary strategies in the management of hepatocellular carcinoma. HPB 2012;2012:154056.

59. Mazzaferro V, Llovet JM, Miceli R, Bhoori S, Schiavo M, Mariani L, et al. Predicting survival after liver transplantation in patients with hepatocellular carcinoma beyond the Milan criteria: a retrospective, exploratory analysis. Lancet Oncol

2009;10:35-43.

60. Gluer AM, Cocco N, Laurence JM, Johnston ES, Hollands MJ, Pleass HCC, et al. Systematic review of actual 10-year survival following resection for hepatocellular carcinoma. HPB 2012;14:285-90.

61. Samuel M, Chow PK, Chan Shih-Yen E, Machin D, Soo KC. Neoadjuvant and adjuvant therapy for surgical resection of hepatocellular carcinoma. Cochrane Database Syst Rev 2009:CD001199.

62. Cucchetti A, Piscaglia F, Caturelli E, Benvegnu L, Vivarelli M, Ercolani G, et al. Comparison of recurrence of hepatocellular carcinoma after resection in patients with cirrhosis to its occurrence in a surveilled cirrhotic population. Ann Surg Oncol 2009;16:413-22.

63. Morimoto O, Nagano H, Sakon M, Fujiwara Y, Yamada T, Nakagawa H, et al. Diagnosis of intrahepatic metastasis and multicentric carcinogenesis by microsatellite loss of heterozygosity in patients with multiple and recurrent hepatocellular carcinomas. J Hepatol 2003;39:215-21.

64. Poon RT, Fan ST, Ng IO, Lo CM, Liu CL, Wong J. Different risk factors and prognosis for early and late intrahepatic recurrence after resection of hepatocellular carcinoma. Cancer 2000;89:500-7.

65. Menon KV, Hakeem AR, Heaton ND. Meta-analysis: recurrence and survival following the use of sirolimus in liver transplantation for hepatocellular carcinoma. Aliment Pharmacol Ther 2013;37:411-9.

66. Waki K, Aikata H, Katamura Y, Kawaoka T, Takaki S, Hiramatsu A, et al. Percutaneous radiofrequency ablation as first-line treatment for small hepatocellular carcinoma: results and prognostic factors on long-term follow up. J Gastroenterol Hepatol 2010;25:597-604.

67. Liu Y, Zheng Y, Li S, Li B, Zhang Y, Yuan Y. Percutaneous microwave ablation of larger hepatocellular carcinoma. Clin Radiol 2013;68:21-6.

68. Itoh S, Ikeda Y, Kawanaka H, Okuyama T, Kawasaki K, Eguchi D, et al. Efficacy of surgical microwave therapy in patients with unresectable hepatocellular carcinoma. Ann Surgical Oncol 2011;18:3650-6.

69. Yang Y, Wang C, Lu Y, Bai W, An L, Qu J, et al. Outcomes of ultrasound-guided percutaneous argon-helium cryoablation of hepatocellular carcinoma. J Hepatobiliary Sci 2012;19:674-84.

70. Cheung TT, Fan ST, Chu FS, Jenkins CR, Chok KS, Tsang SH, et al. Survival analysis of high-intensity focused ultrasound ablation in patients with small hepatocellular carcinoma. HPB 2013;15:567-73.

71. Zhang Y, Zhao J, Guo D, Zhong W, Ran L. Evaluation of short-term response of high intensity focused ultrasound ablation for primary hepatic carcinoma: utility of contrast-enhanced MRI and diffusion-weighted imaging. Eur J Radiol 2011;79:347-52.

72. Kim DJ, Clark PJ, Heimbach J, Rosen C, Sanchez W, Watt K, et al. Recurrence of Hepatocellular Carcinoma: Importance of mRECIST Response to Chemoembolization and Tumor Size. Am J Transplantation 2014;14:1383-90.

73. Park W, Chung Y-H, Kim JA, Jin Y-J, Lee D, Shim JH, et al. Recurrences of hepatocellular carcinoma following complete remission by transarterial chemoembolization or radiofrequency therapy: Focused on the recurrence patterns. Hepatol Res 2013;43:1304-12.

74. Sangro B, Inarrairaegui M, Bilbao JI. Radioembolization for hepatocellular carcinoma. J Hepatol 2012;56:464-73.

75. Tateishi R, Shiina S, Teratani T, Obi S, Sato S, Koike Y, et al. Percutaneous radiofrequency ablation for hepatocellular carcinoma. An analysis of 1000 cases. Cancer 2005;103:1201-9.

76. Cho YK, Kim JK, Kim WT, Chung JW. Hepatic resection versus radiofrequency ablation for very early stage hepatocellular carcinoma: a Markov model analysis. Hepatology 2010;51:1284-90.

77. #xf8, stner AH, Sorensen M, Olesen R, #xe9, Kr, et al. Sorafenib in Advanced Hepatocellular Carcinoma: A Nationwide Retrospective Study of Efficacy and Tolerability. Scientific World J 2013;2013:6.

78. Launay-Vacher V, Deray G. Hypertension and proteinuria: a class-effect of antiangiogenic therapies. Anti Cancer Drugs 2009;20:81-2.

79. Cheng AL, Kang YK, Chen Z, Tsao CJ, Qin S, Kim JS, et al. Efficacy and safety of sorafenib in patients in the Asia-Pacific region with advanced hepatocellular carcinoma: a phase III randomised, double-blind, placebo-controlled trial. Lancet Oncol 2009;10:25-34.

80. Villanueva A, Llovet JM. Targeted therapies for hepatocellular carcinoma. Gastroenterology. 2011;140:1410-26.

81. Maluccio M, Covey A. Recent progress in understanding, diagnosing, and treating hepatocellular carcinoma. CA Cancer J Clin 2012;62:394-9.

82. Cao H, Phan H, Yang LX. Improved chemotherapy for hepatocellular carcinoma. Anticancer Res 2012;32:1379-86.

83. Tse RV, Hawkins M, Lockwood G, Kim JJ, Cummings B, Knox J, et al. Phase I study of individualized stereotactic body radiotherapy for hepatocellular carcinoma and intrahepatic cholangiocarcinoma. J Clin Oncol 2008;26:657-64.

84. Kwon JH, Bae SH, Kim JY, Choi BO, Jang HS, Jang JW, et al. Long-term effect of stereotactic body radiation therapy for primary hepatocellular carcinoma ineligible for local ablation therapy or surgical resection. Stereotactic radiotherapy for liver cancer. BMC Cancer 2010;10:475.

85. Sun JC, Pan K, Chen MS, Wang QJ, Wang H, Ma HQ, et al. Dendritic cells-mediated CTLs targeting hepatocellular carcinoma stem cells Cancer Biol Ther. 2010;10:368-75.

86. Pardee AD, Butterfield LH. Immunotherapy of hepatocellular carcinoma: Unique challenges and clinical opportunities. Oncoimmunology 2012;1:48-55.

87. Kota J, Chivukula RR, O'Donnell KA, Wentzel EA, Montgomery CL, Hwang HW, et al. Therapeutic microRNA delivery suppresses tumorigenesis in a murine liver cancer model. Cell 2009;137:1005-17.

88. Bader AG. miR-34 - a microRNA replacement therapy is headed to the clinic. Front Genet 2012;3:120.

89. Morimoto M, Numata K, Kondou M, Nozaki A, Morita S, Tanaka K. Midterm outcomes in patients with intermediate-sized hepatocellular carcinoma: a randomized controlled trial for determining the efficacy of radiofrequency ablation combined with transcatheter arterial chemoembolization. Cancer 2010;116:5452-60.

90. Lee HY, Rhim H, Lee MW, Kim YS, Choi D, Park MJ, et al. Early diffuse recurrence of hepatocellular carcinoma after percutaneous radiofrequency ablation: Analysis of risk factors. Euro Radiol 2013;23:190-7.

91. Jeng KS, Jeng WJ, Sheen IS, Lin CC, Lin CK. Is less than 5 mm as the narrowest surgical margin width in central resections of hepatocellular carcinoma justified? Am J Surg 2013.

92. Chieh Kow AW, David Kwon CH, Song S, Shin M, Kim JM, Joh JW. Risk factors of peritoneal recurrence and outcome of resected peritoneal recurrence after liver resection in hepatocellular carcinoma: Review of 1222 cases of hepatectomy in a tertiary institution. Ann Surg Oncol 2012;19:2246-55.

93. Berber E, Siperstein A. Local recurrence after laparoscopic radiofrequency ablation of liver tumors: An analysis of 1032 tumors. Ann Surg Oncol 2008;15:2757-64.

94. Nakazawa T, Kokubu S, Shibuya A, Ono K, Watanabe M, Hidaka H, et al. Radiofrequency ablation of hepatocellular carcinoma: Correlation between local tumor progression after ablation and ablative margin. Am J Roentgenol 2007;188:480-8.

95. Xi T, Lai ECH, Min AR, Shi LH, Wu D, Xue F, et al. Adjuvant transarterial chemoembolization after curative resection of hepatocellular carcinoma: A non-randomized comparative study. Hepato-Gastroenterology 2012;59:1198-203.

96. Wu JC, Huang YH, Chau GY, Su CW, Lai CR, Lee PC, et al. Risk factors for early and late recurrence in hepatitis B-related hepatocellular carcinoma. J Hepatol 2009;51:890-7.

97. Nahleh Z, Tfayli A, Najm A, El Sayed A, Nahle Z. Heat shock proteins in cancer: targeting the 'chaperones'. Future Med Chem 2012;4:927-35.

98. Hanahan D, Weinberg RA. Hallmarks of cancer: the next generation. Cell2011;144:646-74.

99. Barrott JJ, Haystead TA. Hsp90, an unlikely ally in the war on cancer. The FEBS J 2013;280:1381-96.

100. Sun Y, Zang Z, Xu X, Zhang Z, Zhong L, Zan W, et al. Differential proteomics identification of HSP90 as potential serum biomarker in hepatocellular carcinoma by two-dimensional electrophoresis and mass spectrometry. Int J Mol Sci 2010;11:1423-33.

101. Bagatell R, Paine-Murrieta GD, Taylor CW, Pulcini EJ, Akinaga S, Benjamin IJ, et al. Induction of a heat shock factor 1-dependent stress response alters the cytotoxic activity of hsp90-binding agents. Clin Cancer Res 2000;6:3312-8.

102. Liu Q, Zhai B, Yang W, Yu LX, Dong W, He YQ, et al. Abrogation of local cancer recurrence after radiofrequency ablation by dendritic cell-based hyperthermic tumor vaccine. Mol Ther 2009;17:2049-57.

103. Kroeze SGC, Van Melick HHE, Nijkamp MW, Kruse FK, Kruijssen LWJ, Van Diest PJ, et al. Incomplete thermal ablation stimulates proliferation of residual renal carcinoma cells in a translational murine model. BJU Int 2012;110:281-6.

104. Sajjadi AY, Mitra K, Grace M. Expression of heat shock proteins 70 and 47 in tissues following short-pulse laser irradiation: Assessment of thermal damage and healing. Med Eng Phys 2013;35:1406-14.

105. Villanueva A, Chiang DY, Newell P, Peix J, Thung S, Alsinet C, et al. Pivotal role of mTOR signaling in hepatocellular carcinoma. Gastroenterology 2008;135:1972-83, 83 e1-11.

106. Chen JS, Wang Q, Fu XH, Huang XH, Chen XL, Cao LQ, et al. Involvement of PI3K/PTEN/AKT/mTOR pathway in invasion and metastasis in hepatocellular carcinoma: Association with MMP-9. Hepatol Res 2009;39:177-86.

107. de La Coste A, Romagnolo B, Billuart P, Renard CA, Buendia MA, Soubrane O, et al. Somatic mutations of the beta-catenin gene are frequent in mouse and human hepatocellular carcinomas. PNAS 1998;95:8847-51.

108. Yoshida T, Hisamoto T, Akiba J, Koga H, Nakamura K, Tokunaga Y, et al. Spreds, inhibitors of the Ras/ERK signal transduction, are dysregulated in human hepatocellular carcinoma and linked to the malignant phenotype of tumors. Oncogene

2006;25:6056-66.

109. Schuierer MM, Bataille F, Weiss TS, Hellerbrand C, Bosserhoff AK. Raf kinase inhibitor protein is downregulated in hepatocellular carcinoma. Oncol Rep 2006;16:451-6.

110. Schmitz KJ, Wohlschlaeger J, Lang H, Sotiropoulos GC, Malago M, Steveling K, et al. Activation of the ERK and AKT signalling pathway predicts poor prognosis in hepatocellular carcinoma and ERK activation in cancer tissue is associated with hepatitis C virus infection. J Hepatol 2008;48:83-90.

111. Ito Y, Sasaki Y, Horimoto M, Wada S, Tanaka Y, Kasahara A, et al. Activation of mitogen-activated protein kinases/extracellular signal-regulated kinases in human hepatocellular carcinoma. Hepatology 1998;27:951-8.

112. Feng DY, Zheng H, Tan Y, Cheng RX. Effect of phosphorylation of MAPK and Stat3 and expression of c-fos and c-jun proteins on hepatocarcinogenesis and their clinical significance. World J Gastroenterol 2001;7:33-6.

113. Amann T, Bataille F, Spruss T, Muhlbauer M, Gabele E, Scholmerich J, et al. Activated hepatic stellate cells promote tumorigenicity of hepatocellular carcinoma. Cancer Sci 2009;100:646-53.

114. Wynn TA. Cellular and molecular mechanisms of fibrosis. J Pathol 2008;214:199-210.

115. Sun JM, Yoon JH, Bo HK, Lee JH, Eun UJ, Lee HS. Heat shock protein 90 inhibitor induces apoptosis and attenuates activation of hepatic stellate cells. J Pharmacol Exp Ther 2009;330:276-82.

116. Gray R, Peto R, Brantom P, Grasso P. Chronic nitrosamine ingestion in 1040 rodents: the effect of the choice of nitrosamine, the species studied, and the age of starting exposure. Cancer Res 1991;51:6470-91.

117. McGlynn KA, Hunter K, LeVoyer T, Roush J, Wise P, Michielli RA, et al. Susceptibility to aflatoxin B1-related primary hepatocellular carcinoma in mice and humans. Cancer Res 2003;63:4594-601.

118. Weisburger EK. Carcinogenicity studies on halogenated hydrocarbons. Environ Health Perspect 1977;21:7-16.

119. De Minicis S, Kisseleva T, Francis H, Baroni GS, Benedetti A, Brenner D, et al. Liver carcinogenesis: rodent models of hepatocarcinoma and cholangiocarcinoma. Digest Liver Dis 2013;45:450-9.

120. Knight B, Yeoh GC, Husk KL, Ly T, Abraham LJ, Yu C, et al. Impaired preneoplastic changes and liver tumor formation in tumor necrosis factor receptor type 1 knockout mice. J Exp Med 2000;192:1809-18.

121. Yang MC, Chang CP, Lei HY. Induction of liver fibrosis in a murine hepatoma model by thioacetamide is associated with enhanced tumor growth and suppressed antitumor immunity. Lab Invest 2010;90:1782-93.

122. Liu L, Cao Y, Chen C, Zhang X, McNabola A, Wilkie D, et al. Sorafenib blocks the RAF/MEK/ERK pathway, inhibits tumor angiogenesis, and induces tumor cell apoptosis in hepatocellular carcinoma model PLC/PRF/5. Cancer Res 2006;66:11851-8.

123. Ali SH, DeCaprio JA. Cellular transformation by SV40 large T antigen: interaction with host proteins. Semin Cancer Biol 2001;11:15-23.

124. Conner EA, Lemmer ER, Omori M, Wirth PJ, Factor VM, Thorgeirsson SS. Dual functions of E2F-1 in a transgenic mouse model of liver carcinogenesis. Oncogene 2000;19:5054-62.

125. Sun FX, Tang ZY, Lui KD, Ye SL, Xue Q, Gao DM, et al. Establishment of a metastatic model of human hepatocellular carcinoma in nude mice via orthotopic implantation of histologically intact tissues. Int J Cancer 1996;66:239-43.

126. Tian J, Tang ZY, Ye SL, Liu YK, Lin ZY, Chen J, et al. New human hepatocellular carcinoma (HCC) cell line with highly metastatic potential (MHCC97) and its expressions of the factors associated with metastasis. Br J Cancer 1999;81:814-21.

127. Li Y, Tang ZY, Ye SL, Liu YK, Chen J, Xue Q, et al. Establishment of cell clones with different metastatic potential from the metastatic hepatocellular carcinoma cell line MHCC97. World J Gastroenterol 2001;7:630-6.

128. Shouval D, Reid LM, Chakraborty PR, Ruiz-Opazo N, Morecki R, Gerber MA, et al. Tumorigenicity in nude mice of a human hepatoma cell line containing hepatitis B virus DNA. Cancer Res 1981;41:1342-50.

129. Newell P, Villanueva A, Friedman SL, Koike K, Llovet JM. Experimental models of hepatocellular carcinoma. J Hepatol 2008;48:858-79.

130. Bogen KT. Risk extrapolation for chlorinated methanes as promoters vs initiators of multistage carcinogenesis. Fund Appl Toxicol 1990;15:536-57.

131. Bui LA, Butterfield LH, Kim JY, Ribas A, Seu P, Lau R, et al. In vivo therapy of hepatocellular carcinoma with a tumor-specific adenoviral vector expressing interleukin-2. Human Gene Ther 1997;8:2173-82.

132. Fukuda Y, Imai K, Miura K, Matsui M, Nakanishi T, Nakazato H, et al. A monoclonal antibody to the carbohydrate chain on human hepatocellular carcinoma-associated antigen which suppressed tumor growth in nude mice. Cancer Immunol Immunother 1988;27:26-32.

133. Shope RE, Hurst EW. Infectious Papillomatosis of Rabbits : With a Note on the Histopathology. J Exp Med 1933;58:607-24.

134. Kidd JG, Beard JW, Rous P. Serological Reactions with a Virus Causing Rabbit Papillomas Which Become Cancerous : Ii. Tests of the Blood of Animals Carrying Various Epithelial Tumors. J Exp Med 1936;64:79-96.

135. Kidd JG, Rous P. A Transplantable Rabbit Carcinoma Originating in a Virus-Induced Papilloma and Containing the Virus in Masked or Altered Form. J Exp Med 1940;71:813-38.

136. Galasko CSB, Haynes DW. Survival of VX2 carcinoma cells in vitro. Euro J Cancer 1976;12:1025-6.

137. Shah SA, Dickson JA. Preservation of enzymatically prepared rabbit VX2 tumour cells in vitro. Euro J Cancer 1978;14:447-8.

138. Easty DM, Easty GC. Establishment of an in vitro cell line from the rabbit VX2 carcinoma. Virchows Arch B Cell Pathol Incl Mol Pathol 1982;39:333-7.

139. Handal JA, Schulz JF, Florez GB, Kwok SCM, Khurana JS, Samuel SP. Creation of rabbit bone and soft tissue tumor using cultured VX2 cells J Surg Res. 2012.

140. Hoye RC, Thomas LB, Riggle GC, Ketcham A. Effects of neodymium laser on normal liver and Vx2 carcinoma transplanted into the liver of experimental animals. JNCI 1968;41:1071-82.

141. Okuma T, Matsuoka T, Okamura T, Wada Y, Yamamoto A, Oyama Y, et al. 18F-FDG Small-Animal PET for Monitoring the Therapeutic Effect of CT-Guided Radiofrequency Ablation on Implanted VX2 Lung Tumors in Rabbits. J Nucl Med 2006;47:1351-8.

142. Galasko CS, Muckle DS. Intrasarcolemmal Proliferation of the VX2 Carcinoma. Br J Cancer 1974;29:59-65.

143. Vargha G, Miltenyi L, Endes J. A new transplantation method of creating Vx2 kidney carcinoma in rabbits. Res Exp Med (Berl) 1974;164:77-82.

144. Shen N, Wu H, Xu X, Wang J, Hoffman MR, Rieves AL, et al. Cervical Lymph Node Metastasis Model of Pyriform Sinus Carcinoma. ORL 2009;71:129-34.

145. Tabuchi Y, Nakamura T, Saitoh Y. Liver metastases induced by implantation of VX2 cancer into the gastrointestine. J Surg Res 1991;50:216-22.

146. Kim SH, Han JK, Lee KH, Yoon CJ, Kim YI, Lee HS, et al. Experimentally Induced Small-Bowel Tumor in Rabbits: US-guided Percutaneous 18-gauge Core Biopsy1. Radiology 2004;231:150-5.

147. Hoshi S, Mao H, Takahashi T, Suzuki K, Nose M, Orikasa S. Internal Iliac Arterial Infusion Chemotherapy for Rabbit Invasive Bladder Cancer. Int J Urol 1997;4:493-9.

148. Iwamoto KS, Cochran ST, Winter J, Holburt E, Higashida RT, Norman A. Radiation dose enhancement therapy with iodine in rabbit VX-2 brain tumors. Radiother Oncol 1987;8:161-70.

149. Zagzag D, Goldenberg M, Brem S. Angiogenesis and blood-brain barrier breakdown modulate CT contrast enhancement: An experimental study in a rabbit brain-tumor model. Am J Roentgenol 1989;153:141-6.

150. Wong VG, Viola RS. Effect of rH Tumor Necrosis Factor on Experimental Intraocular Tumors. Cornea 1991;10:131-5.

151. BOEHM T, MALICH A, REICHENBACH JR, FLECK M, KAISER WA. Percutaneous Radiofrequency (RF) Thermal Ablation of Rabbit Tumors Embedded in Fat: A Model for RF Ablation of Breast Tumors. Invest Radiol 2001;36:480-6.

152. Hasegawa E, Watanabe H, Machida K, Ohmura G, Hirakawa S, Momose K. Assessment of tissue platinum concentration, X-ray computed tomogram, and microangiography after CDDP intraperitoneal administration in VX2 ovarian tumor. Japan J Cancer Chemother 1991;18:2038-41.

153. Eifler AC, Lewandowski RJ, Virmani S, Chung JC, Wang D, Tang RL, et al. Development of a VX2 Pancreatic Cancer Model in Rabbits: A Pilot Study. J VasC Interv Radiol 2009;20:1075-82.

154. Virmani S, Harris KR, Szolc-Kowalska B, Paunesku T, Woloschak GE, Lee FT, et al. Comparison of two different methods for inoculating VX2 tumors in rabbit livers and hind limbs. J Vasc Interv Radiol 2008;19:931-6.

155. Sotiropoulos GC, Malagó M, Molmenti E, Paul A, Nadalin S, Brokalaki EI, et al. Efficacy of transarterial chemoembolization prior to liver transplantation for hepatocellular carcinoma as found in pathology. Hepato-Gastroenterology 2005;52:329-32.

156. Masui T, Nakanishi H, Inada KI, Imai T, Mizoguchi Y, Yada H, et al. Highly metastatic hepatocellular carcinomas induced in male F344 rats treated with N-nitrosomorpholine in combination with other hepatocarcinogens show a high incidence of p53 gene mutations along with altered mRNA expression of tumor-related genes. Cancer Lett 1997;112:33-45.

157. Evans MJ, Kovacs CJ. Properties of the H 4 II E tumor cell system. I. Growth and cell proliferation kinetics of an experimental hepatoma. Cell Tissue Kinet 1977;10:233-43.

158. Trubenbach J, Graepler F, Pereira PL, Ruck P, Lauer U, Gregor M, et al. Growth characteristics and imaging properties of the morris hepatoma 3924A in ACI rats: a suitable model for transarterial chemoembolization. Cardiovasc Intervent Radiol 2000;23:211-7.

159. Kobayashi K, Fukuoka K, Matsushita F. Transplantation of woodchuck hepatocellular carcinoma in nude mice. Hepatology 1983;3:663-6.

160. Terradillos O, Billet O, Renard CA, Levy R, Molina T, Briand P, et al. The hepatitis B virus X gene potentiates c-myc-induced liver oncogenesis in transgenic mice. Oncogene 1997;14:395-404.

161. He S, Krens SG, Zhan H, Gong Z, Hogendoorn PC, Spaink HP, et al. A DeltaRaf1-ER-inducible oncogenic zebrafish liver cell model identifies hepatocellular carcinoma signatures. J Pathol 2011;225:19-28.

162. Nguyen AT, Emelyanov A, Koh CHV, Spitsbergen JM, Lam SH, Mathavan S, et al. A high level of liver-specific expression of oncogenic Kras V12 drives robust liver tumorigenesis in transgenic zebrafish. DMM 2011;4:801-13.

163. Ringsdorf H. Structure and properties of pharmacologically active polymers. Journal of Polymer Science: Polymer Symposia 1975;51:135-53.

164. Bao G, Mitragotri S, Tong S. Multifunctional nanoparticles for drug delivery and molecular imaging. Ann Rev Biomed Eng 2013; 253-82.

165. Joralemon MJ, McRae S, Emrick T. PEGylated polymers for medicine: from conjugation to self-assembled systems. Chem Commun 2010;46:1377-93.

166. Knop K, Hoogenboom R, Fischer D, Schubert US. Poly(ethylene glycol) in drug delivery: pros and cons as well as potential alternatives. Angewandte Chemie 2010;49:6288-308.

167. Bae YH, Park K. Targeted drug delivery to tumors: myths, reality and possibility. J control Release 2011;153:198-205.

168. Wang R, Billone PS, Mullett WM. Nanomedicine in Action: An Overview of Cancer Nanomedicine on the Market and in Clinical Trials. J Nanomaterials 2013;2013:12.

169. Ventola CL. The nanomedicine revolution: part 2: current and future clinical applications. P & T 2012;37:582-91.

170. Matsumura Y, Maeda H. A new concept for macromolecular therapeutics in cancer chemotherapy: mechanism of tumoritropic accumulation of proteins and the antitumor agent smancs. Cancer Res 1986;46:6387-92.

171. Choi JS, MacKay JA, Szoka FC, Jr. Low-pH-sensitive PEG-stabilized plasmid-lipid nanoparticles: preparation and characterization. Bioconjugate Chem 2003;14:420-9.

172. Walker GF, Fella C, Pelisek J, Fahrmeir J, Boeckle S, Ogris M, et al. Toward synthetic viruses: endosomal pH-triggered deshielding of targeted polyplexes greatly enhances gene transfer in vitro and in vivo. Mol Ther 2005;11:418-25.

173. Knorr V, Allmendinger L, Walker GF, Paintner FF, Wagner E. An acetal-based PEGylation reagent for pH-sensitive shielding of DNA polyplexes. Bioconjugate Chem 2007;18:1218-25.

174. DeRouchey J, Schmidt C, Walker GF, Koch C, Plank C, Wagner E, et al. Monomolecular assembly of siRNA and poly(ethylene glycol)-peptide copolymers. Biomacromolecules 2008;9:724-32.

175. Shin J, Shum P, Thompson DH. Acid-triggered release via dePEGylation of DOPE liposomes containing acid-labile vinyl ether PEG-lipids. Journal Control Release 2003;91:187-200.

176. Xu Z, Gu W, Chen L, Gao Y, Zhang Z, Li Y. A smart nanoassembly consisting of acid-labile vinyl ether PEG-DOPE and protamine for gene delivery: preparation and in vitro transfection. Biomacromolecules 2008;9:3119-26.

177. Wang J, Zhao D, Wang Y, Wu G. Imine bond cross-linked poly(ethylene glycol)-block-poly(aspartamide) complex micelle as a carrier to deliver anticancer drugs. RSC Adv 2014;4:11244-50.

178. Chan Y, Wong T, Byrne F, Kavallaris M, Bulmus V. Acid-labile core cross-linked micelles for pH-triggered release of antitumor drugs. Biomacromolecules 2008;9:1826-36.

179. Huynh VT, Quek JY, de Souza PL, Stenzel MH. Block copolymer micelles with pendant bifunctional chelator for platinum drugs: effect of spacer length on the viability of tumor cells. Biomacromolecules 2012;13:1010-23.

180. Gerweck LE, Seetharaman K. Cellular pH gradient in tumor versus normal tissue: potential exploitation for the treatment of cancer. Cancer Res 1996;56:1194-8.

181. Matsumura Y, Hamaguchi T, Ura T, Muro K, Yamada Y, Shimada Y, et al. Phase I clinical trial and pharmacokinetic evaluation of NK911, a micelle-encapsulated doxorubicin. Br J Cancer 2004;91:1775-81.

182. Hamaguchi T, Kato K, Yasui H, Morizane C, Ikeda M, Ueno H, et al. A phase I and pharmacokinetic study of NK105, a paclitaxel-incorporating micellar nanoparticle formulation. Br J Cancer 2007;97:170-6.

183. Urry DW, Urry KD, Szaflarski W, Nowicki M. Elastic-contractile model proteins: Physical chemistry, protein function and drug design and delivery. Adv Drug Deliv Rev 2010;62:1404-55.

184. Gustafson JA, Price RA, Greish K, Cappello J, Ghandehari H. Silk-elastin-like hydrogel improves the safety of adenovirus-mediated gene-directed enzyme-prodrug therapy. Mol Pharm 2010;7:1050-6.

185. Numata K, Mieszawska-Czajkowska AJ, Kvenvold LA, Kaplan DL. Silk-based

nanocomplexes with tumor-homing peptides for tumor-specific gene delivery. Macromolecular Biosci 2012;12:75-82.

186. Numata K, Reagan MR, Goldstein RH, Rosenblatt M, Kaplan DL. Spider silk-based gene carriers for tumor cell-specific delivery. Bioconjugate Chem 2011;22:1605-10.

187. Tatham AS, Shewry PR. Elastomeric proteins: biological roles, structures and mechanisms. Trends Biochem Sci 2000;25:567-71.

188. Urry DW, Shaw RG, Prasad KU. Polypentapeptide of elastin: temperature dependence of ellipticity and correlation with elastomeric force. Biochem Biophys Res Commun 1985;130:50-7.

189. Cappello J, Crissman J, Dorman M, Mikolajczak M, Textor G, Marquet M, et al. Genetic engineering of structural protein polymers. Biotechnol Prog 1990;6:198-202.

190. Meyer DE, Chilkoti A. Genetically encoded synthesis of protein-based polymers with precisely specified molecular weight and sequence by recursive directional ligation: examples from the elastin-like polypeptide system. Biomacromolecules 2002;3:357-67.

191. McDaniel JR, Mackay JA, Quiroz FG, Chilkoti A. Recursive directional ligation by plasmid reconstruction allows rapid and seamless cloning of oligomeric genes. Biomacromolecules 2010;11:944-52.

192. Amiram M, Quiroz FG, Callahan DJ, Chilkoti A. A highly parallel method for synthesizing DNA repeats enables the discovery of 'smart' protein polymers Nature Mater. 2011;10:141-8.

193. Hockney RC. Recent developments in heterologous protein production in Escherichia coli. Trends Biotechnol 1994;12:456-63.

194. Urry DW, Haynes B, Thomas D, Harris RD. A method for fixation of elastin demonstrated by stress/strain characterization. Biochem Biophys Res Commun 1988;151:686-92.

195. McDaniel JR, Radford DC, Chilkoti A. A unified model for de novo design of elastin-like polypeptides with tunable inverse transition temperatures. Biomacromolecules 2013;14:2866-72.

196. Glaves R, Baer M, Schreiner E, Stoll R, Marx D. Conformational dynamics of minimal elastin-like polypeptides: the role of proline revealed by molecular dynamics and nuclear magnetic resonance. Chemphyschem 2008;9:2759-65.

197. Lee H, Kim HR, Larson RG, Park JC. Effects of the Size, Shape, and Structural Transition of Thermosensitive Polypeptides on the Stability of Lipid Bilayers and Liposomes. Macromolecules 2012;45:7304-12.

198. Meyer DE, Chilkoti A. Purification of recombinant proteins by fusion with

thermally-responsive polypeptides. Nat Biotechnol 1999;17:1112-5.

199. Yang K, Su Y, Li J, Sun J, Yang Y. Expression and purification of the antimicrobial peptide cecropin AD by fusion with cationic elastin-like polypeptides. Protein Expr Purif 2012;85:200-3.

200. Hu F, Ke T, Li X, Mao PH, Jin X, Hui FL, et al. Expression and purification of an antimicrobial peptide by fusion with elastin-like polypeptides in Escherichia coli. Appl Biochem Biotechnol 2010;160:2377-87.

201. Banki MR, Feng L, Wood DW. Simple bioseparations using self-cleaving elastin-like polypeptide tags. Nat Methods 2005;2:659-61.

202. McDaniel JR, Bhattacharyya J, Vargo KB, Hassouneh W, Hammer DA, Chilkoti A. Self-Assembly of Thermally Responsive Nanoparticles of a Genetically Encoded Peptide Polymer by Drug Conjugation. Angewandte Chemie Int Ed 2013;52:1683-7.

203. Offenbacher AR, Pagba CV, Polander BC, Brahmachari U, Barry BA. First Site-Specific Incorporation of a Noncanonical Amino Acid into the Photosynthetic Oxygen-Evolving Complex. ACS Chem Biol 2014;9:891-6.

204. Mischenko N, Reynders K, Mortensen K, Scherrenberg R, Fontaine F, Graulus R, et al. Structural Studies of Thermoplastic Triblock Copolymer Gels. Macromolecules 1994;27:2345-7.

205. Reynders K, Mischenko N, Mortensen K, Overbergh N, Reynaers H. Stretching-Induced Correlations in Triblock Copolymer Gels As Observed by Small-Angle Neutron Scattering Macromolecules. 1995;28:8699-701.

206. Valiaev A, Lim DW, Schmidler S, Clark RL, Chilkoti A, Zauscher S. Hydration and conformational mechanics of single, end-tethered elastin-like polypeptides. JACS 2008;130:10939-46.

207. Urry DW, Parker TM, Reid MC, Gowda DC. Biocompatibility of the Bioelastic Materials, Poly(GVGVP) and Its γ-Irradiation Cross-Linked Matrix: Summary of Generic Biological Test Results. J Bioact Compat Pol 1991;6:263-82.

208. Urry DW, Trapane TL, Prasad KU. Phase-structure transitions of the elastin polypentapeptide-water system within the framework of composition-temperature studies. Biopolymers 1985;24:2345-56.

209. Ong SR, Trabbic-Carlson KA, Nettles DL, Lim DW, Chilkoti A, Setton LA. Epitope tagging for tracking elastin-like polypeptides. Biomaterials 2006;27:1930-5.

210. Kim W, Brady C, Chaikof EL. Amphiphilic protein micelles for targeted in vivo imaging. Acta biomaterialia 2012;8:2476-82.

211. Rincon AC, Molina-Martinez IT, de Las Heras B, Alonso M, Bailez C,

Rodriguez-Cabello JC, et al. Biocompatibility of elastin-like polymer poly(VPAVG) microparticles: in vitro and in vivo studies. J Biomed Mater Res 2006;78:343-51.

212. Sallach RE, Cui W, Balderrama F, Martinez AW, Wen J, Haller CA, et al. Long-term biostability of self-assembling protein polymers in the absence of covalent crosslinking. Biomaterials 2010;31:779-91.

213. Srokowski EM, Woodhouse KA. Evaluation of the bulk platelet response and fibrinogen interaction to elastin-like polypeptide coatings. J Biomed Mater Res 2014;102:540-51.

214. MacKay JA, Chen M, McDaniel JR, Liu W, Simnick AJ, Chilkoti A. Self-assembling chimeric polypeptide-doxorubicin conjugate nanoparticles that abolish tumours after a single injection. Nature materials 2009;8:993-9.

215. Liu W, Dreher MR, Furgeson DY, Peixoto KV, Yuan H, Zalutsky MR, et al. Tumor accumulation, degradation and pharmacokinetics of elastin-like polypeptides in nude mice. Journal of Controlled Release 2006;116:170-8.

216. Liu W, Dreher MR, Chow DC, Zalutsky MR, Chilkoti A. Tracking the in vivo fate of recombinant polypeptides by isotopic labeling. Journal of Controlled Release 2006;114:184-92.

217. Yang M, Ding Y, Zhang L, Qian X, Jiang X, Liu B. Novel thermosensitive polymeric micelles for docetaxel delivery. Journal of biomedical materials research Part A 2007;81:847-57.

218. Kohori F, Sakai K, Aoyagi T, Yokoyama M, Yamato M, Sakurai Y, et al. Control of adriamycin cytotoxic activity using thermally responsive polymeric micelles composed of poly(N-isopropylacrylamide-co-N,N-dimethylacrylamide)-b-poly(d,l-lactide). Colloids Surf B 1999;16:195-205.

219. Li W, Li J, Gao J, Li B, Xia Y, Meng Y, et al. The fine-tuning of thermosensitive and degradable polymer micelles for enhancing intracellular uptake and drug release in tumors. Biomaterials 2011;32:3832-44.

220. Liu SQ, Tong YW, Yang YY. Incorporation and in vitro release of doxorubicin in thermally sensitive micelles made from poly(N-isopropylacrylamide-co-N,N-dimethylacrylamide)-b-poly(D,L-lactide-co-glyco lide) with varying compositions. Biomaterials 2005;26:5064-74.

221. Liu B, Yang M, Li R, Ding Y, Qian X, Yu L, et al. The antitumor effect of novel docetaxel-loaded thermosensitive micelles. Euro J Pharm Biophar. 2008;69:527-34.

222. Akimoto J, Nakayama M, Sakai K, Okano T. Temperature-induced intracellular uptake of thermoresponsive polymeric micelles. Biomacromolecules 2009;10:1331-6.

223. Christensen T, Trabbic-Carlson K, Liu W, Chilkoti A. Purification of recombinant

proteins from Escherichia coli at low expression levels by inverse transition cycling. Analy Biochem 2007;360:166-8.

224. Kim JY, O'Malley S, Mulchandani A, Chen W. Genetically engineered elastin-protein A fusion as a universal platform for homogeneous, phase-separation immunoassay. Analy Chem 2005;77:2318-22.

225. Krishnani KK, Chen W, Mulchandani A. Bactericidal activity of elastin-like polypeptide biopolymer with polyhistidine domain and silver. Colloids Surf B 2014;119:66-70

226. Massodi I, Moktan S, Rawat A, Bidwell GL, 3rd, Raucher D. Inhibition of ovarian cancer cell proliferation by a cell cycle inhibitory peptide fused to a thermally responsive polypeptide carrier. Int J Cancer 2010;126:533-44.

227. Giorello L, Clerico L, Pescarolo MP, Vikhanskaya F, Salmona M, Colella G, et al. Inhibition of cancer cell growth and c-Myc transcriptional activity by a c-Myc helix 1-type peptide fused to an internalization sequence. Cancer Res 1998;58:3654-9.

228. Kojima C, Irie K. Synthesis of temperature-dependent elastin-like peptide-modified dendrimer for drug delivery. Biopolymers 2013;100:714-21.

229. Amruthwar SS, Janorkar AV. Preparation and characterization of elastin-like polypeptide scaffolds for local delivery of antibiotics and proteins. J Mater Sci Mater Med 2012;23:2903-12.

230. Wu Y, MacKay JA, McDaniel JR, Chilkoti A, Clark RL. Fabrication of elastin-like polypeptide nanoparticles for drug delivery by electrospraying. Biomacromolecules 2009;10:19-24.

231. Adams SB, Jr., Shamji MF, Nettles DL, Hwang P, Setton LA. Sustained release of antibiotics from injectable and thermally responsive polypeptide depots. Journal of biomedical materials research Part B, Appl Biomater 2009;90:67-74.

232. Wright ER, Conticello VP. Self-assembly of block copolymers derived from elastin-mimetic polypeptide sequences. Adv Drug Deliv Rev 2002;54:1057-73.

233. Walker CR, Pushpavanam K, Nair DG, Potta T, Sutiyoso C, Kodibagkar VD, et al. Generation of polypeptide-templated gold nanoparticles using ionizing radiation. Langmuir 2013;29:10166-73.

234. Bidwell GL, 3rd, Fokt I, Priebe W, Raucher D. Development of elastin-like polypeptide for thermally targeted delivery of doxorubicin. Biochem Pharmacol 2007;73:620-31.

235. Meyer DE, Shin BC, Kong GA, Dewhirst MW, Chilkoti A. Drug targeting using thermally responsive polymers and local hyperthermia. J control Release 2001;74:213-24.

236. Asai D, Xu D, Liu W, Garcia Quiroz F, Callahan DJ, Zalutsky MR, et al. Protein polymer hydrogels by in situ, rapid and reversible self-gelation. Biomaterials 2012;33:5451-8.

237. Martinez-Osorio H, Juarez-Campo M, Diebold Y, Girotti A, Alonso M, Arias FJ, et al. Genetically engineered elastin-like polymer as a substratum to culture cells from the ocular surface. Curr Eye Res 2009;34:48-56.

238. Janorkar AV, Rajagopalan P, Yarmush ML, Megeed Z. The use of elastin-like polypeptide-polyelectrolyte complexes to control hepatocyte morphology and function in vitro. Biomaterials 2008;29:625-32.

239. Lim DW, Nettles DL, Setton LA, Chilkoti A. Rapid cross-linking of elastin-like polypeptides with (hydroxymethyl)phosphines in aqueous solution. Biomacromolecules2007;8:1463-70.

240. McHale MK, Setton LA, Chilkoti A. Synthesis and in vitro evaluation of enzymatically cross-linked elastin-like polypeptide gels for cartilaginous tissue repair. Tissue Eng 2005;11:1768-79.

241. Nicol A, Gowda DC, Urry DW. Cell adhesion and growth on synthetic elastomeric matrices containing Arg-Gly-Asp-Ser-3. J Biomed Mater Res 1992;26:393-413.

242. Lee J, Kim O, Jung J, Na K, Heo P, Hyun J. Simple fabrication of a smart microarray of polystyrene microbeads for immunoassay. Colloids Surf B. 2009;72:173-80.

243. Lao UL, Chen A, Matsumoto MR, Mulchandani A, Chen W. Cadmium removal from contaminated soil by thermally responsive elastin (ELPEC20) biopolymers. Biotechnol Bioeng 2007;98:349-55.

244. Megeed Z, Winters RM, Yarmush ML. Modulation of single-chain antibody affinity with temperature-responsive elastin-like polypeptide linkers. Biomacromolecules 2006;7:999-1004.

245. Kostal J, Prabhukumar G, Lao UL, Chen A, Matsumoto M, Mulchandani A, et al. Customizable Biopolymers for Heavy Metal Remediation. J Nanopart Res 2005;7:517-23.

246. Kim JS, Chu HS, Park KI, Won JI, Jang JH. Elastin-like polypeptide matrices for enhancing adeno-associated virus-mediated gene delivery to human neural stem cells. Gene Therapy 2012;19:329-37.

247. Liu Y, Jia Z, Li L, Chen F. A genetically synthetic protein-based cationic polymer for siRNA delivery. Med Hypotheses 2011;76:239-40.

248. Dash BC, Mahor S, Carroll O, Mathew A, Wang W, Woodhouse KA, et al. Tunable elastin-like polypeptide hollow sphere as a high payload and controlled delivery

gene depot. J Controll Release 2011;152:382-92.

249. Chen THH, Bae Y, Furgeson DY. Intelligent biosynthetic nanobiomaterials (IBNs) for hyperthermic gene delivery. Pharm Res 2008;25:683-91.

250. Edwards MJ. Apoptosis, the heat shock response, hyperthermia, with defects, disease and cancer. Where are the common links? Cell Stress Chaperones 1998;3:213-20.

251. Hornback NB. Historical aspects of hyperthermia in cancer therapy. Radiol Clin North Am 1989;27:481-8.

252. Curley SA, Cusack JC, Jr., Tanabe KK, Stoelzing O, Ellis LM. Advances in the treatment of liver tumors. Curr Probl Surg 2002;39:449-571.

253. Mala T. Cryoablation of liver tumours - A review of mechanisms, techniques and clinical outcome. Minim Invasive Ther Allied Technol 2006;15:9-17.

254. Lencioni R, Cioni D, Crocetti L, Franchini C, Pina CD, Lera J, et al. Early-stage hepatocellular carcinoma in patients with cirrhosis: long-term results of percutaneous image-guided radiofrequency ablation. Radiology 2005;234:961-7.

255. Goldberg SN, Gazelle GS, Dawson SL, Rittman WJ, Mueller PR, Rosenthal DI. Tissue ablation with radiofrequency: effect of probe size, gauge, duration, and temperature on lesion volume. Academic Radiol 1995;2:399-404.

256. Massarweh NN, Cosgriff N, Slakey DP. Electrosurgery: history, principles, and current and future uses. J Am Coll Surg 2006;202:520-30.

257. Pollack SV, Carruthers A, Grekin RC. The history of electrosurgery. Dermatologic Surg 2000;26:904-8.

258. Strasberg SM, Drebin JA, Linehan D. Use of a bipolar vessel-sealing device for parenchymal transection during liver surgery. J Gastrointestinal Surg 2002;6:569-74.

259. Constant DL, Florman SS, Mendez F, Thomas R, Slakey DP. Use of the LigaSure vessel sealing device in laparoscopic living-donor nephrectomy. Transplantation 2004;78:1661-4.

260. Glover JL, Bendick PJ, Link WJ. The use of thermal knives in surgery: electrosurgery, lasers, plasma scalpel. Curr Probl Surg 1978;15:1-78.

261. Brace CL. Microwave ablation technology: what every user should know. Current probl Diagn Radiol 2009;38:61-7.

262. Brace CL. Radiofrequency and microwave ablation of the liver, lung, kidney, and bone: what are the differences? Current probl Diagn Radiol 2009;38:135-43.

263. Schramm W, Yang D, Haemmerich D. Contribution of direct heating, thermal conduction and perfusion during radiofrequency and microwave ablation. Conf Proc IEEE Eng Med Biol Soc 2006;1:5013-6.

264. Simon CJ, Dupuy DE, Mayo-Smith WW. Microwave ablation: principles and applications. Radiographics 2005;25 Suppl 1:S69-83.

265. Skinner MG, Iizuka MN, Kolios MC, Sherar MD. A theoretical comparison of energy sources--microwave, ultrasound and laser--for interstitial thermal therapy. Phys Med Biol 1998;43:3535-47.

266. Martin RCG, Scoggins CR, McMasters KM. Safety and efficacy of microwave ablation of hepatic tumors: A prospective review of a 5-year experience. Ann Surg Oncol 2010;17:171-8.

267. Parrish JA. New concepts in therapeutic photomedicine: photochemistry, optical targeting and the therapeutic window. J Invest Dermatol 1981;77:45-50.

268. Ivarsson K, Olsrud J, Sturesson C, Moller PH, Persson BR, Tranberg KG. Feedback interstitial diode laser (805 nm) thermotherapy system: ex vivo evaluation and mathematical modeling with one and four-fibers. Lasers Surg Med 1998;22:86-96.

269. Jacques SL. Laser-tissue interactions. Photochemical, photothermal, and photomechanical. Surg Clin North Am 1992;72:531-58.

270. McDannold NJ, Jolesz FA. Magnetic resonance image-guided thermal ablations. TMRI 2000;11:191-202.

271. Weigel C, Kirsch M, Mensel B, Nerger U, Hosten N. Percutaneous laser-induced thermotherapy of lung metastases: experience gained during 4 years. Der Radiologe. 2004;44:700-7.

272. Kennedy JE, Ter Haar GR, Cranston D. High intensity focused ultrasound: surgery of the future? Br J Radiol 2003;76:590-9.

273. Beerlage HP, van Leenders GJ, Oosterhof GO, Witjes JA, Ruijter ET, van de Kaa CA, et al. High-intensity focused ultrasound (HIFU) followed after one to two weeks by radical retropubic prostatectomy: results of a prospective study. The Prostate 1999;39:41-6.

274. ter Haar G, Rivens I, Chen L, Riddler S. High intensity focused ultrasound for the treatment of rat tumours. Phys Med Biol 1991;36:1495-501.

275. Kennedy JE. High-intensity focused ultrasound in the treatment of solid tumours. Nat Rev Cancer 2005;5:321-7.

276. Chatterjee DK, Diagaradjane P, Krishnan S. Nanoparticle-mediated hyperthermia in cancer therapy. Ther Deliv 2011;2:1001-14.

277. Song CW, Kang MS, Rhee JG, Levitt SH. Effect of hyperthermia on vascular function in normal and neoplastic tissues. Ann NY Aca Sci 1980;335:35-47.

278. Dudar TE, Jain RK. Differential response of normal and tumor microcirculation to hyperthermia. Cancer Res 1984;44:605-12.

279. Song CW, Kang MS, Rhee JG, Levitt SH. The effect of hyperthermia on vascular function, pH, and cell survival. Radiology 1980;137:795-803.

280. Wust P, Hildebrandt B, Sreenivasa G, Rau B, Gellermann J, Riess H, et al. Hyperthermia in combined treatment of cancer. Lancet Oncol 2002;3:487-97.

281. Cho JA, Park H, Kim HK, Lim EH, Seo SW, Choi JS, et al. Hyperthermia-treated mesenchymal stem cells exert antitumor effects on human carcinoma cell line. Cancer 2009;115:311-23.

282. Lepock JR. How do cells respond to their thermal environment? Int J Hyperthermia 2005;21:681-7.

283. Hildebrandt B, Wust P, Ahlers O, Dieing A, Sreenivasa G, Kerner T, et al. The cellular and molecular basis of hyperthermia. Crit Rev Oncol Hematol 2002;43:33-56.

284. Lefor AT, Makohon S, Ackerman NB. The effects of hyperthermia on vascular permeability in experimental liver metastasis. J Surg Oncol 1985;28:297-300.

285. Hosono MN, Hosono M, Endo K, Ueda R, Onoyama Y. Effect of hyperthermia on tumor uptake of radiolabeled anti-neural cell adhesion molecule antibody in small-cell lung cancer xenografts. Socie Nucl Med 1994;35:504-9.

286. Schuster JM, Zalutsky MR, Noska MA, Dodge R, Friedman HS, Bigner DD, et al. Hyperthermic modulation of radiolabelled antibody uptake in a human glioma xenograft and normal tissues. Int J Hyperthermia 1995;11:59-72.

287. Hauck ML, Coffin DO, Dodge RK, Dewhirst MW, Mitchell JB, Zalutsky MR. A local hyperthermia treatment which enhances antibody uptake in a glioma xenograft model does not affect tumour interstitial fluid pressure. Int J Hyperthermia 1997;13:307-16.

288. Jain RK. Barriers to drug delivery in solid tumors. Sci Am 1994;271:58-65.

289. Gnant MF, Noll LA, Terrill RE, Wu PC, Berger AC, Nguyen HQ, et al. Isolated hepatic perfusion for lapine liver metastases: impact of hyperthermia on permeability of tumor neovasculature. Surgery 1999;126:890-9.

290. Monsky WL, Fukumura D, Gohongi T, Ancukiewcz M, Weich HA, Torchilin VP, et al. Augmentation of transvascular transport of macromolecules and nanoparticles in tumors using vascular endothelial growth factor. Cancer Res 1999;59:4129-35.

291. Kong G, Braun RD, Dewhirst MW. Hyperthermia enables tumor-specific nanoparticle delivery: effect of particle size. Cancer Res 2000;60:4440-5.

292. Turi A, Lu RC, Lin PS. Effect of heat on the microtubule disassembly and its relationship to body temperatures. Biochem Biophys Res Commun 1981;100:584-90.

293. Dermietzel R, Streffer C. The cytoskeleton and proliferation of melanoma cells under hyperthermal conditions. A correlative double immunolabelling study. Strahlenther Onkol 1992;168:593-602.

294. Glass JR, DeWitt RG, Cress AE. Rapid loss of stress fibers in Chinese hamster ovary cells after hyperthermia. Cancer Res 1985;45:258-62.

295. Liu P, Zhang A, Xu Y, Xu LX. Study of non-uniform nanoparticle liposome extravasation in tumour. Int J Hyperthermia 2005;21:259-70.

296. Issels RD, Prenninger SW, Nagele A, Boehm E, Sauer H, Jauch KW, et al. Ifosfamide plus etoposide combined with regional hyperthermia in patients with locally advanced sarcomas: a phase II study. J Clin Oncol 1990;8:1818-29.

297. van Bree C, van der Maat B, Ceha HM, Franken NA, Haveman J, Bakker PJ. Inactivation of p53 and of pRb protects human colorectal carcinoma cells against hyperthermia-induced cytotoxicity and apoptosis. J Cancer Res Clin Oncol 1999;125:549-55.

298. Wiedemann GJ, Siemens HJ, Mentzel M, Biersack A, Wossmann W, Knocks D, et al. Effects of temperature on the therapeutic efficacy and pharmacokinetics of ifosfamide. Cancer Res 1993;53:4268-72.

299. Streffer C. Aspects of metabolic change after hyperthermia. Recent results in cancer research Fortschritte der Krebsforschung Progres dans les recherches sur le cancer 1988;107:7-16.

300. Keen AR, Frelick RW. Response of tumors to thermodynamic stimulation of the immune system. Delaware Med J 1990;62:1155-6, 9-64.

301. Bae Y, Buresh RA, Williamson TP, Chen TH, Furgeson DY. Intelligent biosynthetic nanobiomaterials for hyperthermic combination chemotherapy and thermal drug targeting of HSP90 inhibitor geldanamycin. J Control Release 2007;122:16-23.

302. Nishimura Y, Ono K, Hiraoka M, Masunaga S, Jo S, Shibamoto Y, et al. Treatment of murine SCC VII tumors with localized hyperthermia and temperature-sensitive liposomes containing cisplatin. Radiation Res 1990;122:161-7.

303. Urano M, Begley J, Reynolds R. Interaction between adriamycin cytotoxicity and hyperthermia: growth-phase-dependent thermal sensitization. Int J Hyperthermia 1994;10:817-26.

304. Urano M, Kuroda M, Nishimura Y. For the clinical application of thermochemotherapy given at mild temperatures. Int J Hyperthermia 1999;15:79-107.

305. Istomin YP, Zhavrid EA, Alexandrova EN, Sergeyeva OP, Petrovich SV. Dose enhancement effect of anticaner drugs associated with increased temperature in vitro. Exp Oncol 2008;30:56-9.

306. Urano Y, Watanabe K, Sakaki A, Arase S, Watanabe Y, Shigemi F, et al. Immunohistochemical demonstration of peptidylarginine deiminase in human sweat glands. Am J Dermatopathol 1990;12:249-55.

307. Schmitt E, Gehrmann M, Brunet M, Multhoff G, Garrido C. Intracellular and extracellular functions of heat shock proteins: repercussions in cancer therapy. J leukocyte Biol 2007;81:15-27.

308. Ritossa P. [Problems of prophylactic vaccinations of infants. Rivista dell'Istituto sieroterapico italiano. 1962;37:79-108.

309. Katschinski DM. On heat and cells and proteins. News Physiol Sci. 2004;19:11-5.

310. Eickelberg O, Geibel J, Seebach F, Giebisch G, Kashgarian M. K(+)-induced HSP-72 expression is mediated via rapid Ca(2+) influx in renal epithelial cells. Am J Physiol Renal Physiol 2001;281:F280-7.

311. Aufricht C. HSP: helper, suppressor, protector. Kidney Int 2004;65:739-40.

312. Luk JM, Lam CT, Siu AF, Lam BY, Ng IO, Hu MY, et al. Proteomic profiling of hepatocellular carcinoma in Chinese cohort reveals heat-shock proteins (Hsp27, Hsp70, GRP78) up-regulation and their associated prognostic values. Proteomics 2006;6:1049-57.

313. Ciocca DR, Calderwood SK. Heat shock proteins in cancer: diagnostic, prognostic, predictive, and treatment implications. Cell Stress Chaperones 2005;10:86-103.

314. Arzumanyan A, Reis HM, Feitelson MA. Pathogenic mechanisms in HBV- and HCV-associated hepatocellular carcinoma. Nat Rev Cancer 2013;13:123-35.

315. Lim SO, Park SG, Yoo JH, Park YM, Kim HJ, Jang KT, et al. Expression of heat shock proteins (HSP27, HSP60, HSP70, HSP90, GRP78, GRP94) in hepatitis B virus-related hepatocellular carcinomas and dysplastic nodules. World J Gastroenterol 2005;11:2072-9.

316. Federico A, Tuccillo C, Terracciano F, D'Alessio C, Galdiero M, Finamore E, et al. Heat shock protein 27 expression in patients with chronic liver damage. Immunobiology 2005;209:729-35.

317. Vabulas RM, Raychaudhuri S, Hayer-Hartl M, Hartl FU. Protein folding in the cytoplasm and the heat shock response. Cold Spring Harbor Perspect Biol

2010;2:a004390.

318. Suto R, Srivastava PK. A mechanism for the specific immunogenicity of heat shock protein-chaperoned peptides. Science 1995;269:1585-8.

319. Samali A, Holmberg CI, Sistonen L, Orrenius S. Thermotolerance and cell death are distinct cellular responses to stress: dependence on heat shock proteins. FEBS Lett 1999;461:306-10.

320. Shin E, Ryu H, Kim S-H, Jung H, Jang J-J, Lee K. The clinicopathological significance of heat shock protein 70 and glutamine synthetase expression in hepatocellular carcinoma. J Hepato-biliary-pancreatic Sci 2011;18:544-50.

321. Yao DF, Wu XH, Su XQ, Yao M, Wu W, Qiu LW, et al. Abnormal expression of HSP gp96 associated with HBV replication in human hepatocellular carcinoma. Hepatobiliary & pancreatic diseases international : HBPD Int 2006;5:381-6.

322. Lim SO, Park SG, Yoo JH, Park YM, Kim HJ, Jang KT, et al. Expression of heat shock proteins (HSP27, HSP60, HSP70, HSP90, GRP78, GRP94) in hepatitis B virus-related hepatocellular carcinomas and dysplastic nodules. World J Gastroenterol 2005;11:2072-9.

323. Yi X, Luk JM, Lee NP, Peng J, Leng X, Guan XY, et al. Association of mortalin (HSPA9) with liver cancer metastasis and prediction for early tumor recurrence. Mol Cell Proteomics 2008;7:315-25.

324. King KL, Li AF, Chau GY, Chi CW, Wu CW, Huang CL, et al. Prognostic significance of heat shock protein-27 expression in hepatocellular carcinoma and its relation to histologic grading and survival Cancer. 2000;88:2464-70.

325. Gibert B, Hadchity E, Czekalla A, Aloy MT, Colas P, Rodriguez-Lafrasse C, et al. Inhibition of heat shock protein 27 (HspB1) tumorigenic functions by peptide aptamers. Oncogene 2011;30:3672-81.

326. Kamada M, So A, Muramaki M, Rocchi P, Beraldi E, Gleave M. Hsp27 knockdown using nucleotide-based therapies inhibit tumor growth and enhance chemotherapy in human bladder cancer cells. Mol Cancer Ther 2007;6:299-308.

327. Asaum J, Matsuzaki H, Kawasak S, Kuroda M, Takeda Y, Kishi K, et al. Effects of quercetin on the cell growth and the intracellular accumulation and retention of adriamycin. Anticancer Res 2000;20:2477-83.

328. Knowles LM, Zigrossi DA, Tauber RA, Hightower C, Milner JA. Flavonoids suppress androgen-independent human prostate tumor proliferation. Nutrition Cancer 2000;38116-22.

329. So FV, Guthrie N, Chambers AF, Carroll KK. Inhibition of proliferation of estrogen receptor-positive MCF-7 human breast cancer cells by flavonoids in the

presence and absence of excess estrogen. Cancer Lett 1997;112:127-33.

330. Yoshida M, Sakai T, Hosokawa N, Marui N, Matsumoto K, Fujioka A, et al. The effect of quercetin on cell cycle progression and growth of human gastric cancer cells. FEBS Lett 1990;260:10-3.

331. Propper DJ, Braybrooke JP, Taylor DJ, Lodi R, Styles P, Cramer JA, et al. Phase I trial of the selective mitochondrial toxin MKT077 in chemo-resistant solid tumours. Ann Oncology 1999;10:923-7.

332. Rousaki A, Miyata Y, Jinwal UK, Dickey CA, Gestwicki JE, Zuiderweg ER. Allosteric drugs: the interaction of antitumor compound MKT-077 with human Hsp70 chaperones. J Mol Biol 2011;411:614-32.

333. Massey AJ, Williamson DS, Browne H, Murray JB, Dokurno P, Shaw T, et al. A novel, small molecule inhibitor of Hsc70/Hsp70 potentiates Hsp90 inhibitor induced apoptosis in HCT116 colon carcinoma cells. Cancer Chemother Pharmacol 2010;66:535-45.

334. Krause SW, Gastpar R, Andreesen R, Gross C, Ullrich H, Thonigs G, et al. Treatment of colon and lung cancer patients with ex vivo heat shock protein 70-peptide-activated, autologous natural killer cells: a clinical phase i trial. Clin Cancer Res 2004;10:3699-707.

335. Taipale M, Jarosz DF, Lindquist S. HSP90 at the hub of protein homeostasis: emerging mechanistic insights. Nat Rev Mol Cell Biol 2010;11:515-28.

336. Moser C, Lang SA, Kainz S, Gaumann A, Fichtner-Feigl S, Koehl GE, et al. Blocking heat shock protein-90 inhibits the invasive properties and hepatic growth of human colon cancer cells and improves the efficacy of oxaliplatin in p53-deficient colon cancer tumors in vivo. Mol Cancer Ther 2007;6:2868-78.

337. Neckers L, Schulte TW, Mimnaugh E. Geldanamycin as a potential anti-cancer agent: its molecular target and biochemical activity. Invest New Drugs 1999;17:361-73.

338. Zuehlke A, Johnson JL. Hsp90 and co-chaperones twist the functions of diverse client proteins. Biopolymers 2010;93:211-7.

339. Workman P, Burrows F, Neckers L, Rosen N. Drugging the cancer chaperone HSP90: combinatorial therapeutic exploitation of oncogene addiction and tumor stress. Ann NY Aca Sci 2007;1113:202-16.

340. Schulte TW, Neckers LM. The benzoquinone ansamycin 17-allylamino-17-demethoxygeldanamycin binds to HSP90 and shares important biologic activities with geldanamycin. Cancer Chemother Pharmacol 1998;42:273-9.

341. Heath EI, Hillman DW, Vaishampayan U, Sheng S, Sarkar F, Harper F, et al. A phase II trial of 17-allylamino-17-demethoxygeldanamycin in patients with hormone-

refractory metastatic prostate cancer. Clinical Cancer Res 2008;14:7940-6.

342. Solit DB, Osman I, Polsky D, Panageas KS, Daud A, Goydos JS, et al. Phase II trial of 17-allylamino-17-demethoxygeldanamycin in patients with metastatic melanoma. Clinical Cancer Res 2008;14:8302-7.

343. Ronnen EA, Kondagunta GV, Ishill N, Sweeney SM, Deluca JK, Schwartz L, et al. A phase II trial of 17-(Allylamino)-17-demethoxygeldanamycin in patients with papillary and clear cell renal cell carcinoma. Investi New Drug 2006;24:543-6.

344. Pacey S, Gore M, Chao D, Banerji U, Larkin J, Sarker S, et al. A Phase II trial of 17-allylamino, 17-demethoxygeldanamycin (17-AAG, tanespimycin) in patients with metastatic melanoma. Investi New Drug 2012;30:341-9.

345. Tian ZQ, Liu Y, Zhang D, Wang Z, Dong SD, Carreras CW, et al. Synthesis and biological activities of novel 17-aminogeldanamycin derivatives. Bioorganic Med Chem 2004;12:5317-29.

346. Kummar S, Gutierrez ME, Gardner ER, Chen X, Figg WD, Zajac-Kaye M, et al. Phase I trial of 17-dimethylaminoethylamino-17-demethoxygeldanamycin (17-DMAG), a heat shock protein inhibitor, administered twice weekly in patients with advanced malignancies. Euro J Cancer 2010;46:340-7.

347. Lancet JE, Gojo I, Burton M, Quinn M, Tighe SM, Kersey K, et al. Phase I study of the heat shock protein 90 inhibitor alvespimycin (KOS-1022, 17-DMAG) administered intravenously twice weekly to patients with acute myeloid leukemia. Leukemia 2010;24:699-705.

348. Jhaveri K, Taldone T, Modi S, Chiosis G. Advances in the clinical development of heat shock protein 90 (Hsp90) inhibitors in cancers. Biochim Biophys Acta 2012;1823:742-55.

349. Sydor JR, Normant E, Pien CS, Porter JR, Ge J, Grenier L, et al. Development of 17-allylamino-17-demethoxygeldanamycin hydroquinone hydrochloride (IPI-504), an anti-cancer agent directed against Hsp90. PNAS 2006;103:17408-13.

350. Oh WK, Galsky MD, Stadler WM, Srinivas S, Chu F, Bubley G, et al. Multicenter phase II trial of the heat shock protein 90 inhibitor, retaspimycin hydrochloride (IPI-504), in patients with castration-resistant prostate cancer. Urology 2011;78:626-30.

351. Jhaveri K, Ochiana SO, Dunphy MP, Gerecitano JF, Corben AD, Peter RI, et al. Heat shock protein 90 inhibitors in the treatment of cancer: current status and future directions. Expert Opin Invest Drug 2014;23:611-28.

352. Bae Y, Fukushima S, Harada A, Kataoka K. Design of environment-sensitive supramolecular assemblies for intracellular drug delivery: polymeric micelles that are responsive to intracellular pH change. Angewandte Chemie 2003;42:4640-3.

353. Kratz F, Beyer U, Schutte MT. Drug-polymer conjugates containing acid-cleavable bonds. Crit Rev Ther Drug Carrier Syst 1999;16:245-88.

354. Tian ZQ, Wang Z, MacMillan KS, Zhou Y, Carreras CW, Mueller T, et al. Potent cytotoxic C-11 modified geldanamycin analogues. J Med Chem 2009;52:3265-73.

CHAPTER 3

THERMO-TARGETED DRUG DELIVERY OF GELDANAMYCIN TO HYPERTHERMIC TUMOR MARGINS WITH DIBLOCK ELASTIN-BASED BIOPOLYMERS

3.1 Introduction

As introduced in the previous chapter, traditional chemotherapy exerts limited efficacy due in large part to poor drug solubility, formulation, off-target toxicity, and plasma instability. Polymer-drug conjugates have been proposed to improve the drug water solubility and supply multiple conjugation sites to maximize the drug loading onto a single macromolecular backbone. In addition, the large macromolecular weight constitutes a Ringsdorf model which provides additional sites for active targeting modalities or therapeutic enhancements (viz. diagnostic agents)[(1)]. Polymer-drug conjugates also display prolonged plasma half-life and may be passively targeted to tumor beds via the enhanced permeability and retention (EPR) effect alone[(2)]. However, there are still a number of limitations. Synthetic polymer delivery vehicles are often made in toxic organic solvents with long and complex postreaction purifications. Also, the reaction extent is hard to control from batch to batch, which results in variable and high polydispersity. These limitations are a primary impetus for this study.

Recombinant elastin-like polypeptide (ELP)-based biopolymers, a linear and random coiled polymer, have shown great potential in replicating the Ringsdorf model as

previously described, especially for anticancer treatment[3-5]. To date, multiple ELP-based structures have been developed[6-8]. However, this study presents a unique approach with ELP-based delivery vehicles. ELP consists of pentapeptide repeats with the monomer unit $(GXGVP)_n$ where X (guest residue) can be any amino acid except proline[9]. Without using deleterious solvents, ELP-based biopolymers are designed by protein engineering and expressed in bacteria, resulting in high yields, high purity, and low cost for industrial scale-up. In addition, ELP enjoys a modular structural design[10], easy and monodisperse synthesis, and excellent biotolerance[11], which when combined provide for rapid pre-clinical development. Most importantly, for active drug targeting, ELP boasts a unique inverse phase transition behavior upon heating; it remains water-soluble under its thermal transition temperature (T_t) ($T < T_t$), which is fully tunable by biopolymer molecular weight, ELP concentration, and guest residue composition, and collapses at $T > T_t$ forming aggregates. This temperature phase transition behavior is fully reversible and exploited as a nonchromatographical method to purify not only multiblock, ELP-based biopolymers but also fusion products with both high yields and purity[12, 13]. This unique property has been explored to achieve prolonged drug release, enhanced tumor accumulation[14, 15], and delayed tumor progression in tumor models[16]. The rapid thermal transition kinetics of ELP and ELP-based biopolymers promote an exciting course for adjuvant chemo- and/or radiotherapy in conjunction with established clinical thermal ablation or hyperthermic procedures to target the tumor margins, which are the barrier to cancer eradication for tumors > 3 cm[17].

With cancer, there is no lack of potential therapeutic targets; however, to promote additive and possibly synergistic effects with a thermal-based delivery system, heat shock

proteins (HSPs) have emerged as prime cancer targets. HSPs are shown to be upregulated in heat stressed conditions, such as hyperthermia[18, 19], and overexpressed in many cancer tissues including HCC[20-24]. HSP90 is a vital molecular chaperone for the correct folding of many oncogenic proteins such as Akt, HIF-1, mTOR, Erb2, and MMP2[25-28] and highly expressed at the tumor margins[29]. Therefore, the inhibition of HSP90, especially with concurrent application of thermal therapy, holds great potential for multitargeting various cancer signaling pathways without the complexity of drug-drug interactions, off-target effects, systemic toxicity, or multidrug resistance[27, 30]. The most potent inhibitor of HSP90 developed so far is geldanamycin (GA)[31]. However, although successful in preclinical trials, GA clinical trials have stopped due to extremely poor water solubility and hepatotoxicity[32]. A GA derivative, 17-AAG (17-allylamino-17-demethoxygeldanamycin), has been entered into clinical trials, but the formulation requires toxic Cremophor EL (CrEL) and DMSO to solubilize the drug[33]. More soluble derivatives such as 17-DMAG (17-demothoxy-N,N -dimethylaminoethylaminogeldanamycin) still suffer from non-tumor-specific targeting which requires a delivery strategy to improve its pharmacokinetic profile[34, 35]. Rather than administration of free GA or GA-derivatives, we propose a thermo-targeted biopolymer-GA delivery system to increase drug solubility, reduce off-target toxicities, and specifically target hyperthermic ablative tumor margins with application of thermal ablation lethal to the tumor core. Thermal ablation is the first line nonsurgical treatment option for most HCC patients who are not eligible for surgical resection due to impaired hepatic function[36, 37]. To enhance ablation efficiency, a positively charged, but possibly toxic copolymer K8-ELP(1-60) system was conjugated with GA with significant *in vitro*

tumor cell cytotoxicity[38]. ELP nomenclature is presented as “ELP1-n” representing the guest residue substitution (ELP1 – V5:A2:G3) and “60” the number of pentapeptide repeats. However, the relatively small number (n=8) of lysine residues limited drug loading capacities. Lysines also provided a four methylene spacer between the active functional group and biopolymer backbone, which might result in delayed drug release kinetics[5]. Furthermore, the low molecular weight of the total construct (25.4 kDa) might not provide sufficient stealth properties, thus limiting evasion of the reticuloendothelial system (RES) and the degree of EPR targeting. Last but not least, the positive charges trigger natural defense of bacteria which results in very poor yields. Here, we present the first generation of ELP-based biopolymers is comprised of 15 aspartic (D) or 15 glutamic acids (E) and ELP(1-60/90/180) block. E15-ELP(1-90) was chosen as the initial candidate for GA conjugation due to its higher T_t ~ 40°C (pertinent to microwave antenna *in silico* and *ex vivo* data at T > 40^{o}C, peripheral isotherms > 3 cm away from the microwave antenna (data not shown)); a sublethal temperature but sufficiently adequate for thermo-sensitive chemotherapy via E15-GA-ELP(1-90) biopolymer-conjugates). A covalent, pH-sensitive hydrazone bond was designed to release GA specifically within the acidic tumor microenvironment or within the acidic endosomes or late lysosomes of tumor cells[38], which is yet another active targeting modality against the tumor margins. We were able to obtain covalently conjugated GA in nearly 50-67% capacity while retaining thermo-responsive properties to target hyperthermic tumor margins with clinically established ablation.

3.2 Materials and methods

3.2.1 Materials

Oligonucleotides were synthesized at the Research Core Facility, University of Utah (UU). DH5α cells and fetal bovine serum (FBS) were purchased from Invitrogen (Carlsbad, CA); pET25b+ expression vector and *E. coli* BLR (DE3) strains were obtained from Novagen (Madison, WI). T4 DNA ligase, restriction enzymes, calf intestinal alkaline phosphatase (CIP), and pUC19 cloning vector were purchased from New England Biolabs (Beverly, MA). Circle-Grow culture medium was purchased from Q-BIOgene (Carlsbad, CA). Geldanamycin (GA) was obtained from LC Laboratories (Woburn, MA) and structure confirmed upon receipt by ^{1}H-NMR. Carbenecillin sodium salt was purchased from ISC Bioexpress (Kaysville, UT). Aminoacetaldehyde diethyl acetal (AAADA), chloroform, carbohydrazide, 1-ethyl-3-(3-dimethylaminopropyl) carbodiimide (EDC)·HCl, sulfo-*N*-hydroxysuccinimide (NHS), and dimethyl sulfoxide (DMSO) were from Sigma-Aldrich (Milwaukee, WI) and used as received.

3.2.2 Construction of diblock biopolymers: D15- or E15-ELP(1-60/90/180)

First, oligos encoding 15 aspartic (D15) or 15 glutamic (E15) acids were designed with ApE software, optimized for bacterial expression, and synthesized by the UU Core Facility:

- D15 forward: 5’-gtggacgatgatgacgatgatgatgacgatgatgatgacgatgatgatggtggc-3'
- D15 reverse: 5'-accatcatcatcgtcatcatcatcgtcatcatcatcgtcatcatcgtccacgcc-3'
- E15 forward: 5'-gtggaggaagaagaggaagaagaagaggaagaagaagaggaagaagaaggtggc-3'
- E15 reverse: 5'-accttcttcttcctcttcttcttcctcttcttcttcctcttcttcctccacgcc-3'

The oligos were annealed to form a double-stranded DNA cassette with *Pfl*MI compatible ends at the 5'. Second, ELP(1-60/90/180) were polymerized from ELP(1-10), where “1” stands for a “X” guest residue substitution of V5:A2:G3, “10” represents 10 amino acids in total, through recursive directional ligation (RDL)[39]. Both agarose gel electrophoresis and DNA sequencing verified correct insertions. The validated ELP(1-60/90/180) pUC19 plasmids were further digested with *Pfl*MI restriction enzymes, dephosphorylated by CIP, and ligated with annealed D15/E15 oligos. The cloning scheme starting from the ELP homopolymer is illustrated in **Figure 3.1**. Sequence verified plasmids were transformed into DH5α cells by heat shock. After amplification at 37°C overnight, plasmids were purified using a QIAGEN Miniprep Kit (Valencia, CA), double digested with *Nde* I and *HinD* III, and ligated to compatible pET25b+ expression vectors to yield D15- or E15-ELP(1-60/90/180) expression vectors. The expression vectors were transformed into *E. coli* BLR (DE3) strain by heat shock. The diblock copolymers were expressed at 37°C for 9 h at 230 rpm, followed by shaking incubation at room temperature for another 15 h. After the removal of cell lysate by centrifugation and sonication, the diblock biopolymers were purified by inverse transition cycling (ITC) [40] with pH adjustment to neutral using 1M HCl before the first hot spin. The purity and molecular weight of the biopolymers were confirmed by tris-glycine SDS-PAGE and mass spectrometry analysis. The biopolymers were lyophilized and stored at -20°C for future use.

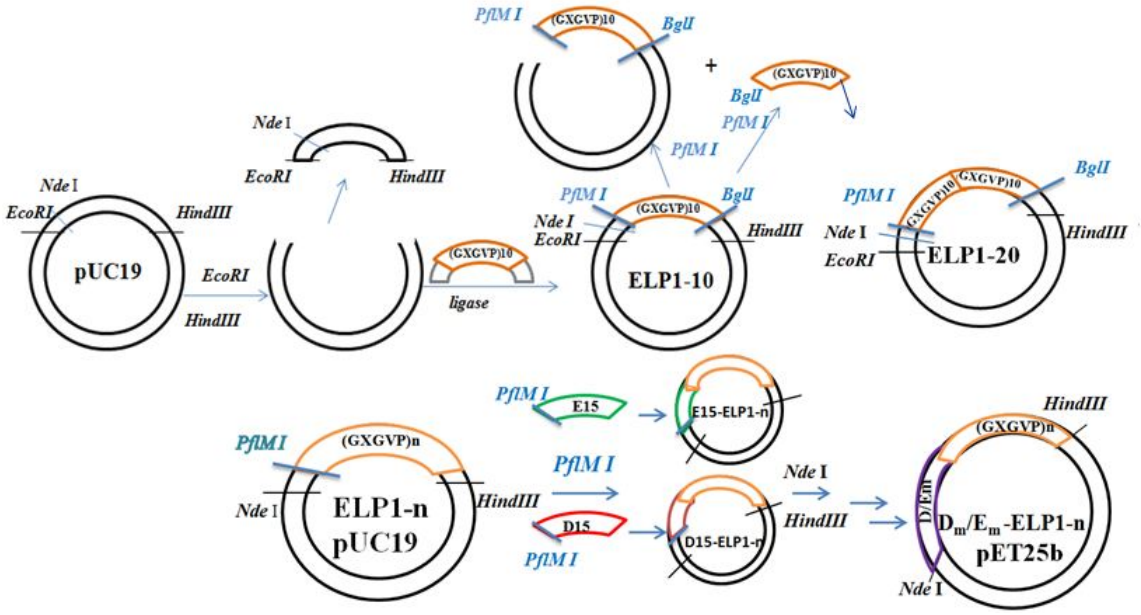

Figure 3.1. A typical round of RDL for homopolymer cloning.

"1" stands for a "X" guest residue substitution of V5:A2:G3, "n" stands for total number of amino acids comprising ELP, "m" indicates total aspartic(D)/glutamic(E) acid repeats. Further insertion of D/E15 components was realized using *PflM*I restriction enzyme. The final construct was transferred to a pET25b+ plasmid for expression.

3.2.3 Thermal transition temperature profile of D15/E15-ELP (1-60/90/180) diblock biopolymers

Inverse phase transition is the key parameter to realize thermo-targeted drug delivery. It has been demonstrated that the thermal transition temperature (T_t) of the ELP homopolymers is affected by ELP length, concentration, and hydrophobicity[39]. This generation of ELP-based diblock biopolymers is entirely unique with the addition of 15 consecutive hydrophilic amino acids; hence, thermal transition profiles demonstrate new features distinct from ELP homopolymers. The T_t as a function of ELP length, concentration, and pH was measured using a CARY 100-Bio UV-Vis spectrophotometer (Palo Alto, CA). The optical density at 650 nm was monitored at 1°C/min temperature increments in the range of 25-75°C. The T_t was determined as the temperature at the maximum derivative of turbidity at the wavelength of 650 nm. This wavelength was chosen to avoid the influence of high absorption from GA.

3.2.4 Activation of geldanamycin (GA) and D15-ELP(1-60) and E15-ELP(1-90) biopolymers

GA is a potent HSP90 inhibitor extracted from *Streptomyces hygroscopicus*[41]. To retain biofunctionality following bond cleavage from the biopolymers, the 17-methoxy was converted to an aldehyde using amino acetaldehyde diethyl acetal (AAADA) as described elsewhere[42]. The final purple colored product was washed with anhydrous chloroform, which was eliminated by overnight rotary evaporation. Product purity was confirmed by TLC and ^{1}H-NMR (d_6-DMSO). The carboxyl groups of the diblock biopolymers were converted to amines using carbohydrazide. Briefly, freeze-dried copolymers were dissolved in 0.1M sodium phosphate buffer (10-20 mg/mL)

supplemented with 32 mg/mL carbohydrazide. EDC (50 mM) and sulfo-NHS (5 mM) were then added and stirred at room temperature (450 rpm) for 4 h. The activated diblock copolymers were purified by size exclusion chromatography (SEC) using a PD-10 column eluted with water. Products were lyophilized and stored at -20°C.

3.2.5 Hydrazone conjugation of GA to ELP-biopolymers

25 mg of activated diblock biopolymer was mixed with activated GA-aldehyde (molar ratio 1:2) in anhydrous DMSO, as shown in **Figure 3.2.** The reaction mixture was stirred at 23°C for three days and the product was then dialyzed in water for two days to eliminate residual solvent. Insoluble GA-aldehyde was further removed by both centrifugation and PD-10 SEC. The final conjugated product was lyophilized for future characterization. The GA:biopolymer conjugation ratio was determined by a UV-Vis calibration curve and further confirmed by MS. To reduce the space for nomenclature, we will use GA-D15-n or GA-E15-n for GA diblock biopolymer conjugates with hydrazone linkages, where "n" stands for the total number of total amino acids for ELP(1-n) library (60 or 90).

3.2.6 Physical stability of GA- ELP biopolymer conjugates

3.2.6.1 Particle size distribution and zeta potential analysis

Diblock biopolymer and GA conjugates were dissolved in 0.8 mL PBS and purified through a 0.2 μm filter with the final concentration ranging from 10-25 μM determined by a UV-Vis calibration curve. Particle size was measured at 25°C using a BI-200SM, dynamic light scanning (DLS) system (Holtsville, NY). Particle size was also measured in PBS containing 20% FBS to mimic *in vivo* stability. Particle size distribution was

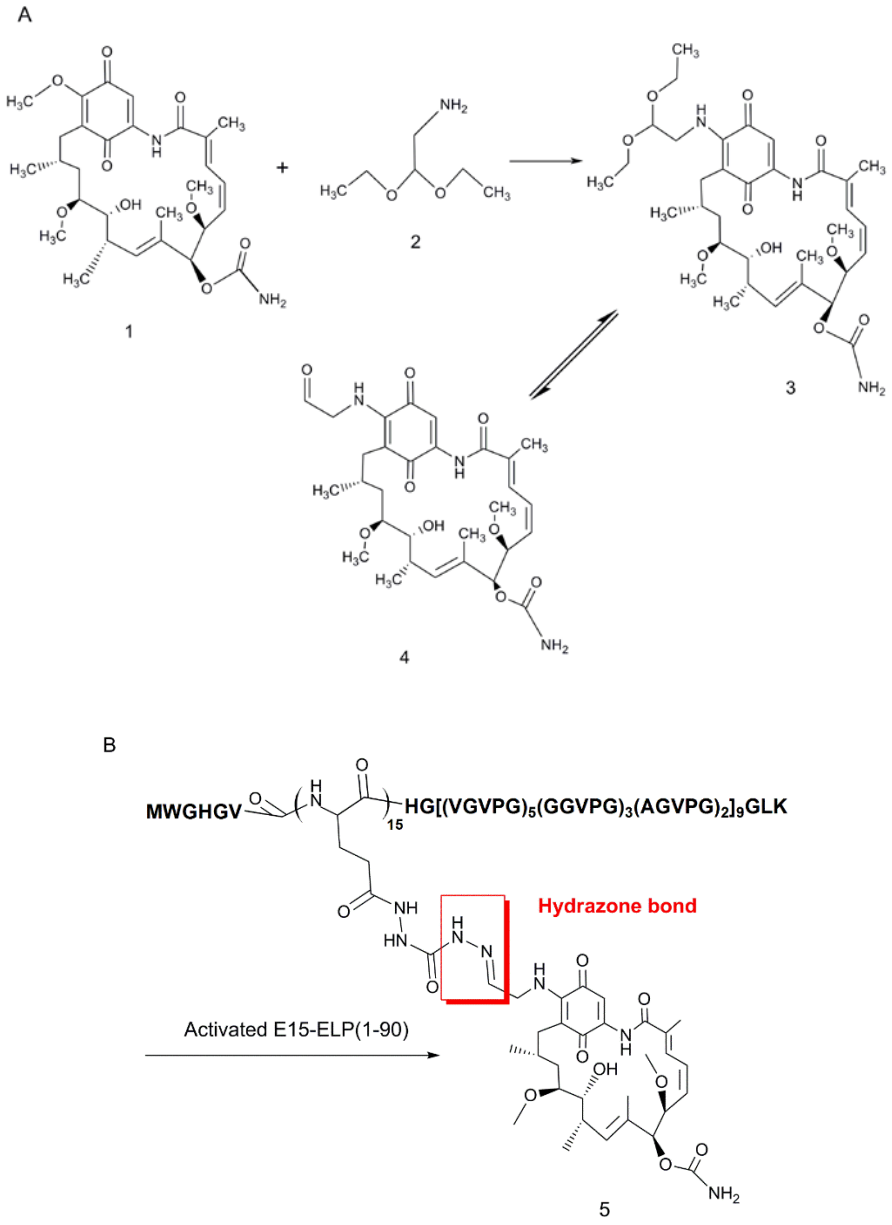

Figure 3.2. Chemical schemes of geldanamycin (GA) activation.

(A) GA activation and conjugation with E15-ELP(1-90) through pH-sensitive hydrazone linkages (B). 1, Geldanamycin (GA); 2, aminoacetaldehyde diethyl acetal (AAADA); 3, acetal modified GA by-products; 4, aldehyde-modified GA (GA-CHO); and 5, GA-E15-90.

further validated by transmission electron microscopy (TEM). Briefly, small drops of purified biopolymers and conjugate solutions (25 μM) were air-dried on carbon-coated copper electron microscopy grids for 10 min. Protein nanoparticles were negatively stained with 2% phosphotungstic acid for 30 s and excess liquid was removed by filters. Grids were examined in a TEM (PHILIP) at 120 kV and resulting images were acquired by a charge-coupled digital camera. Concurrently, the zeta potential of the biopolymer-GA drug conjugates was measured at the same conditions using a ZetaPALS zeta potential analyzer at 25^{o}C (Holtsville, NY). Data for both sets represent three independent trials.

3.2.6.2 Thermal transition profile of biopolymer-GA conjugates

The hydrophobicity of the GA directly affects the macromolecular assembly of the biopolymer-GA conjugates; therefore, the thermal transition behavior at the same ELP length and concentration would be expected to be different. The thermal responses of conjugates were measured both in PBS and 20% FBS as monitored by UV-Vis at wavelength of 650 nm.

3.2.7 Drug release profile of GA- ELP biopolymer conjugates

The pH release kinetics at both acidic and neutral pH were performed on an Alliance RP-HPLC equipped with an absorbance reader. 25 μM GA-E15-90 samples (concentration based on the ELP) were prepared in 1 mL of PBS at pH 4.5 or pH 7 and were shaken at 37°C or 45°C at 180 rpm . 100 μL samples (cooled on ice first) were loaded at 0, 3, 6, 12, 24, 48, and 72 h with a 75 μL injection volume. GA-E15-90 and free GA were separated on a diphenyl column (Waters) using a H_2O/90% DCM gradient with

0.1% v/v TFA. Initially, the binary gradient was 70:30 for 10 min at which point the 90% DCM concentration was raised to 60% over 30 min followed by a static 10 min period. The flow rate was 1.0 mL/min. Percent of GA release as a function of time was based upon a drop in the GA-E15-90 peak area percent, normalized to the 0 h time point[5]. These runs were repeated three times for each GA-E15-90 conjugate.

3.3 Results and discussion

An ELP(1-n) library starting from the ELP(1-10) monomer was successfully cloned using the RDL approach, as delineated in **Figure 3.3**. Insertion of D15 or E15 blocks was confirmed by an additional sequencing step in both the pUC19 vector, and the subsequently subcloned pET25b+ vector, which was eventually transformed and allowed to express proteins in BLR (DE3) cells. The typical purification steps of E15-ELP(1-90) diblock copolymer are described in **Figure 3.4**. A slight modification was made before the first hot spin step due to the insertion of ample carboxyl groups, whose protonation creates a stiff hydrogen bonding block leading to higher transition temperatures. Typically, two rounds of ITC were sufficient to obtain products with high purity, as suggested by the SDS-PAGE. Due to the random coil, linear structure of the polypeptide, ELP-based biopolymers showed higher molecular weights than expected (>40 kDa estimated by the gel); therefore, the precise molecular weight was further validated by electro-spray ionization mass spectrometry (ESI-MS) (**Figure 3.5**). Using the simple and efficient purification methods, a large library of ELP diblock copolymers was constructed and summarized in **Table 3.1**.

The ELP diblock biopolymers displayed interesting thermal transition behaviors. **Figure 3.6A** demonstrated that T_t was not a function of concentration for D15-ELP(1-60),

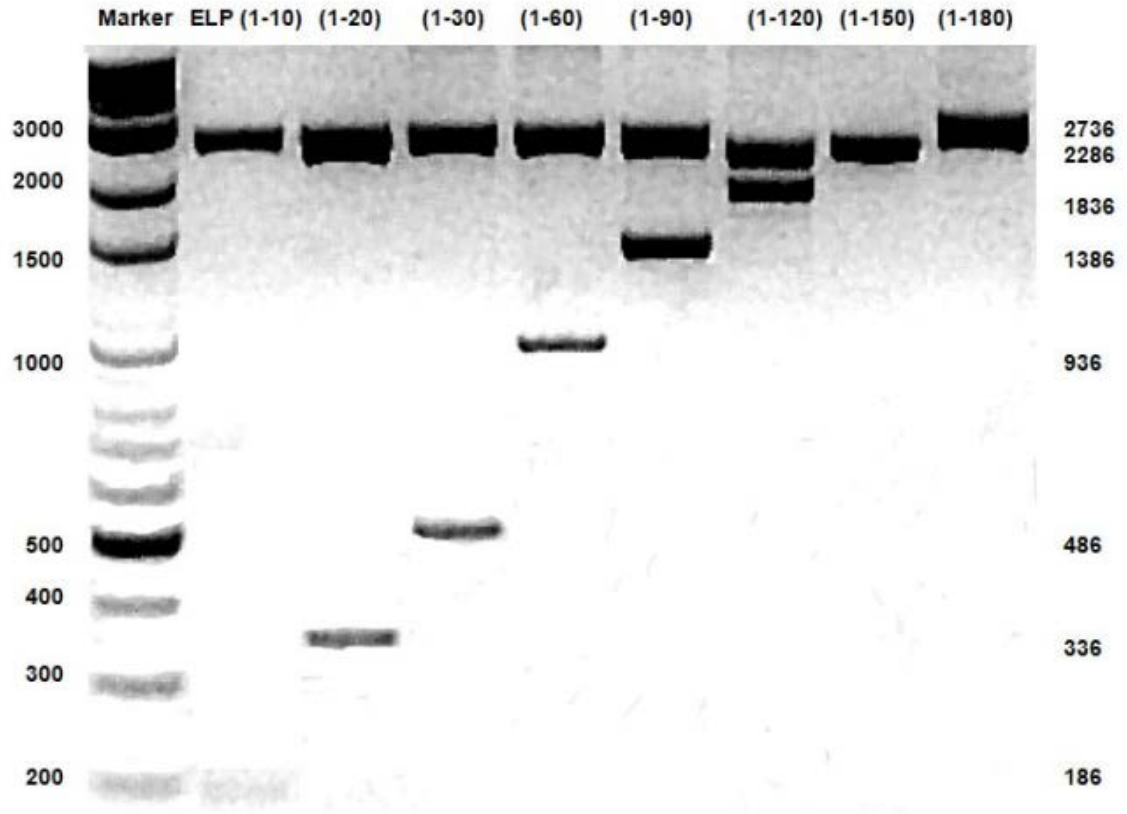

Figure 3.3. ELP(1-n) homopolymer libraries.

The expected band lengths are denoted at the right panel of the gel picture. Gel composition and running conditions: 1.8% agarose, 70V, 3 h.

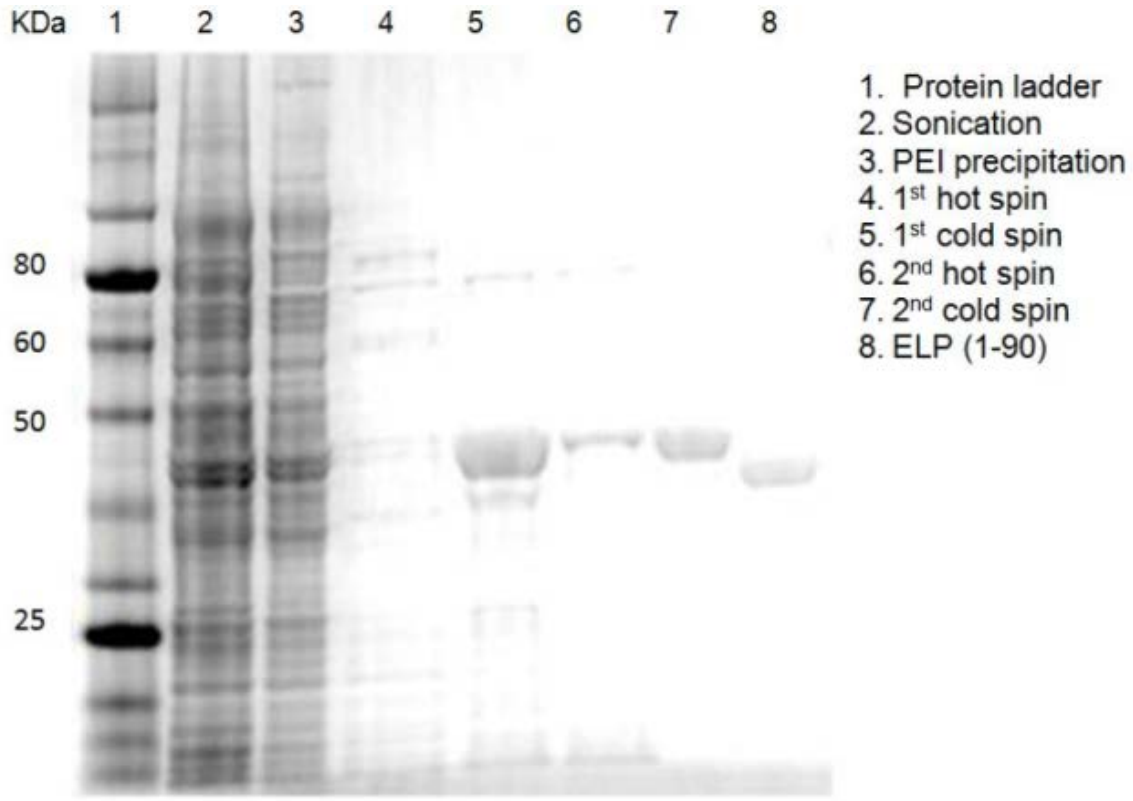

Figure 3.4. A typical 4-20% Tris-glycine SDS-PAGE of E15-ELP(1-90).

Gel was run at 90 V for 150 min stained with Invitrogen safeblue®. Samples from lanes 2-7 were taken after each purification step designated in the box. ELP(1-90) was also loaded as a control for purity verification. A MW shift indicates the insertion of the new poly(E) block.

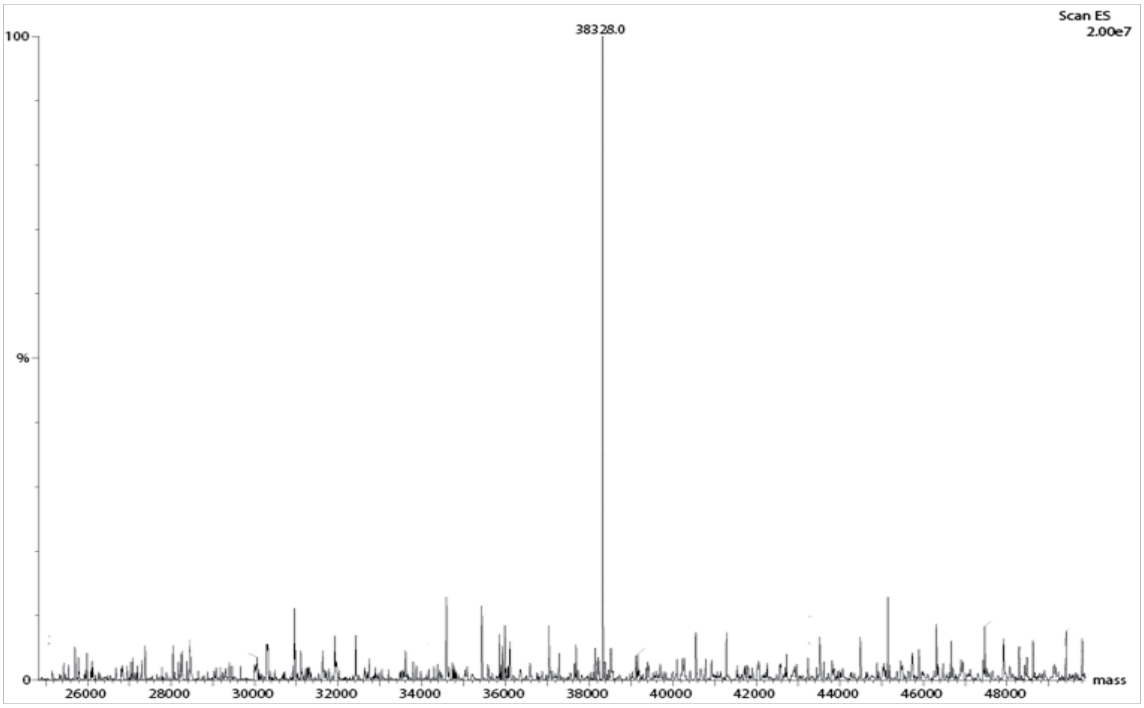

Figure 3.5. Electrospray ionization mass spectrometry (ESI-MS) of E15-ELP(1-90).

The molecular weight is in accordance with the expected value (38328.6 Da).

Table 3.1. Summary of ELP-based diblock copolymers expressed.

Biocopolymer amino acid sequence	**Monomers**	**Mw (KDa)**	**Yields (mg/L culture)**	**Tt [a](°C) (25μM)**
MWGHGV-$(E)_m$-H-$(GXGVP)_n$-GGLK	m (15) n (90,180)			
$(E)_m$-ELP(1-*n*)	E15-(1-90)	38.3	15	35.5
	E15-(1-180)	73.5	20	33.0
MWGHGV-$(D)_m$-H-$(GXGVP)_n$-GGLK	m (15); n(60, 90,180)			
$(D)_m$-ELP(1-*n*)	D15-(1-60)	26.3	15	39.1
	D15-(1-90)	38.1	20	37.0
	D15-(1-180)	73.2	40	34.0

[a]Transition temperatures were calculated at normalized concentration of 25 μM in PBS

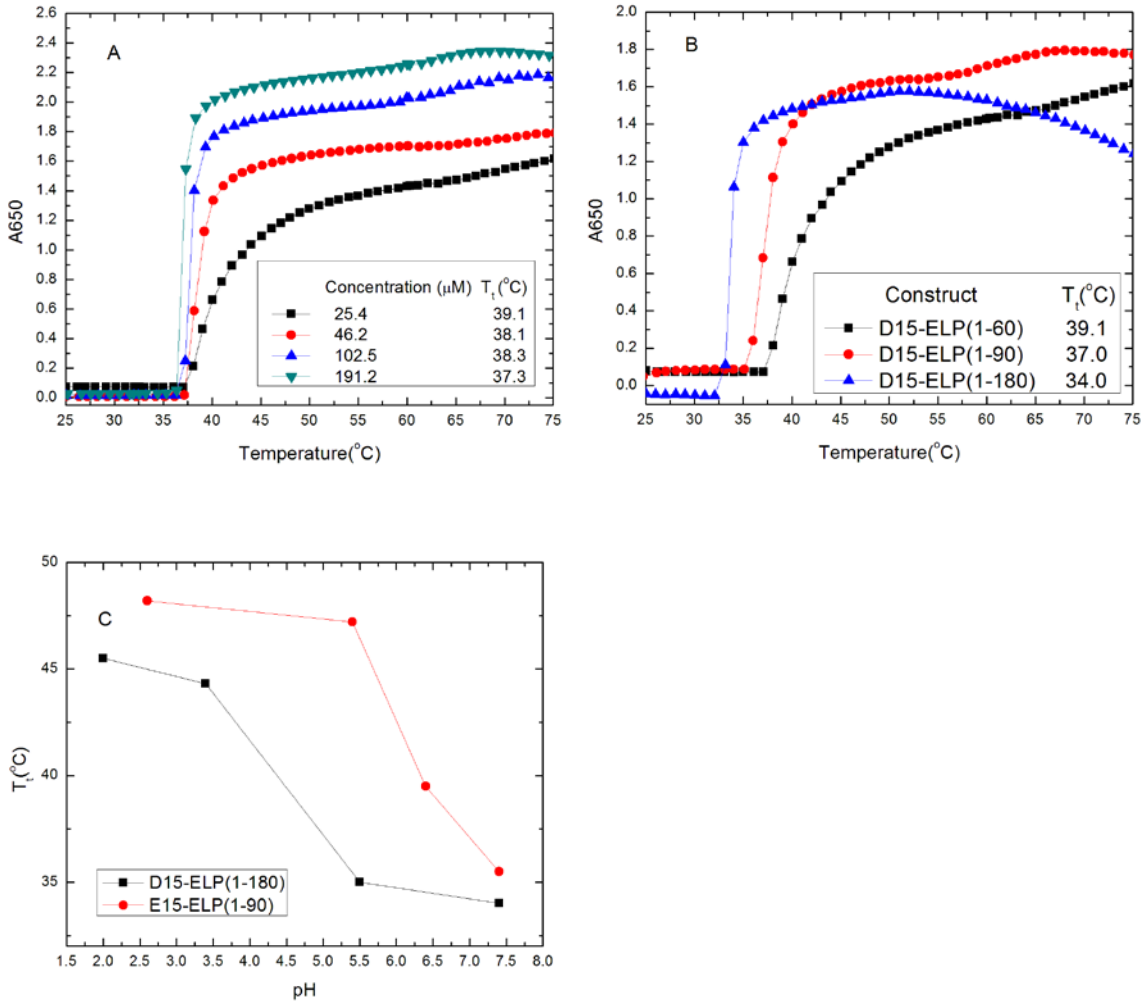

Figure 3.6. Temperature transition behaviors of ELP-diblock copolymers.

(A) T_t under different concentrations of D15-ELP(1-60); (B) T_t as function of molecular weight; (C) pH influence on T_t. Both D15-ELP(1-180) and E15-ELP(1-90) display the same pattern of increased T_t at lower pH. All measurements were conducted at 25 μM in PBS (pH7.4, 147 mM), n=3.

or any other copolymers we have made, which is not the case for ELP alone[43]. We propose that the addition of 15 more hydrophilic amino acids promotes the self-assembly of the copolymer to a micelle-like structure, where the intramolecular hydrophobic interactions are greatly enhanced. This hypothesis remains to be validated. The proposal is further supported by the DLS data and TEM image in **Figure 3.7** where spherical structures with size ca. 50 – 100 nm were observed. On the other hand, T_t remains a function of molecular weight suggested by **Figure 3.6B** – T_t dropped as the length of ELP-block increased. T_t shows strong dependence on pH where T_t increased with the decrease of pH values (**Figure 3.6C**) except for the point approximate to the pKa of glutamic/aspartic acid where precipitation might occur to reduce the apparent concentration. We believe that the ample carboxyl groups exposed to the water interface can form stiff intermolecular hydrogen bonds that require more heat to destabilize the supramolecular self-assembled structures.

Drug conjugation ratios of GA-conjugates were confirmed by UV spectrometry and MS. As shown in **Figure 3.8**, GA-E15-90 showed a significant increase in UV absorbance at 337 nm, which is the distinctive absorption peak for GA-CHO. The drug loading was calculated using a calibration curve of both GA-CHO and ELP diblock biopolymers. We show 46-67% of the available sites successfully conjugated onto the D/E side chains. Drug content was further confirmed by MALDI-TOF MS where a significant shift of the molecular weight was obtained (**Figure 3.8**). Since the GA-CHO is very hydrophobic, the high drug conjugation ratio could facilitate a core-shell self-assembly of the conjugate, where the drug is shielded in a hydrophobic core away from the aqueous milieu, while the ELP homopolymer blocks are exposed to the water

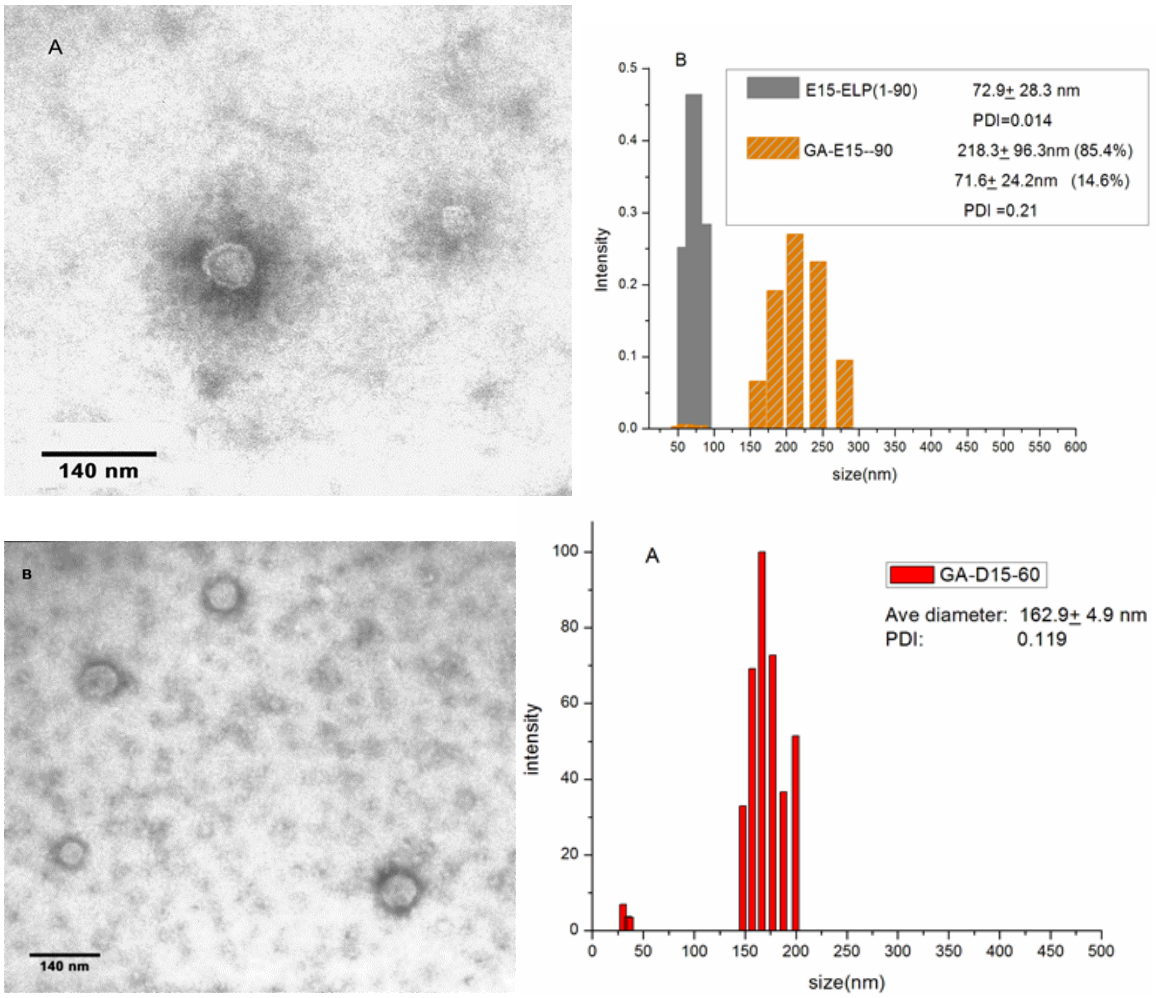

Figure 3.7. Morphology and size distribution of polymer and conjugates by DLS and TEM.

(A) TEM images of Native copolymer E15-ELP (1-90) shows a particle size (50-100 nm). (B) TEM images of GA-D15-60 (100-150 nm). (C) Size distributions of E15-ELP(1-90) copolymer and GA-E15-90 conjugate. (D) Size distributions of GA-D15-60 conjugate; All samples were measured three times in PBS (25 μM), data represented with standard error of the mean at 25 °C. Particle sizes lower than that obtained from dynamic light scattering (DLS) presumably due to dehydration.

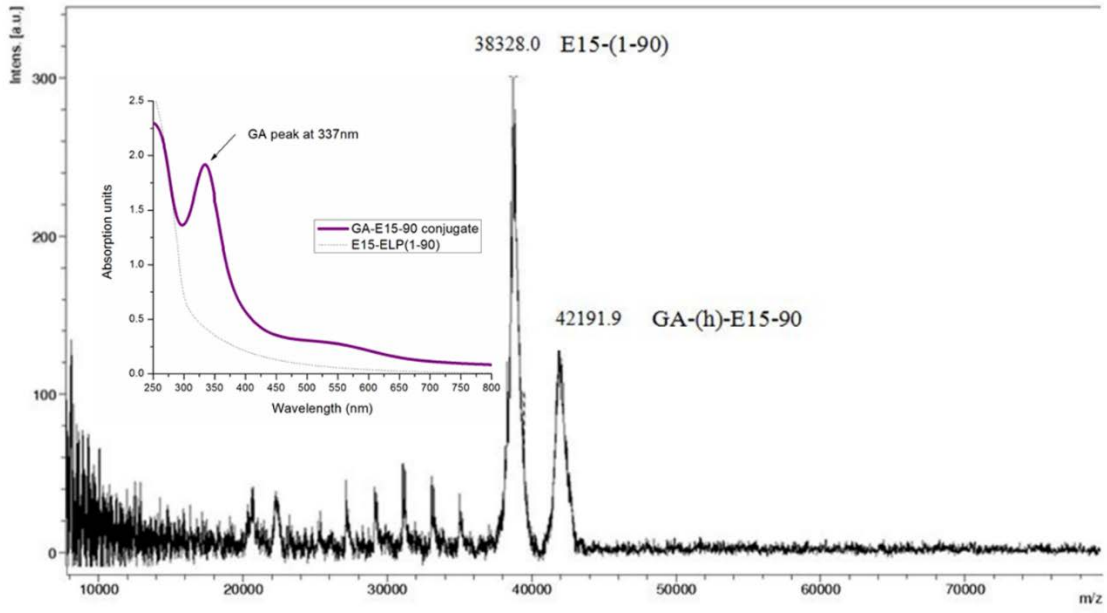

Figure 3.8. MALDI-TOF mass spectrometry and UV-Vis profile of GA-E15-90 conjugate.

GA-CHO has a peak wavelength at 337 nm. The distinct peak of conjugates demonstrated a high conjugation ratio of GA-CHO to the activated ELP bio-copolymer. The molecular weight shift on the MALDI TOF confirmed that approximately seven GA molecules were conjugated per ELP-biopolymer (9.2 wt %). All samples were measured at 25 °C.

interface. We have observed that higher drug conjugation ratios result in a narrower size distribution, as seen in **Figure 3.7D**, where 10 out of 15 available hydrazides on the activated D15-ELP(1-60) were occupied by GA-CHO; whereas the E15-ELP(1-90) counterpart, which has 20% less degree of conjugation, demonstrated a higher poly-dispersity, as indicated in **Figure 3.7C**. Both constructs displayed a slightly positive charge (+2.6 - 3.3mV), suggesting high drug conjugation and stable nanostructures have been formed. The ample carboxyl group exposed to the water resulted in a negative surface charge (-20 ± 2.9 mV) of ELP diblock biopolymer. After activation with the carbohydrazide, the zeta potential was converted to the positive by the attached amine groups (+16 ± 3.3 mV) not conjugated to GA. The charges were further reduced through the conjugation of multiple GAs which form neutral hydrazone bonds. It has been shown that nanoparticles with slight surface charge achieve higher accumulation in tumors[44] as well as less systemic aggregation[45, 46]. We are optimizing the preparation methods to engineer even smaller nanoparticles.

The transition profiles of the GA conjugates are summarized in **Figure 3.9**. Similar independence of concentration on T_t was observed for all three conjugates; however, a moderate concentration of conjugate (> 25 μM) may be needed to ensure fast transition kinetics. As the molecular weight of the ELP block decreases, a higher T_t was obtained. The influence of serum on the transition behavior is reported in **Figure 3.10**. The transition kinetics were slightly slower due to the mixed population proteins; however, it is to our advantage that the T_t increases after the addition of serum which reaches hyperthermic temperature (> 41°C). In order to test the reproducibility of the thermal transition, we conducted two consecutive thermal runs under the same experimental

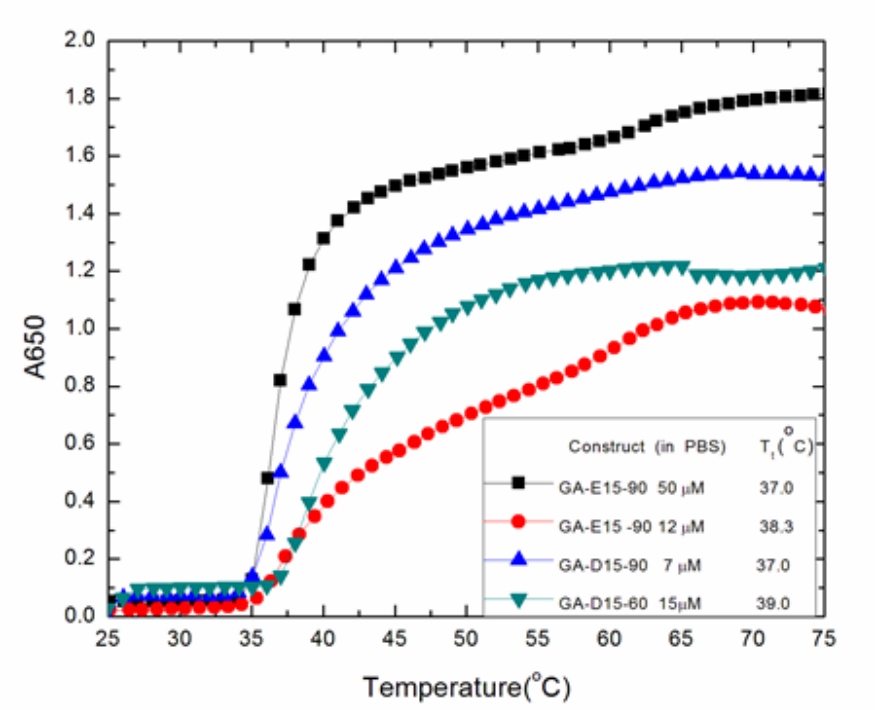

Figure 3.9 Thermal transition behavior of GA-polymer conjugates.

For GA-E15-90, 50 μM is sufficient for rapid thermal kinetics. The effect of concentration on T_t is again not pronounced, which is similar to the effect on the ELP copolymer. T_t can be increased by shortening the ELP block length (less intermolecular hydrophobic interaction).

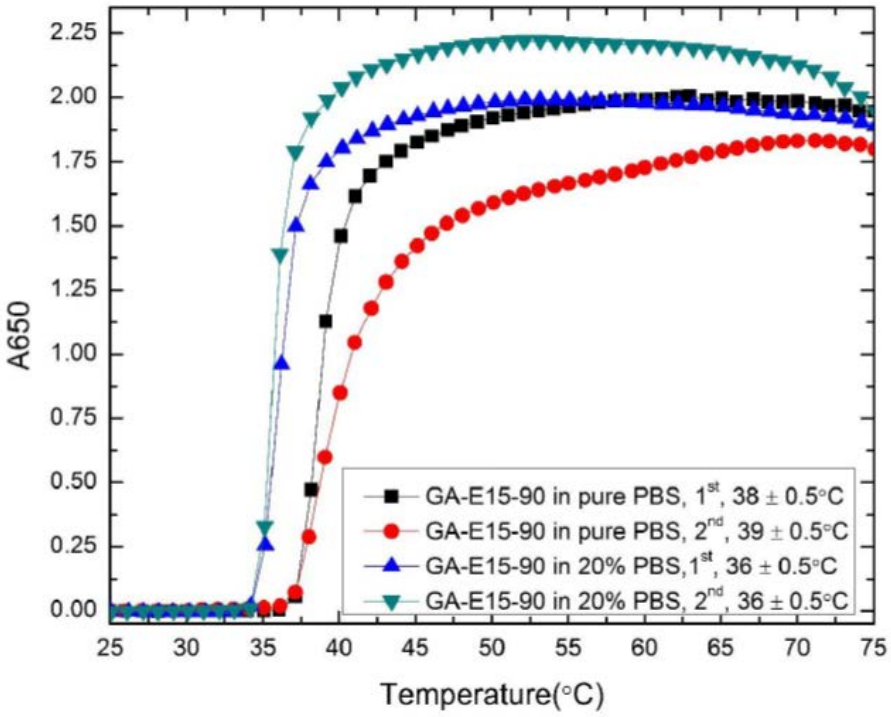

Figure 3.10 Thermal transition behavior of GA-E15-90 in 20% serum.

Comparable kinetics have been achieved with lowered Tt. The thermal profile was repeated once under the same conditions (2nd runs). Similar thermokinetics and Tt have been achieved. All conjugates contain 25μM equivalent ELP in PBS (147 mM), n=3.

conditions. The second thermal transition is affected by the serum due to some aggregation of ELP with serum proteins as suggested by the downscan of the first run. However, the thermal kinetics are still retained despite the presence of serum. Rapid aggregation of ELP can be achieved simply by increasing the concentration of the conjugates. Further studies are ongoing evaluating the length of polyD/E and ELP composition to tailor the transition temperature by promoting intramolecular hydrophobic interactions.

The release of GA-CHO as a function of time from copolymer conjugates was assessed in PBS buffer at pH 4.5 and pH 7.4. GA-E15-90 (R_t 26 min), ELP copolymer (R_t 22 min), and free GA-CHO (R_t 18 min) can be separated using the binary gradient in a 52 min run. By calculating the percentage drop in the GA-E15-90 peak area, over 60% GA is considered to be released from the ELP backbone, while only about 20% of GA is released at neutral pH over the three-day time frame (**Figure 3.11**). Initial burst releases were observed at both pH, which can be attributed to physically-bound free drugs. In order to understand the release kinetics at hyperthermic conditions, we also conducted release study at 45 °C at both pH for three days. The release is almost complete at pH 4.5 with much faster kinetics than the release at the 37 °C. Interestingly, the release at neutral pH is also greatly increased by the high temperature. It has been found that hydrolysis kinetics of hydrazone is much higher at high temperatures[47-49]. Kovaríková *et al.* have also demonstrated that the break-down rate of hydrazone bonds increases 3-fold at 40 °C[50]. The significant release at even neutral pH will not cause unwanted side effects since the drug is still released at ablated/tumor margins where the particles have hydrophobically aggregated. We are optimizing the ELP structures to achieve even faster

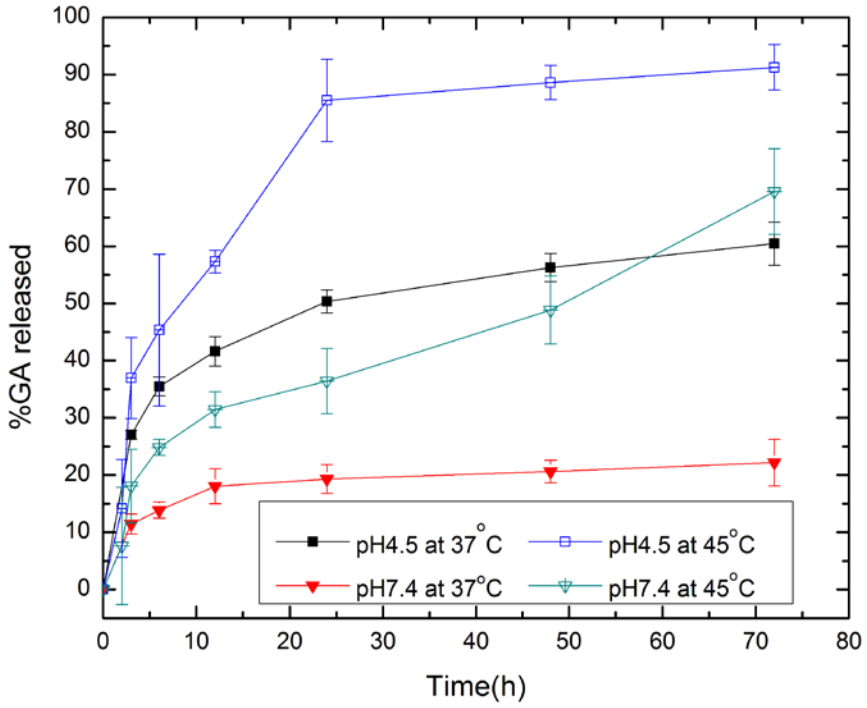

Figure 3.11 GA release from GA-E15-90 (25 μM in PBS) as function of time.

Release profile at pH 4.5 and pH 7.4, under both normothermia (37 °C) and hyperthermia (45°C), were recorded. Data reported as mean ± S.D., n =3.

drug release at 45 °C under the presence of serum. The fast kinetics at high temperature will ensure an acute killing of cancer cells before the expression of heat shock proteins which might account for focal, local-regional tumor recurrence.

3.4. Conclusion

We have successfully constructed a new breed of ELP-based diblock copolymers featuring poly glutamic/aspartic acids for facile drug conjugation and thermo-targeted chemotherapy of hyperthermic tumor margins. D15/E15-ELP(1-60/90) polymers were conjugated with GA-CHO and high drug loadings were achieved with retained thermo-responsiveness and particle stability with a unimodal size distribution. The addition of serum proteins does not significantly perturb the thermal transition behavior. Thus, the ELP-based polymer-GA conjugates demonstrate great potential for thermo-targeted chemotherapy of the tumor margins and inhibition of HSP90 at these sites with further synchronous use of thermal ablation. Active targeting will result by thermal precipitation of the biopolymer-GA conjugates at hyperthermic isotherms T > 40°C (verified by *in silico* and *ex vivo* correlation) and pH-sensitive drug release within the acidic tumor microenvironment; passive targeting may occur by the putative EPR effect. A preliminary animal model, a VX2 rabbit model, was used to evaluate the anticancer effects of diblock ELP-GA conjugates and the results are provided in Appendix B. Some palliative effect was observed in a limited number of animals but lung embolus also occurred which require conjugates with a higher Tt. Therefore, an improved design of ELP polymer was introduced with more detailed information provided in Chapter 4.

3.5 References

1. Sternglanz H, Bugg CE. Relationship between the mutagenic and base-stacking properties of halogenated uracil derivatives. The crystal structures of 5-chloro- and 5-bromouracil. Biochim Biophys Acta 1975;378:1-11.

2. Matsumura Y, Maeda H. A new concept for macromolecular therapeutics in cancer chemotherapy: mechanism of tumoritropic accumulation of proteins and the antitumor agent smancs. Cancer Res 1986;46:6387-92.

3. McDaniel JR, Callahan DJ, Chilkoti A. Drug delivery to solid tumors by elastin-like polypeptides. Adv Drug Deliv Rev 2010;62:1456-67.

4. Bidwell GL, 3rd, Davis AN, Raucher D. Targeting a c-Myc inhibitory polypeptide to specific intracellular compartments using cell penetrating peptides. J Control Release 2009;135:2-10.

5. Furgeson DY, Dreher MR, Chilkoti A. Structural optimization of a "smart" doxorubicin-polypeptide conjugate for thermally targeted delivery to solid tumors. J Control Release 2006;110:362-9.

6. Osborne JL, Farmer R, Woodhouse KA. Self-assembled elastin-like polypeptide particles. Acta Biomater 2008;4:49-57.

7. Wright ER, Conticello VP. Self-assembly of block copolymers derived from elastin-mimetic polypeptide sequences. Adv Drug Deliv Rev 2002;54:1057-73.

8. Bessa PC, Machado R, Nurnberger S, Dopler D, Banerjee A, Cunha AM, et al. Thermoresponsive self-assembled elastin-based nanoparticles for delivery of BMPs. J Control Release 2010;142:312-8.

9. Chilkoti A, Dreher MR, Meyer DE. Design of thermally responsive, recombinant polypeptide carriers for targeted drug delivery. Adv Drug Deliv Rev 2002;54:1093-111.

10. Sallach RE, Cui W, Wen J, Martinez A, Conticello VP, Chaikof EL. Elastin-mimetic protein polymers capable of physical and chemical crosslinking Biomaterials. 2009;30:409-22.

11. Woodhouse KA, Klement P, Chen V, Gorbet MB, Keeley FW, Stahl R, et al. Investigation of recombinant human elastin polypeptides as non-thrombogenic coatings. Biomaterials 2004;25:4543-53.

12. Wu WY, Mee C, Califano F, Banki R, Wood DW. Recombinant protein purification by self-cleaving aggregation tag. Nat Protoc 2006;1:2257-62.

13. Christensen T, Amiram M, Dagher S, Trabbic-Carlson K, Shamji MF, Setton LA, et al. Fusion order controls expression level and activity of elastin-like polypeptide fusion proteins. Protein Sci 2009;18:1377-87.

14. Liu W, Dreher MR, Furgeson DY, Peixoto KV, Yuan H, Zalutsky MR, et al. Tumor accumulation, degradation and pharmacokinetics of elastin-like polypeptides in nude mice. J Control Release 2006;116:170-8.

15. Dreher MR, Liu W, Michelich CR, Dewhirst MW, Chilkoti A. Thermal cycling enhances the accumulation of a temperature-sensitive biopolymer in solid tumors. Cancer Res 2007;67:4418-24.

16. Liu W, MacKay JA, Dreher MR, Chen M, McDaniel JR, Simnick AJ, et al. Injectable intratumoral depot of thermally responsive polypeptide-radionuclide conjugates delays tumor progression in a mouse model. J Control Release 2010;144:2-9.

17. Lencioni R, Crocetti L, De Simone P, Filipponi F. Loco-regional interventional treatment of hepatocellular carcinoma: techniques, outcomes, and future prospects. Transpl Int 2010;23:698-703.

18. Hashim IA. Clinical biochemistry of hyperthermia. Ann Clin Biochem 2010;47:516-23.

19. Rylander MN, Feng Y, Bass J, Diller KR. Thermally induced injury and heat-shock protein expression in cells and tissues. Ann N Y Acad Sci 2005;1066:222-42.

20. Yano M, Naito Z, Tanaka S, Asano G. Expression and roles of heat shock proteins in human breast cancer. Jpn J Cancer Res 1996;87:908-15.

21. Senju M, Sueoka N, Sato A, Iwanaga K, Sakao Y, Tomimitsu S, et al. Hsp90 inhibitors cause G2/M arrest associated with the reduction of Cdc25C and Cdc2 in lung cancer cell lines. J Cancer Res Clin Oncol 2006;132:150-8.

22. Schwock J, Pham NA, Cao MP, Hedley DW. Efficacy of Hsp90 inhibition for induction of apoptosis and inhibition of growth in cervical carcinoma cells in vitro and in vivo. Cancer Chemother Pharmacol 2008;61:669-81.

23. Williams CR, Tabios R, Linehan WM, Neckers L. Intratumor injection of the Hsp90 inhibitor 17AAG decreases tumor growth and induces apoptosis in a prostate cancer xenograft model. J Urol 2007;178:1528-32.

24. Sun Y, Zang Z, Xu X, Zhang Z, Zhong L, Zan W, et al. Differential proteomics identification of HSP90 as potential serum biomarker in hepatocellular carcinoma by two-dimensional electrophoresis and mass spectrometry. Int J Mol Sci 2010;11:1423-33.

25. Whitesell L, Lindquist SL. HSP90 and the chaperoning of cancer. Nat Rev Cancer 2005;5:761-72.

26. Eustace BK, Sakurai T, Stewart JK, Yimlamai D, Unger C, Zehetmeier C, et al. Functional proteomic screens reveal an essential extracellular role for hsp90 alpha in cancer cell invasiveness. Nat Cell Biol 2004;6:507-14.

27. Bohonowych JE, Gopal U, Isaacs JS. Hsp90 as a gatekeeper of tumor angiogenesis: clinical promise and potential pitfalls. J Oncol 2010;2010:412985.

28. Blagosklonny MV. Hsp-90-associated oncoproteins: multiple targets of geldanamycin and its analogs. Leukemia 2002;16:455-62.

29. Schueller G, Kettenbach J, Sedivy R, Stift A, Friedl J, Gnant M, et al. Heat shock protein expression induced by percutaneous radiofrequency ablation of hepatocellular carcinoma in vivo. Int J Oncol 2004;24:609-13.

30. Ibrahim NO, Hahn T, Franke C, Stiehl DP, Wirthner R, Wenger RH, et al. Induction of the hypoxia-inducible factor system by low levels of heat shock protein 90 inhibitors. Cancer Res 2005;65:11094-100.

31. Roe SM, Prodromou C, O'Brien R, Ladbury JE, Piper PW, Pearl LH. Structural basis for inhibition of the Hsp90 molecular chaperone by the antitumor antibiotics radicicol and geldanamycin. J Med Chem 1999;42:260-6.

32. Supko JG, Hickman RL, Grever MR, Malspeis L. Preclinical pharmacologic evaluation of geldanamycin as an antitumor agent. Cancer Chemother Pharmacol 1995;36:305-15.

33. Sausville EA, Tomaszewski JE, Ivy P. Clinical development of 17-allylamino, 17-demethoxygeldanamycin. Curr Cancer Drug Targets 2003;3:377-83.

34. Egorin MJ, Lagattuta TF, Hamburger DR, Covey JM, White KD, Musser SM, et al. Pharmacokinetics, tissue distribution, and metabolism of 17-(dimethylaminoethylamino)-17-demethoxygeldanamycin (NSC 707545) in CD2F1 mice and Fischer 344 rats. Cancer Chemother Pharmacol 2002;49:7-19.

35. Xiong MP, Yanez JA, Remsberg CM, Ohgami Y, Kwon GS, Davies NM, et al. Formulation of a geldanamycin prodrug in mPEG-b-PCL micelles greatly enhances tolerability and pharmacokinetics in rats. J Control Release 2008;129:33-40.

36. Rahbari NN, Mehrabi A, Mollberg NM, Muller SA, Koch M, Buchler MW, et al. Hepatocellular carcinoma: current management and perspectives for the future. Ann Surg 2011;253:453-69.

37. Verslype C, Van Cutsem E, Dicato M, Arber N, Berlin JD, Cunningham D, et al. The management of hepatocellular carcinoma. Current expert opinion and recommendations derived from the 10th World Congress on Gastrointestinal Cancer, Barcelona, 2008. Ann Oncol 2009;20 Suppl 7:vii1-vii6.

38. Bae Y, Nishiyama N, Kataoka K. In vivo antitumor activity of the folate-conjugated pH-sensitive polymeric micelle selectively releasing adriamycin in the intracellular acidic compartments. Bioconjug Chem 2007;18:1131-9.

39. Meyer DE, Chilkoti A. Genetically encoded synthesis of protein-based polymers

with precisely specified molecular weight and sequence by recursive directional ligation: examples from the elastin-like polypeptide system. Biomacromolecules 2002;3:357-67.

40. Meyer DE, Kong GA, Dewhirst MW, Zalutsky MR, Chilkoti A. Targeting a genetically engineered elastin-like polypeptide to solid tumors by local hyperthermia. Cancer Res 2001;61:1548-54.

41. DeBoer C, Meulman PA, Wnuk RJ, Peterson DH. Geldanamycin, a new antibiotic. J Antibiot (Tokyo) 1970;23:442-7.

42. Bae Y, Buresh RA, Williamson TP, Chen TH, Furgeson DY. Intelligent biosynthetic nanobiomaterials for hyperthermic combination chemotherapy and thermal drug targeting of HSP90 inhibitor geldanamycin. J Control Release 2007;122:16-23.

43. Urry DW. Physical chemistry of biological free energy transduction as demonstrated by elastic protein-based polymers. J Phys Chem B 1997;101:11007-28.

44. Floss DM, Schallau K, Rose-John S, Conrad U, Scheller J. Elastin-like polypeptides revolutionize recombinant protein expression and their biomedical application. Trends Biotechnol 2010;28:37-45.

45. Calvo P, Vila-Jato JL, Alonso MJ. Effect of lysozyme on the stability of polyester nanocapsules and nanoparticles: stabilization approaches. Biomaterials 1997;18:1305-10.

46. Karmali PP, Simberg D. Interactions of nanoparticles with plasma proteins: implication on clearance and toxicity of drug delivery systems. Expert Opinion on Drug Delivery 2011;8:343-57.

47. R. L. Cousins G, Poulsen S-A, K. M. Sanders J. Dynamic combinatorial libraries of pseudo-peptide hydrazone macrocycles. Chemical Communications 1999;16:1575-6.

48. Polyakov VA, Nelen MI, Nazarpack-Kandlousy N, Ryabov AD, Eliseev AV. Imine exchange in O-aryl and O-alkyl oximes as a base reaction for aqueous ‘dynamic’ combinatorial libraries. A kinetic and thermodynamic study. J Phys Org Chem 1999;12:357-63.

49. Cousins GR, Furlan RL, Ng YF, Redman JE, Sanders JK. Identification and isolation of a receptor for N-Methyl alkylammonium salts: molecular amplification in a pseudo-peptide dynamic combinatorial library. Angew Chem Int Ed Engl 2001;40:423-8.

50. Kovaríková P, Mokrý M, Klimes J, Vávrová K. HPLC study on stability of pyridoxal isonicotinoyl hydrazone. J Pharm Biomed Anal 2006;40:105-12.

CHAPTER 4

TUMOR ERADICATION USING SYNCHRONOUS THERMAL ABLATION AND HSP90 CHEMOTHERAPY WITH PROTEIN ENGINEERED TRIBLOCK BIOPOLYMER-GELDANAMYCIN CONJUGATES

4.1 Introduction

Thermal ablation is widely utilized in clinics to treat unresectable, primary liver tumors such as hepatocellular carcinoma (HCC). Although ablative technology has been improved over the years with increased coagulation efficiency and lowered complication rates, a range of high tumor recurrence rates for HCC (4-84%)[1-3] remain among the current ablation modalities. Recent reports of 5-year tumor recurrence rates for HCC treated with ablation include: radiofrequency ablation (RFA) 26-84%[4], cryoablation (CA) 31-55%[5, 6], high intensity focused ultrasound (HIFU) 18-58%[7, 8], and microwave thermal ablation (MWA) 31-65%[9, 10].

Multiple factors contribute to incomplete tumor ablation such as irregular, nonuniform tumor size and shape[11, 12], high tumor tissue heterogeneity, liver cirrhosis, heat sink effects caused by proximate capillary drainage[13-15], and the extreme difficulty of 3-D and real-time visualization of all viable tumor tissues[16] particularly at the polyclonal tumor margins (TMs)[17-19]. The TMs are of particular interest, having been identified as one of the major risks of local tumor recurrence and patient mortality[20, 21]. In addition, reports have shown that thermal ablation alters the tumor microenvironment by

modulation of molecular signaling pathways involving growth factors, kinases, and cytokines[22, 23]. Cellular growth kinetics, including those of hepatic stellate cells, macrophages, and cancer-associated fibroblasts, have also been increased postablation[24]. Stroma cells, in particular, have been shown to recruit tumor cells to the margins in preparation for neoplastic growth[25]. All these factors, together with activated tumor stromal interactions, present dynamic and daunting barriers towards tumor remission. To combat local tumor recurrence following incomplete thermal ablation, complementary chemo- and/or radiotherapies have been combined for additive or synergistic benefit. For example, adjuvant chemotherapy with MWA increased recurrence-free survival 7-fold in large-HCC patients compared to MWA alone[26]. RFA has been applied to animal tumor models with concomitant liposomal doxorubicin[27], paclitaxel[28], and quercetin[29] achieving a 1.2-1.5-fold increase of apoptosis compared to each treatment alone. An ongoing Phase II clinical trial combines Sorafenib, a RAF kinase inhibitor, given orally twice daily with RFA to treat medium-sized HCC (clinical trial #NCT00813293). The benefit of neoadjuvant Sorafenib to RFA efficiency remains to be seen.

Since the tumor microenvironment involves numerous cellular and molecular components, a systemic therapy aiming at a single pathway may eventually experience drug resistance and tolerance. Indeed, cells treated by ablation induce various growth factors such as vascular endothelial growth factor (VEGF), fibroblast growth factors (FGFs), and tumor growth factor-beta (TGF-β)[30, 31]. Among those growth factors, VEGF and FGF-2 expression are observed to be overexpressed by ~ 15% at the ablated margins[31]. Similarly, HSPs are induced under thermal stress caused by hypo- or hyperthermic ablation, which may lead to thermo-tolerance[6, 32, 33]. Two major HSPs,

HSP70 and HSP90, have been characterized in several animal tumor models[34]. For example, in a renal tumor model, these two HSPs are upregulated at the ablated margins. HSP70 displays a 3-8% increase up to seven days after both CA and RFA, whereas HSP90 shows an even higher elevation up to 15% in three days, but only with RFA[32]. However, significant suppression of neither HSP70 nor HSP90 has yet been achieved to prevent postablation recurrence. Our group is particularly interested in HSP90, an endogenous protein accounting for 1-2% of total cytosolic protein[35] and elevated 2-4-fold in viable, thermal stressed cells[36]. In human HCC tissue samples, HSP90 has shown a 7-fold upregulation compared to basal hepatocyte levels[37]. More importantly, HSP90 chaperones over 200 oncogenic proteins such as receptors for all the growth factors mentioned above and various kinases, including mTOR, Akt, and HIF-1[38], critical for tumor angiogenesis[39], invasion, and progression[40]. Although it remains to be revealed how HSP90 is directly involved in the ablation-altered tumor microenvironment, compounds for HSP90 suppression hold potential to further increase ablation–induced tissue coagulation and, most importantly, eradicate the thermal stressed, residual viable cells at the HCC tumor margins.

In this chapter, we continue to use geldanamycin (GA), a potent HSP90 inhibitor, used as an adjuvant chemotherapeutic in combination with thermal ablation, to induce apoptosis by destabilizing client proteins critical for tumor survival[41-43]. Past studies with GA have been plagued with solubilization issues and acute systemic toxicity. To solubilize this extremely hydrophobic agent (~20-50 μM in water) and lower systemic toxicity, we propose a new generation of elastin-based biopolymers to carry high concentrations of GA for focal, locoregional drug targeting to hyperthermic tumor

margins (41-45 ^{o}C).

Previously in Chapter 3, we constructed a diblock ELP copolymer and achieved rapid transition kinetics (ELP1-60-D15, ELP1 library has a guest residue ratio of V: G: A=5:3:2)[44]. However, the transition temperature (Tt) of this copolymer is about 38 ºC, which is not high enough to avoid aggregation upon systemic injection. Based on the physicochemical properties of ELP biopolymers, Tt can be raised to hyperthermic temperatures (41-45 ºC) by constructing a new biopolymer with a more hydrophilic guest-residue, or by making shorter ELPs with smaller molecular weight, and/or decreasing the polymer concentration or the ionic strength of the surrounding medium. We chose to add a hydrophilic block upstream of the ELP1-60 since decreased biopolymer concentration or molecular weight will hinder the acuteness of phase transition. Additionally, there are no charged residues on ELPs and the ionic strength of the blood is fixed. In order to have more control of the Tt, we inserted hydrophilic ELPs with a guest residue ratio of V1:A10 (ELPVA library) up-stream of ELP1-60 (ELPVA-ELP1-60). One valine was designed for cloning feasibility and repeats of alanine, although not as hydrophilic as glycine, retained robust expression achieving high yields (> 50 mg/liter culture), as observed by other groups[45]. We also inserted alanine between the aspartic acids (DADAV) to avoid steric hindrance to drug conjugation. Therefore, the sequence of our final construct from N to C-terminus is [ELPVA$_n$-60-(DADAV)$_7$D]. GA will be conjugated via pH-sensitive hydrazone linkers. This system is designed for site-specific targeting of hyperthermic tumor margins and pH-sensitive GA release in the acidic, tumor microenvironment. Clinically established electrocauterization will be the thermal ablation method of choice for tumor elimination due to the simplicity and

availability here at University of Utah. Electrocautery works similar to radiofrequency which is the leading thermal ablation modality used in clinics. With this technique, it is believed that ELP-GA bioconjugates can work more efficient than clinically-relevant GA controls in preventing tumor recurrence in addition to potent anticancer efficacy and minimum systemic toxicity.

4.2 Materials and methods

4.2.1 Materials

4.2.1.1 Reagents

Oligonucleotides were synthesized at the Research Core Facility, University of Utah (UU). DH5α cells and fetal bovine serum (FBS) were purchased from Invitrogen (Carlsbad, CA); pET25b + expression vector and E. coli BLR (DE3) strains were obtained from Novagen (Madison, WI). T4 DNA ligase, calf intestinal alkaline phosphatase (CIP), restriction enzymes, and buffers were purchased from New England Biolabs (Beverly, MA). Circle-Grow culture medium was purchased from Q-Biogene (Carlsbad, CA). Geldanamycin (GA), 7-*N*-allylamino-17-demethoxygeldanamycin (17-AAG) was obtained from LC Laboratories (Woburn, MA) and structure confirmed upon receipt by ^{1}H-NMR. Carbenecillin sodium salt, PBS tablets, and TBST (0.5 M Tris-buffered saline with 0.5% Tween 20) buffer were purchased from ISC Bioexpress (Kaysville, UT). Aminoacetaldehyde diethyl acetal (AAADA), chloroform, carbohydrazide, 1-ethyl-3-(3-dimethylaminopropyl) carbodiimide (EDC) hydrocholide, sulfo-*N*-hydroxysuccinimide (NHS), Atto 488 NHS ester, and dimethyl sulfoxide (DMSO) were from Sigma-Aldrich (St. Louis, MO), and used as received. Molecular sieves were added to nonaqueous solvents to retain anhydrous conditions.

4.2.1.2 Cell culture

HepG2 (ATCC HB-8065; human HCC) and Hep3B (ATCC HB-8064; human HCC) were purchased from ATCC (Manassas, VA). Cells were cultured as per ATCC instructions. Briefly, HepG2 cells were cultured in Dulbecco's modified Eagle's medium (DMEM) supplemented with 10% fetal bovine serum (FBS) and 1% penicillin streptomycin; Hep3B cells were cultured in modified Eagle's medium (MEM) supplemented with 10% FBS and 1% penicillin streptomycin. Cell culture supplies were purchased from Invitrogen (Carlsbad, CA). All cells were grown and maintained at 37 °C, 5% CO_2, and routinely washed and subcultured at ~90% confluence. A primary antibody against HSP90 and secondary mouse IgG antibody were purchased from Abcam (Cambridge, MA). Immunohistochemistry of HSP90 was conducted by ARUP laboratories (UT) who provided all the reagents.

Animals: 4-5 weeks old, female athymic nude mice were purchased from Simonsen Laboratories (Gilroy, CA). Animal studies were completed according to the University of Utah IACUC approved protocols.

4.2.1.3 Nomenclature

ELPVA has a guest residue ratio of V: A=1:10. ELPVAn stands for ELPs with different repeats of ELPVA monomer. E.g.: ELPVA20 is dimer of ELPVA with 22 amino acids: 2 valines and 20 alanines. ELPVA40 has 4 repeats of ELPVA with 4 valines and 40 alanines. ELP1 library has a guest residue ratio of V:G:A= 5:3:2. E.g: ELP1-60 stands for 6 repeats of V5G3A2, 60 amino acids in total.

ELP diblock copolymer (no spacer): ELP1-60-D15

ELP triblock copolymer: ELPVAn-60-$(DADAV)_7$D

The ELP-GA conjugates, unless otherwise stated, stand for ELPVA40-60-$(Asp)_8GA_7$

ELP-fluorescein conjugates: ELPVA40-60-$(Asp)_6Fl_9$

4.2.2 Cloning, expression, and purification of triblock ELP biopolymers

To construct an ELPVA library, three type II restriction enzymes were used to seamlessly link two VA10 monomers. Briefly, a cDNA of ELPVA monomer containing VA10 and a PvuI restriction site was synthesized by the core facility at the University of Utah. Four oligos comprising VA10 monomer were separately synthesized. Oligo sequences are provided below:

Oligo 1

5′-CGCGACATATGGGCGGACACGGCGTGGGTGTTCCGGGCGCAGGTGTTCCG GGCGCAGGTG TTCCGGGCGCAGGTGTTCCGGGCGCAGGTGTTCCGGGC-3′

Oligo 2

5′-GCAGGTGTTCCGGGCGCAGGTGTTCCGGGCGCAGGTGTTCCGGGCGCAGG TGTTCCGGGCGCAGGTGTTCCGGGCGCAGGTGTGCCGGGCTGGCTGGGATGA AGCTTGC-3′

Oligo 3

5′-CGCGGCAAGCTTCATCCCAGCCAGCCCGGCACACCTGCGCCCGGAACACC TGCGCCCGGAACACCTGCGCCCGGAACACCTGCGCCCGGAACACCTGCGCC-3′

Oligo 4

5′-CGGAACACCTGCGCCCGGAACACCTGCGCCCGGAACACCTGCGCCCGGAA CACCTGCGCCCGGAACACCTGCGCCCGGAACACCCACGCCGTGTCCGCCCAT ATGT-3′

Each oligo was first resuspended in ligation buffer (NEB, MA) and heated to 95 °C for 5 min. Annealing was completed through a slow cool down to 25 °C over 3 h. Initially, the cloning vector (pIDT) was kindly provided by Dr. Amanda Brooks, University of Utah. The vector was first double digested with P*vu*I and D*ra*III to yield vector Fragment I. Fragment II was simultaneously obtained by P*vu*I and B*gl*I digestion. CIP was added to each digestion to prevent self-ligation. After digestion for an hour at 37 ºC, the bands were separated on an agarose gel (1.5 %, 90 V, 1 h). Each fragment with the expected size was cut and DNA was extracted from the gel using a QIAGEN extraction kit. The compatible ends of B*gl*I and D*ra*III were recognized by ligase and the two fragments, each carrying one VA10 monomer, were ligated to obtain a new vector having VA10 dimers (VA20) **(Figure 4.1)**. Additional VA repeats (e.g., VA30, VA40 etc.) were obtained by the same method. The ELPVAn was then inserted at the N-terminus of ELP1-60 using the D*ra*III recognition site. The block for drug conjugation—$(DADAV)_7D$—was placed at the C-terminus of ELP1-60 using two oligos synthesized by the Core Facility. Sequences are provided below for completeness:

Oligo 1

5′-TGGCTGGATGCAGACGCAGTGGATGCAGACGCAGTTGATGCAGATGCAGT
GGATGCAGATGCAGTTGATGCAGATGCAGTGGATGCAGATGCAGTTGATGCA
GATGCAGTG-3′

Oligo 2

5′-TCAATCCACTGCATCTGCATCAACTGCATCTGCATCCACTGCATCTGCATCA
ACTGCATCTGCATCCACTGCATCTGCATCAACTGCGTCTGCATCCACTGCGTC
TGCATC-3′

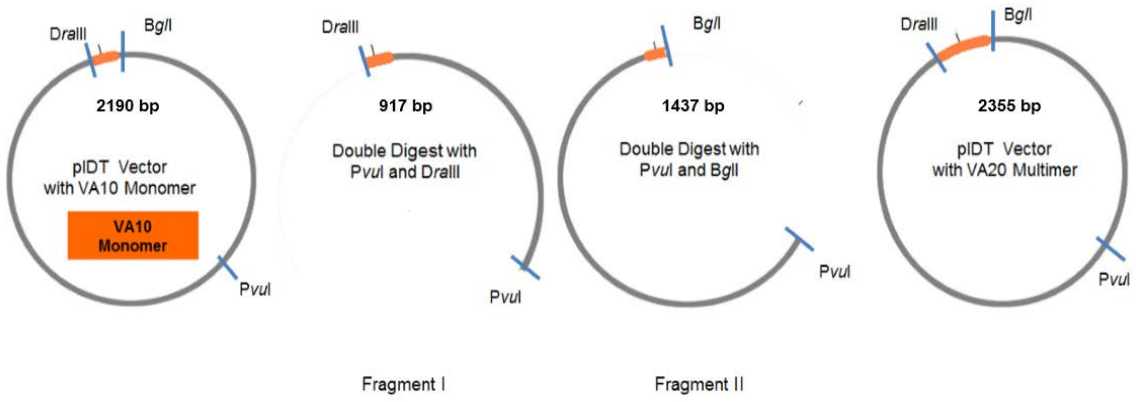

Figure 4.1. Cloning scheme for building up ELPVAn library.

The PIDT vector with VA monomer was first double digested with P*vu*I and D*ra*III to yield vector Fragment I. Fragment II was simultaneously obtained by P*vu*I and B*gl*I digestion. The compatible ends of B*gl*I and D*ra*III were recognized by ligase and the two fragments, each carrying one VA10 monomer, were ligated to obtain a new vector having VA10 dimers (VA20).

The annealing and insertion of $(DADAV)_7D$ was performed the same as D15 in our previous construct[44]. The final DNA with both ELPVAn (N-terminal) and $(DADAV)_7D$ (C-terminal) was verified by both a diagnostic digest and DNA sequencing. The completed construct was then digested with N*de*I and H*ind*III, transferred to a pET25b expression plasmid, and transformed into BLR cells for expression. A complete sequence of the verified gene and translated amino acid sequence was provided in Appendix A. A single colony on the petri dish was inoculated in 5 mL Circle Grow media containing 60 mg/mL carbenicillin at 240 rpm and 37 °C. After overnight shaking, the cell culture was centrifuged at 4000 rpm and 4 °C for 10 min to separate dead cells in the supernatant. The resultant pellet was resuspended in fresh media, and transferred to 4L culture flasks to shake under the same conditions for another 24 h for large-scale production. Typical yields of the triblock ELP biopolymer were 75-100 mg/liter culture. The purification of the ELP was realized by three rounds of hot/cold spin cycles (cf. inverse transition cycling; ITC) as previously reported[44]. The purity and precision of ELP triblock copolymers were characterized by both SDS-PAGE and mass spectrometry.

4.2.3 Synthesis and characterization of triblock ELP-GA conjugates

Aldehyde-modified geldanamycin (GA-CHO) was conjugated to carbohydrazide modified ELP triblock copolymer to yield a pH-sensitive (hydrazone) bond[44]. The conjugation ratio (GAs per biopolymer) was calculated by both UV-spectrometry (Agilent, CA) and ESI mass spectrometry. Particle size (hydrodynamic radius, Rh) is an extremely delicate parameter; therefore, samples were solubilized in molecular biology grade water and measured by dynamic light scattering with a laser goniometer (Brookhaven, NY). The radius of gyration (R_g) of all polymers were measured by static

light scattering (SLS) using the same instrument. Briefly, BI-200SM Goniometer (Hotsville, NY) was used after calibration. Measurements from 12 angles from 15° to 155º were used to generate a static light scattering plot for each triblock copolymers and GA-conjugates at 25 μM ELP concentrations in PBS (pH 7.4, 147 mM) at 25 °C. R_g is calculated from the limiting slope of the extrapolated line at zero concentration. Assuming all nanocomplexes are near spherical structures, R_g was also calculated by $R_g^2 = 3/5\ R^2$, where R is the radius of the sphere. Under the same conditions, the surface charge densities of both free biopolymer and biopolymer-GA conjugates were acquired on an Aetasizer Nano ZS (Malvern Inc, MA). To ensure thermo-targeting of hyperthermic tumor margins (~ 41-45 °C), rapid thermal kinetics within this temperature range are essential. The thermal transition behaviors of the biopolymer alone and biopolymer-GA conjugates were monitored using UV-Vis spectrophotometry as previously described[44]. Briefly, 25 μM triblock ELP or ELP-GA equivalent conjugates were solubilized in PBS and heated at a speed of 1 °C/min from 25 °C-85 °C, and absorption at 650 nm was recorded as a function of temperature. Tt was calculated as the temperature at the maximum derivative of turbidity at 650 nm. All measurements were conducted in triplicate and expressed as mean ± SD.

4.2.4 Drug release profile of GA-ELP biopolymer conjugates

The pH release kinetics at both acidic and neutral pH were monitored on an Alliance RP-HPLC equipped with an absorbance reader. 25 μM ELP conjugates (concentration based on the ELP) were prepared in 1 mL of PBS at pH 5.0 or pH 7.4 and shaken at 37 °C or 43 °C at 180 rpm. 100 μL samples (cooled on ice first) were loaded at 0.5, 2, 6, 12, 24, 48, and 72 h with a 75 μL injection volume. ELP-GA conjugates and free GA-

CHO were separated on a diphenyl column (Waters, MA) using an H_2O/80% DCM gradient with 0.1% v/v TFA. Initially, the binary gradient was 80:20 for 10 min at which point the 80% DCM concentration was raised to 100% over 35 min followed by a static 15 min period. The flow rate was 0.5 mL/min. Percent of GA release as a function of time was based upon GA peak area under the curve normalized to the 0 h time point (n=3).

4.2.5 Cytotoxicity

Cell Counting Kit-8 (CCK-8, Dojindo, MD) was used to evaluate cell viability through assessing mitochondrial dehydrogenase activity of cells treated with 17-AAG, the clinically tested GA analog, GA-CHO, free ELP triblock biopolymer, and ELP-GA conjugates at both 37 °C and 43 °C. Briefly, HepG2 (in DMEM) and Hep3B (in MEM) cells were seeded onto 96-well culture plates (5000/well, n=3) until 70% confluence. Thermo-treated groups were incubated at 43 °C for 30 min while the normothermia groups were incubated at standard 37 °C. After 10 min of recovery, each well was treated with 100 µL drug containing solution. Specifically, 17-AAG and GA-CHO were freshly solubilized in 10 µL DMSO while ELP and conjugates were solubilized in 10 µL PBS. 90 µL media was added to each solution to reach ELP-normalized concentrations ranging from 10 nM to 100 µM. Cells were further incubated at 37 °C for another 48 h period before the CCK-8 assay. Here, 30 µL of diluted CCK-8 agent were added to each well and further incubated at 37 °C for an hour. As per the vendor's instructions, absorption at 450 nm was measured using a SpectraMax M2 microplate reader (Molecular Devices, CA). The cytotoxicity is presented by IC50 values defined as the drug concentrations eliciting a 50% decrease in absorbance of untreated control wells.

Thermal Enhancement Ratio (TER) was calculated by IC_{50} at 37 °C divided by IC_{50} at 43 °C.

Cytotoxicity profiles were further evaluated using propidium iodine (PI) staining. Cancer cells were plated on 6-well plates with 3-5×10^5 cells/well in 2 mL media. Cells were treated to the previously described hyperthermic/normothermic conditions. After 48 h of total treatment, the cells were harvested by trypsinization, centrifuged at 1000 rpm for 3 min, and resuspended in 500 µL cold PBS with 5 µL PI (100×, 20 mL PBS, 20 µL 0.1% Triton X-100, 2900 mg/mL RNAse, and 20 µg/mL PI). The final cell suspension was transferred into FACS tubes and incubated on ice for an additional 5-10 min. The stained cells were captured with a DxP cytometer (Cytek Development, CA) and cell viability was analyzed using FlowJo CE software (Tree Star Inc, OR).

4.2.6 Cell uptake

4.2.6.1 Conjugation of fluorophore to biopolymers

Carbohydrazide modified ELP was conjugated with Atto 488 NHS ester (Sigma Aldrich, MO) to study the cell uptake after hyperthermia and normothermia. Briefly, Atto 488 NHS was dissolved in DMSO at a concentration of 10 mg/mL. 150 µL of dye solution was then mixed with 25 mg ELP in 2 mL Na_2HCO_3 buffer (0.1 M, pH 8.3 ± 0.2) and stirred in the dark at 25 °C for an hour. Free dye was removed by filtration through a PD-10 column (GE Healthcare, Buckinghamshire, UK) and dialysis overnight against PBS. The final product was lyophilized for long-term storage. The concentration of loaded dye was measured using a Nanodrop spectrometer (Thermoscientific, MA), which has built-in software for widely used fluorescein. The loading capacity was calculated by concentration after lyophilization and divided by total concentration in the start solution.

4.2.6.2 Flow cytometry and microscopy

Cellular uptake was monitored using flow cytometry. Hep3B cancer cells were grown on a 6-well plate until 70-80% confluent. Endocytosis inhibitors (amiloride (0.08 mg/mL), mβCD (2.0 mg/mL), and chlorpromazine (10 μg/mL) inhibiting macropinocytosis, caveolae, and clathrin-mediated endocytosis, respectively) were administered, and cells were incubated at 37 °C for 30 min. Hyperthermia was performed after the endocytosis inhibition for 30 min at 43 °C. Free dye in 1% DMSO, ELPVA40-60-Fl (1 μM equivalent dye) in PBS was administered to the cells and incubated for an additional 4 h and 48 h. Cells were thoroughly washed by PBS three times, followed by trypsinization and resuspension in fresh PBS before cell sorting.

For nucleus staining by fluorescence, each treated well was stained with one drop of Hoechst stain (Invitrogen, CA) for nucleus visualization. Excessive dye in each well was washed away with PBS five times before fluorescence microscopy (Olympus IX71Ftware, PA). All acquired images were processed by Image J software (NIH, MD)

4.2.7 Colocalization of polymer-conjugates with lysosomes

The colocalization of fluorescence and lysosomes was monitored using confocal microcopy (Nikon A1R, NY) at 60 × magnification. Hep3B cells were cultured on a Lab-Tek 8-chamber coverglass system at a density of ~10000 cells/chamber. After cells reached 70% in confluence, 2 μL of Lysotracker RFP (Invitrogen, CA) was administered for lysosome staining. After overnight incubation, the coverglass system was placed on a Nikon A1R Confocal Microscope and heated at 43 °C for 30 min (5% CO_2 maintained). The temperature was then returned to 37 °C and 1 μM equivalent Atto 488 (Fl) or conjugated ELPVA40-60 -Fl was administered to the labeled cells. Before imaging, the

cell nucleus was labeled with Hoechst stain (50 ×). Images were taken at 60 × with fixed positions every hour up to 12 h, using the following excitation/emission wavelengths (nm): for Hoechst, 350/461 nm; for Atto-488 fluorescein, 498/520 nm; for Lysosome-RFP, 555/584 nm. The level of colocalization was calculated using Image J software by computing the overlap of individual pixels from two fluorescence channels. The effect of endocytosis on colocalization was evaluated using the same endocytosis inhibitors as in the cell uptake study.

4.2.8 Western blotting of HSP90

To evaluate the inhibition of each drug, 20000 cells were cultured in 6-well plates and grown until 70-80% confluent. Cells in each well were lysed with 150 µL SDS buffer (0.1M Tris HCl, pH 8.3, 1% protease inhibitor). Total protein concentration was determined by BCA assay per vender instruction (Thermoscientific, MA). 10-20 µg total protein was separated on a 4-12% Bis-Tris SDS gel (Invitrogen, CA) and transferred to a PVDF membrane for electroblotting. Primary antibodies against rabbit HSP90 (1:1000) and β-actin (1:2000) were incubated at 4 °C overnight, followed by a 1 h incubation of rabbit anti-mouse IgG secondary antibody. The membranes were washed three times with TBST buffer, incubated with a chemiluminescent reagent (ISC Bioexpress, UT), and visualized on a FluoroChem FC2 camera (AlphaInnotech, CA).

4.2.9 Tumor implantation

HepG2 cells were cultured in DMEM media in a 175 cm^2 tissue flask until 70-80 % confluent. Cells were washed with PBS, trypsinized, and centrifuged at 1000 rpm for 3 min. Cells were reconstituted in cold DMEM-Matrigel (BD Biosciences, CA) solution

(50:50, v/v). The right flank of each nude mouse was sterilized with isopropyl alcohol prior to injecting a 200 µL suspension (2-3×10^6 cells) under general anesthesia. Animal weight and tumor size were recorded twice weekly according to the approved IACUC protocol.

4.2.10 *In vivo* assessment of anticancer efficacy of biopolymer-GA conjugates

Tumors reaching 5 mm in all dimensions were subsequently intravenously injected with 200 µL of PBS, 17-AAG, or ELP-GA conjugates (3.7 mg/kg equivalent GA dose) twice weekly (for a total of seven doses) through the tail vein. Animal weight and tumor sizes were monitored up to 21 days after treatment. Tumor volume was calculated by 0.5×(length of tumor)×(width of tumor)^2.

4.2.11 Electrocauterized thermal ablation

Each animal was anesthetized via inhalation of 5% isoflurane with a nose cone and subsequently placed on a sterile electrical grounding pad. A heating lamp was placed beside the animal to keep it warm during anesthesia. The tumor area was sterilized with an alcohol swab and a 1 cm small incision was made to expose the tumor. Cauterization was accomplished with an ESU-30 system (Olympus, FL) at 25 W with coagulation mode with an electrical pencil (Covidien, MA) placed in the center of the tumor. To ensure that we could achieve hyperthermic margins, we first conducted a thermometry study where a temperature probe (Fluke, 80PK-25, WA) was placed consecutively at three positions (~5 mm away from the pencil tip) and temperatures were recorded after demarcation appeared. The electrical surgery unit is able to achieve an ablated margin

around 42 ºC (supporting information). For tumor treatment, the duration of cauterization was dependent on the tumor size and a 3-5 mm peripheral margin was left unablated. 200 μL Rimadyl (50 mg/mL) was subcutaneously injected after the ablation and the incision was closed with a surgical staple (3M Health Care, MN)

4.2.12 Combination therapy of electrocauterization and biopolymer-GA conjugates

To evaluate additive and/or synergistic effects of combination therapy, each sample (PBS, 17-AAG, ELP-GA) was initially normalized to 3.7 mg/kg GA equivalents and intravenously injected. We kept the same dose in the combination while the flank HCC tumors on the mice were first cauterized and the tumor core coagulated. The injection of therapeutics was then performed immediately after the cauterization and wound closure. Three days following the first dose, a second dose was administered, with two more doses injected twice weekly. Physical activity and eating/drinking habits were monitored daily. The animal weight and tumor size were recorded twice weekly up to 90 days.

4.2.13 Histology and HSP90 immunohistochemistry

Animals were euthanized when a tumor reached 2 cm in any dimension, or >20% loss of body weight was observed, or one day after the last treatment by CO_2 inhalation, and the tissue samples were collected promptly. Briefly, a 0.5 cm incision was performed on the flank skin to expose the tumor. The fascia was removed and tumor washed three times by PBS. Two pieces at both the ablated tumor core and tumor margins (tissues next to the demarcation, 3-5 mm long, and 100-200 mg), were excised from each animal. One piece of sample was immediately put into 10% neutral buffered formalin for 36-40 h.

Fixed tissues were then transferred to 70% alcohol for storage prior to paraffin embedding. Tissue samples were dehydated through graded alcohol and xylene, embedded in paraffin, and sectioned at a thickness of 5 μm with a microtome. 10 slices were obtained per sample. Each slide was either stained with hematoxylin and eosin (H&E) for gross histopathological analysis or processed for HSP90 immunochemistry (ARUP laboratories, UT). Briefly, slides were pretreated with monoclonal rabbit anti-HSP90 (Cell Signaling Technology, MA) for 60 min, followed by a 20 min incubation of mouse IgG blocker (BioCare Medical, CA) to block endogenous mouse IgG. The primary antibody was then applied at a dilution of 1:50 for 2 h at 37 °C. A secondary antibody (mouse $F(ab)_2$) (Dako; Carpinteria, CA) was applied for 4 min at a dilution of 1:100. The slides were imaged with an IVIEW DAB detection kit (Ventana Medical Systems; Tucson, AZ) and visualized under optical microscopy with 10 × and 40 × magnification (assisted by Prof. Theodore Pysher, Division Chief of Pediatric Pathology, University of Utah). The relative HSP90 expression was analyzed using ImageJ. For each slide, three random positions were selected at the tumor margins with the same areas of pixels to calculate HSP90 intensity relative to untreated control.

The second section (100-200 mg) from the same tumor sample was flash frozen in liquid nitrogen and homogenized for Western blot. Tumor tissues were homogenized in lysis buffer (100 mg tissue/ mL) for 20 sec on ice and immediately centrifuged at 12000 rpm for 10 min at 4 °C. Protein concentrations were determined by BCA assay and samples loaded onto an SDS protein gel followed by electroblotting and processed as described in Section 4.2.5.

4.2.14 Statistical analysis

One-way analysis of variance (one-way ANOVA) with the Bonferroni *post-hoc* analysis was used to compare three or more groups. A Student's t-test was used for two groups; $p < 0.05$ indicated statistically significant differences between the groups.

4.3 Results

4.3.1 Characterization of triblock ELP biopolymers and conjugates

To avoid potential aggregation upon systemic injection observed from conjugates in Chapter 3, we introduced a hydrophilic ELPVA library to the diblock polymer (ELP1-60-D15) to increase Tt to the hyperthermic range (41-45°C). The insertion of more VA repeats, as we expected, increased hydrophilicity (determined as solubilization and no precipitation) of the polymer and resulted in elevated Tt. Briefly, the smallest VA polymer, VA20, has a Tt at 39 °C and the Tt rises to 43 °C for larger and more hydrophilic polymer VA40, as shown in **Figure 4.2A**. Thus, we chose the VA40-construct for drug conjugation and future experiments.

The insertion of alanine spacers between aspartic repeats [$(DADAV)_7D$] reduces the steric hindrance for drug conjugation and allows more aldehyde-modified GAs to access and react with the primary amines conjugated on aspartic acids. Therefore, the conjugation ratios (47-53%), although not dramatically increased (Mass Spec data provided in Appendix A), were more consistent and reproducible than our previous di-block and no-spacer construct. The insertion of VA and spacers also contributes to the hydrodynamic stability of the construct. The increasing number of VA repeats showed gradual reduction of the hydrodynamic radius despite the increase of molecular weight (**Table 4.1**). The radius of gyration (R_g) has slightly lower value than the hydrodynamic

A B

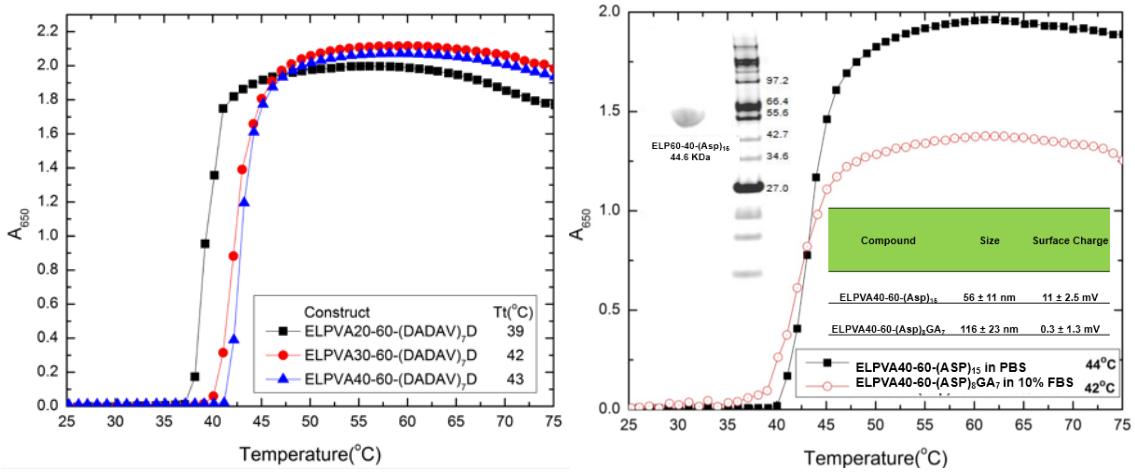

Figure 4.2. Physicochemical properties of ELP-biopolymer and GA conjugates.

A) Physicochemical properties of a new breed of ELP-VA library. The insertion of VA increases the molecular weight and reduces hydrophobicity of ELP triblock polymers. All ELP triblock copolymers were evaluated at 25µM in PBS (pH7.4, 147mM). B) Purity and molecular weight of the triblock polymer were displayed in an SDS gel. The thermo-responsiveness behavior in PBS and 10% serum after conjugation. The conjugates maintain the acute responsiveness within the desired hyperthermia range (41-45 °C) for combination therapy in the presence of serum. ELP triblock copolymer and conjugates were evaluated at 25µM (ELP equivalent) in PBS (pH7.4, 147mM) and PBS with 10% serum (v/v).

Table 4.1. Characterization of ELP triblock copolymers.

Construct	Tt (^oC)	R_h (nm)	PDI	R_g (nm)	R_{gs} (nm)	ρ	Zeta Potential (mV)
$ELP(VA_{10})_8$	75 ± 0.5	10.8 ± 3.6	0.011	3.5 ± 0.6	4.1 ± 1.4	0.32	0.8 ± 0.5
$ELP(VA_{10})_2$-ELP(1-60)-$(DADAV)_7D$	38 ± 0.5	107 ± 20	0.203	85 ± 6.7	83 ± 14	0.79	-16.8 ± 0.5
$ELP(VA_{10})_3$-ELP(1-60)-$(DADAV)_7D$	42 ± 0.5	80 ± 14	0.14	66 ± 5.1	62 ± 10	0.82	-17.4 ± 1.9
$ELP(VA_{10})_4$-ELP(1-60)-$(DADAV)_7D$	44 ± 0.5	56 ± 11	0.121	25 ± 4.1	43 ± 8.2	0.45	-18.1 ± 0.3
$ELP(VA_{10})_4$-ELP(1-60)-$D_8A_{14}V_7$-GA_7 conjugates	43 ± 0.5	116 ± 23	0.126	85 ± 7.6	90 ±11	0.73	0.3 ± 1.3

25 μM ELPs in PBS (147mM, pH 7.4) were standardized in both DLS and SLS. All samples were recorded at 25°C and reported as mean ± SD (n=3). Rh is the hydrodynamic radius obtained from DLS and R_g is the radius of gyration measured by SLS. R_{gs} is the calculated R_g assuming constructs are spherical. The results from measurements and calculations are very similar.

radius (R_h), since it is the root mean square distance of the polymers from the center of the polymer mass and less dependent on the surrounding medium. R_gs measured by SLS further confirmed the decrease of the sizes with addition of hydrophobic VA block, which may result from increased side chain contacts. Combined with R_h, R_g can be used to describe the morphology of nanoparticles. The morphology of the polymers can be deduced from shape factor ρ, which is calculated by R_g / R_h. Distinct from triblock copolymers, the homopolymers ($ELP(VA10)_8$) have much smaller ρ value, which is largely affected by the absence of charged, hydrophilic amino acids present in the triblock copolymers. Therefore, the homopolymers have more compact structures in water (not a good solvent) which leads to smaller R_g and subsequent smaller ρ value. For small protein nanoparticles, small-angle-X-ray scattering may provide better information since it has lower background noise (noticing that SD of VA80 is bigger than the rest). On the other hand, the conjugates and the triblock copolymers, except for VA40, have ρ values ranging from 0.73 to 0.82, indicating that those polymers have near-spherical structures resulting from macromolecular self-assembly. Typical value for a globular protein is around 0.77[46], but values between 0.5 to 0.8 are generally considered to suggest a spherical morphology of the polymer[47]. Interestingly, the VA40 copolymers have a ρ value slightly lower than 0.5, which suggest a different axial ratio and core-shell structure caused by the increased hydrophobicity of extra valines and alanines. The added concentration of nonpolar amino acids increases the compactness of the polymer in the water-based medium, which leads to smaller R_g value. It is hard to predict the exact number of hydrophobic amino acids to achieve the critical R_g for morphology distinction, but our observation suggests that R_g with R_h can be used to design protein polymers and

tailor the shape for specific needs without using costly imaging analysis or molecular simulations.

The conjugate displayed an approximate hydrodynamic size of 116 nm and neutral surface charge, as shown in **Figure 4.2B**, which may pass into the tumor through its leaky vasculature to exploit the enhanced permeation and retention (EPR) effect[48]. Additional data of DLS, TEM, and SLS were also provided in Appendix A.

The pH sensitivity of the conjugates was characterized in both neutral and acidic buffers. A pH of 5.0 was chosen to mimic endosomal/lysosomal pH[49] where the drug is cleaved. The drug release was significantly higher (~70%) and faster in the acidic environment compared to normal physiological pH (~15%) within 72 h (**Figure 4.3**). More importantly, more than 50% of the drug was released within 12 h of administration, ensuring a more efficient tumor kill postablation with less systemic toxicity.

4.3.2 Cytotoxicity and HSP90 inhibition of ELP-GA conjugates

CCK-8 assay was used to measure the level of formazan, which can be extrapolated to represent the percentage of viable cells. The IC_{50} value was defined as the concentration causing 50% cell death of the nontreated controls. Complementarily, we also used propidium iodide (PI) staining to sort the dead cells (unstained cells) with flow cytometry to confirm the cytotoxicity elicited by 17- AAG and conjugates (data not shown). Aldehyde-modified GA (GA-CHO) showed slightly better cytotoxicity than the clinically-tested GA analog, 17-AAG, with the lowest IC_{50} around 160 nM. The triblock copolymer ELP was not toxic within the tested concentrations, but the resultant conjugate maintained strong cytotoxicity with IC_{50} below μM range, as shown in **Table 4.2**.

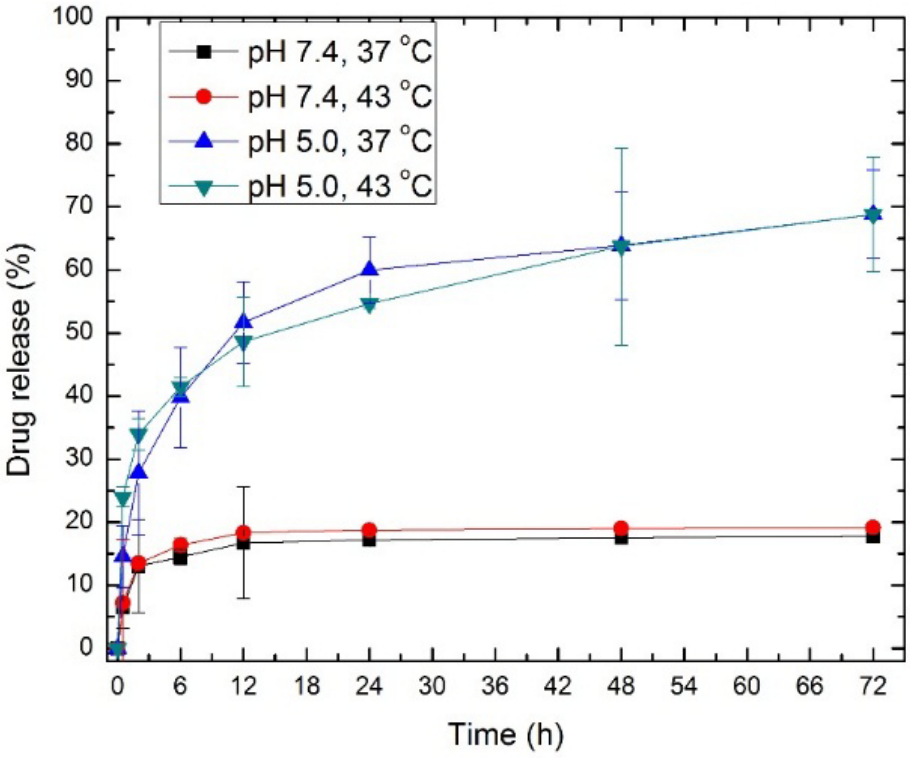

Figure 4.3. Release profile from ELP-GA conjugates at neutral and acidic pH under both normothermia (37 °C) and hyperthermia (43 °C).

The concentration of GA and ELP free polymer were derived from the standard curves at 337 and 220 nm, respectively. Using the binary gradient, ELPVA40-60-(Asp)15 copolymer (Rt= 22 min) and free GA-CHO (Rt =27 min) can be separated according to HPLC chromatography. We calculated the percent of GA release as a function of time based upon a drop in the conjugate peak area percent, normalized to the 0 h time point. These runs were repeated three times for each ELP-GA conjugate.

Table 4.2. Cytotoxicity of free drug, free polymer, and ELP-GA conjugates to HCC cell lines.

Compound	IC_{50} (μM, 43°C)	IC50 (μM, 37 °C)	IC_{50} (μM, 43°C)	IC50 (μM, 37 °C)
	HepG2		Hep3B	
17-AAG	0.18 ± 0.03	0.24 ± 0.04	0.07 ± 0.01	2.35 ± 0.05
GA-CHO	0.16 ± 0.02	0.20 ± 0.01	0.06 ± 0.01	2.15 ± 0.11
ELPVA40-	>100	>100	>100	>100
ELP VA40-	0.79 ± 0.13	1.29 ± 0.19	0.87 ± 0.13	2.57 ± 0.17

Tested concentrations ranged from 0.01-10 μM. IC50 were calculated using Prism Graphpad software. Data were expressed as mean ± SD, n=3.

Hyperthermia further enhances the cytotoxicity of GA and conjugates by 1.3-3.0-fold. GA has shown elevated toxicity upon hypothermia in various cancer cell lines, including breast cancer[50], melanoma[51], and prostate cancer cells[52]. Here, we achieved ubiquitous toxicity enhancement in both HCC cell lines. The increased toxicity can be attributed to the following reasons. First, hyperthermia is known to increase cell membrane mobility and permeability[53], which allow more efficient cellular uptake for large molecules[54]. At the same time, thermo-sensitive ELP conjugates form aggregates, which can be internalized more into the cells as a result of increased hydrophobicity, and function as a drug depot to kill the cells around aggregate domains. Those cells further increase the sensitivity of adjacent cells to chemotherapy (bystander effect) to cause vast and efficient cell depletion. Finally, the hyperthermia synergistically enhances the cellular ATPase activity, which directly links to the favored mechanism of HSP90 and increases the rate of GA binding to HSP90 to elicit the cytotoxic effect.

HSP90 level was measured in the cells treated at the same conditions in the cytotoxicity studies. **Figure 4.4** shows a dose- and time-dependent inhibition of HSP90 by ELP-GA conjugates. The cellular HSP90 was depleted at 21 h around the IC_{50} concentration, further substantiating that effective HSP90 suppression leads to efficient cell death.

4.3.3 Characterization and cellular uptake of ELP-Fl conjugates

Since HSP90 is mostly present in the cytosol, we confirmed that conjugates are encapsulated in the cells and released GA in the cytoplasm. To visualize the ELP-based polymer, Atto 488, a stable and reliable imaging agent, was linked to the ELP triblock

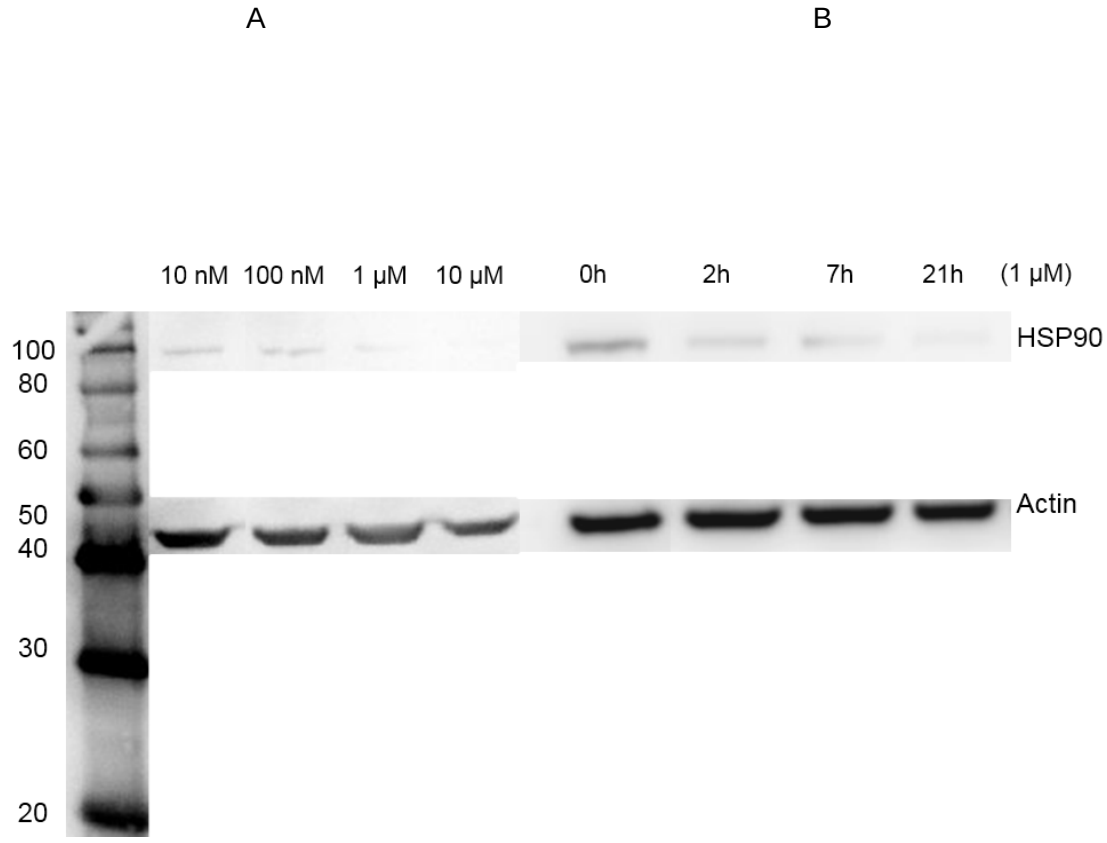

Figure 4.4. Quantitative western blotting of HSP90 expression in HepG2 cells after treatment of ELP-GA conjugates as a function of dose and time.

A) Samples were taken at 48 h after each concentration (same as cytotoxicity studies). HSP90 was inhibited at a dose of 1 µm GA equivalent. B) HSP90 level as a function of time, treated by conjugates with a 1 µm GA equivalent concentration.

copolymer backbone as a mimic of the ELP-GA conjugates to probe the extent and mechanism of cellular uptake. The same conjugation chemistry and purification was used for the ELP-Fl conjugate, which yielded a conjugate similar to GA's, as shown in **Table 4.3**.

Both confocal microscopy and flow cytometry were conducted to examine the level of internalization to the cytosol and lysosome. **Figure 4.5** shows the cellular uptake by both free drug and conjugate after 30 min treatment at 43°C. The conjugate showed enhanced uptake at both 4 h and 48 h, during which 60% of the drug was still bound to the ELP backbone (confirmed by release studies using HPLC). At the same time, lysosome tracker was used to stain the lysosome and monitor the colocalization level of fluorescence and lysosome up to 48 h. Peak localization (20%, calculated by ImageJ) was observed for conjugates while only trace levels were detected for the free fluorescent dye.

Localization is important due to the fact that low pH of the lysosome provides cleavage of GA from the ELP backbone for therapeutic effect. To examine the molecular mechanisms of internalization, three inhibitors: amiloride, mβCD, and chlorpromazine, suppressing three major pathways of endocytosis were applied to the cell culture. All inhibitors decreased the level of colocalization, as shown in **Figure 4.6**, suggesting that mixed and dynamic internalization pathways exist for ELP-based biopolymers. Temperature also plays a major role in cellular uptake. As observed by other researchers, hyperthermia increases the fluidity of the cellular membrane[55], which facilitates the dynamic interaction of ELP with the cell membrane. A higher temperature also contributes to increased cellular uptake[56, 57] allowing targeted and efficient cancer cell abrogation. Hence, cellular uptake was confirmed using flow cytometry at the same dose

Table 4.3. Physicochemical characterization of ELP-Fl conjugates.

Loading effciency (%)	Tt (^{o}C)	Size (nm)	PDI	Zeta Potential (mV)
60	41.5 ± 0.5	127 ± 33	0.133	0.1 ± 0.5

All characterization was performed with 25 μM equivalent ELP, in PBS (pH 7.4, 147 mM). Hydrodynamic radius (size) and zeta potential were measured at 25 ºC. PDI represents polydispersity of the nanoparticles. All results were mean ± SD, n=3.

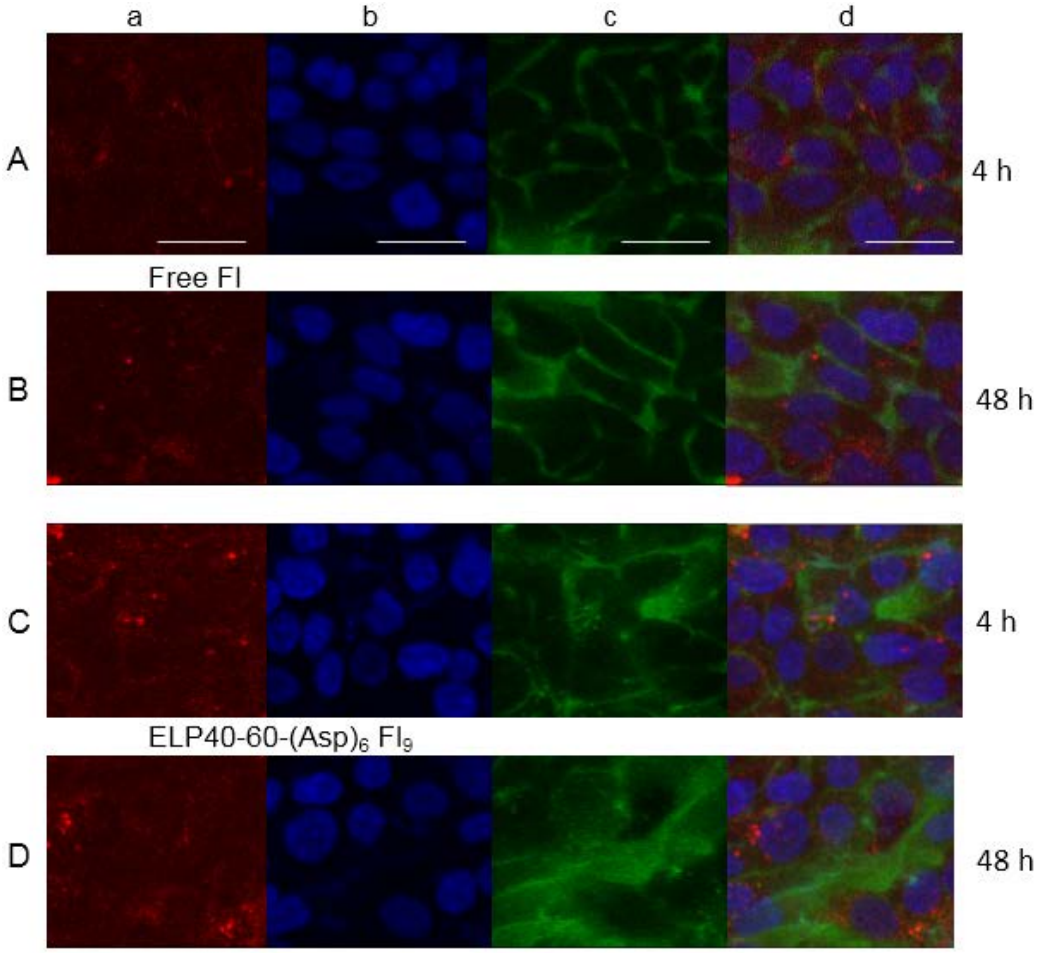

Figure 4.5. Confocal microscopy images of cell uptake of Fluorescein only (Fl, panel A&B) and ELP-Fluorescein (ELPVA40-60-$(Asp)_6Fl_9$ conjugates, panel C&D).

Images were taken after 4 h and 48 h incubation. a) Lysosome tracker (red, Lysosomes-RFP); b) Cell nuclei (blue, Hoechst); c) Fluorescein (green, Fl or ELP-Fl); d) Merge (scale bar, 20 μm).

A B

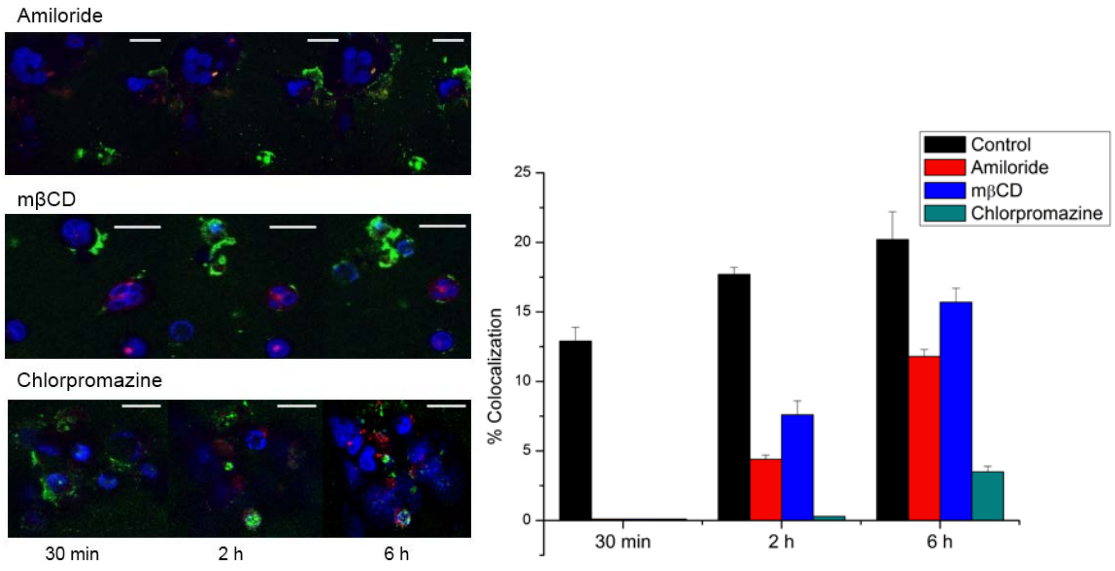

Figure 4.6. Colocalization studies monitored using confocal microscopy.

A) Representative confocal images of cells taken at 30 min, 2 h, and 6 h after endocytosis inhibition. B) Level of co-localization with lysosomes as calculated from over-lapping pixels of lysosome-RFP and Fl divided by total Fl pixels. (Scale bar, 20 µm)

under normo- and hyperthermia. Cells were analyzed at both 4 h and 48 h posttreatment. Again, the free dye signal was sparse after extensive washing, while the conjugates maintained strong signals up to 48 h. The same endocytosis, inhibitors were used to examine the mechanism of internalization. We found that all inhibitors had some effect on endocytosis, as shown in **Figure 4.7**. Chlorpromazine, which inhibits the clathrin-mediated endocytosis pathway[58], displayed the most suppression of cellular uptake, similar to the findings in confocal microscopy studies.

4.3.4 Antitumor efficacy and histological evaluation

Tumor growth rate for each treatment is summarized in **Figure 4.8**. Due to the aggressive nature of HCC, most animals in the PBS group were quickly (15-20 days) subject to euthanasia as the tumor size reached 2 cm in one dimension. The conjugates and free drug displayed limited efficacy in tumor stasis. However, the ELP-GA achieved slower tumor growth than the free drug ($p < 0.05$), which is in accordance with the level of HSP90 inhibition.

All mice tolerated the drug throughout the course of the treatment since the doses were given at 50% of the MTD. No severe distress, weight loss, or death were observed. There are some side effects for the combination therapy. First, the mice experienced 3-5% weight loss at the first day after treatment. The activity level was restored with time, but they displayed slower weight gain compared to untreated controls. The mice also showed was effective in killing the tumors. As shown in **Figure 4.9A**, the power and duration of the cauterization achieved >50% tissue necrosis; there are distinct regions where clusters of cells remained viable. Indeed, one of the major limitations for all ablation modalities is

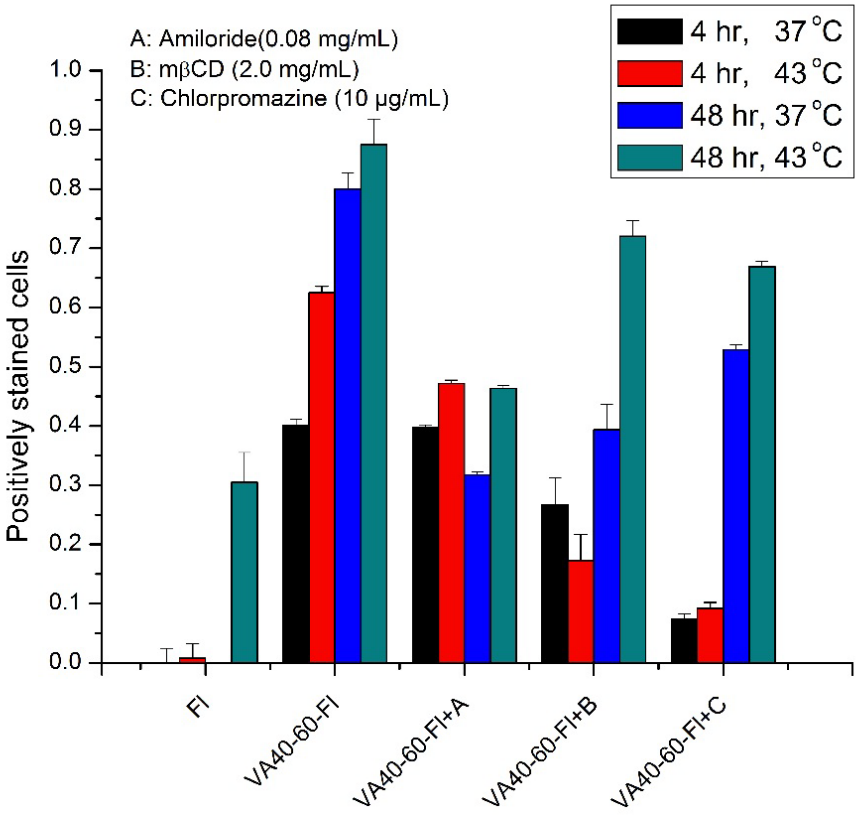

Figure 4.7. Fluorescent dye uptake of Hep3B cells after 30 min of endocytotic inhibition.

The percent of gated fluorescing cells was quantified by flow cytometry at 4 h and 48 h after treatment of conjugates and equivalent doses of fluorescein (1 µm). The results are shown as mean ± SD, n = 3.

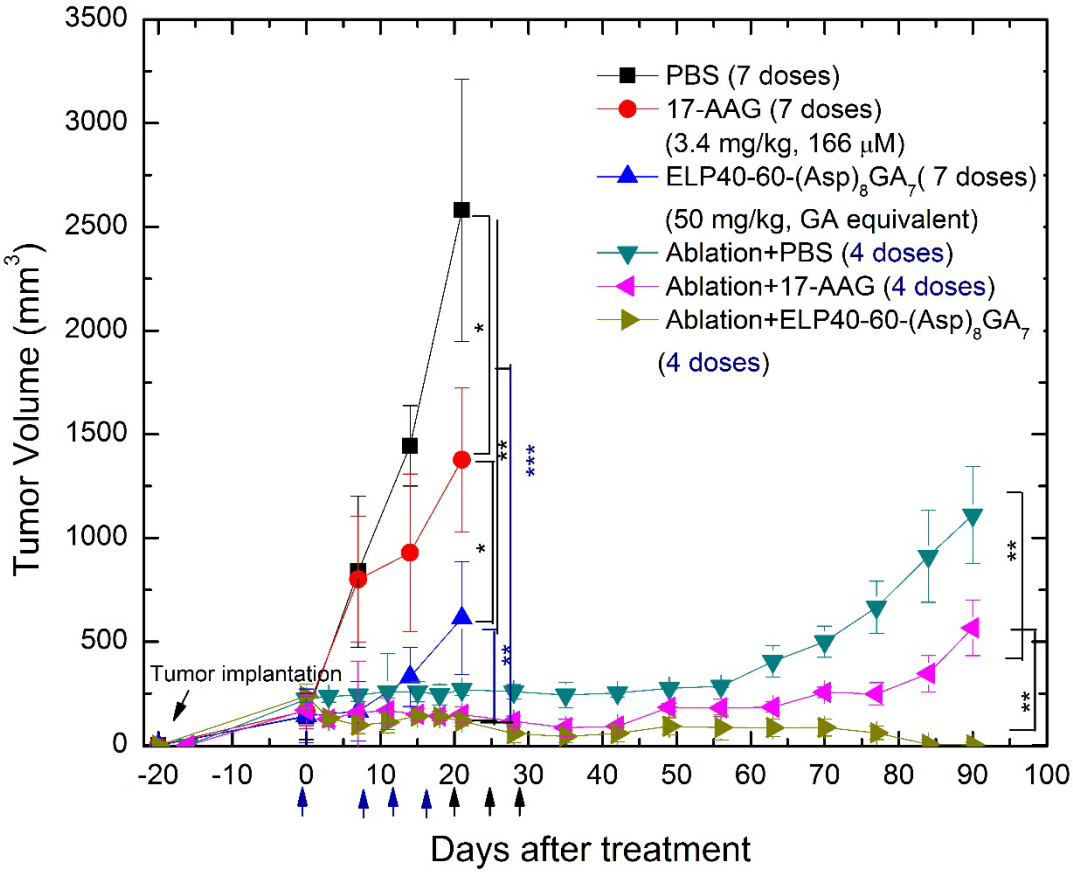

Figure 4.8. Tumor growth following treatment with intravenous free 17-AAG, ELP-GA conjugates, and/or ablation (electrocautery).

The conjugates were given twice weekly, 7 doses in total. Combination of ablation and 4 doses of adjuvant therapy (either with 17-AAG or ELP-GA or PBS) resulted in tumor regression up to 90 days (*$p < 0.05$, **$p < 0.01$, *** $p < 0.001$). Studies were terminated at 90 days due to significant weight loss in other groups.

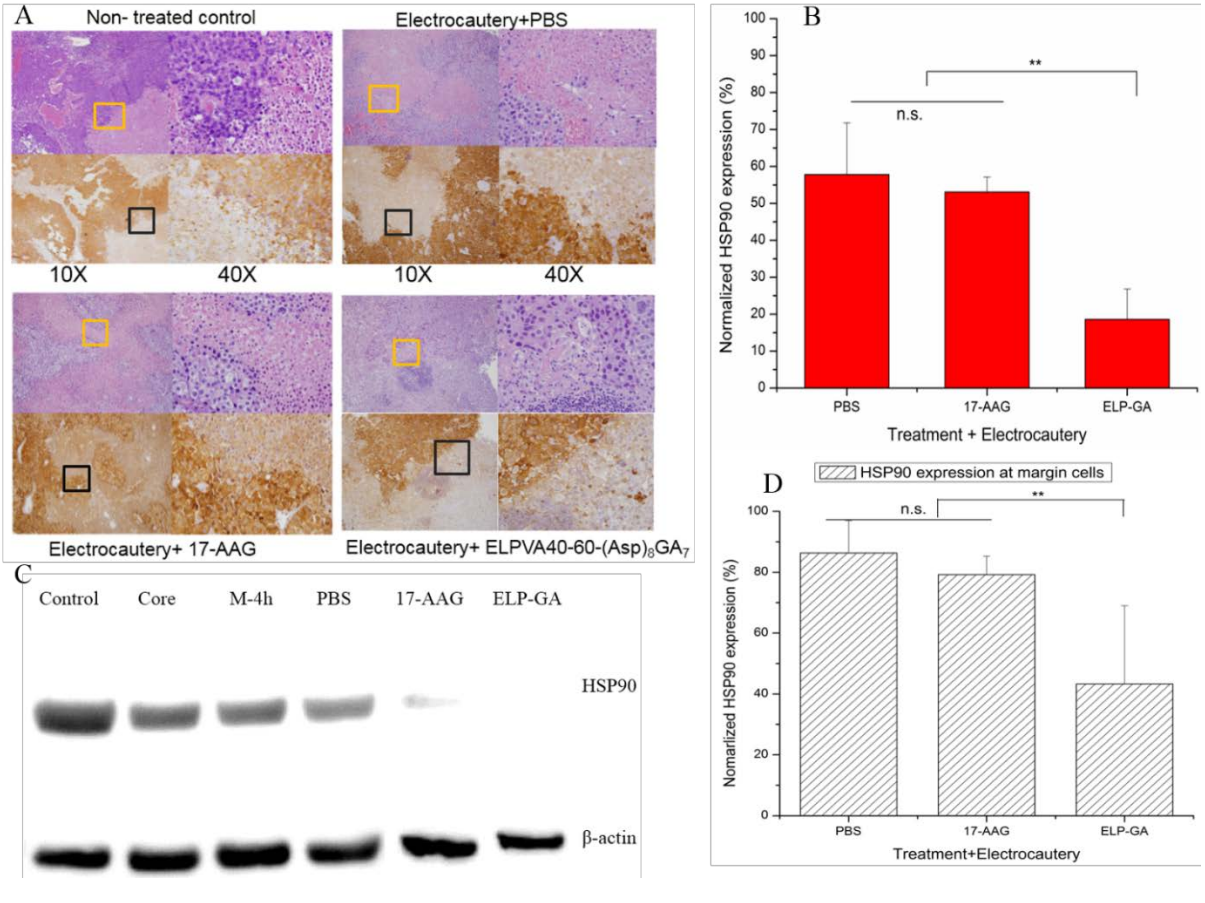

Figure 4.9. HSP90 quantification by immunohistochemisty and Western blot.

A) Histology and HSP90 immunohistochemistry of tumor margin samples taken after combination therapy. Square on low magnification is the region of high magnification image. Original magnification 25 ×. B) HSP90 expression levels after each combination treatment (normalized to ablation-only controls). C) Quantitative Western blotting of HSP90 in tumor samples excised after ablation only (tumor core, margin, 4 h post-ablation), and from tumor margins after combined treatment (electrocautery with PBS, 17-AAG, and ELP-GA) following the last dose. D) HSP90 expression levels from margin cells (viable cells adjacent to necrotic cells) after combination treatment. The results are shown as mean ± SD, n = 3. (**, $p < 0.01$)

that the heat is not evenly distributed and is significantly affected by the tumor size, location, cell type, and adjacency to large blood vessels. As a result, HSP90 immunohistochemistry showed variable intensity of staining. However, only cells with less reduced physical strength in clawing and declined response to other stimuli. Before the combination therapy, we did a thermometry study to confirm that the electrocautery strong staining HSP90, usually stronger than the untreated control cells, remained viable and possibly responsible for tumor recurrence. The levels of HSP90 expression were confirmed by Western blot in **Figure 4.9C** where ELP-GA conjugates displayed the most inhibition of HSP90 compared to other treatments. No tumor growth was observed over 60 days after reduction of tumor was achieved at first 10 days of treatment. However, slow tumor growths (compared to nontreated control) at the ablated tumor site were observed in ablation (Electrocautery) alone and with the 17-AAG group. Therefore, the conjugate played a critical role in preventing the tumor recurrence by superior HSP90 inhibition in tumors in general (**Figure 4.9B)**, as well as the margins cells (cells adjacent to necrotic cells), as shown in **Figure 4.9D**.

4.4 Discussion

Primary HCC accounts for more than 90% of liver cancers and the 5-year survival rate remains as low as 12%[59]. Despite the higher response rates and longer survival afforded by current treatment modalities, the vast majority of patients die due to recurrent tumors or distant metastasis. Thermal ablation treatment is widely used in HCC patients, who are not eligible for surgery or transplantation. However, prevention of postablation recurrence remains underexplored and requires targeted molecular intervention for better prognosis. Thermal ablation is effective in killing cells at hyperthermic conditions[60]. At

temperatures > 60°C, almost all cells undergo coagulation necrosis with massive protein denaturation and DNA damage[61]. With advanced mathematical simulation and technical developments, faster hyperthermic kinetics, better probe design, and larger coagulation zones have been achieved in major ablation modalities[62-64]. Paradoxically, tumor thermal ablation has also been shown to enhance tumor progression and recurrence, regardless of the extent of ablation[32]. Not all tumor cells can be ablated. It has been shown that the location of the tumor has been one of the risk factors of incomplete tumor ablation and recurrence[56].

Specifically, tumor cells adjacent to large blood vessels not only have better nutrient supplies, but also receive less heating, either due to the position of the probe (usually away from major vessels to avoid bleeding) or to the heat sink effect, which is more pronounced in liver cancer due to its abundant vasculature. Limited clinical efficacy also persists among large tumors (>3 cm)[65, 66], which cannot be overcome even by multiple ablations. More importantly, the cells further from the ablation tip, especially those at the periphery of ablated tumors, will not experience coagulation necrosis, but rather sub-lethal hyperthermia or mild heat stress. In such cases, protein denaturation and DNA impairment occur at a much lower level[67]. The cells are able to express and secrete multiple cellular factors to minimize the impact of thermal stress for survival and serve as new niches for neoplastic growth[25].

In this study, we used electrocauterization, a simplified but widely used clinical ablation device, to ablate tumors in a HCC murine model. Up to 40% tumor relapse was observed after a single ablation treatment, despite strong evidence of cell killing by histology studies. In order to increase ablation efficiency and decrease tumor recurrence,

several groups have combined thermal ablation with either chemotherapy or radiation[68-70]. These adjuvant therapies can target tumor cells at the ablated margins by inducing cell apoptosis and enhancing cytotoxicity. Chemotherapies can also fill the gaps inside the high temperature area as observed by other groups and confirmed in this study. Specifically, Lindner *et al* used RFA combined with Thermo-Dox to deliver the doxorubicin in breast cancer cells[71, 72]. This combination has displayed superior efficacy over either ablation or chemotherapy alone and the study is currently moving into clinical trials (# NCT00617981). The formulation of Thermo-Dox has been optimized such that the therapeutic payload is preferentially released at hyperthermic temperatures. Further studies have been encouraging as it achieved a 2-fold increase of cell apoptosis compared with free drug ablation[28]. Using similar formulations, Yang *et al* further delivered both paclitaxel and HSP70 inhibitor quercetin to a rat breast cancer model with increased tumor abrogation[29].

To explore more significant clinical benefits of combined chemotherapy and ablation, a logical step forward is to exploit the synergy between ablation and adjuvant chemotherapies to obtain optimal tumor cell injury. Several groups have probed the molecular mechanisms of tumor recurrence in the context of ablation. Our study reconciles these observations, identifying that HSP90 is upregulated after tumor ablation and recurrence occurred in murine models receiving ablation only. Therefore, we proposed a synchronous thermal ablation with systemic HSP90 inhibition through thermo-responsive ELP-GA conjugates to not only kill the tumor cells around the ablation core but also to eradicate the cells at the ablated margins where viable cells express more HSP90.

HSP90 inhibitors have been developed over three decades and continuous effort has been made to develop more potent agents as more understanding of the heat shock pathway in cancer is revealed. Numerous oncogenic proteins remain targets as client proteins of HSP90. Thus, inhibition of HSP90 can lead to suppression of multiple targets with reduced drug resistance, drug tolerance, or drug-drug interaction. We chose geldanamycin (GA) for its high potency and improved cytotoxicity when combined with hyperthermia. However, GA has limited clinical use due to its hepatotoxicity, therefore requiring an advanced formulation. We demonstrated that thermo-responsive ELP-based biopolymers not only increase GA's water solubility but also achieve lower systemic toxicity though the conjugation with a pH-sensitive hydrozone linkage. We achieved a 2-3-fold increase of cell eradication when exposed to 30 min of hyperthermia *in vitro* with strong suppression of HSP90.

The safety of conjugates was further confirmed by toxicity studies, including blood chemistry and endotoxin testing (results not shown). ELP-GA is biocompatible *in vivo* and the maximum tolerated dose (MTD, 100 mg/kg) is 200-times that of IC50 *in vitro*. We arbitrarily chose half of the MTD and administered GA twice weekly in an aggressive HCC murine model and showed that downregulation of HSP90 contributed significantly to slower tumor progression. However, although the conjugates alone displayed superior efficacy to the free drug (17-AAG) and controls, they are still limited for tumor regression. Sufficient drug delivery into the tumor has been a daunting task where multiple barriers, including high interstitial pressure, limited EPR effect, and tumor cell heterogeneity, are yet to be overcome. Impressively, when ELP-GA conjugates were combined with thermal ablation (electrocautery), we achieved > 90%

cell eradication, greater HSP90 inhibition, and no tumor recurrence up to 70 days. Ongoing studies are comparing the concentration of GA in both the tumor core and tumor margins after single or combined treatment. This information will help probe the mechanism of two-way synergy between ablation and macromolecular drug delivery. Given the fact that blood circulation of mice is 5-6 seconds, immediate injection after ablation is unlikely to get no benefit from hyperthermia as a result of ablation. However, the therapeutic potential of ELP phase transition can be further illustrated by a control study where ELP conjugates are injected long after ablation to rule out the effect of hyperthermia. In addition, we initially designed the ELPVA80 polymer to be the thermal-insensitive control, but the yields were too poor for animal studies due to its higher Tt. Nevertheless, a separate animal study to quantify ELP concentrations as a function of ablation is ideal. This information will help improve the design of ELP-based polymer conjugates to rapidly aggregate at the ablated site to achieve maximum accumulation and distribution into tumor tissues. Continued effort is also needed to optimize the dosing regimens and improve the ablation method to further exploit thermal targeting of ELP conjugates. For a translational point of view, an orthotropic liver cancer model, which has a more comprehensive tumor microenvironment and similarity to human HCCs, should be further pursued and optimized for clinical development of chemotherapy combined with thermal ablation. Our study paves the way for combining other chemotherapies, especially those with HSP90-sensitive clients (e.g., HER2), to achieve better clinical outcomes.

4.5 Conclusion

In this chapter, ELP triblock biopolymers conjugated with GA were synthesized and characterized. Conjugates offered high yield, purity, and conjugation with rapid thermo transition behavior in cell culture conditions. pH-sensitive drug release at the lysosomal state was also achieved. When combined with hyperthermia, conjugates exert more cytotoxicity in both HepG2 and Hep3B cells than normothermia control. The hyperthermia treatment also enhanced the cellular uptake of conjugates despite endocytosis inhibition. HSP90 levels were inhibited with a IC_{50} dose within one day of treatment. The in vivo results further substantiate the finding that a combination of thermal ablation and adjuvant HSP90 inhibition via thermo-responsive ELP-GA conjugates can exert a superior antitumor effect in an HCC murine model. The vast tumor eradication provides compelling rationale for further exploring the postablation kinetics of HSP90 expression for optimal dosing to achieve progression-free and long-term survival of HCC patients.

4.6 Reference

1. Lu MD, Xu HX, Xie XY, Yin XY, Chen JW, Kuang M, et al. Percutaneous microwave and radiofrequency ablation for hepatocellular carcinoma: a retrospective comparative study. J Gastroenterol 2005;40:1054-60.

2. Lu DS, Yu NC, Raman SS, Limanond P, Lassman C, Murray K, et al. Radiofrequency ablation of hepatocellular carcinoma: treatment success as defined by histologic examination of the explanted liver. Radiology 2005;234:954-60.

3. Park W, Chung YH, Kim JA, Jin YJ, Lee D, Shim JH, et al. Recurrences of hepatocellular carcinoma following complete remission by transarterial chemoembolization or radiofrequency therapy: Focused on the recurrence patterns. Hepatol Res 2013;43:1304-12.

4. Waki K, Aikata H, Katamura Y, Kawaoka T, Takaki S, Hiramatsu A, et al. Percutaneous radiofrequency ablation as first-line treatment for small hepatocellular carcinoma: results and prognostic factors on long-term follow up. J Gastroenterol Hepatol

2010;25:597-604.

5. Yang Y, Wang C, Lu Y, Bai W, An L, Qu J, et al. Outcomes of ultrasound-guided percutaneous argon-helium cryoablation of hepatocellular carcinoma. HPB 2012;19:674-84.

6. Liu Q, Zhai B, Yang W, Yu LX, Dong W, He YQ, et al. Abrogation of local cancer recurrence after radiofrequency ablation by dendritic cell-based hyperthermic tumor vaccine. Mol Ther 2009;17:2049-57.

7. Zhang Y, Zhao J, Guo D, Zhong W, Ran L. Evaluation of short-term response of high intensity focused ultrasound ablation for primary hepatic carcinoma: Utility of contrast-enhanced MRI and diffusion-weighted imaging. Eur J Radiol 2011;79:347-52.

8. Cheung TT, Fan ST, Chu FS, Jenkins CR, Chok KS, Tsang SH, et al. Survival analysis of high-intensity focused ultrasound ablation in patients with small hepatocellular carcinoma. HPB 2013;15:567-73.

9. Itoh S, Ikeda Y, Kawanaka H, Okuyama T, Kawasaki K, Eguchi D, et al. Efficacy of surgical microwave therapy in patients with unresectable hepatocellular carcinoma. Ann Surg Oncol 2011;18:3650-6.

10. Liu Y, Zheng Y, Li S, Li B, Zhang Y, Yuan Y. Percutaneous microwave ablation of larger hepatocellular carcinoma. Clin Radiol 2013;68:21-6.

11. Veltri A, Guarnieri T, Gazzera C, Busso M, Solitro F, Fora G, et al. Long-term outcome of radiofrequency thermal ablation (RFA) of liver metastases from colorectal cancer (CRC): size as the leading prognostic factor for survival. Radiol Med 2012;117:1139-51.

12. Yamakado K, Nakatsuka A, Ohmori S, Shiraki K, Nakano T, Ikoma J, et al. Radiofrequency ablation combined with chemoembolization in hepatocellular carcinoma: Treatment response based on tumor size and morphology. J Vasc Interv Radiol 2002;13:1225-32.

13. Mulier S, Ni Y, Jamart J, Ruers T, Marchal G, Michel L. Local recurrence after hepatic radiofrequency coagulation: multivariate meta-analysis and review of contributing factors. Ann Surg 2005;242:158-71.

14. Lin SM, Lin CJ, Lin CC, Hsu CW, Chen YC. Randomised controlled trial comparing percutaneous radiofrequency thermal ablation, percutaneous ethanol injection, and percutaneous acetic acid injection to treat hepatocellular carcinoma of 3 cm or less. Gut 2005;54:1151-6.

15. Wiggermann P, Puls R, Vasilj A, Sieron D, Schreyer AG, Jung EM, et al. Thermal ablation of unresectable liver tumors: factors associated with partial ablation and the impact on long-term survival. Med Sci Monit 2012;18:CR88-92.

16. Schumann C, Rieder C, Bieberstein J, Weihusen A, Zidowitz S, Moltz JH, et al. State of the art in computer-assisted planning, intervention, and assessment of liver-tumor ablation. Crit Rev Biomed Eng 2010;38:31-52.

17. Goldberg SN, Solbiati L. Tumor dissemination after radiofrequency ablation of hepatocellular carcinoma. Hepatology 2001;34:609; author reply 10-1.

18. Kuszyk BS, Boitnott JK, Choti MA, Bluemke DA, Sheth S, Magee CA, et al. Local tumor recurrence following hepatic cryoablation: radiologic-histopathologic correlation in a rabbit model. Radiology 2000;217:477-86.

19. Supic G, Kozomara R, Jovic N, Zeljic K, Magic Z. Prognostic significance of tumor-related genes hypermethylation detected in cancer-free surgical margins of oral squamous cell carcinomas. Oral Oncol 2011;47:702-8.

20. Kim YS, Rhim H, Cho OK, Koh BH, Kim Y. Intrahepatic recurrence after percutaneous radiofrequency ablation of hepatocellular carcinoma: analysis of the pattern and risk factors. Eur J Radiol 2006;59:432-41.

21. Berber E, Siperstein A. Local recurrence after laparoscopic radiofrequency ablation of liver tumors: an analysis of 1032 tumors. Ann Surg Oncol 2008;15:2757-64.

22. Yoshida S, Kornek M, Ikenaga N, Schmelzle M, Masuzaki R, Csizmadia E, et al. Sublethal heat treatment promotes epithelial-mesenchymal transition and enhances the malignant potential of hepatocellular carcinoma. Hepatology 2013;58:1667-80.

23. Burks SR, Ziadloo A, Hancock HA, Chaudhry A, Dean DD, Lewis BK, et al. Investigation of cellular and molecular responses to pulsed focused ultrasound in a mouse model. PloS One 2011;6:e24730.

24. Yang JD, Nakamura I, Roberts LR. The tumor microenvironment in hepatocellular carcinoma: current status and therapeutic targets. Semin Cancer Biol 2011;21:35-43.

25. Quail DF, Joyce JA. Microenvironmental regulation of tumor progression and metastasis. Nat Med 2013;19:1423-37.

26. Groeschl RT, Wong RK, Quebbeman EJ, Tsai S, Turaga KK, Pappas SG, et al. Recurrence after microwave ablation of liver malignancies: a single institution experience. HPB 2013;15:365-71.

27. Goldberg SN, Kamel IR, Kruskal JB, Reynolds K, Monsky WL, Stuart KE, et al. Radiofrequency ablation of hepatic tumors: increased tumor destruction with adjuvant liposomal doxorubicin therapy. Am J Roentgenol 2002;179:93-101.

28. Yang W, Ahmed M, Elian M, Hady el SA, Levchenko TS, Sawant RR, et al. Do liposomal apoptotic enhancers increase tumor coagulation and end-point survival in percutaneous radiofrequency ablation of tumors in a rat tumor model? Radiology

2010;257:685-96.

29. Yang W, Ahmed M, Tasawwar B, Levchenko T, Sawant RR, Collins M, et al. Radiofrequency ablation combined with liposomal quercetin to increase tumour destruction by modulation of heat shock protein production in a small animal model. Int J Hyperthermia 2011;27:527-38.

30. von Breitenbuch P, Köhl G, Guba M, Geissler E, Jauch KW, Steinbauer M. Thermoablation of colorectal liver metastases promotes proliferation of residual intrahepatic neoplastic cells. Surgery 2005;138:882-7.

31. Nikfarjam M, Muralidharan V, Christophi C. Altered growth patterns of colorectal liver metastases after thermal ablation. Surgery 2006;139:73-81.

32. Kroeze SGC, Van Melick HHE, Nijkamp MW, Kruse FK, Kruijssen LWJ, Van Diest PJ, et al. Incomplete thermal ablation stimulates proliferation of residual renal carcinoma cells in a translational murine model. BJU Int 2012;110:281-6.

33. Sajjadi AY, Mitra K, Grace M. Expression of heat shock proteins 70 and 47 in tissues following short-pulse laser irradiation: Assessment of thermal damage and healing. Med Eng Phys 2013;35:1406-14.

34. Kroeze SG, van Melick HH, Nijkamp MW, Kruse FK, Kruijssen LW, van Diest PJ, et al. Incomplete thermal ablation stimulates proliferation of residual renal carcinoma cells in a translational murine model. BJU Int 2012;110:E281-6.

35. Parsell DA, Lindquist S. The function of heat-shock proteins in stress tolerance: degradation and reactivation of damaged proteins. Ann Rev Genetics 1993;27:437-96.

36. Yavelsky V, Vais O, Piura B, Wolfson M, Rabinovich A, Fraifeld V. The role of Hsp90 in cell response to hyperthermia. J Therm Biol 2004;29:509-14.

37. Sun Y, Zang Z, Xu X, Zhang Z, Zhong L, Zan W, et al. Differential proteomics identification of HSP90 as potential serum biomarker in hepatocellular carcinoma by two-dimensional electrophoresis and mass spectrometry. Int J Mol Sci 2010;11:1423-33.

38. Koga F, Kihara K, Neckers L. Inhibition of cancer invasion and metastasis by targeting the molecular chaperone heat-shock protein 90. Anticancer Res 2009;29:797-807.

39. Bohonowych JE, Gopal U, Isaacs JS. Hsp90 as a gatekeeper of tumor angiogenesis: clinical promise and potential pitfalls. J Oncol 2010;2010:412985.

40. Teng Y, Ngoka L, Mei Y, Lesoon L, Cowell JK. HSP90 and HSP70 Proteins Are Essential for Stabilization and Activation of WASF3 Metastasis-promoting Protein. J Biol Chem 2012;287:10051-9.

41. Roe SM, Prodromou C, O'Brien R, Ladbury JE, Piper PW, Pearl LH. Structural

basis for inhibition of the Hsp90 molecular chaperone by the antitumor antibiotics radicicol and geldanamycin. J Med Chem 1999;42:260-6.

42. Blagosklonny MV, Toretsky J, Neckers L. Geldanamycin selectively destabilizes and conformationally alters mutated p53. Oncogene 1995;11:933-9.

43. Supko JG, Hickman RL, Grever MR, Malspeis L. Preclinical pharmacologic evaluation of geldanamycin as an antitumor agent. Cancer Chemother Pharmacol 1995;36:305-15.

44. Chen Y, Youn P, Furgeson DY. Thermo-targeted drug delivery of geldanamycin to hyperthermic tumor margins with diblock elastin-based biopolymers. J Control Release 2011;155:175-83.

45. Fujita Y, Mie M, Kobatake E. Construction of nanoscale protein particle using temperature-sensitive elastin-like peptide and polyaspartic acid chain. Biomaterials 2009;30:3450-7.

46. Antonietti M, Heinz S, Schmidt M, Rosenauer C. Determination of the micelle architecture of polystyrene/poly(4-vinylpyridine) block copolymers in dilute solution. Macromolecules 1994;27:3276-81.

47. Callahan DJ, Liu W, Li X, Dreher MR, Hassouneh W, Kim M, et al. Triple stimulus-responsive polypeptide nanoparticles that enhance intratumoral spatial distribution. Nano letters 2012;12:2165-70.

48. Maeda H, Wu J, Sawa T, Matsumura Y, Hori K. Tumor vascular permeability and the EPR effect in macromolecular therapeutics: a review. J Control Release 2000;65:271-84.

49. Szmacinski H, Lakowicz JR. Optical measurements of pH using fluorescence lifetimes and phase-modulation fluorometry. Anal Chem 1993;65:1668-74.

50. Bae Y, Buresh RA, Williamson TP, Chen THH, Furgeson DY. Intelligent biosynthetic nanobiomaterials for hyperthermic combination chemotherapy and thermal drug targeting of HSP90 inhibitor geldanamycin. J Control Release 2007;122:16-23.

51. Ito A, Saito H, Mitobe K, Minamiya Y, Takahashi N, Maruyama K, et al. Inhibition of heat shock protein 90 sensitizes melanoma cells to thermosensitive ferromagnetic particle-mediated hyperthermia with low Curie temperature. Cancer Sci 2009;100:558-64.

52. Larson N, Gormley A, Frazier N, Ghandehari H. Synergistic enhancement of cancer therapy using a combination of heat shock protein targeted HPMA copolymer–drug conjugates and gold nanorod induced hyperthermia. J Control Release 2013;170:41-50.

53. Song CW, Kang MS, Rhee JG, Levitt SH. The effect of hyperthermia on vascular

function, pH, and cell survival. Radiology 1980;137:795-803.

54. Kong G, Anyarambhatla G, Petros WP, Braun RD, Colvin OM, Needham D, et al. Efficacy of liposomes and hyperthermia in a human tumor xenograft model: importance of triggered drug release. Cancer Res 2000;60:6950-7.

55. Hildebrandt B, Wust P, Ahlers O, Dieing A, Sreenivasa G, Kerner T, et al. The cellular and molecular basis of hyperthermia. Crit Rev Oncol Hematol 2002;43:33-56.

56. Huang HW. Influence of blood vessel on the thermal lesion formation during radiofrequency ablation for liver tumors. Med Phys. 2013;40:073303.

57. Raucher D, Chilkoti A. Enhanced uptake of a thermally responsive polypeptide by tumor cells in response to its hyperthermia-mediated phase transition. Cancer Res 2001;61:7163-70.

58. Wang LH, Rothberg KG, Anderson RG. Mis-assembly of clathrin lattices on endosomes reveals a regulatory switch for coated pit formation. J Cell Biol 1993;123:1107-17.

59. Szklaruk J, Silverman PM, Charnsangavej C. Imaging in the diagnosis, staging, treatment, and surveillance of hepatocellular carcinoma. Am J Roentgenol 2003;180:441-54.

60. Nikfarjam M, Muralidharan V, Christophi C. Mechanisms of focal heat destruction of liver tumors. J Surg Res 2005;127:208-23.

61. Chu KF, Dupuy DE. Thermal ablation of tumours: biological mechanisms and advances in therapy. Nat Rev Cancer 2014;14:199-208.

62. Wright AS, Lee FT, Jr., Mahvi DM. Hepatic microwave ablation with multiple antennae results in synergistically larger zones of coagulation necrosis. Ann Surg Oncol 2003;10:275-83.

63. Dong BW, Zhang J, Liang P, Yu XL, Su L, Yu DJ, et al. Sequential pathological and immunologic analysis of percutaneous microwave coagulation therapy of hepatocellular carcinoma. Int J Hyperthermia 2003;19:119-33.

64. Mala T. Cryoablation of liver tumours - a review of mechanisms, techniques and clinical outcome. Minim Invasive Ther Allied Technols 2006;15:9-17.

65. de Baere T, Elias D, Dromain C, Din MG, Kuoch V, Ducreux M, et al. Radiofrequency ablation of 100 hepatic metastases with a mean follow-up of more than 1 year. Am J Roentgenol 2000;175:1619-25.

66. Wood TF, Rose DM, Chung M, Allegra DP, Foshag LJ, Bilchik AJ. Radiofrequency ablation of 231 unresectable hepatic tumors: indications, limitations, and complications. Ann Surg Oncol 2000;7:593-600.

67. Fajardo LF, Egbert B, Marmor J, Hahn GM. Effects of hyperthermia in a malignant tumor. Cancer 1980;45:613-23.

68. Grieco CA, Simon CJ, Mayo-Smith WW, DiPetrillo TA, Ready NE, Dupuy DE. Percutaneous image-guided thermal ablation and radiation therapy: outcomes of combined treatment for 41 patients with inoperable stage I/II non-small-cell lung cancer. J Vasc Interv Radiol 2006;17:1117-24.

69. Ahmed M, Goldberg SN. Combination radiofrequency thermal ablation and adjuvant IV liposomal doxorubicin increases tissue coagulation and intratumoural drug accumulation. Int J Hyperthermia 2004;20:781-802.

70. Horkan C, Dalal K, Coderre JA, Kiger JL, Dupuy DE, Signoretti S, et al. Reduced tumor growth with combined radiofrequency ablation and radiation therapy in a rat breast tumor model. Radiology 2005;235:81-8.

71. Goldberg SN, Girnan GD, Lukyanov AN, Ahmed M, Monsky WL, Gazelle GS, et al. Percutaneous tumor ablation: increased necrosis with combined radio-frequency ablation and intravenous liposomal doxorubicin in a rat breast tumor model. Radiology 2002;222:797-804.

72. Lindner LH, Eichhorn ME, Eibl H, Teichert N, Schmitt-Sody M, Issels RD, et al. Novel temperature-sensitive liposomes with prolonged circulation time. Clin Cancer Res 2004;10:2168-78.

CHAPTER 5

IN VIVO BIODISTRIBUTION AND TUMOR DRUG ACCUMULATION OF ELP-GA CONJUGATES UNDER HYPERTHERMIA

5.1 Introduction

Accumulation of chemotherapeutics in the tumor tissues remains a big challenge for anticancer therapy. Although amount of dosage administered for the patient highly depends on the drug and tumor, there is still much room for improvement to the current methodology. Being small in molecular weight and poorly soluble in water, systemic chemotherapeutics exhibit unfavorable pharmacokinetic characteristics, trigger systemic toxicity and side effects, and rapidly clear out demanding repeated injection. Macromolecular drug delivery carriers have been shown to increase the half-life of the chemotherapeutics from minutes to days, aid safe transportation in the bloodstream, and reach the desired tumor tissue with a localized high concentration. It has been shown that with the aid of high molecular weight carrier, the amount of the intratumoral concentration has increased from the original 1-2% to about 10%[1, 2]. The 500% improvement is phenomenal; nevertheless, there are still 90% of highly potent drugs remaining in the body and may trigger unwanted toxicity.

Hyperthermia has been used as an adjuvant anticancer therapy and exploited as an active targeting strategy for higher drug accumulation[3]. Using radiofrequency ablation (RFA) and liposomal doxorubicin, the combination therapy achieved 2-14-fold increase

of drug accumulation in tumor[4]. Similarly, high intensity focused ultrasound (HIFU) is used to deliver temozolomide and achieved 2-4-fold increase of localization in brain tumor[5]. There are clear indications that the combination therapy has synergistic effect, but the mechanisms are still unclear. Our group has been interested in thermal ablation since it is widely used in interventional oncology; however, such treatment method also has high recurrence rate[6-10]. We hypothesize that although ablation is highly effective in killing the tumor core with high temperature, it also creates a hyperthermic margin and survival through upregualtion of heat shock proteins (HSPs). To deliver the highly hydrophobic, but potent HSP90 inhibitor geldanamycin (GA), we proposed using thermo-responsive, elastin-like polypeptides (ELP) as macromolecular drug carriers. We have shown in Chapter 4 that high concentrations of GA can be conjugated onto the ELP backbone. The conjugates achieved significant cytotoxicity and HSP90 depletion in liver cancer cells. In addition, the combination of thermal ablation (electrocautery) and heat shock protein inhibition exerted superior anticancer efficacy through efficient HSP90 suppression, which results in long-term tumor remission. To answer whether the effect is a result of thermo-targeting and higher accumulation at the heated tumor, biodistribution and intratumoral accumulation studies were conducted to quantify the amount of GA. In the meantime, we have reviewed the plasma stability and acute toxicity profile from the maximum tolerated dose (MTD) study and the ELP-GA conjugates were prepared as previously described. The conjugates showed little degradation over 72 h in fresh mouse plasma. In MTD studies, different concentrations of free drug or conjugates were intravenously (i.v.) injected through the tail vein to both normal and tumor-bearing mice. The biodistribution of the free drug 17-AAG and ELP-GA conjugates in major organs

and tumor margins with or without ablation were measured at different time points up to 72 h postinjection (p.i.). The result suggests that the ELP-GA conjugates with ablation achieve 80% higher accumulation in the tumor margin than the nonablated at 4 h postablation, and the accumulation is 10 times higher than that of free drug; therefore, the synergistic anticancer effect is partially attributed by the enhanced accumulation of GA conjugates after a single dose.

5.2 Materials and methods

5.2.1 Materials

E. coli BLR (DE3) strains were obtained from Novagen (Madison, WI). Circle-Grow culture medium was purchased from Q-Biogene (Carlsbad, CA). Geldanamycin (GA), 7-N-allylamino-17-demethoxygeldanamycin (17-AAG) was obtained from LC Laboratories (Woburn, MA) and structure confirmed upon receipt by 1H-NMR. Carbenecillin sodium salt, PBS tablets were purchased from ISC Bioexpress (Kaysville, UT). Aminoacetaldehyde diethyl acetal (AAADA), chloroform, carbohydrazide, 1-ethyl-3-(3-dimethylaminopropyl) carbodiimide (EDC) hydrocholide, sulfo-N-hydroxysuccinimide (NHS), Atto 488 NHS ester, and dimethyl sulfoxide (DMSO) were from Sigma-Aldrich (St. Louis, MO), and used as received. Cell culture: HepG2 (ATCC HB-8065; human HCC). Cells were cultured as per ATCC instructions. Briefly, HepG2 cells were cultured in Dulbecco's modified Eagle's medium (DMEM) supplemented with 10% fetal bovine serum (FBS) and 1% penicillin streptomycin; All cells were grown and maintained at 37 °C, 5% CO2, and routinely washed and subcultured at ~90% confluence. Animals: 4-10 week old, female athymic nude mice were purchased from Simonsen Laboratories (Gilroy, CA). Animal studies were completed according to the University of Utah

IACUC guidelines.

5.2.2 Synthesis and characterization of triblock ELP-GA conjugates

Aldehyde-modified geldanamycin (GA-CHO) was conjugated to carbohydrazide modified ELP triblock copolymer, which yields a pH-sensitive (hydrazone) bond, shown in **Figure 5.1**. The conjugation ratio (GAs per biopolymer) was calculated by both UV-spectrometry (Agilent, CA) and ESI mass spectrometry. Particle size was measured by dynamic light scattering with a laser goniometer (Brookhaven, NY). The surface charge densities of both free biopolymer and biopolymer-GA conjugates were acquired on an Aetasizer Nano ZS (Malvern Inc, MA). The thermal transition behaviors of the biopolymer alone and biopolymer-GA conjugates were monitored using UV-Vis spectrophotometry as previously described[(11)]. 25 μM triblock ELP or ELP-GA equivalent conjugates were solubilized in DMEM culture media and heated at a speed of 1°C/min from 25 °C-85 °C, and absorption at 650nm was recorded as a function of temperature. The thermal transition temperature (Tt) was calculated as the temperature at the maximum derivative of turbidity at 650 nm. All measurements were conducted in triplicate and expressed as mean ± standard error.

5.2.3 Stability assay in fresh plasma

The *in vitro* degradation profile was determined by incubating 10 μl of ELP-GA conjugates with 90 μl of fresh mouse plasma (from blood collected via cardiac puncture before euthanization and stored in heparin-coated tubes), resulting in a final ELP concentration of 25 μM, at 37 °C. Samples were collected from this mixture at 4, 24, and 72 h and immediately stored at −20 °C. ELP conjugates were purified with a mini ITC

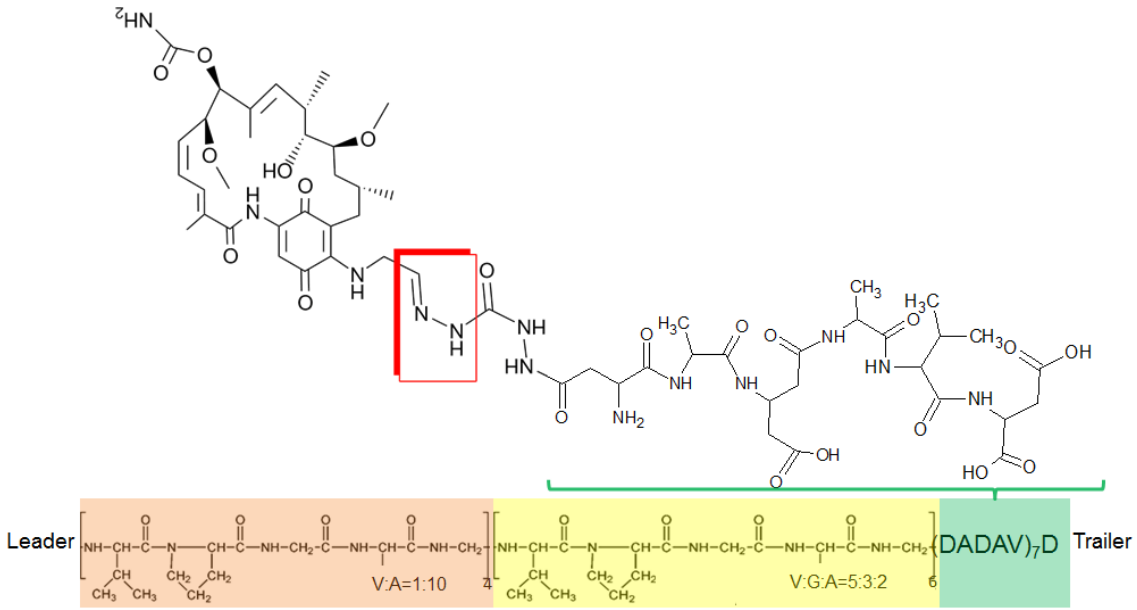

Figure 5.1. Structure of ELP-GA conjugates [ELPVA40-60-$(DADAV)_7D$].

method where conjugates' solution was spiked with 5M NaCl and heated on a heating block at 85 °C for 5 min. Soluble plasma proteins were removed by centrifugation at 16000 rpm at room temperature for 5 min. Next, ELP was resolublized in 500 µL cold PBS and centrifuged again at 4 °C for 5 min. This hot-cold spin was repeated twice before loading onto a Bis-Tris gel for SDS-PAGE (Invitrogen, CA).

5.2.4 Endotoxin assay

Since ELPs are expressed from bacteria culture, they may contain a certain level of bacteria endotoxins. Endotoxins are known to cause fever, diarrhea, and other toxicities in animals[(12)]. Therefore, all drug solutions were subject to endotoxin assay before injection into the animals. Due to the lack of guidance in the literature, the universal acceptable safe endotoxin level is set to be between 0.1-1 EU/mL for injections. If the endotoxin levels are high, drug solutions are filtered through Piece High-Capacity resin (Thermo scientific, IL) until the level is no longer detectable per vendor instruction. The endotoxin level was measured using LAL turbidimetric assay (Lonza, Walkersville, MD). Briefly, endotoxin standards were diluted to various concentrations and vortexed vigorously with the chromogenic agents. 200 µL solutions were added to 96-well plates and incubated in a 37 ºC dry bath for 30 min. A standard curve was generated for a linear relation of endotoxin content and absorption value. The endotoxin levels in all reagents were determined using the standard curve.

5.2.5 Maximum tolerated dose (MTD) determination

Tumor-free nude mice were randomly distributed into several groups with five animals per group and were subject to intravenous injection of drug solution (200 µL) according

to a dose response model for 10 days[13]. Drug suspensions were freshly prepared in sterile PBS for ELP biopolymer and ELP-GA conjugates. GA-CHO was first solubilized in DMSO and diluted 10 times in PBS. Equivalent volume of PBS was also given to mice as control. In a dose escalation model shown in **Table 5.1**, the starting dose of GA-CHO, ELP biopolymer, and ELP-biopolymer was chosen to be 10, 5, and 5 mg/kg, respectively[11]. The animals that survived the injections were weighed daily over a period of 10 days.

Major adverse reactions from mice upon injection include the following symptoms: impaired mobility, severe stress, over 10% weight loss or death, etc. If these major adverse reactions were not observed in all animals receiving the same treatment within 10 days, the next dose level was reached until one or more animals exhibited the major adverse reactions. All surviving animals at the end of the dose response study were euthanized after blood was collected from cardiac puncture. For animals showing major adverse reactions, blood was collected and they were euthanized promptly. No blood sample is recovered from dead animals. Any value in blood chemistry or weight that is over three times of the standard deviation from the mean of the control groups is also considered as evidence of major adverse reaction. The dose is determined as the maximum tolerated dose (MTD) where all animals are free of major adverse events with no abnormal parameters in their blood chemistry. Otherwise, a further decreased dose was selected until all major adverse reactions mentioned above were absent in all animals. **Table 5.1** summarizes the dose and concentrations of each agent given to animals.

Table 5.1. Dose escalation model for MTD study.

Compound	Dose (mg/kg)					
	GA concentration (μM)					
GA-CHO	10	30	50			
	1800	**5300**	**8800**			
ELP triblock	5	10	30	50	100	200
	12	*25*	*75*	*150*	*300*	*600*
ELP-GA		5	10	30	50	100
		60	**140**	**420**	**840**	**1680**

5.2.6. Blood biochemistry

Blood was withdrawn from the cardiac puncture after brief anesthesia through inhalation of isoflurane. The collected blood (0.4-0.9 mL) was stored in heparin-coated centrifuge tubes on ice and was briefly centrifuged at 1000 rpm for 2 min at 4 ºC to collect the supernatant in the upper layer. Serum samples were sent to ANTECH Diagnosis (Irvine, CA) for overnight processing.

Major parameters of toxicity include liver function, which was examined with serum levels of total bilirubin levels (TBIL), alanine aminotransferase (ALT), and aspartate aminotransferase (AST). Renal toxicity was evaluated by and creatinine (Cr) blood urea nitrogen (BUN)). Albumin (ALB) or globulin (GLOB) was tested as parameters of tissue damage or inflammation.

5.2.7 Tumor implantation and electrocautery

HepG2 cells were cultured in DMEM media in a 175 cm^2 tissue flask until 70-80 % confluent. Cells were washed with PBS, trypsinized, and centrifuged at 1000 rpm for 3 min. Cells were reconstituted in cold DMEM-Matrigel (BD Biosciences, CA) solution (50:50, v/v). The right flank of each nude mouse was sterilized with isopropyl alcohol prior to injecting a 200 µL suspension ($2\text{-}3\times10^6$ cells) under general anesthesia. Animal weight and tumor size were recorded twice weekly according to the approved IACUC protocol. Once the tumor reaches 5-7 mm in each dimension, each animal was anesthetized via inhalation of 5% isoflurane with a nose cone and subsequently placed on a sterile electrical grounding pad. A heating lamp was placed beside the animal to keep it warm during anesthesia. The tumor area was sterilized with an alcohol swab and a 1-cm small incision was made to expose the tumor. Cauterization was accomplished via an

ESU-30 system (Olympus, FL) at 25 W, coagulation mode, with an electrical pencil (Covidien, MA) placed in the center of the tumor for 5-10 sec.

5.2.8 Biodistribution assays

Tumor-bearing mice were i.v. injected with 200 μL of normal saline, which contains 17 mg/kg 17-AAG or equivalent ELP-GA conjugates. For the combination groups, electrocautery was performed and immediately followed by dependent biodistribution studies carried out by sacrificing mice at 4, 24, and 72 h. At the time of euthanasia, blood was collected as described above. During necropsy, whole organ tissue samples were obtained from lung, liver, kidneys, spleen, and plasma. Whole animal blood was put into a centrifuge tube with separator to harvest the plasma. Tumor margins were defined as 3-5 mm rim from the visible tumor edge or 5 mm away from the ablated tumor core. All tissues were weighed, washed with PBS, and subject to flash freezing and then homogenized in 1 mL lysis buffer using Polytron homogenizer (Westbury, NT). Briefly, tissue samples were homogenized at level 4 for 30 sec on ice until no visible chuck remains. Tissue solution was extracted with 1 mL acetonitrile and extracted with additional 1 mL EtOAc and vortexed for 1 min. The resulting organic layer was transferred to 10 × 75 mm glass culture tubes. Sample in the centrifuge tube was extracted again using the same method and dried under nitrogen flush. Combined samples were finally reconstituted for HPLC analysis (n=3).

5.2.9 Evaluation of drug concentrations in tumor margins

Two separate groups of animals were used for two time points each. 150-200 μL blood was collected[4] through the tail vein at 30 min or 4 h p.i. (Group 1, Group 2). No saline

was replaced as pharmacokinetic parameters would be altered. The weight of the animals were carefully monitored as no animals underwent >10 % weight loss. A second blood collection (24 h for Group 1 and 72 h for Group 2) was realized through cardiac puncture and followed by euthanization[14].

Relative concentrations of drug in tumors following treatment with free drug or copolymer-drug conjugates were evaluated in HCC tumor-bearing mice. Mice were injected (i.v.) via the tail vein with sterile solutions of 17 mg/kg drug equivalent ELP-GA conjugates and 17-AAG. Cohorts of 3 mice per treatment group were sacrificed at 4 h, and 24, 72 h p.i.. Tumors were harvested immediately after euthanization and stored at -80 ºC until analysis. Concentrations of GA-CHO in tumors were determined with HPLC using modification of previously described procedures[11]. Tumor samples were thawed and homogenized using a Brinkman homogenizer (Westbury, NY) in 1 part (weight to volume) PBS[11]. 10 μL of 100 μg/mL 17-AAG (internal standard, IS) in acetonitrile was added to a 240 μL sample of tumor homogenate and mixed[15]. Samples were extracted with 1 mL of ethyl acetate (EtOAc) by vortexing and centrifuged at 14000 rpm for 5 min, and the resulting organic layer was transferred to 10 × 75 mm glass culture tubes. The samples were extracted with an additional 1 mL of EtOAc and the organic layer was combined with the first batch. After drying under nitrogen, resulting residue was dissolved in 100μL of mobile phase and filtered with 0.2 μm polypropylene syringe filter units (Whatman,, NJ) and finally placed in Waters Total Recovery glass vials (Waters Corporation, Milford, MA). 75 μL was injected into the HPLC system as previously described.

A calibration curve was generated for GA-CHO at concentrations of 1, 10, and 100 μg/mL in control tissue homogenate and processed as described above. The curve was constructed by plotting the peak area ratio of GA-CHO to the IS and has shown a linear relationship from 1 to 100 μg/mL. Recovery of 17-AAG standard was 93 ± 3.5%. GA-CHO in tissue samples was quantitated using the ratio of found GA peak area to IS peak area. Major organs were also collected at the point of euthanization and drug was extracted the same way in the tumor.

5.2.10 Statistical analysis

Differences in organ accumulation of the copolymer conjugates and tumor drug concentration were analyzed using one-way ANOVA. Where differences were detected, Boferonni's *post hoc* test was used to test for pairwise differences between the groups.

5.3 Results

5.3.1 Synthesis and characterization of ELP-GA conjugates

We first synthesized ELP triblock copolymer [ELPVA40-60-DADAV)$_7$D] and modified the aspartic acids to introduce reactive amine groups. The aldehyde-modified GA was reacted with amine groups on ELP copolymer to result in a pH-sensitive, hydrozone linker, as shown in **Figure 5.1**. Physicochemical properties of ELP conjugates were summarized in **Table 5.2.** Briefly, high purity ELP was achieved by three rounds of inverse transition cycling (ITC). 4-8 GAs are conjugated onto the ELP backbone determined by mass spectrometry and UV-vis spectrometry. ELP conjugates have a hydrodynamic size just above 100 nm and slightly neutral surface charge. The conjugates also display reproducible transition behavior in culture media with Tt between 42-44 ºC.

Table 5.2. Physicochemical properties of ELP-GA conjugates.

Physicochemical Parameters				
Molecular Weight (Da)	GA content (% wt/wt)	Size (nm)	Charge (mV)	Tt (°C)
48	7.1 ± 2.0	116 ± 23	0.3 ± 1.3	43 ± 1

Hydrodynamic radius and zeta potential were measure at 25 °C with 25 equivalent ELP in PBS (pH7.4, 147 mM), n=3.

5.3.2 Plasma stability and endotoxin levels of ELP conjugates

To predict the stability of conjugates in the blood circulation, conjugates were incubated with mouse plasma incubated at 37 °C up to 72 h. At designated time points, ELP was purified through the mini-ITC method and loaded onto Bis-Tris gel. Overall, most conjugates stay intact over 72 h. However, a certain amount of conjugates were physically bound to plasma proteins, resulting in new bands with larger molecular weights. Degradation by the proteinase is obvious as low molecular weight proteins were shown on the gel in **Figure 5.2**. Increasing amount of lower MW ELP conjugates is observed as a function of time, which can be attributed to GA release from the polymer. The endotoxin level of purified ELP is not detectable by the LAL assay but is higher in the conjugates due to the positive charge. Therefore, the conjugates were subject to an endotoxin removal assay until no endotoxin level was below 1 EU/mL.

5.3.3 Maximum tolerated dose (MTD) and acute toxicity of GA compounds

MTD is defined as the highest dose showing no major adverse reactions in mice over 10 days p.i.. In this study, the animal weight and physical activities were monitored daily with blood chemistry taken at the end. According to the dose escalation model, MTD was determined based on summarized physiological and hematological examinations, as shown in **Table 5.3**. Any values beyond three SDs in the parameters of blood chemistry were considered as a significant difference and the correspondent dose, or any occurrence of animal death, was determined as toxic dose (TD). For the doses given in **Table 5.1**, one animal was dead on the day after injection at 50 mg/kg for GA group; therefore, the MTD for GA is determined to be 30 mg/kg. Animals in both ELP and ELP-GA conjugates' group survived throughout the course of the study with no sign of severe

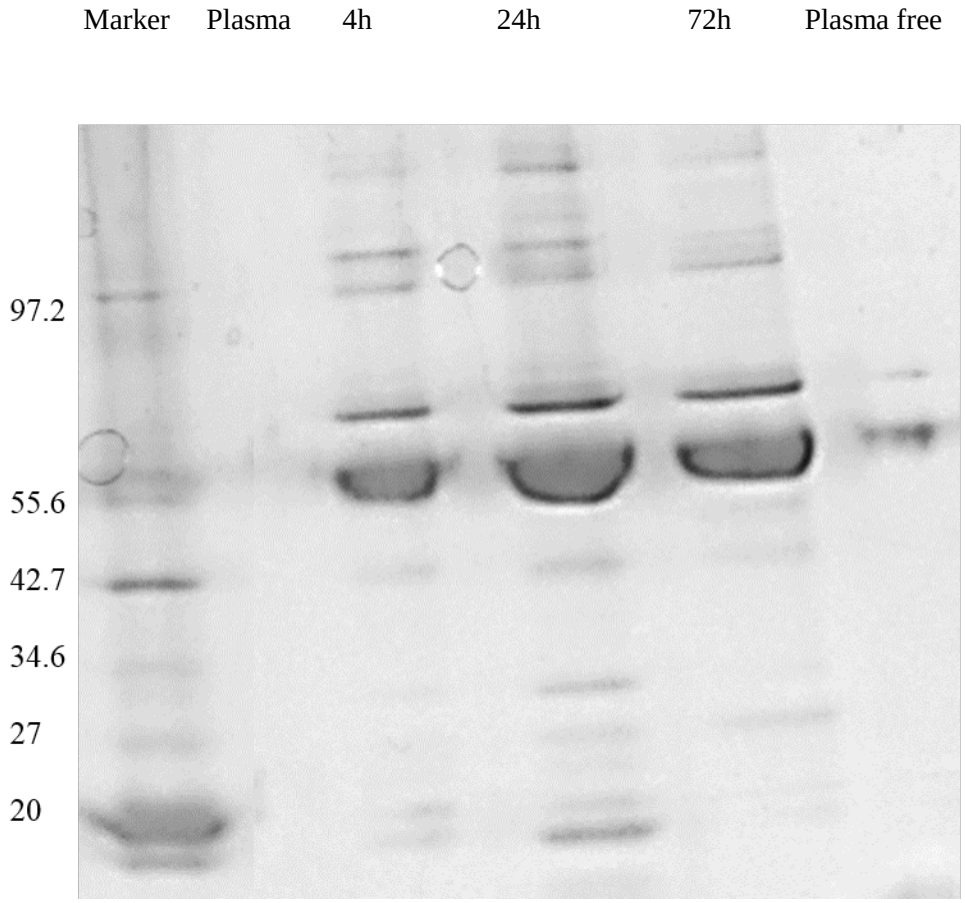

Figure 5.2. *In vitro* plasma stability assay.

ELP degradation visualized by SDS-PAGE after incubation *in vitro* with fresh mouse plasma at 37 °C. The MW is indicated with the MW marker in the left lane and the incubation time is indicated above each lane. The plasma only sample was purified in the same way as incubated ELP-conjugates. Few bands are detectable due to extensive purification from ITC. The plasma free sample contains fresh conjugates in plain PBS.

Table 5.3. Blood chemistry results of mice which exhibited toxicity or death(s) post-injection.

Drug	PBS	GA-CHO	GA-CHO	ELP	ELP	ELP-GA	ELP-GA
MTD (mg/kg)		**30**	50	**100**	200	**50**	100
Chemistry							
Albumin	3.6 ± 1.0	3.4 ± 0.1	n/a [a]	2.5 ± 0.3	2.9 ± 0.3	3.9 ± 0.0	3.6 ± 10.8
Globulin	2.4 ± 0.2	3.2 ± 0.4	n/a	3.2 ± 0.2	3.1 ± 0.3	2.8 ± 0.2	2.7 ± 0.2
BUN	21 ± 2	23 ± 4	n/a	20 ± 4	*28 ± 2* [*]	21 ± 2	*31± 11* [*]
Creatinine	0.2	0.2	n/a	0.2	0.2	0.2	0.3
AST	402 ± 33	472 ± 160	n/a	314 ± 133	*518 ± 100* [*]	391 ± 116	400 ± 146
ALT	55 ± 11	87 ± 17	n/a	85 ± 0.2	81 ± 76	62 ± 2	73 ± 11
Total Bilirubin	0.1 ± 0.1	0.2 ± 0.1	n/a	0.1 ± 0.1	0.1 ± 0.1	0.1 ± 0.1	0.1 ± 0.1
Weight change (%)	4.1 ± 2.5	-5.3 ± 1.5	n/a	-1.5 ± 0.2	-4.1 ± 0.6	1.5 ± 0.2	*-11.5 ± 1.2* [*]

[a] n/a as result of animal death

[*] $p < 0.05$

distress or compromised physical activity. No significant changes were observed in blood biochemical indices[16] except renal toxicity as a result of increased level of BUN for both ELPs and conjugates at 200 and 100 mg/kg, respectively. Therefore, those doses were determined as the toxic dose (TD). Liver dysfunction is evident in TD of ELP shown by increased levels of AST. No inflammatory responses were observed in all animals by albumin or globulin level. Mice in the ELP-GA, 100 mg/kg group, had significant weight loss (>10%) on the day after the injection, although the weight slowly improved to pre-injection state in the following three or four days. Therefore, the MTD dose is determined as 100 and 50 mg/kg for ELP and ELP-GA, respectively.

5.3.4 Biodistribution of ELP-GA conjugates

The results of a 3-day biodistribution study of free-17-AAG, ELP-GA conjugates under both normothermia (NT) and hyperthermia (HT), at 17 mg/kg doses in tumor-bearing mice is shown in **Figure 5.3**. The ablation does not significantly alter the biodistribution with major accumulation in liver and kidney. Specifically, the accumulations of both the conjugates and 17-AAG decrease from 4 h while the free drug is not detectable at 24 h and beyond after injection. Therefore, only 4 h time points were taken for the 17-AAG group (**Figure 5.3.A**). The conjugates, on the other hand, prolong the accumulation until 72 h **(Figure 5.3.B**, $p<0.01$). Drug concentrations in tumor margins are not significant under normothermia, but the conjugates have a higher accumulation than the free drug. Accumulation in all other organs appears to decrease with time. The application of thermal ablation, however, significantly increases the drug accumulation by 80%, but no such difference was observed in 17-AAG group.

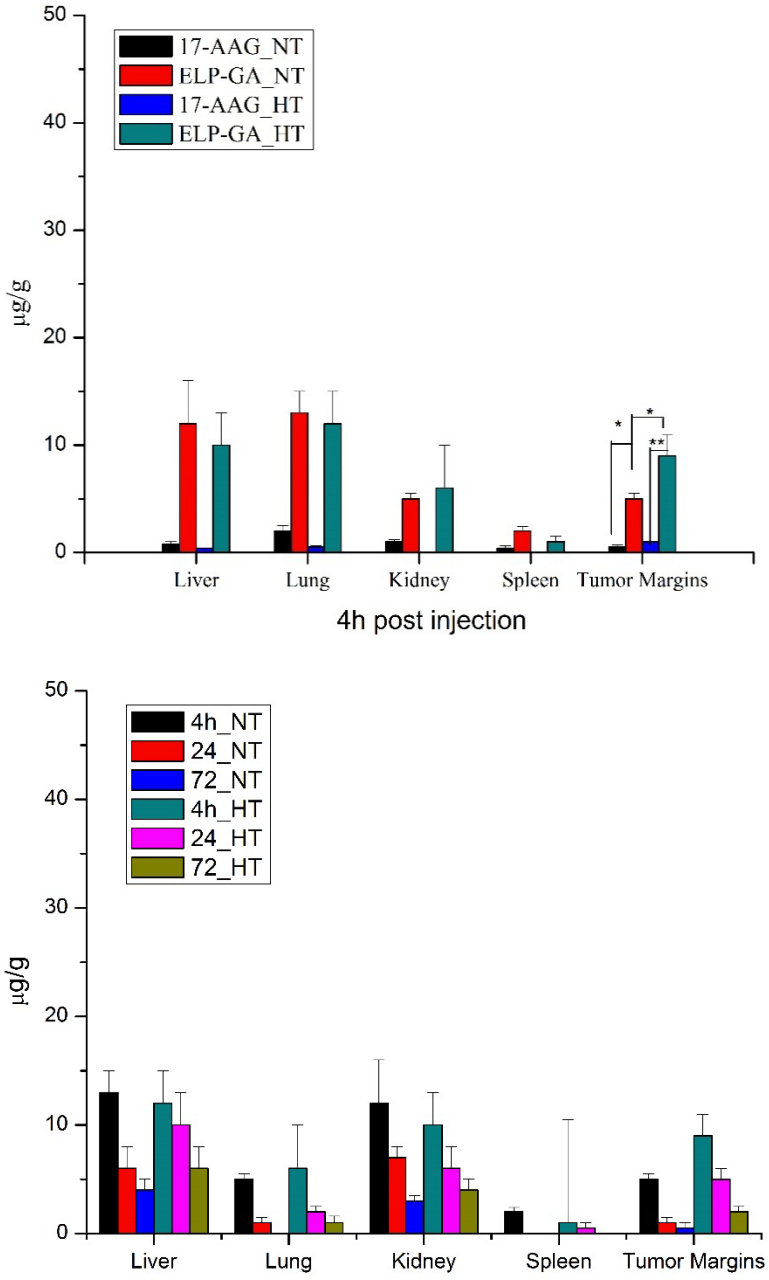

Figure 5.3. Biodistribution of 17-AAG and ELP-GA conjugates.

A) Levels of GA in major organs at 4 h p.i. for both 17-AAG and ELP-GA conjugates. B) Biodistribution of ELP-GA conjugates. Data expressed as mean ± SD, n=3. * $p < 0.05$, ** $p < 0.01$.

Rapid blood clearance was observed for both free drug and conjugates within 24 h p.i., as shown in **Figure 5.4.** Similar to the results in organ accumulation, ELP-GA conjugates displayed a prolonged presence in the blood up to 24 h compared to 17-AAG alone. Total blood concentration over a 4 h period is less than the free drug because a more significant amount of GA may likely be in an aggregated state within the ELP than the free17-AAG. The hyperthermia does have some effect on the systemic circulation of conjugates as less GA was detected within the initial phase (4h); however, the accumulated amount of drug concentrations over 72 h is higher than those of nonablated groups.

5.4 Discussion

The concept of combining chemotherapy with other therapeutic modalities was introduced in the early 1970s[17]. Improved cure rates were achieved by Emil Fei and colleagues who used adjuvant chemotherapy in osteosarcoma patients[18]. However, one of the limitations of this approach is the difficulty to choose suitable compounds. There is increasing awareness in choosing and dosing the drug that gets the best synergistic benefit and improved clinical outcome. In this study, we combine a commonly used thermal ablation modality with heat shock protein (HSP) inhibition that show superior anticancer efficacy in tumor-bearing mice. HSP90 inhibitor, GA, is carried by ELP triblock copolymer that provides rapid thermo-responsiveness upon hyperthermia.

In this study, the ELP conjugates were first tested in fresh mouse serum to monitor their stability and potential reaction with serum. The majority of ELP-conjugates stayed intact during the 72 h incubation time with certain degradation and serum interaction. Shah and colleagues have shown that both elastase and collagenase endopeptidases can

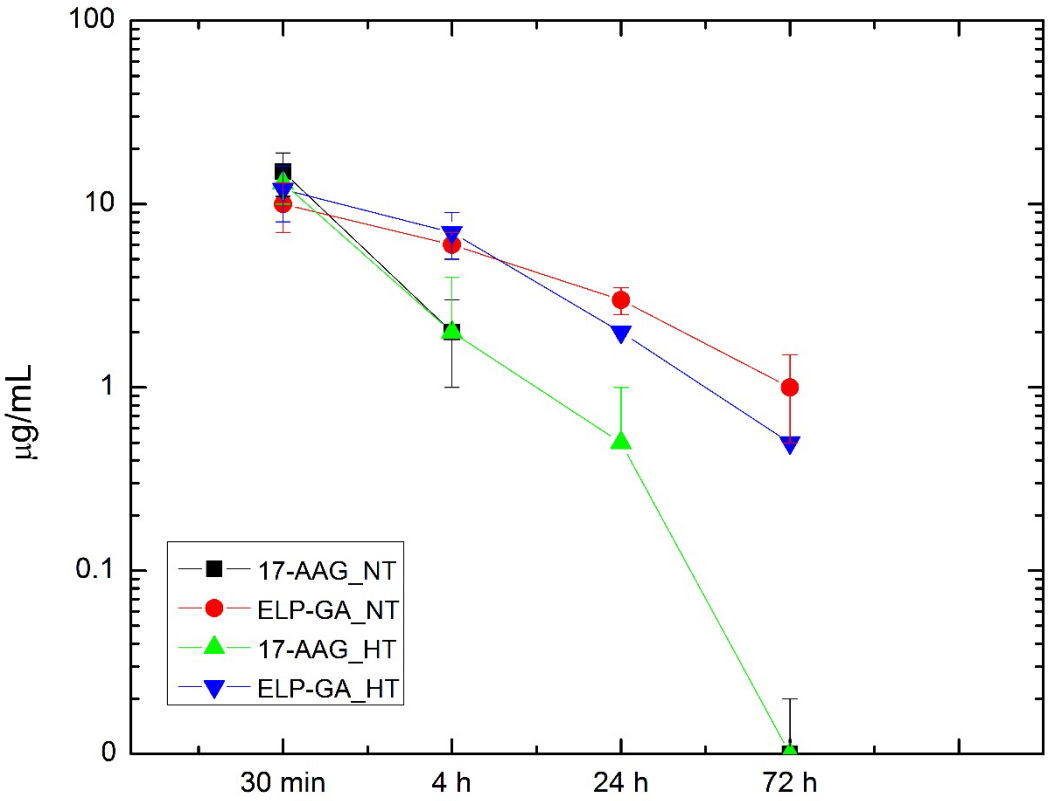

Figure 5.4. Blood concentration of 17-AAG and ELP-GA conjugates with (HT) or without hyperthermia (NT).

Data expressed as mean ± SD, n=3.

proteolytically degrade soluble ELPs[19]. Surprisingly, the degradation can be intervened by the inverse transition behavior. As a result, the half-life of ELP can be increased when hyperthermia is applied over a substantial period of time. It indicates that the repeated thermal ablation hyperthermia at the tumor region following the initial ablation treatment can contribute to even more pronounced accumulation of ELP-based conjugates.

To probe the polymer-drug behavior after systemic injection for better dosing regimen, the concentration of drug in major organs and tumor margins as a function of time needs to be established. Firstly, the toxicities of GA analog 17-AAG, ELP, and conjugates were evaluated in a dose escalation model. GA-CHO released from the conjugates is highly effective in suppressing HSP90 expression postablation; however, it can trigger systemic toxicity when repeatedly injected at high doses. GA-CHO induced acute toxicity at 50 mg/kg, which is higher than the clinically tested 17-AAG, which is shown to be 175-300 mg/kg in humans[20, 21]. Both ELP and ELP conjugates are well tolerated by nude mice even at high concentrations. In addition to its biodegradability, engineered ELP-based biopolymer exhibited excellent biocompatibility in mice or rabbit models[22], with reported MTD up to 800 mg/kg[23]. ELP copolymer presented in this study does not trigger noticeable toxicity until 200 mg/kg. Similarly, the conjugates, although they carry high concentrations of potent GA-CHO, have a MTD dose up to 100 mg/kg, which is 30 times of the dose used in our previous tumor treatment and 6 times of the biodistribution study. The conjugation to a biocompatible ELP-based polymer is to reduce dose-limiting toxicities and improve tumor response through residence of drug at the viable tumor margin. After tissue homogenization, we measured the drug concentrations at major organs, as well as ablated tumor margins with or without thermal ablation. The blood

concentration after the systemic injection does not vary much between 17-AAG and ELP-GA conjugates with 17-AAG slightly higher than the conjugates at early time points. The half-life of 17-AAG has been shown to be around 4 h[24]; therefore, it is anticipated that blood concentration rapidly drops after 4 h p.i., which coincides with others' findings[25]. However, most GA remains bound to the polymer backbone in the 72 h time frame; therefore, the plasma concentration is sustained until after 24 h. GA is designed to release mostly in an acidic environment, not in neutral pH in the circulation. Therefore, it is anticipated that the blood concentration in early time points will not be higher than the free drug. It has been observed by many other groups that efficacy of conjugates does not necessarily correlate to the amount of drug released[15, 26].

The biodistribution of 17-AAG and ELP-GA conjugates was evaluated using a higher dose (17 mg/kg drug equivalent) than the therapeutic dose due to the detection limit of HPLC systems. Nevertheless, this dose is still below the MTD; therefore, single injections at this dose are not expected to trigger toxicity in 72 h. Both free and conjugated drug were rapidly cleared to an undetectable level in 72 h among all tissues with preferential accumulation in liver and kidney[27]. The accumulation may be higher at higher dose as suggested by MTD results where 100 mg/kg of ELP-GA conjugates triggered renal and liver toxicity in one of the treated animals. Whether the accumulation is dose-dependent needs further investigation, and more time points before 24 h are necessary to understand the retention pattern of the conjugates.

Our laboratory, as well as other groups, has shown that ELP polymer conjugates can enhance accumulation in solid tumors compared to nonconjugated drug alone[28, 29]. Drug concentrations after the application of ablation are consistent with other published

results[28, 30] that demonstrated greater accumulation in heated tumor tissues. We specifically excise the tissue from ablated tumor margins as those are the areas where cells evade from thermo-killing, induce heat shock proteins, and promote survival and proliferation. The effect of hyperthermia on EPR effect remains to be investigated. However, high accumulation in the ablated tissue samples, particularly at early time points, is partly due to enhanced permeability of blood vessels and increased blood flow[30, 31]. We anticipate that longer treatment of hyperthermia may contribute to even higher accumulation until the drug transport is saturated. It has also been suggested that higher accumulation is facilitated by the phase transition of ELP under hyperthermia. The conjugates were injected immediately after ablation, which creates a hyperthermic rim for less than 10 sec. Theoretically, blood circulation (5-6 s typically for mice) should allow ELP to reach the tumor site. Therefore, there is a large room of improvement for drug localization using a more powerful ablation device where longer duration of hyperthermia can be achieved.

There are several limitations of the pilot study. Ideally, a control polymer without thermo-sensitivity should be included to further investigate the therapeutic benefit from thermo-targeting. We did design a thermo-insensitive, ELPVA80 homopolymer as the control. It has a Tt around 70ºC and can be regarded as thermo-insensitive, but the yields were too low to conduct a full set of toxicity and biodistribution study. Therefore, we only compared the amount of conjugated GA and free 17-AAG to examine the effect of thermal ablation (hyperthermia) on the accumulation in the tumor margins. Another limitation of the study is the lack of quantification of ELP amounts at the tissue sites. This can be achieved by radio-labeling of ELP-GA conjugates or using ELP that

expressed in media with isotopes[31].

Similar to other combination therapies, the inherent complexity of adjuvant chemotherapy may bring about more questions regarding the proper dosing regimens, and more comprehensive clinical trials are needed to standardize the decision-making process. As thermal ablation is routinely used in the clinics, the adjuvant therapies on a personalized level can be achieved with rational drug selection and dosing for an optimal clinical outcome.

5.5 Conclusion

Long-circulating, ELP-GA conjugates were successfully synthesized to measure their biodistribution and intratumoral accumulation, particularly at the tumor margins. After i.v. injection, the polymer conjugates accumulated preferentially in the liver and kidney, with 5% of injected dose accumulating in tumor margin areas. However, when the injection was performed immediately after the ablation, the accumulation at the margin was raised by 80% in the first 4 h, and has prolonged accumulation until 72 h. Data presented here are the first study evaluating the effect of thermo-responsive, polymer drug carrier on systemically injected HSP90 inhibitor in a clinically relevant setting. The hyperthermia created by thermal ablation can be used to tailor the pharmacokinetics of chemotherapeutics to further augment the cytotoxic effect with less systemic dose. Taken together, this information sheds light on the possibility to reduce excessive dosing on patients and ultimately shorten the treatment duration and to achieve better quality of life.

5.6 Reference

1. Bae YH, Park K. Targeted drug delivery to tumors: myths, reality and possibility. J Control Release 2011;153:198-205.

2. Kwon IK, Lee SC, Han B, Park K. Analysis on the current status of targeted drug delivery to tumors. J Control Release 2012;164:108-14.

3. Larson N, Gormley A, Frazier N, Ghandehari H. Synergistic enhancement of cancer therapy using a combination of heat shock protein targeted HPMA copolymer-drug conjugates and gold nanorod induced hyperthermia. J Control Release 2013;170:41-50.

4. Monsky WL, Kruskal JB, Lukyanov AN, Girnun GD, Ahmed M, Gazelle GS, et al. Radio-frequency ablation increases intratumoral liposomal doxorubicin accumulation in a rat breast tumor model. Radiology 2002;224:823-9.

5. Wei KC, Chu PC, Wang HY, Huang CY, Chen PY, Tsai HC, et al. Focused ultrasound-induced blood-brain barrier opening to enhance temozolomide delivery for glioblastoma treatment: a preclinical study. PloS One 2013;8:e58995.

6. Huang HW. Influence of blood vessel on the thermal lesion formation during radiofrequency ablation for liver tumors. Med Phys 2013;40:073303.

7. Groeschl RT, Wong RK, Quebbeman EJ, Tsai S, Turaga KK, Pappas SG, et al. Recurrence after microwave ablation of liver malignancies: a single institution experience. HPB 2013;15:365-71.

8. Cheung TT, Fan ST, Chu FS, Jenkins CR, Chok KS, Tsang SH, et al. Survival analysis of high-intensity focused ultrasound ablation in patients with small hepatocellular carcinoma. HPB 2013;15:567-73.

9. Yang Y, Wang C, Lu Y, Bai W, An L, Qu J, et al. Outcomes of ultrasound-guided percutaneous argon-helium cryoablation of hepatocellular carcinoma. J Hepatobiliary Pancreat Sci 2012;19:674-84.

10. Kroeze SGC, Van Melick HHE, Nijkamp MW, Kruse FK, Kruijssen LWJ, Van Diest PJ, et al. Incomplete thermal ablation stimulates proliferation of residual renal carcinoma cells in a translational murine model. BJU Int 2012;110:E281-E6.

11. Chen Y YP, Furgeson D.Y. Thermo-targeted drug delivery of geldanamycin to hyperthermic tumor margins with diblock elastin-based biopolymers. J Control Release 2011;155:175-183.

12. Snell ES. Gram-negative bacterial endotoxin and the pathogenesis of fever. Prog Drug Res 1975;19:402-11.

13. Greish K, Thiagarajan G, Herd H, Price R, Bauer H, Hubbard D, et al. Size and surface charge significantly influence the toxicity of silica and dendritic nanoparticles. Nanotoxicology 2012;6:713-23.

14. Veltri A, Guarnieri T, Gazzera C, Busso M, Solitro F, Fora G, et al. Long-term outcome of radiofrequency thermal ablation (RFA) of liver metastases from colorectal cancer (CRC): size as the leading prognostic factor for survival. Radiol Med 2012;117:1139-51.

15. Borgman MP, Aras O, Geyser-Stoops S, Sausville EA, Ghandehari H. Biodistribution of HPMA copolymer-aminohexylgeldanamycin-RGDfK conjugates for prostate cancer drug delivery. Mol Pharm 2009;6:1836-47.

16. Mitruka BM RH. Clinical, biochemical and hematological reference values in normal experimental animals and normal humans. J Clin Pathol 1979;32:96.

17. M S. Sabatine's essentials fo internal medicine. Philadelphia: Williams -Wilkins; 2007.

18. DeVita VT, Jr., Chu E. A history of cancer chemotherapy. Cancer Res 2008;68:8643-53.

19. Shah M, Hsueh PY, Sun G, Chang H, Janib SM, MacKay JA. Biodegradation of elastin-like polypeptide nanoparticles. Prot Sci 2012;21:743-50.

20. Heath EI, Hillman DW, Vaishampayan U, Sheng S, Sarkar F, Harper F, et al. A phase II trial of 17-allylamino-17-demethoxygeldanamycin in patients with hormone-refractory metastatic prostate cancer. Clin Cancer Res 2008;14:7940-6.

21. Ramanathan RK, Trump DL, Eiseman JL, Belani CP, Agarwala SS, Zuhowski EG, et al. Phase I pharmacokinetic-pharmacodynamic study of 17-(allylamino)-17-demethoxygeldanamycin (17AAG, NSC 330507), a novel inhibitor of heat shock protein 90, in patients with refractory advanced cancers. Clin Cancer Res 2005;11:3385-91.

22. Urry DW, Parker TM, Reid MC, Gowda DC. Biocompatibility of the Bioelastic Materials, Poly(GVGVP) and Its γ-Irradiation Cross-Linked Matrix: Summary of Generic Biological Test Results. J Bioact Compat Pol 1991;6:263-82.

23. Walker L, Perkins E, Kratz F, Raucher D. Cell penetrating peptides fused to a thermally targeted biopolymer drug carrier improve the delivery and antitumor efficacy of an acid-sensitive doxorubicin derivative. Int J Pharm 2012;436:825-32.

24. Goetz MP, Toft D, Reid J, Ames M, Stensgard B, Safgren S, et al. Phase I trial of 17-allylamino-17-demethoxygeldanamycin in patients with advanced cancer. J Clin Oncol 2005;23:1078-87.

25. Daozhen C, Lu L, Min Y, Xinyu J, Ying H. Synthesis of (131)I-labeled-[(131)I]iodo-17-allylamino-17-demethoxy geldanamycin ([(131)I]iodo-17-AAG) and its biodistribution in mice. Cancer Biother Radiopharm 2007;22:607-12.

26. Rihova B, Strohalm J, Hovorka O, Subr V, Etrych T, Chytil P, et al. Doxorubicin release is not a prerequisite for the in vitro cytotoxicity of HPMA-based pharmaceuticals: in vitro effect of extra drug-free GlyPheLeuGly sequences. J Control Release 2008;127:110-20.

27. Sun J, Liu L, Jiang X, Chen D, Huang Y. Therapeutic effects of radiolabeled 17-allylamino-17-demethoxygeldanamycin on human H460 nonsmall-cell lung carcinoma xenografts in mice. Cancer Biother Radiopharm 2010;25:155-64.

28. Meyer DE, Shin BC, Kong GA, Dewhirst MW, Chilkoti A. Drug targeting using thermally responsive polymers and local hyperthermia. J Control Release 2001;74:213-24.

29. Moktan S, Perkins E, Kratz F, Raucher D. Thermal Targeting of an Acid-Sensitive Doxorubicin Conjugate of Elastin-like Polypeptide Enhances the Therapeutic Efficacy Compared with the Parent Compound In Vivo. Mol Cancer Ther 2012;11:1547-56.

30. Liu W, Dreher MR, Furgeson DY, Peixoto KV, Yuan H, Zalutsky MR, et al. Tumor accumulation, degradation and pharmacokinetics of elastin-like polypeptides in nude mice. J Control Release 2006;116:170-8.

31. Liu W, Dreher MR, Chow DC, Zalutsky MR, Chilkoti A. Tracking the in vivo fate of recombinant polypeptides by isotopic labeling. J Control Release 2006;114:184-92.

CHAPTER 6

CONCLUSIONS AND FUTURE DIRECTIONS

6.1 Conclusions

As cancer cases continue to rise each year, with high mortality rates, effective treatments remain in desperate demand. Anticancer chemotherapy is still the most widely used treatment for all cancer types; yet, the efficacy and safety of this method remains a major issue to be addressed. Since patients are usually alive for a long period while tumors develop into their very late stages, cancer has, to a large extent, become a chronic disease with a huge burden for both the diseased individual and the health care system. From a drug delivery point of view, a better treatment can be achieved through the use of a system initially proposed as the “magic bullet”, which can carry highly concentrated drugs to the specific tumor site, executing fast-acting and sustained cytotoxicity, with little systemic side effects or long-term toxicity. However, despite 120 years of effort, thousands of papers, and billions of dollars in research funding, no one-size-fits-all, “magic bullet” approach has been found that can ensure both efficacy and a desirable safety profile. We have, on the other hand, learned much during this time about the complex nature of carcinogenesis, drug resistance, cancer heterogeneity, and multiple barriers to the direct targeting of the tumor. It is certain that a better drug delivery system cannot be achieved without a more in-depth understanding of the disease, and how patients respond to treatments. A multipronged approach armed with advanced

technologies—such as the approach introduced in this dissertation—can provide a carrier to overcome some, if not all, barriers to increasing intratumoral drug accumulation with the desired pharmacologic response.

The work performed in this dissertation originated from the observation of a universally high recurrence rate among HCC patients treated by thermal ablation. This shows that there is a critical need to design a treatment that can not only overcome the limitations of ablation, but also exert sufficient cytotoxicity to prevent future tumor relapse. In order to achieve this goal, we designed and evaluated a combination therapy that uses electrocautery with heat shock targeted chemotherapy to achieve a synergistic, long-term anticancer effect in HCC tumor models. The delivery of HSP90 inhibitor is realized through biocompatible, thermo-responsive ELP biopolymer carriers, which show increased drug delivery to tumors upon hyperthermia[1-3].

In the dissertation, it was first necessary to demonstrate that ELP-based polymer conjugates can be efficiently produced and that they exhibit acute thermo-responsiveness upon hyperthermia. In Chapter 3, ELP diblock copolymer conjugates were successfully synthesized and characterized. The HSP90 inhibitor, GA-CHO, was conjugated through a pH-sensitive, hydrazone linker and released preferentially at acidic pH levels. The ability of conjugates to rapidly aggregate upon heat was evaluated by UV-Vis spectrometry and showed excellent reproducibility. The rapidness was maintained in cell culture media with little interaction with serum. In a small pilot study, the copolymer conjugates showed a palliative effect in a very aggressive, rabbit VX2 tumor model where the clinically-tested, free drug, 17-AAG, showed little efficacy and severe side effects such as significant weight loss and eating difficulties. The conjugates, however, exhibited low

transition temperature (~38 ºC) that posed a potential risk for lung embolus in 25% of the animals. Therefore, a new construct with higher transition temperature, smaller, more uniform particle size, and higher hydrodynamic stability was introduced in Chapter 4. The new construct was expanded into three blocks and achieved an even higher yield than the previous diblock copolymers. Upon conjugation to GA, the conjugates displayed desirable physicochemical properties with a transition temperature within 42-44 ºC. It was demonstrated that the conjugates exerted increased cytotoxicity in both HCC cancer cells lines upon 30-min hyperthermia, with effective inhibition of HSP90 in a time- and dose-dependent manner. The thermally enhanced cytotoxicity was more pronounced with the conjugates than with free drug 17-AAG or saline controls, without contribution from the copolymer itself.

Based on the promising results *in vitro,* analogous experiments were performed *in vivo* to further evaluate the benefit of combination therapy. First, we demonstrated that by using a clinically available cautery machine, a thermal ablation with high temperature (>70 ºC) could be achieved along with coagulation necrosis in the ablation core. Meanwhile, the ablated margin area was exposed to a short pulse of hyperthermia, just sufficient to trigger upregulation of HSP90. Next, we combined our pharmacological treatment with the ablation. After ablation and thermal pulse, we immediately injected ELP-GA conjugates intravenously and monitored the tumor growth, as well as HSP90 levels, at the end of the chemotherapy treatment. The conjugates plus ablation displayed superior anticancer efficacy; no tumor relapses were observed at 90 days after treatment, while 25-50% of animals in the ablation only or ablation + free drug groups experienced tumor regrowth. Moreover, HPS90 levels in ELP-GA and the ablation groups were

significantly lower, which are in accordance with the remission of tumors.

To further understand the mechanism of this improved therapeutic outcome, a biodistribution and intratumoral drug concentration study was performed in Chapter 5. Conjugates showed 80% higher accumulation in the tumor compared to the nonablated control, and 10 times higher accumulation than the free drugs. The biodistribution data also suggest nonspecific accumulation in the major organs, but the combination group showed much less accumulation in the liver and kidney, where the toxicity of ELP conjugates can be mainly expected, as suggested by MTD study. This is the first *in vivo* study that comprehensively illustrates the efficacy, accumulation, and the toxicity profile of thermo-responsive ELP conjugates, which can be used to achieve long-term anticancer effect.

In conclusion, this dissertation investigated the use of thermal ablation to effectively abrogate tumor cells at the ablated core and create hyperthermia isotherms to increase the delivery of ELP-GA conjugates for killing the sublethal cells expressing HSPs for survival and recurrence. Data were collected to support the overall hypothesis, and the efficacy was demonstrated in a murine xenograft model. Overall, these results exhibit the potential for the combination of thermal ablation and targeted heat shock inhibition to be used as a tool to increase drug delivery to stressed, inadequately ablated tumor cells and prevent recurrence of HCCs.

6.2 Future directions

Although the work in this dissertation is largely a proof of concept for the application of clinical hyperthermia with targeted, thermo-responsive drug delivery in cancer, there are clear indications that this potential treatment will show a synergistic anticancer effect.

It is also notable that although the drug accumulation is increased with the use of hyperthermia, there is plenty of room to improve the method and its results. Because of tumor heterogeneity and the chaotic structure of blood vessels, one application of ablation may not result in uniform heating in the ablated periphery, and the collapsed tumor tissue may present another barrier for efficient macromolecular transport. This limitation can be partly addressed by multiple applications of short-pulse ablation, each followed by delivery of smaller amounts of polymer conjugates to further increase the intratumoral uptake. Complimentary pharmacokinetic studies are also needed to provide guidance on the proper interval between ablation and systemic chemotherapeutic injection.

Mechanistically, it is important to understand how the combinatorial anticancer effect is related to the biological features of tumors, especially the interstitial fluid pressure (IFP). High IFP at the tumor core is one of the leading barriers for drug delivery[4, 5]. The pressure gradient in tumors originates from morphologically and functionally abnormal blood vessels and a lack of functional lymphatic vessels[6]. Since the vascular density is higher at the tumor periphery, blood flow inside a tumor is often intermittent, which limits the extravasation of macromolecular, nanoparticulate drug delivery systems. Various reports have shown that drug accumulation in the tumor can be significantly increased when the IFP is reduced. It has been shown that hyperthermia can reduce the IFP of tumors up to 78%, which is more effective than many chemicals or enzymes disrupting collagens or normalizing tumor vasculatures[7]. However, it is still unknown what kind of drug-heat sequence and heating dosing regimen can improve drug accumulation, and inconsistent heating remains a challenge. Therefore, it will be very

helpful to develop a thermo-responsive imaging system that can track temporospatial distributions of the nanoparticles upon hyperthermia in real-time fashion. At the same time, it is also equally important to develop a measurement technique that can relate pressure gradients with the delivery of the nanoparticles as a function of particle size, heating temperature, and duration. Once these techniques are established, the model will shed light on the biological response of the tumor to heat, and will aid in understanding how IFP alters the fate of macromolecules. Ideally, this correlation can be developed into a simulation and modeling program where drug intake can be predicted beforehand in order to rationally design delivery systems that best suit the particular tumor type and patient.

Judging from the modest success of these pilot studies, combinatorial therapy using ablation and thermally targeted heat shock inhibition may be clinically beneficial for cancer patients. However, there are multiple limitations to be addressed to achieve a better therapeutic outcome.

First, the release profile from the polymer backbone needs to be optimized to overcome the release burst at the initial stage. Although a library of ELP copolymers was generated in this dissertation, suitable candidates for conjugates are few. In almost 20% of cases, the therapeutic drug was released within 2 h of the administration, which may account for unspecific accumulation in other but vital organs. This issue may be addressed by controlling the size and length of each block, as well as the spacer between the drug and polymer.

Secondly, although the production of the polymer itself can be precisely controlled by genetic engineering, the drug loading is still subject to poly-dispersity, resulting in batch-

to-batch variance. A potential strategy to avoid inconsistency is to use click chemistry and introduce a nonconical amino acid loaded at a designated position in the polymer so that the conjugation ratio will be consistent among batches. However, special attention must be paid to the biocompatibility and immune responses of those nontraditional ELPs, as they may trigger an unwanted immune response.

Another unanswered question of this dissertation is the GA/ELP accumulation kinetics at the ablated sites. To quantify the actual amount of drug in each tissue, the animals need to be sacrificed at specific time points and the actual extraction and purification of the materials are very laborious. Furthermore, the real-time imaging of ELP remains a challenge, as no reliable quantification has been established. ELP has been expressed from radiolabeled media but the overall yield has been too poor to perform imaging studies. With the introduction of noncanonical amino acids, whole body imaging with highly specific and sensitive probes can be realized as a way to understand ELP transport, accumulation, and extravasation in the tumor.

Also, the invasive nature of thermal ablation adds clinical difficulty for treating tumors deep inside the body. Hence, edema and other complications resulting from damage to the surrounding normal tissues might limit those types of application in cancer patients. Therefore, continuing efforts are needed to achieve more uniform heat penetration at the tumor regions. One possible approach would be to use ELP-conjugated magnetic particles, which can be attracted to the tumor regions and emit energy upon application of an external magnetic field. At the same time, the metal materials can be used as diagnostic agents and provide real-time pharmacokinetic information of the conjugates in general. As a final recommendation, with the increase in understanding about the role of

HSPs in cancer and their behavior after thermal stress, a combined inhibition of HSP90 with heat shock factor-1(HSF-1)[8, 9] should be studied. Other HSPs have been observed to be elevated following HSP90 inhibition, possibly comprising the anticancer benefit of HSP90 alone.

As shown by multitudes of cancer research, it is clear that there currently exists no magic drug/target for all cancer types; therefore, personalized monitoring should be established to achieve a more specific treatment regimen for the individual patient. Since it is difficult to associate personalized therapy with combination therapies similar to adjuvant chemotherapies, the thermal ablation method, dosing regimens, heat-drug sequence, and pharmacokinetic modeling need to be fully developed in order to achieve a real transition from bench top to bed. A platform, preferentially using computer modeling, can be very useful for doctors in prescribing treatment based on the individual patient and may help in achieving timely intervention to avoid future recurrence of HCC. Clinical investigation of this type would increase the likelihood of each patient to achieve the best treatment outcome, with more effective and less toxic cancer therapies. It is anticipated that the combination therapy built upon this work will assist in the translation of advanced drug delivery systems into clinical use, in order to fight cancer in the long run and allow a faster victory over the disease.

6.3 References

1. Meyer DE, Shin BC, Kong GA, Dewhirst MW, Chilkoti A. Drug targeting using thermally responsive polymers and local hyperthermia. J Control Release 2001;74:213-24.

2. Dreher MR, Liu W, Michelich CR, Dewhirst MW, Chilkoti A. Thermal cycling enhances the accumulation of a temperature-sensitive biopolymer in solid tumors. Cancer Res 2007;67:4418-24.

3. Kim MS, Lee D-W, Park K, Park S-J, Choi E-J, Park ES, et al. Temperature-triggered tumor-specific delivery of anticancer agents by cRGD-conjugated thermosensitive liposomes. Colloids Surf B 2014;116:17-25.

4. Milosevic M, Fyles A, Hedley D, Pintilie M, Levin W, Manchul L, et al. Interstitial fluid pressure predicts survival in patients with cervix cancer independent of clinical prognostic factors and tumor oxygen measurements. Cancer Res 2001;61:6400-5.

5. Wiig H, Swartz MA. Interstitial fluid and lymph formation and transport: physiological regulation and roles in inflammation and cancer. Physiol Rev 2012;92:1005-60.

6. Carmeliet P. Angiogenesis in life, disease and medicine. Nature 2005;438:932-6.

7. Leunig M, Goetz AE, Dellian M, Zetterer G, Gamarra F, Jain RK, et al. Interstitial fluid pressure in solid tumors following hyperthermia: possible correlation with therapeutic response. Cancer Res 1992;52:487-90.

8. Akerfelt M, Morimoto RI, Sistonen L. Heat shock factors: integrators of cell stress, development and lifespan. Nat Rev Mol Cell Biol 2010;11:545-55.

9. Fang F, Chang R, Yang L. Heat shock factor 1 promotes invasion and metastasis of hepatocellular carcinoma in vitro and in vivo. Cancer 2012;118:1782-94.

APPENDIX A

PHYSICOCHEMICAL CHARACTERIZATION OF ELP TRIBLOCK COPOLYMERS AND CONJUGATES

A.1 Materials and methods

Detailed description of materials and methods were provided in Chapter 4, materials and methods section.

A.2 Results

A.2.1 Complete gene and amino acid sequence of ELP triblock copolymers

Sequences were verified by the core sequencing facility in University of Utah.

A.2.1.1 ELPVA20-1-60-$(DADAV)_7$D

From start to stop codon, including trailer sequences:

5′-ATGGGCGGACACGGCgtgggtgttccgggcgcaggtgttccgggcgcaggtgttccgggcgcaggtgttcc
gggcgcaggtgttccgggcgcaggtgttccgggcgcaggtgttccgggcgcaggtgttccgggcgcaggtgttcc
gggcgcaggtgttccgggcgcaggtgttccgggcgcaggtgttccgggcgcaggtgttccgggcgcaggtgtt
ccgggcgcaggtgttccgggcgcaggtgttccgggcgcaggtgttccgggcgcaggtgttccgggcgcaggtgtt
ccgggcgcaggtgttccgggcgcaggtgttccgggcgcaggtgttccgggcgcaggtgttccgggcgcaggtgtt
gcaggtgttccgggcgcaggtgtgccgggcgcGTGGGTGTTCCGGGCGTGGGTGTTCCGGGTG
GCGGTGTGCCGGGCGCACCTGTTCCTGGTGTAGGTGTGCCGGGTGTTGGTGTG
CCGGGTGTTGGTGTACCAGGTGGCGGTGTTCCGGGTGCAGGCGTTCCGGGTG

GCGGTGTGCCGGGCGTGGGTGTTCCGGGCGTGGGTGTTCCGGGTGGCGGTGT

GCCGGGCGCAGGTGTTCCTGGTGTAGGTGTGCCGGGTGTTGGTGTGCCGGGT

GTTGGTGTACCAGGTGGCGGTGTTCCGGGTGCAGGCGTTCCGGGTGGCGGTG

TGCCGGGCGTGGGTGTTCCGGGCGTGGGTGTTCCGGGTGGCGGTGTGCCGGG

CGCAGGTGTTCCTGGTGTAGGTGTGCCGGGTGTTGGTGTGCCGGGTGTTGGTG

TACCAGGTGGCGGTGTTCCGGGTGCAGGCGTTCCGGGTGGCGGTGTGCCGGG

CGTGGGTGTTCCGGGCGTGGGTGTTCCGGGTGGCGGTGTGCCGGGCGCAGGT

GTTCCTGGTGTAGGTGTGCCGGGTGTTGGTGTGCCGGGTGTTGGTGTACCAGG

TGGCGGTGTTCCGGGTGCAGGCGTTCCGGGTGGCGGTGTGCCGGGCGTGGGT

GTTCCGGGCGTGGGTGTTCCGGGTGGCGGTGTGCCGGGCGCAGGTGTTCCTG

GTGTAGGTGTGCCGGGTGTTGGTGTGCCGGGTGTTGGTGTACCAGGTGGCGG

TGTTCCGGGTGCAGGCGTTCCGGGTGGCGGTGTGCCGGGCGTGGGTGTTCCG

GGCGTGGGTGTTCCGGGTGGCGGTGTGCCGGGCGCAGGTGTTCCTGGTGTAG

GTGTGCCGGGTGTTGGTGTGCCGGGTGTTGGTGTACCAGGTGGCGGTGTTCCG

GGTGCAGGCGTTCCGGGTGGCGGTGTGCCGGGCTGGCTGgatgcagacgcagtggatgc

agacgcagttgatgcagatgcagtggatgcagatgcagttgatgcagatgcagtggatgcagatgcagttgatgcagatgcagt

ggattga-3′

A.2.1.2 Amino acid sequence of ELPVA20-1-60-$(DADAV)_7$D

5′-MGGHGVGVPGAGVPGAGVPGAGVPGAGVPGAGVPGAGVPGAGVPGAGVPG

AGVPGAGVPGVGVPGAGVPGAGVPGAGVPGAGVPGAGVPGAGVPGAGVPGAG

VPGAGVPGAGVPGVGVPGVGVPGGGVPGAGVPGVGVPGVGVPGVGVPGGVPG

AGVPGGGVPGVGVPGVGVPGGGVPGAGVPGVGVPGVGVPGVGVPGGGVPGAG

VPGGGVPGVGVPGVGVPGGGVPGAGVPGVGVPGVGVPGVGVPGGGVPGAGVP

GGGVPGVGVPGVGVPGGGVPGAGVPGVGVPGVGVPGVGVPGGGVPGAGVPGG

GVPGVGVPGVGVPGGGVPGAGVPGVGVPGVGVPGVGVPGGGVPGAGVPGGGV

PGVGVPGVGVPGGGVPGAGVPGVGVPGVGVPGVGVPGGGVPGAGVPGGGVPG

WLDADAVDADAVDADAVDADAVDADAVDADAVDADAVD*-3′

A.2.1.3 Gene sequence of ELPVA30-1-60-$(DADAV)_7$D

5′-ATGGGCGGACACGGCgtgggtgttccgggcgcaggtgttccgggcgcaggtgttccgggcgcaggtgttcc

gggcgcaggtgttccgggcgcaggtgttccgggcgcaggtgttccgggcgcaggtgttccgggcgcaggtgttccgggcgc

aggtgttccgggcggcaggtgttccgggcgcaggtgttccgggcgcaggtgttccgggcgcaggtgttccgggcgcaggtgt

tccgggcgcaggtgtgccgggcgtgggtgttccgggcgcaggtgttccgggcgcaggtgttccgggcgcaggtgttccgggc

gcaggtgttccgggcgcaggtgttccgggcgcaggtgttccgggcgcaggtgttccgggcgcaggtgttccgggcgcaggtg

ttccgggcgcaggtgtgccgggcGTGGGTGTTCCGGGCGTGGGTGTTCCGGGTGGCGGTG

TGCCGGGCGCAGGTGTTCCTGGTGTAGGTGTGCCGGGTGTTGGTGTGCCGGG

TGTTGGTGTACCAGGTGGCGGTGTTCCGGGTGCAGGCGTTCCGGGTGGCGGT

GTGCCGGGCGTGGGTGTTCCGGGCGTGGGTGTTCCGGGTGGCGGTGTGCCGG

GCGCAGGTGTTCCTGGTGTAGGTGTGCCGGGTGTTGGTGTGCCGGGTGTTGGT

GTACCAGGTGGCGGTGTTCCGGGTGCAGGCGTTCCGGGTGGCGGTGTGCCGG

GCGTGGGTGTTCCGGGCGTGGGTGTTCCGGGTGGCGGTGTGCCGGGCGCAGG

TGTTCCTGGTGTAGGTGTGCCGGGTGTTGGTGTGCCGGGTGTTGGTGTACCAG

GTGGCGGTGTTCCGGGTGCAGGCGTTCCGGGTGGCGGTGTGCCGGGCGTGGG

TGTTCCGGGCGTGGGTGTTCCGGGTGGCGGTGTGCCGGGCGCAGGTGTTCCT

GGTGTAGGTGTGCCGGGTGTTGGTGTGCCGGGTGTTGGTGTACCAGGTGGCG

GTGTTCCGGGTGCAGGCGTTCCGGGTGGCGGTGTGCCGGGCGTGGGTGTTCC

GGGCGTGGGTGTTCCGGGTGGCGGTGTGCCGGGCGCAGGTGTTCCTGGTGTA

GGTGTGCCGGGTGTTGGTGTGCCGGGTGTTGGTGTACCAGGTGGCGGTGTTCC
GGGTGCAGGCGTTCCGGGTGGCGGTGTGCCGGGCGTGGGTGTTCCGGGCGTG
GGTGTTCCGGGTGGCGGTGTGCCGGGCGCAGGTGTTCCTGGTGTAGGTGTGC
CGGGTGTTGGTGTGCCGGGTGTTGGTGTACCAGGTGGCGGTGTTCCGGGTGC
AGGCGTTCCGGGTGGCGGTGTGCCGGGCTGGCTGgatgcagacgcagtggatgcagacgcag
ttgatgcagatgcagtggatgcagatgcagttgatgcagatgcagtggatgcagatgcagttgatgcagatgcagtgg attga-
3′

A.2.1.4 Amino acid sequence of ELPVA30-1-60-$(DADAV)_7$D

5′-MGGHGVGVPGAGVPGAGVPGAGVPGAGVPGAGVPGAGVPGAGVPGAGVPG
AGVPGAGVPGVGVPGAGVPGAGVPGAGVPGAGVPGAGVPGAGVPGAGVPGAG
VPGAGVPGAGVPGVGVPGAGVPGAGVPGAGVPGAGVPGAGVPGAGVPGAGVP
GAGVPGAGVPGAGVPGVGVPGVGVPGGGVPGAGVPGVGVPGVGVPGVGVPGG
GVPGAGVPGGGVPGVGVPGVGVPGGGVPGAGVPGVGVPGVGVPGVGVPGGGV
PGAGVPGGGVPGVGVGVGVPGGGVPGAGVPGVGVPGVGVPGVGVPGGGVPGA
GVPGGGVPGVGVPGVGVPGGGVPGAGVPGVGVPGVGVPGVGVPGGGVPGAGV
PGGGVPGVGVPGVGVPGGGVPGAGVPGVGVPGVGVPGVGVPGGGVPGAGVPG
GGVPGVGVPGVGVPGGGVPGAGVPGVGVPGVGVPGVGVPGGGVPGAGVPGGG
VPGWLDADAVDADAVDADAVDADAVDADAVDADAVDADAVD*-3′

A.2.1.5 Gene sequence of ELPVA40-1-60-$(DADAV)_7$D

5′-atgggcggacacggcgtgggtgttccgggcgcaggtgttccgggcgcaggtgttccgggcgcaggtgttccgggcgcag
gtgttccgggcgcaggtgttccgggcgcaggtgttccgggcgcaggtgttccgggcgcaggtgttccgggcgcaggtgttccg
ggcgcaggtgtgccgggcgtgggtgttccgggcgcaggtgttccgggcgcaggtgttccgggcgcaggtgttccgggcgca

ggtgttccgggcgcaggtgttccgggcgcaggtgttccgggcgcaggtgttccgggcgcaggtgttccgggcgcaggtgttcc

gggcgcaggtgtgccgggcgtgggtgttccgggcgcaggtgttccgggcgcaggtgttccgggcgcaggtgttccgggcgc

aggtgttccgggcgcaggtgttccgggcgcaggtgttccgggcgcaggtgttccgggcgcaggtgttccgggcgcaggtgttc

cgggcgcaggtgtgccgggcgtgggtgttccgggcgcaggtgttccgggcgcaggtgttccgggcgcaggtgttccgggcg

caggtgttccgggcgcaggtgttccgggcgcaggtgttccgggcgcaggtgttccgggcgcaggtgttccgggcgcaggtgtt

ccgggcgcaggtgtgccgggcGTGGGTGTTCCGGGCGTGGGTGTTCCGGGTGGCGGTGT

GCCGGGCGCAGGTGTTCCTGGTGTAGGTGTGCCGGGTGTTGGTGTGCCGGGT

GTTGGTGTACCAGGTGGCGGTGTTCCGGGTGCAGGCGTTCCGGGTGGCGGTG

TGCCGGGCGTGGGTGTTCCGGGCGTGGGTGTTCCGGGTGGCGGTGTGCCGGG

CGCAGGTGTTCCTGGTGTAGGTGTGCCGGGTGTTGGTGTGCCGGGTGTTGGTG

TACCAGGTGGCGGTGTTCCGGGTGCAGGCGTTCCGGGTGGCGGTGTGCCGGG

CGTGGGTGTTCCGGGCGTGGGTGTTCCGGGTGGCGGTGTGCCGGGCGCAGGT

GTTCCTGGTGTAGGTGTGCCGGGTGTTGGTGTGCCGGGTGTTGGTGTACCAGG

TGGCGGTGTTCCGGGTGCAGGCGTTCCGGGTGGCGGTGTGCCGGGCGTGGGT

GTTCCGGGCGTGGGTGTTCCGGGTGGCGGTGTGCCGGGCGCAGGTGTTCCTG

GTGTAGGTGTGCCGGGTGTTGGTGTGCCGGGTGTTGGTGTACCAGGTGGCGG

TGTTCCGGGTGCAGGCGTTCCGGGTGGCGGTGTGCCGGGCGTGGGTGTTCCG

GGCGTGGGTGTTCCGGGTGGCGGTGTGCCGGGCGCAGGTGTTCCTGGTGTAG

GTGTGCCGGGTGTTGGTGTGCCGGGTGTTGGTGTACCAGGTGGCGGTGTTCCG

GGTGCAGGCGTTCCGGGTGGCGGTGTGCCGGGCGTGGGTGTTCCGGGCGTGG

GTGTTCCGGGTGGCGGTGTGCCGGGCGCAGGTGTTCCTGGTGTAGGTGTGCC

GGGTGTTGGTGTGCCGGGTGTTGGTGTACCAGGTGGCGGTGTTCCGGGTGCA

GGCGTTCCGGGTGGCGGTGTGCCGGGCTGGCTGgatgcagacgcagtggatgcagacgcagtt

gatgcagatgcagtggatgcagatgcagttgatgcagatgcagtggatgcagatgcagttgatgcagatgcagtggattga-3′

A.2.1.6 Amino acid sequence of ELPVA40-1-60-$(DADAV)_7$D

5′-MGGHGVGVPGAGVPGAGVPGAGVPGAGVPGAGVPGAGVPGAGVPGAGVPG
AGVPGAGVPGVGVPGAGVPGAGVPGAGVPGAGVPGAGVPGAGVPGAGVPGAG
VPGAGVPGAGVPGVGVPGAGVPGAGVPGAGVPGAGVPGAGVPGAGVPGAGVP
GAGVPGAGVPGAGVPGVGVPGAGVPGAGVPGAGVPGAGVPGAGVPGAGVPGA
GVPGAGVPGAGVPGAGVPGVGVPGVGVPGGGVPGAGVPGVGVPGVGVPGVGV
PGGGVPGAGVPGGGVPGVGVPGVGVPGGGVPGAGVPGVGVPGVGVPGVGVPG
GGVPGAGVPGGGVPGVGVPGVGVPGGGVPGAGVPGVGVPGVGVPGVGVPGGG
VPGAGVPGGGVPGVGVPGVGVPGGGVPGAGVPGVGVPGVGVPGVGVPGGGVP
GAGVPGGGVPGVGVPGVGVPGGGVPGAGVPGVGVPGVGVPGVGVPGGGVPGA
GVPGGGVPGVGVPGVGVPGGGVPGAGVPGVGVPGVGVPGVGVPGGGVPGAGV
PGGGVPGWLDADAVDADAVDADAVDADAVDADAVDADAVDADAVD*-3′.

A.2.2 Physicochemical characterization of ELP triblock copolymers and conjugates

The exact expression of amino acid sequences was further verified by Mass Spectrometry analysis. Representative Mass Spec plots were provided in **Figure A.1.** Size distributions of all ELP polymers from DLS were shown in **Figure A.2**. The filtration did not change the size distribution (data not shown) as copolymers do not aggregate at 25 μM but form stable nanoparticles. Each chemical reaction from GA modification to bioconjugation to ELPs was summarized in **Table A.1** where yield and purity of each step were listed. Purity of modified GA and conjugates was verified mostly

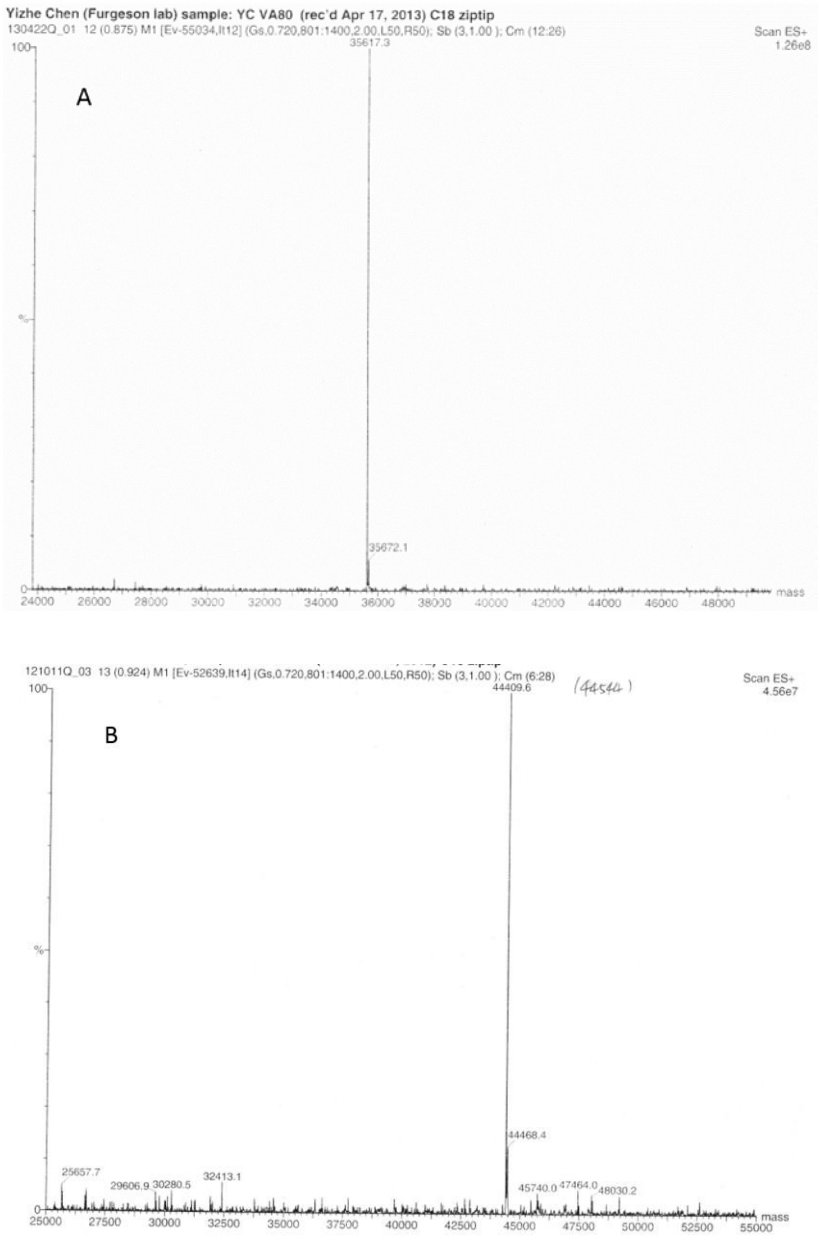

Figure A.1 Mass Spectrometry (ESI) of A) ELPVA homopolymers (ELPVA80) and B) ELP triblock copolymer (ELPVA40-60-(DADAV)$_7$D).

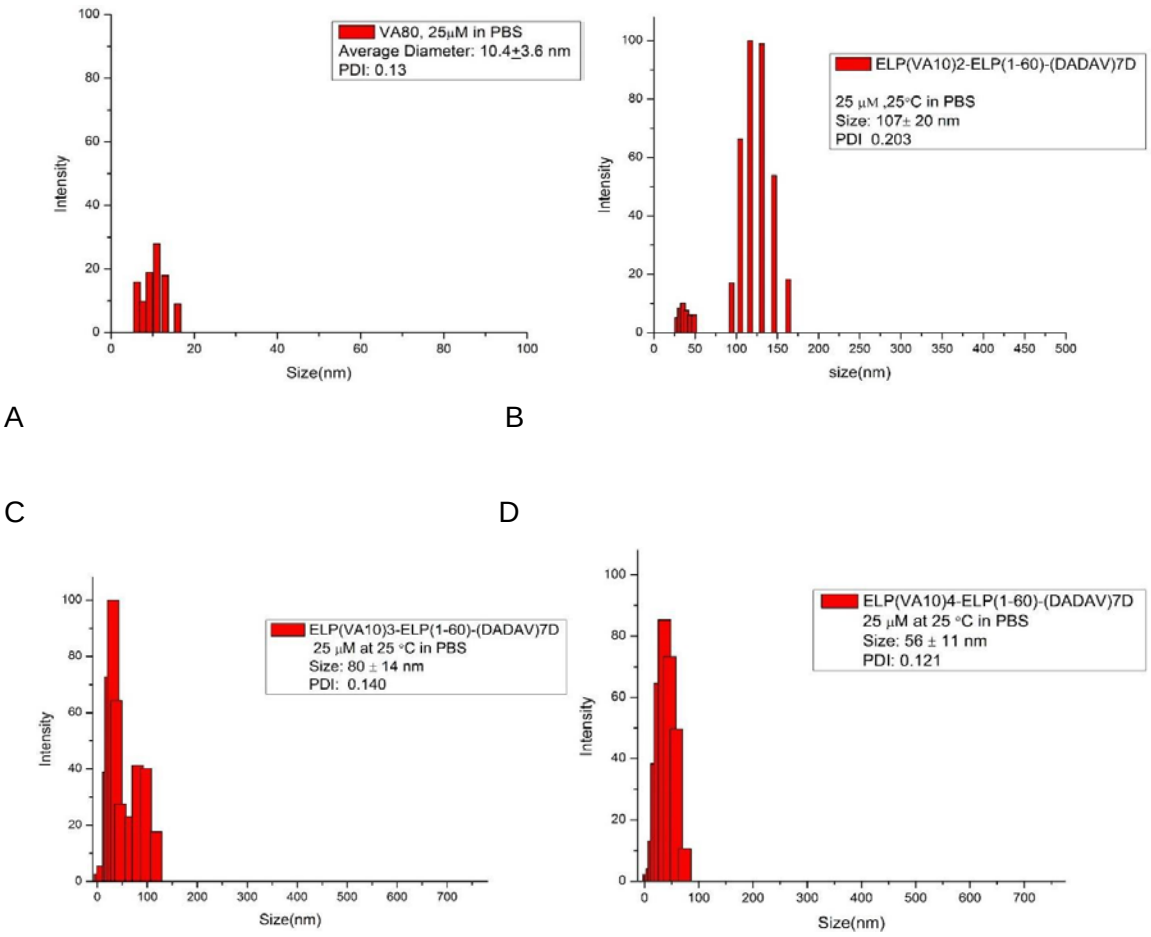

Figure A.2 Size distributions of ELP biopolymers.

The hydrodynamic radius of polymers was measured at 25μM in PBS (pH7.4, 147mM) at 25 °C by DLS, n=3.

Table A.1. Summary of yield and purity of chemical reactions in bio-conjugation of GA to ELP biopolymers.

Reaction	Yield	Purity
GA modification		
Diethal acetal formation	95%	>95%
Acid hydrolysis	90%	90%
GA-aldehyde formation	70%	>95%
Polymer modification		
NHS formation	90%	90%
End product, lyophilized	75%	90%
Hydrazone formation	65-75%	Varies depends on drug conjugation number
Conjugates, lyophilized	40-50%	Varies depends on drug conjugation number

by NMR, as shown in **Figure A.3**. The molecular weight distribution and absence of free drugs were verified by both Mass Spectrometry (ESI and MALDITOF) in **Figure A.4** to **Figure A.6**. Similar to the free copolymer, the particle size distribution of ELP-GA conjugates was evaluated by both DLS and SLS in **Figure A.7** and **Figure A.8**. An additional TEM image was provided for conjugates, suggesting that the conjugates self-assembled into spherical structures.

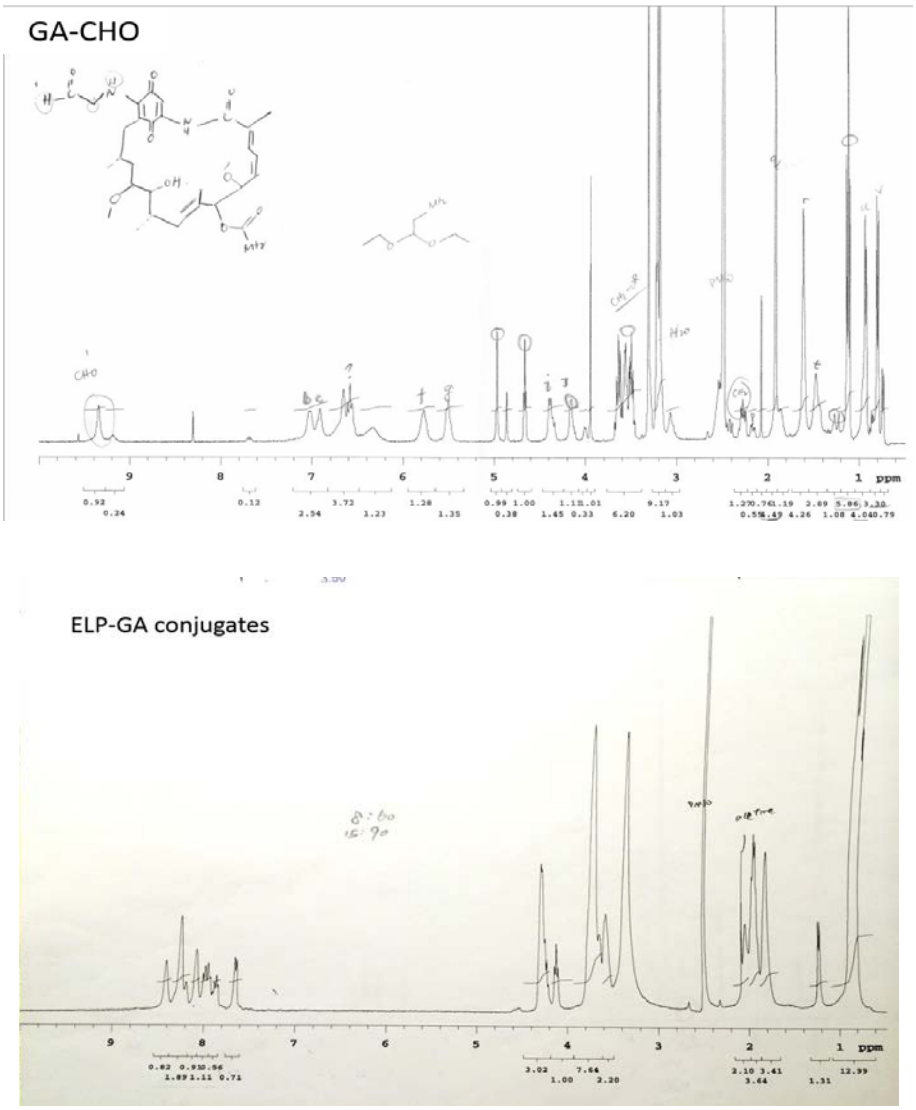

Figure A.3 NMR of modified GA(GA-CHO) and ELP-GA conjugates.

1mg GA-CHO or equivalent conjugates were dissolved in *d6*-DMSO for ^{1}H-NMR analysis. No CHO-signal from free drug was detected.

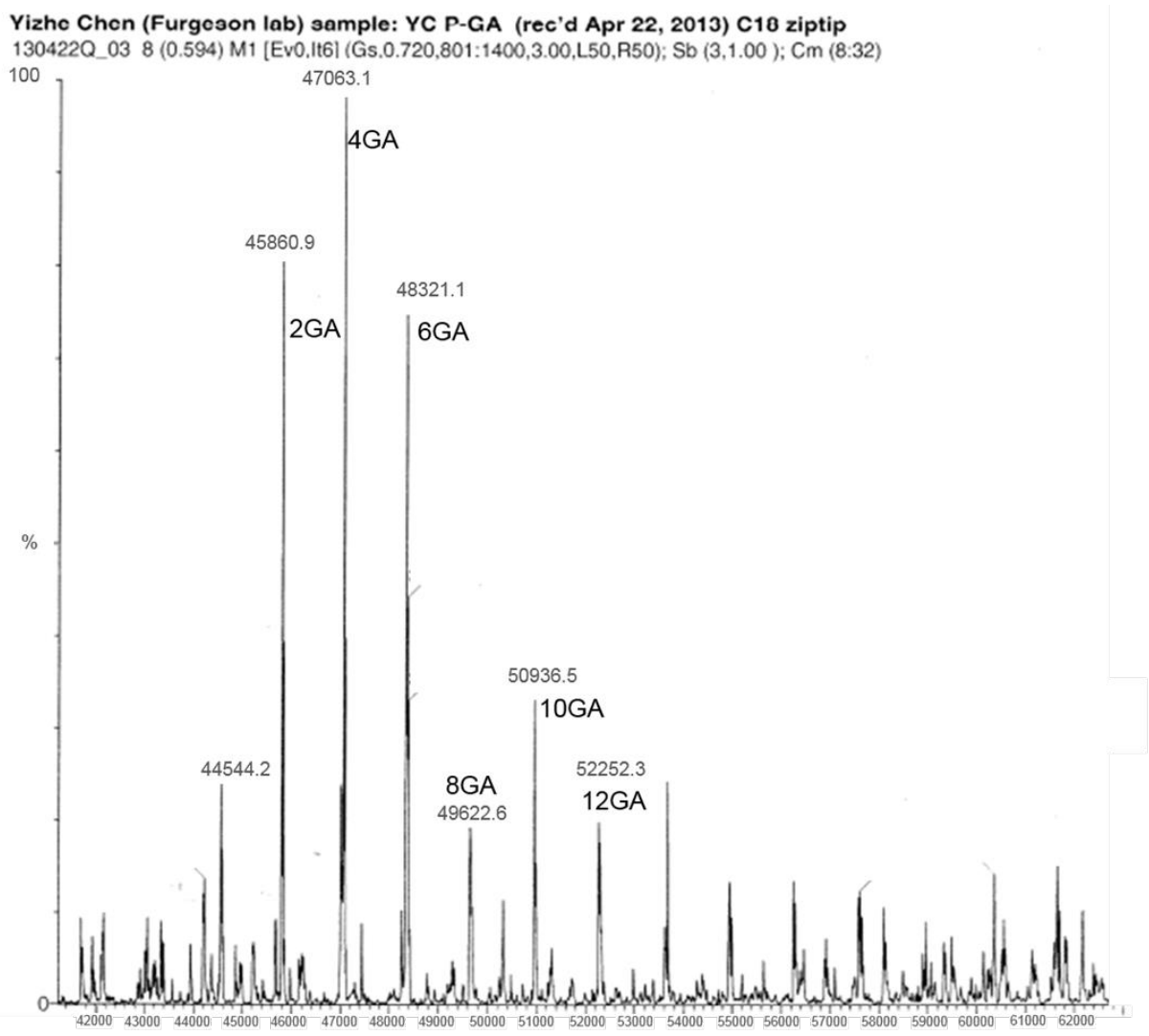

Figure A.4 Mass Spec of ELP triblock copolymer conjugates (ESI).

Peaks were assigned based on precise calculation from molecular weight of modified GA. A distribution of 2-12 GAs can be detected by ESI.

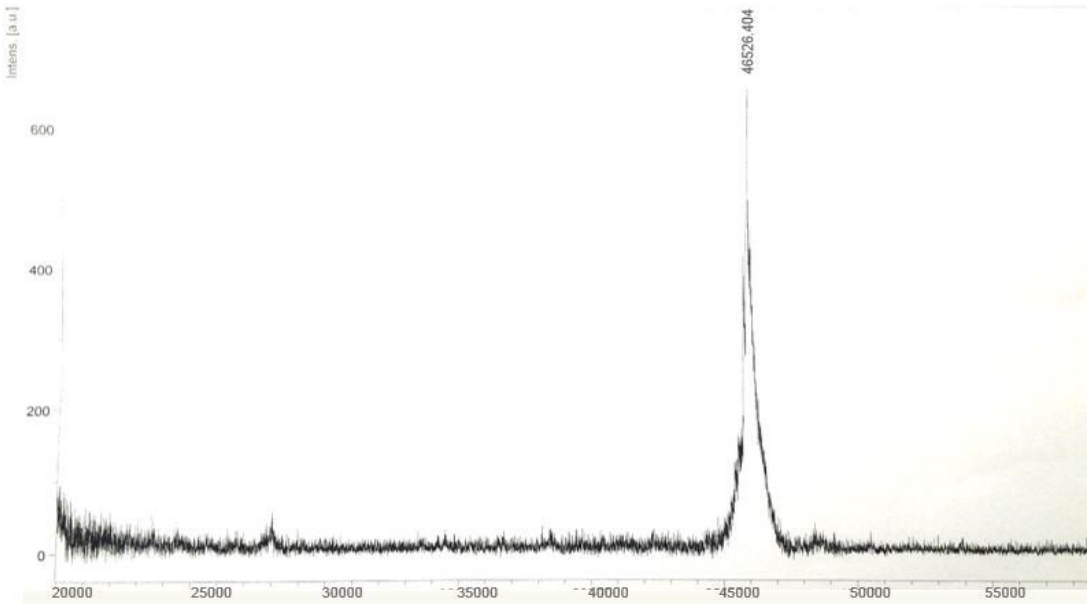

Figure A.5 Mass Spec of ELP triblock copolymer conjugates (MALDI-TOF).

A distribution of molecular weight from 45000 to 48000 Da was detected by MALDI-TOF.

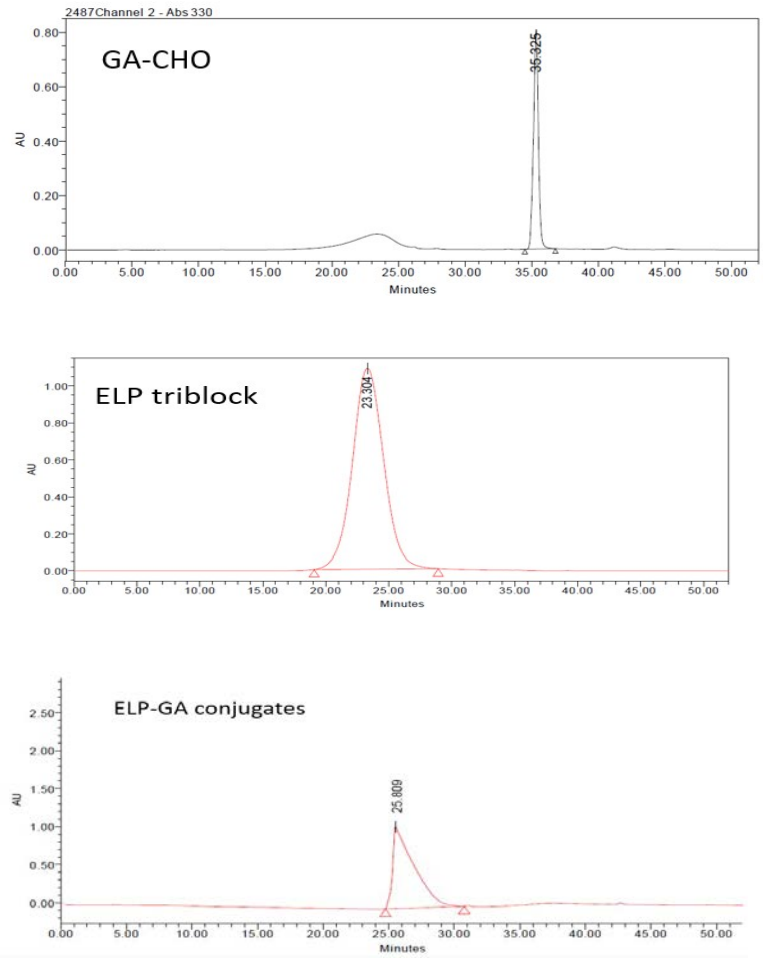

Figure A.6. HPLC graphs of free drug, free polymer, and ELP-GA conjugates.

ELPs were loaded at 25 μM standard concentrations. Initially, the binary gradient was 70:30 for 10 min at which point the 90% DCM concentration was raised to 60% over 30 min followed by a static 10 min period. The flow rate was 0.3 mL/min. Using the binary gradient, ELP copolymer (R_t= 23 min), conjugates (R_t =26 min), and free GA-CHO (R_t =35min) can be separated. Concentrations were determined from the standard curve at 337 and 220 nm.

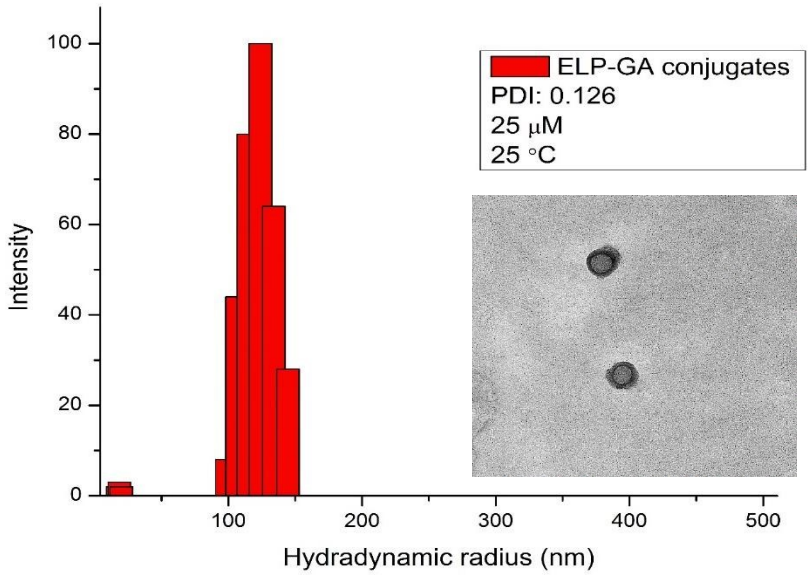

d	G(d)	C(d)	d	G(d)	C(d)	d	G(d)	C(d)
14.69	0	0	33.97	0	2	78.57	0	2
15.85	0	0	36.66	0	2	84.79	0	2
17.10	2	1	39.56	0	2	91.51	0	2
18.46	3	2	42.70	0	2	98.75	8	5
19.92	2	2	46.08	0	2	106.58	44	18
21.50	0	2	49.73	0	2	115.02	80	42
23.20	0	2	53.67	0	2	124.13	100	72
25.04	0	2	57.92	0	2	133.96	64	91
27.02	0	2	62.51	0	2	144.57	28	100
29.16	0	2	67.46	0	2	156.03	0	100
31.47	0	2	72.80	0	2	168.38	0	100

Figure A.7 DLS and TEM of ELP-GA conjugates.

Conjugates containing 25 μM ELP were measured at 25 °C in PBS (pH 7.4, 147 mM). Representative histogram plot were generated from raw data (representative table provided, n=3.

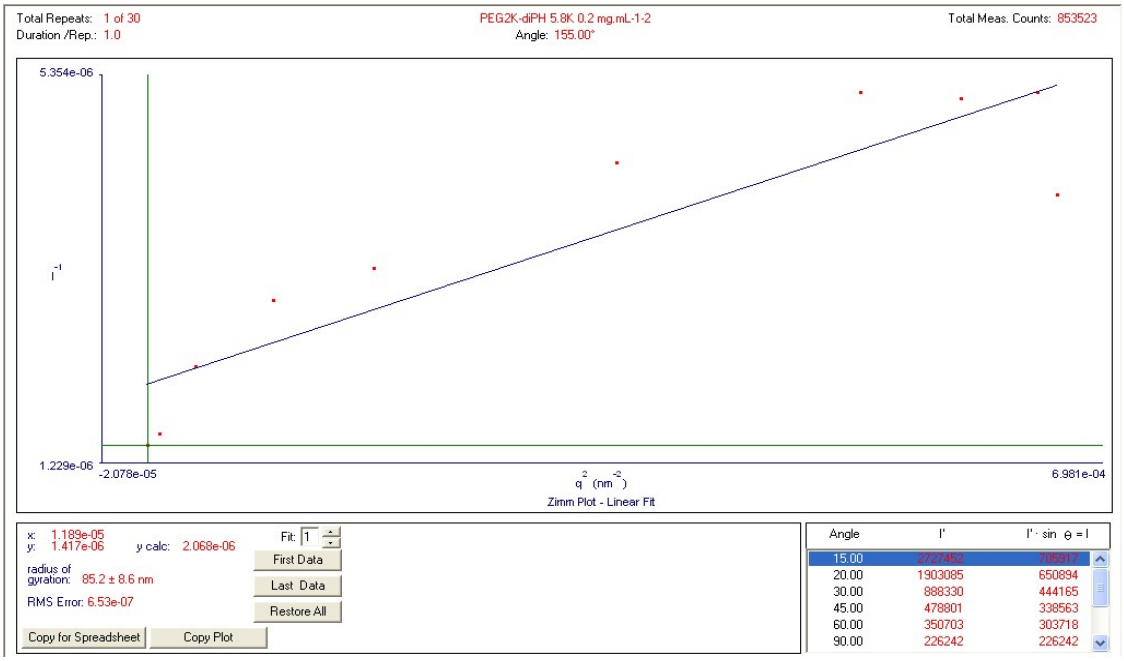

Figure A.8 Representative SLS of ELP-GA conjugates.

Conjugates containing 25 µM ELP were measured at 25 °C in PBS (pH 7.4, 147 mM). 12 angles from 15°C to 155°C were measured to generate the SLS plot.

APPENDIX B

IN VIVO EFFICACY OF ELP-DIBLOCK COPOLYMER GA CONJUGATES IN RABBIT TUMOR MODELS: A PRELIMINARY STUDY

B.1 Materials and methods

B.1.1 Establishing VX2 tumor model in donor animals

Female New Zealand white rabbits (NZ-WR), 18-24 months old, were anesthetized with a mixture of ketamine and xylazine (28.6 mg/kg ketamine, 4.8 mg/kg xylazine, I.M.) and maintained with 1-3% isoflurane using a mask/nose cone. Donor animals (one donor animal per group) were bilaterally inoculated with ~2 x 10^6 VX2 cells (kindly donated by Dr. Ashish Ranjan, Former Fellow-Center for Interventional Oncology; NIH) in the superficial thigh muscles of hind limb under anesthesia and aseptic conditions. VX2 inoculated NZ-WR was monitored biweekly by ultrasound to determine the size of the tumor. A Vevo 2100 ultrasound (Visualsonics, CA) was used without contrast to monitor tumor growth in the ultrasound facility.

B.1.2 Transplantation of VX2 tumor fragments through ultrasound-guided, percutaneous injection into the subcapsular region of the liver

Under anesthesia and aseptic conditions, the VX2 tumors were harvested from the donor animals, dissected to ~ 1 mm^3 fragments, minced, and suspended in normal saline,

and 0.2 mL of minced tumor suspension was loaded into 18-gauze jelco catheters. Following this, the minced tumor suspension were percutaneously injected into the subcapsular parenchyma of the left lateral lobe of the liver by passing the loaded catheter through a 16-g Jelco catheter using a blunt stylet under ultrasound guidance. The donor animals were humanely euthanized.

B.1.3 Abrogation of tumor growth, tumor growth kinetics, and endpoint survival

Each animal in treatment groups was systemically injected with 3.1 mg/kg equivalent dose of 17-AAG, ELP-GA conjugates, and PBS control. Tumor volume was monitored by ultrasound and weight was recorded twice weekly. Standard anesthesia, prep, ventilation, and post-op care was applied. Animals having any evidence of excessive tumor burden, severe distress or infection, > 20% loss of body weight, or tumor size > 3 cm in one dimension were euthanized.

B.2 Results and discussion

Due to the aggressiveness of VX2 tumor, all donor rabbits (n=3) showed fast tumor growth in their hind limbs within three-weeks of injection. Representative image of tumor tracked by ultrasound is shown in **Figure B.1.** We had significant technical problems with tumor transplantation where 25% of animals died due to severe GI tract infection. However, the successful implantations did achieve rapid growth of a liver tumor, as shown in **Figure B.2**. By the point of treatment, only three animals were tested with similar tumor size and burden (n=1). ELP-GA diblock copolymer conjugates were synthesized and characterized as shown in Figure **3.7** and **3.9**. Three study groups were

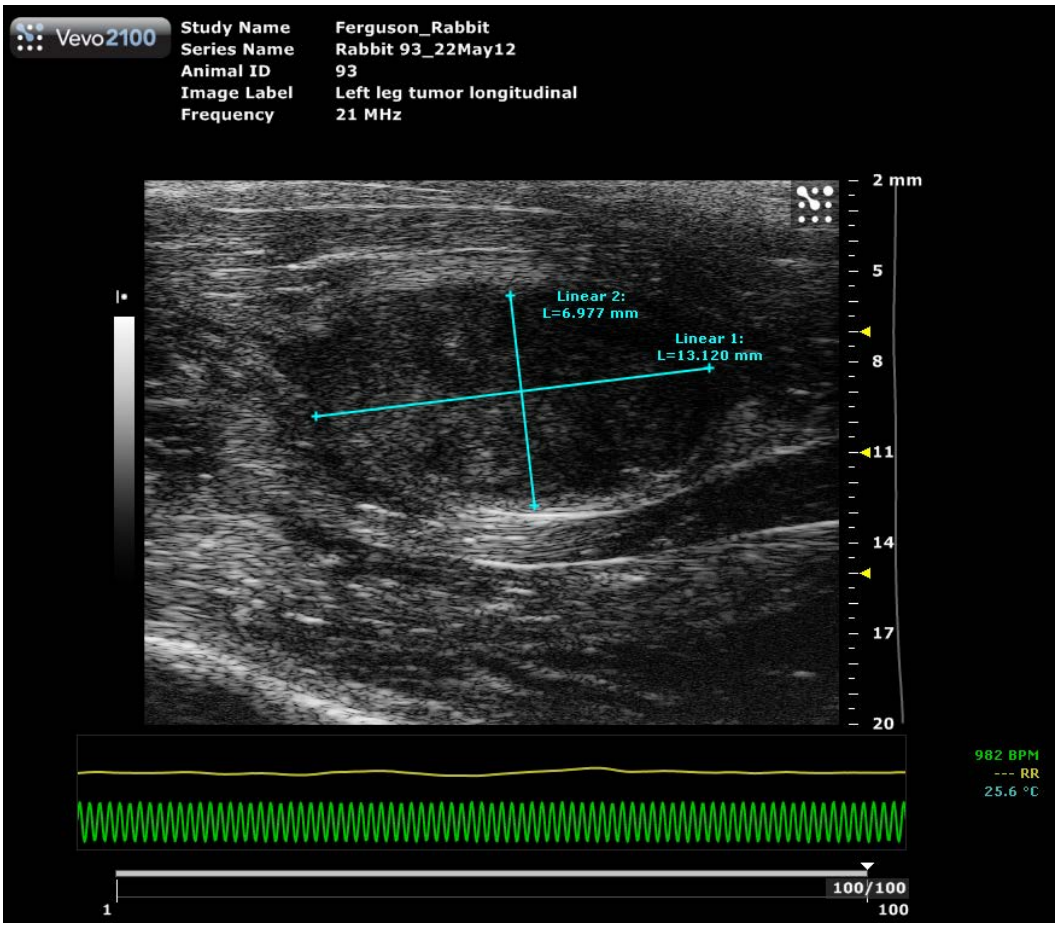

Figure B.1 Ultrasound image of a single tumor at left hind limb of a donor rabbit (B mode).

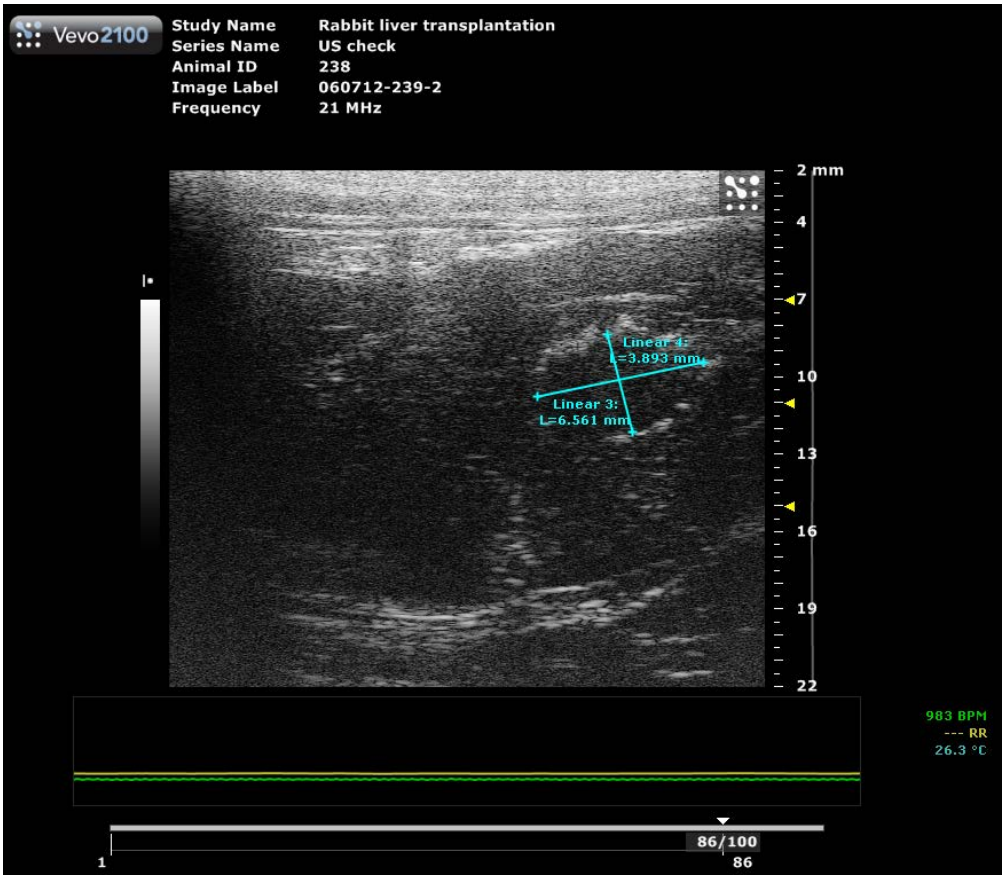

Figure B.2 Ultrasound image of a single liver tumor in a recipient rabbit (B mode).

systemically injected through the ear vein (solubilized in 1.5 mL of PBS). The negative control (PBS) were quickly subject to euthanasia due to severe tumor metastasis. The rabbit receiving 17-AAG showed no sign of tumor suppression and experienced significant weight loss before the endpoint. The ELP-GA conjugates displayed slowest tumor growth and noticeable palliative effect for the diseased animal, as summarized in **Figure B.3.**

Although the animal numbers are too few to draw solid conclusions, there is great potential of using ELP-GA conjugates for HCC treatment, but the conjugates need to be optimized. Therefore, a new library of triblock copolymers was designed and synthesized, as detailed in Chapter 4.

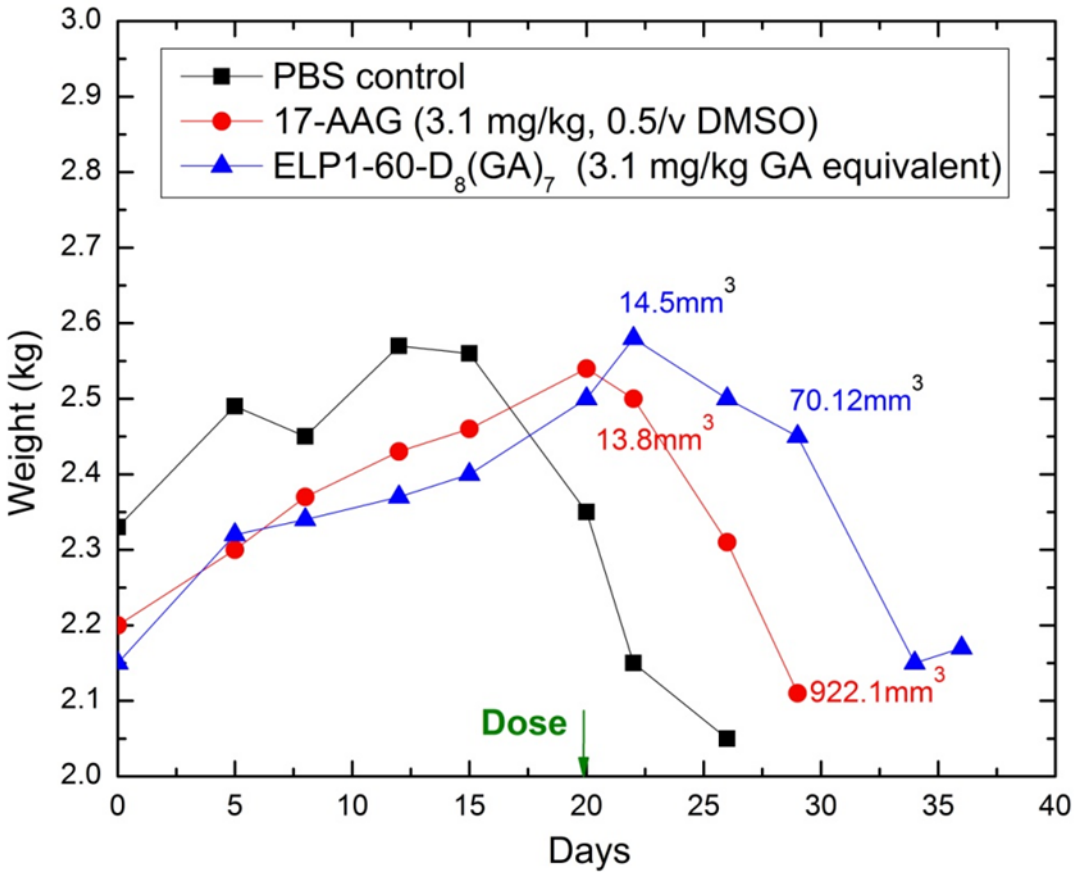

Figure B.3 Weights and tumor volumes of treated animals.

Each rabbit was dosed (i.v.) 20 days post-tumor injection. Tumor volumes for 17-AAG and conjugate were tracked at 22 and 29 days. At 26 days, the PBS control was euthanized and the 17-AAG rabbit was euthanized at 29 days due to >20% weight loss. The conjugate rabbit was able to sustain its weight up to 36 days, but the tumor reached a size > 4 cm in diameter so the study was ended, n=1.